HIGH VOLUME PRECIPITATION OF COPPER POWDER BY DISPROPORTIONATION

Rajender Singh Sipehia

A Thesis

in

The Department

of

Chemistry

Presented in Partial Fulfilment of the Requirements
for the degree of Doctor of Philosophy at
Concordia University
Montréal, Quebec, Canada

August 1980

To

My Mother Gita

and

My Wife Esther

ABSTRACT

HIGH VOLUME PRECIPITATION OF COPPER POWDER BY DISPROPORTIONATION

Rajender Singh Sipehia, Ph.D.
Concordia University, 1980

Copper powder was produced by the disproportionation of cuprous ion in acidified aqueous solution. The process was studied in a dynamic system, in which solutions of cupric sulphate in sulphuric acid were continuously streamed over copper wire, using a series of peristaltic pumps to effect circulation. The system was capable of a maximum yield of 3.5 grams of powder per hour; but this was limited only by the size of the apparatus used.

The size and yield of the copper powder produced were studied as functions of the flow rate of solution, the duration of the experiment, the concentration of copper sulphate, the mass of copper wire within the apparatus, and the temperature of crystallization. The powder yield increased with the duration of the experiment, the concentration of cupric sulphate and the flow rate of solution. The yield varied only slightly with the mass of copper

wire in the apparatus, and it was independent of the temperature of crystallization.

Size classification of the powder was done using the Andreasen pipette method. The pipette was modified, to produce a more easily operated instrument, and gave results that were very reproducible, and believed to be accurate.

At low flow rates of circulating fluid, the particle size of the powder decreased, as the flow rate was increased. But, above a certain flow rate of solution, the particle size increased, as the flow rate was increased. This apparent paradox was ascribed to partial loss of control of the temperature of crystallization, at high flow rates, and this in turn was due to inadequacies in the design of the apparatus. At low flow rates of solution, an increase in the temperature of crystallization led to an increase in the average particle size of the powder.

The particle size of the powder showed only a relatively insignificant effect on the apparent density of the powder. Tensile strength measurements made on compacts formed from the powder, after being sintered by a commercial process, showed that the tensile strength increased, as the particle size decreased. Furthermore, compared to compacts made from commercially available copper powder, compacts made from powder produced in this work showed

significantly higher tensile strengths.

A theoretical analysis of the crystallization process occurring within the apparatus was developed, and from this analysis, the kinetics of nucleation, and of growth of the copper powder were determined. The theoretical analysis supported the experimental results.

ACKNOWLEDGEMENTS

The author wishes to express his sincere gratitude to:

Dr. R. A. Westbury for his guidance, encouragement and extreme degree of understanding throughout the investigation and for his assistance in the preparation of the thesis;

Professor J. G. Dick and Dr. J.R. Ufford for their interest and advice;

My brother Inder who inspired and encouraged me to come abroad for graduate study.

Thanks are also due to Mr. Daniel Dallenbach for typing.

Finally, I would like to record my thanks to my wife, Esther, for her patience and understandimg and my parents, brothers and sisters whose foresight and devotion made this thesis possible.

TABLE OF CONTENTS

LIST OF TABLES

LIST OF FIGURES

INTRODUCTION

The preparation of metals by reduction from their compounds has been known for centuries. It is equally well known that metals are oxidized by various solutions. However, the disproportionation reaction, whereby a metal is oxidized by a hot solution and the resulting solution is then reduced back to the metallic state on cooling, has only been known for about a hundred and fifty years.

This disproportionation, in the case of copper, was first observed by Berzelius (1), who noted that metallic copper was attacked by a hot solution containing cupric ion in such a way that copper powder precipitated from this solution when it was cooled. The reaction was suggested to occur via an intermediate oxidation state, which became more stable when the solution was heated, but rapidly lost its stability upon the solution being cooled again. The reaction would be written as

$$Cu^{2+} + Cu \underset{\text{cold}}{\overset{\text{hot}}{\rightleftharpoons}} 2\ Cu^{+} . \qquad (1)$$

In spite of the fact that this disproportionation reaction has been known for a long time, little attention has been paid to it. Furthermore, those few studies that have been done on the reaction have been restricted

mainly to investigations in a static system.

The disproportionation can be carried out in a dynamic system, and in this case the only result appears to be mass transfer of the metallic copper from a hot section of the apparatus to a cooler section.

The only known investigations in a dynamic system have been done by Ufford (2) and by de Ga (3). Ufford was primarily concerned with the factors which affected or governed the crystal habits of the metal powder produced in the apparatus; and the effect of these variables on the rate of production of crystals and their size were of only secondary concern to him. Also there was an uncontrollable variable inherent in his apparatus, and hence Ufford did not offer a definitive picture concerning the factors which affect the yield and size of the copper crystals produced by this technique.

The investigation of some factors affecting the yield and size of copper powder formed by reaction (1) in a dynamic system was also studied by de Ga (3). De Ga encountered difficulties in her investigation, due mainly to the apparatus design, and she was unable to completely resolve the factors affecting yield and particle size of copper powder produced by this method.

This investigation was undertaken to study reaction (1) in greater detail in a dynamic system. It was decided

that only yield, size and some of the physical characteristics of copper powder produced by this technique would be examined.

THE CHEMICAL REACTIONS

Berzelius (1) speculated about the existence of cuprous sulphate as an intermediate, when he investigated the attack of cupric sulphate solution on copper metal. This reaction was then attempted by other workers as a method for the preparation of cuprous sulphate without success (2).

Recoura (5) prepared cuprous sulphate as a gray powder by reacting cuprous oxide with dimethyl sulphate. The powder was found to be stable in dry air but reacted with water exothermically (2) as follows:

$$Cu_2SO_4 + nH_2O \longrightarrow CuSO_4(aq.) + Cu.$$

Recoura explained the instability of cuprous sulphate in solution as a result of this reaction (2).

Reaction (1) was reported to have proceeded faster when copper sheets were placed in cupric nitrate solutions, instead of cupric sulphate solutions (4). Forster and Seidel (4) reported an increased attack on the metal with increasing temperature. They also found that copper was precipitated on cooling.

Geneslay (6) reported that a solution of cupric sulphate in contact with copper plates results in the deposi-

tion of Cu_2O and $CuSO_4.2Cu(OH)_2$. The formation of oxide was observed first, and this reacted with O_2 and $CuSO_4$ to form the oxysalt. Reaction (1) was not observed.

From the results which he obtained, Ufford (2) concluded that the presence of sulphuric acid, capable of oxidizing action, in the circulating solution containing cupric sulphate over the copper wire, was necessary. This oxidation action of sulphuric acid prevented the coating of copper wire with oxidation products which caused the formation of copper crystals to cease. He also concluded that increasing the acid concentration had little effect on either yield or size of crystals.

Ufford also obtained yields of copper formed, when the circulating solutions of various other sulphates in sulphuric acid were circulated over copper wire. He presumed that these salts acted reversibly as oxidizing agents, attacking the metallic copper with cupric ion formation which in its turn attacked the copper wire to form crystals. From the investigation carried out to study the effect of flow rate on the size of copper powder formed by reaction (1), de Ga (3) concluded that the effect of flow rate was more complex.

Abel (7) made one of the earliest determinations of the equilibrium constant for the disproportionation of cuprous ion. He reported a value of 1.515×10^8 for the

ratio $\left[Cu^{2+}\right] / \left[Cu^{+}\right]^2$; which was found to be high when compared with later work. Luther (8) reported a value of 1.5×10^6 for the same ratio, but he disregarded the influence of complexes which were shown by Abel (7) to be present in significant amount in sulphate solution (9). Bodlander and Storbedk (10) obtained values ranging from 1.6×10^4 to 2.0×10^4.

Fenwick (9) determined the value of 1×10^6 for the equilibrium constant at 25°C. She also established the standard reduction potentials for the $Cu^+ \longrightarrow Cu$ and $Cu^{2+} \longrightarrow Cu^+$ reactions as 0.522 and 0.167 v respectively. Heinerth (11) redetermined the value of the equilibrium constant and reported a value of 1.19×10^6 in sulphate solution at 25°C. He also obtained a value of 0.525 v for $Cu^+ \longrightarrow Cu$ equilibrium. Latimer's values (12) are 0.521 v for $Cu^+ \longrightarrow Cu$ and 0.153 v for $Cu^{2+} \longrightarrow Cu^+$, so that for the total disproportionation reaction,

$$2\ Cu^+ \rightleftharpoons Cu + Cu^{2+}$$

$E^o = 0.355$ v, by the calculation from Fenwick's data, or 0.368 v, by calculation from Latimer's values.

Heinerth (11) also determined the value of the heat of reaction for the reaction (1) in sulphate solution at 25°C. The heat of reaction was 18,800 calories per mole.

A solution of sulphuric acid will attack metallic copper to form cupric sulphate, which in turn then reacts with the metal according to equation (1). Hence, a solution of sulphuric acid can eventually have the same effect on metallic copper as solutions of cupric sulphate (2).

GENERAL THEORY OF REDOX REACTIONS IN SOLUTION

The term "redox reaction" is used to describe a reaction in which electrons are transferred from one substance (the reducing agent) to another (the oxidizing agent), effecting a change in the oxidation number of both substances. The transfer of electron in aqueous solution is usually accompanied by atom or group transfer (13,14). For example, Fe(II) ion may act as a reducing agent by transferring a hydrogen atom from its hydration shell to the substrate: i.e.

$$Fe(H_2O)_6^{2+} + R^{\cdot} \longrightarrow Fe(H_2O)_5OH^{2+} + RH,$$

and in this case transfer of a positive atom or group is equivalent to the loss of electrons. The transfer of a negative atom or group is equivalent to a gain of electrons, as Iron (III) ion may act as an oxidizing agent by transferring a hydroxyl radical to a substrate: i.e.

$$Fe(H_2O)_6^{3+} + R^{\cdot} \longrightarrow Fe(H_2O)_5^{2+} + H^{+} + ROH.$$

There are two well established general mechanisms for electron transfer processes in solution; these mechanisms being referred to as "inner-sphere" and "outer-sphere" (13,15,16). In the inner-sphere mechanism, the metal ions are connected by a common bridging group, while

in the outer-sphere mechanism, the coordination shells of the two metal ions remain intact. Since transfer of the bridging group, from the oxidizing agent to the reducing agent, frequently occurs in inner-sphere reactions, the immediate products of inner-sphere reactions are usually different from those of outer-sphere reactions. Thus valuable information is provided concerning the reaction mechanism, such as in the following cases (17):

$$(H_2O)_5FeX^{2+} + Cr(H_2O)_6^{2+} \xrightarrow{\text{inner sphere}} Fe(H_2O)_6^{2+} + (H_2O)_5CrX^{2+}$$

$$(H_2O)_5FeX^{2+} + Cr(H_2O)_6^{2+} \xrightarrow{\text{outer sphere}} (H_2O)_5FeX^{+} + Cr(H_2O)_6^{3+}$$

In the outer-sphere mechanism, an electron appears to be transferred directly from one complex to the other, without interpenetration of the coordination shells of the metal ions. The elementary steps whereby electron transfer proceeds, in the case of outer-sphere mechanism, have been schematically illustrated by Sutin (17) as follows, where "||" denotes that no chemical bonds have been made or broken:

$$A + B \rightleftharpoons A \,||\, B$$

$$A \,||\, B \rightleftharpoons [A \,||\, B]^*$$

$$[A \,||\, B]^* \rightleftharpoons \bar{A} \,||\, \bar{\bar{B}}$$

$$\bar{A} \,||\, \bar{\bar{B}} \rightleftharpoons A^- + B^+.$$

The steps in the pathway by which inner-sphere reactions proceed could be schematically illustrated (17,18) as follows:

$$AX + B(H_2O) \rightleftharpoons AXB + H_2O$$

$$AXB \rightleftharpoons [AXB]^*$$

$$[AXB]^* \rightleftharpoons \bar{A}\bar{X}\bar{B}$$

$$\bar{A}\bar{X}\bar{B} + H_2O \rightleftharpoons A(H_2O)^- + BX^+$$

For both mechanisms the first step involves the formation of a precursor complex. For the outer-sphere mechanism, no chemical bonds are made or broken during this step, but for the inner-sphere mechanism, the precursor complex must be formed by substitution or addition, such that the two metal ions are bridged by a ligand common to both coordination spheres. Reorganization of the precursor complex to form an activated complex occurs in the second step, and electron transfer usually occurs during the latter stages of this reorganization. The third step involves the deactivation of the activated complex to form a successor complex. While the electron distribution in the precursor complex corresponds to that of the reactants, the electron distribution in the successor complex corresponds to that of the products of the reaction. Finally, the successor (binuclear) complex dissociates into mononuclear products, and the overall redox reaction has been consummated.

For the specific disproportionation reaction (1), i.e.

$$Cu^{2+} + Cu \rightleftharpoons 2Cu^{+}$$

a mechanism was proposed by deGa (3) and her proposal can be considered to be of the inner-sphere variety. Thus, she suggested that, in the reaction vessel, at approximately 100°C, the bisulphate ions act as bridging agents between metallic copper and cupric ions in solution. The bisulphate bridge facilitates the transfer of an electron from the copper wire to the cupric ion, resulting in the formation of two cuprous ions. Denoting the metallic copper as Cu^{*}, the reaction would be depicted as

$$Cu^{*} + HSO_4^{-} + Cu^{2+} \rightleftharpoons \left[Cu^{*}---HSO_4---Cu\right]^{+}.$$

Electron transfer from Cu^{*} to Cu^{2+} then occurs: the complex breaks up

$$\left[Cu^{*} --- HSO_4 --- Cu\right]^{+} \rightleftharpoons Cu^{*}HSO_4 + Cu^{+}$$

and this is immediately followed by

$$CuHSO_4 \rightleftharpoons Cu^{+} + HSO_4^{-}$$

Having brought the copper into solution, in the hot aqueous solution, deGa then faced the necessity of explaining the precipitation of metallic copper as the solution was cooled, and this she did by suggesting a series of reactions in the cooled portion of the apparatus. Thus,

she suggested, as the initial step

$$2CuHSO_4 \rightleftharpoons [Cu \text{ --- } HSO_4 \text{ --- } HSO_4 \text{ --- } Cu]$$

followed by electron exchange within the complex, to yield the species $CuHSO_4^-$ and $CuHSO_4^+$. The two bisulphate complexes then simultaneously ionize: i.e.

$$CuHSO_4^- \longrightarrow Cu^o + HSO_4^-$$

$$CuHSO_4^+ \longrightarrow Cu^{2+} + HSO_4^-.$$

It was proposed that atomic clusters of copper metal are probably formed by the mechanism

$$nCu^o \longrightarrow (Cu^o)_n.$$

Atomic clusters of copper metal formed with n = 5, grow rapidly and result in the formation of microscopic particles: i.e.

$$(Cu^o)_5 \xrightarrow[\text{growth}]{\text{fast}} \text{microscopic particle}$$

and the resultant particle would serve as a nucleus for further growth.

This latter portion of the mechanism was in accord with the theories of crystal growth from solution (20).

CRYSTAL GROWTH

Any crystallization operation can be considered to comprise three basic steps:

(a). Achievement of supersaturation, usually by supercooling;

(b). Formation of crystal nuclei;

and (c). Growth of the crystals.

All three processes may be occurring simultaneously in different regions of a crystallization unit. Supersaturation of a system may be achieved by cooling, evaporation, the addition of precipitant, or as a result of a chemical reaction between two homogeneous phases (19,20).

In the second step, minute solid bodies known as nuclei are formed, which grow into crystals. Nucleation may occur spontaneously or it may be induced artificially; these two cases are referred to as homogeneous and heterogeneous respectively, in systems that do not contain crystalline matter. Nucleation resulting from the presence of crystals in supersaturated systems is called secondary nucleation (20,23). Thus, nucleation nomenclature can be represented as follow:

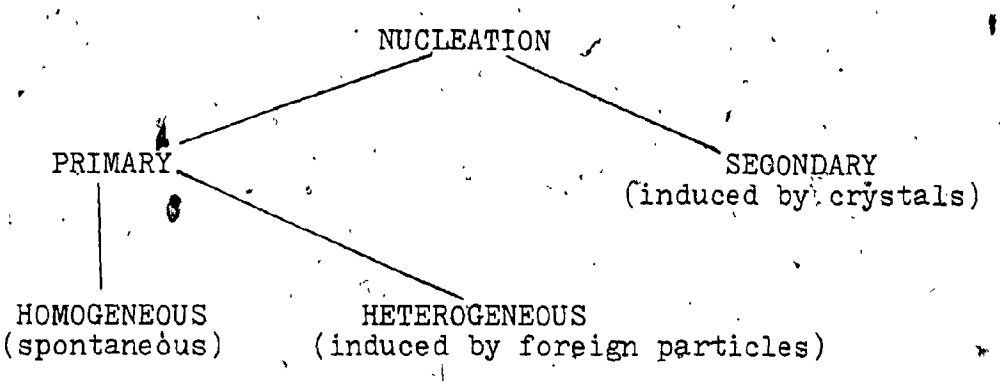

TYPES OF NUCLEATION

Prior to nucleation there is continous formation and dissolution of ionic or molecular clusters in equilibrium with all other clusters. But if the concentration of solute ions or molecules is large enough and a degree of supersaturation exists, then the clusters become sufficiently large to consolidate into small nuclei, whereupon the supposedly irreversible crystal growth ensues. The stable nucleus, which may exist before spontaneous crystallization, is referred to as the critical cluster. The formation of the critical cluster containing 'n' molecules could take place by bimolecular addition of the molecules. Further molecular additions to the critical cluster would result in nucleation followed by crystal growth (20, 21) as shown below:

$$A + A \rightleftharpoons A_2$$

$$A_2 + A \rightleftharpoons A_3$$

$$A_{n-1} + A \rightleftharpoons A_n \text{ (critical cluster)}$$

$$A_n + A \xrightarrow{\text{nucleation}} A_{n+1}$$

$$A_{n+1} + A \longrightarrow \text{crystal growth.}$$

A state of supersaturation is essential for crystallization to occur, and the degree of supersaturation can be expressed by means of the expression:

$$S = \frac{C}{C^*}$$

where C is the concentration of the solution and C^* is the equilibrium saturation concentration at the same temperature. For a saturated solution S = 1; S < 1 denotes undersaturation, while S > 1 indicates supersaturation. Other common expressions concerning supersaturation are the concentration driving force, ΔC, and the relative supersaturation, β , defined respectively by

$$\Delta C = C - C^*$$

and

$$\beta = \frac{\Delta C}{C^*} = S-1$$

and these mathematical relationships will be used later in this thesis.

The free energy changes associated with the process of homogeneous nucleation have been treated mathematically (20), and an outline of the reasoning is as follows. The over-all excess free energy, ΔG, between a small solid particle of solute (of radius = r) and the solute in solution is equal to the sum of the surface excess free energy, ΔG_s, and the volume excess free energy, ΔG_v; i.e.

$$\Delta G = \Delta G_s + \Delta G_v$$

where ΔG_s - the surface excess free energy - represents the excess free energy between the surface of the particle and the bulk of the particle, and ΔG_v - the volume excess free energy - represents the excess free energy between a very large particle (i.e. $r = \infty$) and the solute in solution. ΔG_s is a positive quantity, and its magnitude is proportional to r^2. In a supersaturated solution ΔG_v is a negative quantity, proportional to r^3.

Thus, the above equation for ΔG may be expanded as

$$\Delta G = 4 \pi r^2 \zeta + \frac{4}{3} \pi r^3 \Delta G'_v \qquad (2)$$

where ζ = surface free energy of the particle per unit area

and $\Delta G'_v$ = free energy change of the transformation per unit volume.

The maximum value of ΔG, designated as ΔG_{crit}, which corresponds to the critical nucleus, of radius r_c, may be obtained by differentiating equation (2) with respect to r, and setting $d\Delta G/dr = 0$. This yields

$$\frac{d\Delta G}{dr} = 8\pi r_c \zeta + 4\pi r_c^2 \Delta G_v' = 0 \qquad (3)$$

which reduces to $$r_c = -\frac{2\zeta}{\Delta G_v'} \qquad (4)$$

remembering that $\Delta G_v'$, since it is derived from ΔG_v, must also be a negative quantity. Hence, by substituting (4) into (2), there is obtained an equation which, after some mathematical rearrangement, reduces to the completely equivalent expressions

$$\Delta G_{crit} = \frac{16\pi \zeta^3}{3(\Delta G_v')^2} \qquad (5a)$$

and/or

$$\Delta G_{crit} = \frac{4\pi\zeta r_c^2}{3} \qquad (5b)$$

These expressions for ΔG_{crit}, the critical excess free energy between a solid particle of solute, of radius r_c, and the solute in solution, will be used later in this thesis.

The critical size r_c represents the minimum size of a stable nucleus. A particle smaller than r_c will dissolve

in order to achieve a reduction in its free energy, while a particle larger than r_c will continue to grow.

The rate of nucleation, B^o, (i.e. the number of nuclei formed per unit time per unit volume), can be expressed in the form of the Arrhenius reaction velocity equation (20,23) as follows:

$$B^o = A \exp(-\Delta G/kT) \qquad (6a)$$

where k = the Boltzmann constant

T = the absolute temperature

A = a pre-exponential factor

and ΔG = critical excess free energy of formation of nuclei i.e. ΔG_{crit}

This equation can be modified.

The Gibbs-Thomson equation (56) has suggested that the degree of supersaturation of a crystal can be related to other physical properties of the crystal by the relationship

$$\ln S = \frac{2\sigma \bar{V}}{kTr} \qquad (6b)$$

where $\bar{V}$ is the molar volume of the substance crystallizing, r is the radius of the crystal and the other symbols have been defined previously. Using equations (4) and (6b), we may obtain

$$\Delta G_v = \frac{kT \ln S_c}{\bar{V}} \qquad (6c)$$

where S_c represents the critical degree of supersaturation corresponding to the nucleation rate B^o. Now, equation (6c), upon substitution into equation (5a), yields

$$\Delta G_{crit} = \frac{16 \pi \zeta^3 \bar{V}^2}{3(kT \ln S_c)^2} \qquad (6d)$$

and (6d) in turn, upon substitution into equation (6a), produces an expression for the rate of nucleation as follows:

$$B^o = A \exp - \frac{16 \pi \zeta^3 \bar{V}^2}{3k^3 T^3 (\ln S_c)^2} \qquad (7)$$

Equation (7) predicts an explosive increase in the nucleation rate above a certain level of supersaturation. But the equation is of little practical value, insofar as industrial crystallization is concerned, because under industrial conditions, primary nucleation is predominantly heterogeneous, while the concepts used to develop equation (7) assumed that the primary nucleation was homogeneous.

Nyvlt (22), and Mullin and co-workers (24), have applied an empirical equation, of the form

$$B^o = K_n \Delta C_{max}^m \qquad (8)$$

to industrial crystallization studies, where

B^o = the nucleation rate

K_n = nucleation rate constant

m = the order of the nucleation process

and ΔC_{max} = the maximum allowable supersaturation

This equation can be modified considerably. The maximum allowable supersaturation, ΔC_{max}, may be expressed in terms of the maximum temperature difference during the supersaturation process. Thus, if θ represents the temperature, then the maximum temperature experienced during supercooling can be written as $\Delta\theta_{max}$, and hence ΔC_{max} can be written as

$$\Delta C_{max} = \left(\frac{dC^*}{d\theta}\right)\Delta\theta_{max} \qquad (9)$$

at least as a first approximation. Similarly the nucleation rate may be expressed (22) in terms of the rate at which supersaturation is created by cooling: i.e.

$$B^o = qb \qquad (10)$$

where b = rate of cooling of the solution, i.e. $-\frac{d\theta}{dt}$

and q = mass of solid deposited, per unit mass of free solvent present, when the solution is cooled by one degree Celsius.

The parameter represented by "q" is a function of the change of concentration, and of the crystallizing species.

In general,

$$q = \varepsilon \frac{dC^*}{d\theta} \qquad (11)$$

and $\varepsilon = 1$, if the salt crystallises in an anhydrous form.

Thus, using equations (9) - (11), equation (8) can be rewritten as

$$\varepsilon\, b\left(\frac{dC^*}{d\theta}\right) = K_n \left[\left(\frac{dC^*}{d\theta}\right) \Delta\theta_{max} \right]^m \qquad (12)$$

or, taking common logarithms,

$$\log b = (m-1) \log \left(\frac{dC^*}{d\theta}\right) - \log \varepsilon + \log K_n + m \log \Delta\theta_{max} \qquad (13)$$

which indicates that a plot of log b versus $\log \Delta\theta_{max}$ will be linear, and the slope of the line will give the order of the nucleation process, "m". Mullin et al (24) studied the nucleation and growth of ammonium sulphate crystals from aqueous solution, and equation (13) was applied to enable the order of the nucleation process, for both seeded and unseeded solutions, to be determined. The order of nucleation was found to be 2.6 and 6.4 for unseeded and seeded solutions, respectively, which suggested to the authors that the mechanisms of primary and secondary nucleation were different.

As in the case of nucleation, the classical theories of crystal growth have not led to relationships that are considered useful in studying crystallization on an industrial scale. For a given crystallizer design, an assessment of the rate of growth of crystals is most conveniently expressed by the relationship (23)

$$G = K_g(\Delta C)^g \qquad (14)$$

where G = rate of growth of crystals

ΔC = supersaturation

g = order of the growth process

K_g = growth rate constant

An investigation aimed at studying the size distribution of crystals in a continuous crystallizer was carried out by McCabe (28). The analysis of the problem of crystal size distribution led to the development of what is now known as the "ΔL" law, where L refers to the characteristic linear dimension of a crystal, and hence ΔL is a measure of the growth of the crystal within the crystallizer.

In the development of the law, McCabe made the following assumptions:

(a). A crystal that grows under constant external

conditions remains very nearly geometrically similar to its original shape;

(b). The crystals grow invariantly, (i.e. the growth rate is independent of crystal size);

(c). Supersaturation is constant throughout the crystallizer;

(d). No nucleation occurs;

(e). No size classification occurs in the crystallizer;

(f). The relative velocity between crystals and liquor remains constant.

With these assumptions, McCabe was able to derive an expression for the growth of product crystals; and an outline of his reasoning follows:

For a crystal of length L, the mass could be calculated from the expression

$$\text{mass} = \alpha \rho L^3$$

where ρ = density of the solid material

α = a volume shape factor.

For a number of crystals, dN, the mass would be given by

$$dW = \alpha \rho L^3 dN$$

which leads, after rearrangement, to

$$dN = \frac{dW}{\alpha \rho L^3}$$

Assuming no nucleation, the number of seed crystals, dN_s, of length L_s, must be equal to the number of product crystals, dN_p, of length L_p; i.e.

$$\frac{dW_s}{\alpha \rho L_s^3} = \frac{dW_p}{\alpha \rho L_p^3} = \frac{dW_p}{\alpha \rho (L_s + \Delta L)^3}$$

The extension of this formula is obvious, since it is readily apparent that the expression

$$L_p = L_s + \Delta L$$

must hold, since ΔL is the growth increment within the crystallizer.

The expression can be rearranged,

$$dW_p = \frac{(L_s + \Delta L)^3}{L_s^3} \, dW_s$$

and integrated

$$\int_0^{W_p} dW_p = \int_0^{W} \left[1 + \frac{\Delta L}{L_s}\right]^3 dW_s$$

to yield, finally

$$W_p = \int_0^{W_s} \left[1 + \frac{\Delta L}{L_s}\right]^3 dW_s \qquad (15)$$

where W_p is the mass of product crystals obtained from an initial mass of seed crystals, W_s.

The ideal conditions assumed by McCabe are unlikely to be attained in a real crystallizer. Temperature and supersaturation gradients are unavoidable; invariant growth is comparatively rare because different crystal faces usually grow at different rates; and the crystal growth rate depends on solution velocity, in which case large crystals may grow faster than small (24, 27). However, a feature of the derivation is that the dependence of growth rate on supersaturation need not be known. Despite its limitation, McCabe's derivation provided a simplified approach to the development of the crystal size distribution of a product obtained from a crystallizer.

In the analysis of any system involving crystallization, an important consideration is the study of the factors influencing the size distribution of the crystalline product produced. It is the relationship between the competing kinetic rates of nucleation and crystal growth that determines the size distribution of the product.

For the complete description of the crystal size distribution in a continously operated crystallizer it is necessary to quantify the nucleation and growth kinetics, and to apply the conservation laws of mass, energy and numbers of crystals. The recognition of this latter requirement, the concept of the population density, has been a major contribution to the subject of crystallizer analysis (25, 26, 27) and design.

The population density, symbolized by n, is defined by the expression

$$n = \frac{dN}{dl} = \lim_{\Delta L \to o} \frac{\Delta N}{\Delta L} \qquad (16)$$

where n = population density, i.e. number of particles per unit length per unit slurry volume

ΔN = the number of particles in the size range L_1 to L_2

$\Delta L = L_2 - L_1$

However, because of the inevitable distribution of particle sizes within a sample, the value of n will be determined by the crystal size at which the interval ΔL is taken. Consequently, n is a function of L and has the dimensions of number per unit size per unit volume of the system.

The total number of crystals per unit volume, in the size range L_1 to L_2, is given by

$$\Delta N = \int_{L_1}^{L_2} n dL \qquad (17)$$

Application of the population balance has been demonstrated, with reference to a continuous mixed-suspension mixed-product-removal crystallizer, by Larson and Randolph (25). These authors assumed that no particles entered with the feed and that there was no attrition of the particles, i.e. the crystallization process was assumed to be taking place under steady state conditions. Assuming this, a population balance (input = output) in a system of volume, V, for an arbitrary size range L_1 to L_2, and for an arbitrary time interval Δt, is

$$n_1 V G_1 \Delta t = n_2 V G_2 \Delta t + Q\bar{n} \Delta L \Delta t \qquad (18)$$

where Q = volumetric feed and discharge rate

G = linear growth rate (dL/dt)

n = population density

$\bar{n}$ = average population density

The left-hand side of equation (18) represents the number of crystals growing into the range being studied over the

time interval. The right-hand terms represent the number of crystals (a) growing out of the range being studied over the time interval, and (b) still within the size range when removed from the crystallizer.

Dropping the time interval, Δt, from equation (18), it rearranges to:

$$\frac{V\,(G_2 n_2 - G_1 n_1)}{\Delta L} + Q\,\bar{n} = 0 \qquad (19)$$

and in the limit, as $\Delta L \to 0$, and $G_2 n_2 - G_1 n_1 = \Delta\,(Gn)$, we may write

$$V \frac{d(nG)}{dL} + Qn = 0 \qquad (20)$$

Letting $V/Q = T$, the mean residence time within the crystallizer, and assuming that McCabe's ΔL law holds, that is, growth is independent of size (i.e. $dG/dL = 0$), then equation (20) may be simplified to:

$$\frac{dn}{dL} + \frac{n}{GT} = 0 \qquad (21).$$

If n^o is the population density of the zero size particles or nuclei population density, then integration of equation (21) gives:

$$\int_{n^o}^{n} \frac{dn}{n} = \int_{0}^{L} -\left(\frac{dL}{GT}\right) \qquad (22)$$

and, integrating,

$$n = n^o \exp(-L/GT) \qquad (23)$$

Equation (23) is the fundamental relationship between L and n characterizing the crystal size distribution. A plot of ln n versus L should give a straight line with an intercept at L = 0 equal to ln n^o and a slope of -1/GT. Hence, if the residence time, T, is known, the crystal growth rate G, can be calculated.

The parameter n^o and the growth rate G can be related to the kinetics of nucleation. The nucleation rate may be expressed as

$$B^o = \left|\frac{dN}{dt}\right|_{L=o} = \frac{dN^o}{dt} \qquad (24)$$

where the dimensions of B^o are number/time-volume; and ΔN, as defined previously on page 27, represents the total number of particles in the size range L_1 to L_2.

Also, the growth rate G may be expressed in the differential form as

$$G = \frac{dL}{dt} \qquad (25)$$

There is also available the relationship from calculus

$$\frac{dN^o}{dt} = \left(\frac{dN}{dt}\right)_{L=o} = \left(\frac{dN}{dL}\right)_{L=o}\left(\frac{dL}{dt}\right) \qquad (26)$$

and from the definition of n^o, the nuclei population density, we may write

$$\left(\frac{dN}{dL}\right)_{L=o} = n^o \qquad (27)$$

Hence, by combining equations (24 - 27 inclusive), the nucleation rate, B^o, can be expressed in terms of the nuclei population density, n^o, and the growth rate, G, as

$$B^o = n^o G \qquad (28)$$

From the crystal size distribution the population density at the mean size of each of the various size fractions can be calculated by the equation

$$n = \frac{W}{\alpha \varrho L^3 \Delta L} \qquad (29)$$

where W = mass fraction of product within two size ranges

α = the volume shape factor

ϱ = density of material of which particles are composed

ΔL = as before, the difference between the two size ranges under consideration

L = average particle size in the fraction

If the size distribution of the product crystals should fit equation (23), then the nucleation rate and the growth rate of crystals can be obtained.

Robinson and Roberts (29) proposed an experimental relationship between nucleation rate, B^o, and supersaturation, S, of the form:

$$B^o = K_1 S^i \qquad (30)$$

where K_1 is a coefficient that is probably temperature dependent, and i is a power that might also be a function of nucleation temperature.

McCabe (28) observed that each crystal in suspension grows at the same rate, regardless of its size, if subjected to the same conditions. The expression for the growth rate of crystals can be written as follows:

$$G = \frac{dL}{dt} = K_g S \qquad (31)$$

where K_g is a proportionality constant for the crystal growth rate.

Since equation (31) indicates a linear relationship

between the growth rate of particles, and the supersaturation of the solution, equation (30) was modified, by Lawson and Gench (30), to yield the relationship

$$B^o = K_2 G^i \qquad (32)$$

where G, as before, represents the growth rate of crystals and B^o is the nucleation rate.

A combination of equations (28) and (32), at the steady state, yielded, for the nuclei population density,

$$n^o = K_2 G^{i-1} \qquad (33)$$

and this equation allows determination of the kinetic order of nucleation, in addition to yielding the basic relationship that determines the crystal size distribution. The method of solution of equation (33) involves the use of a set of values of n^o and G which are obtained at different residence times for a constant suspension density. The exponent (i-1) can then be calculated from a plot of log n^o versus log G.

Lawson and Gench (30) investigated the effect of the temperature of crystallization on the size distribution of crystals of potassium nitrate, and of potassium chloride, as produced in a mixed-suspension mixed-product-remover

(MSMPR) crystallizer. These authors found that equations (30) and (32) took the following forms, when the nucleation kinetics of potassium nitrate were studied:

Temperature (°C)	B^o from eqn.(32)	B^o from eqn.(30)
11.0	$5.63 \times 10^8 G^{1.3}$	$K_1(T)S^{1.3}$
20.8	$4.94 \times 10^8 G^{1.3}$	$K_1(T)S^{1.3}$
31.0	$3.32 \times 10^8 G^{1.3}$	$K_1(T)S^{1.3}$
40.0	$2.30 \times 10^8 G^{1.3}$	$K_1(T)S^{1.3}$

Lawson and Gench observed, during their work with potassium nitrate, that the crystal size increased with an increase in temperature. Their studies also showed that the rate of nucleation decreased as the temperature increased, and this is apparent in the several expressions calculated for B^o, at different temperatures, as derived from equation (32).

Lawson and Gench attributed this increase in the size of crystals to the increased growth rate, which would have caused a considerable decrease in the extent of supersaturation which the system could support. In addition, the lowering of the supersaturation would have foreshadowed any increase in the nucleation rate constant.

Lawson and Gench (30) also studied the growth and

nucleation kinetics of potassium chloride, with the following results:

Temperature (°C)	B^o from eqn.(32)	B^o from eqn.(30)
12.0	$9.08 \times 10^9 G^{2.55}$	$K_1(T)S^{2.55}$
20.8	$1.12 \times 10^{10} G^{2.55}$	$K_1(T)S^{2.55}$
30.0	$1.33 \times 10^{10} G^{2.55}$	$K_1(T)S^{2.55}$

In this work, it was observed that the growth rates decreased with increasing temperature, and also, as the temperature increased, the size distribution decreased. It was also noted, and this is apparent in the table, that the nucleation rate increased as the temperature increased.

These observations for potassium chloride are the opposite of those observed for potassium nitrate.

For potassium chloride the nucleation rate constant was found to be more sensitive to the temperature change than the growth rate constant, thus causing a decrease in size with increased temperature. The increased nucleation rate produced more crystals per unit mass of suspension, causing more surface area to be formed (per unit mass of suspension). This increased area reduced the level of supersaturation which could be supported and consequently

reduced the growth rate.

If nucleation and growth are viewed as parallel kinetic reactions, the former determining the rate of particle formation and the latter the rate of deposition of solute onto existing particles, then it follows that the final crystal size distribution obtained can be controlled by varying the relative rate of nucleation as compared to growth (31). Thus, if it is desirable that the mean crystal size be increased during a crystallization process, then nucleation must be suppressed relative to growth, and this will result in larger crystals. On the other hand, if a smaller mean crystal size is desired, then growth must be suppressed relative to nucleation.

GENERAL THEORY OF PARTICLE-SIZE ANALYSIS

The size of a particle is that dimension which best describes its state of sub-division. For a spherical particle, the diameter is the dimension that can be used as its size. For a cuboid the length along one edge is characteristic, and for other regular shapes there are other equally appropriate dimensions. Most powders are irregularly shaped, and consequently for irregular particles the assigned size usually depends upon the physical principles employed (32, 33) in the determination procedure. The true diameter convention is used for microscopic count, the average diameter for sedimentation, and for sieving the smallest cross-section through which the particle will pass (33). Provided the particles of a sample are randomly oriented and a large-enough number of them are present, then some average linear measurement of the projection of many particles in a fixed direction is taken to be statistically adequate for describing the size distribution.

The most common methods of size analysis are listed in Table 1, which summarises the approximate size range of particles that can most suitably be measured by each technique. The size-discriminating property on which each method is based is given by Lapple (34). He also included

Table 1

Common Methods of Particle-Size Analysis

Method	Size Range (Diameter) in microns	References
SIEVING	> 50	32,33,35, 37,39.
Dry		32,33,35, 36
Wet		35,36
GRAVITATION SEDIMENTATION	2-50 (with some variation between methods)	32,33,35, 37,39
Sedimentation balance		32,37,38
Manometer		32,35
Divers		32,33,35
Andreasen pipette		32,33,35
Hydrometer		32,33,35
Photo-electric		32
CENTRIFUGAL SEDIMENTATION	0.005-15	32,36,39, 40
COULTER COUNTER	0.5 - 400	35,40
MICROSCOPIC COUNTING	0.5 - 500	32,35
Optical microscope		32,35,37, 38
AEROSOL ANALYSIS		32
Gravitational settling	> 0.3	32

Table 1 (continued)

Method	Size Range (Diameter) in microns	References
Filtration	> 0.1	32
Cascade impactor	0.2 - 100	32,37,41
Centrifugal impactor	> 1	32,37,42
Thermal Precipitation	< 10	32
Light scattering	> 0.2	32
Elutriation	5 - 200	32,33,37
Micromerograph	1 - 250	32

a list of commercially available equipment for almost every technique. The theories of sieving and sedimentation will be discussed, since these were the only methods employed in this research work. References to the best discussions found in the literature on all the methods listed are also included in Table 1.

Sieving is probably the simplest, fastest and most widely used method of determining particle-size distributions. The method involves agitating the sample through a stack of several sieves arranged in order of decreasing aperture size. The sample is classified into a series of fractions on the individual sieves. Agitation may be manual or mechanical. There are many standardized sieve series, the two used most commonly on this continent being the United States and Tyler Standard Sieve Series. The dimensions of the openings of the sieves in both series are listed by Hausner (43).

Sieve sizes, the minimum square through which the particles can pass, are usually designated as "mesh" sizes. The larger the number of mesh size, the smaller the size of the openings. For practical purposes the screen with the smallest sieve openings is the 325-mesh screen, with a sieve opening of 44 microns. Thus, in practice, this method discriminates between particle which are larger than 44 μ and "fines", which are smaller. With recent advances in tech-

nology, the range of sieving tests has been extended as low as 10 μ (35).

Sieving permits the determination of size ranges rather than of actual particle size. The size range is designated as "-(size of mesh through which powder passes)", and "+(mesh size on which powder is retained)". Thus, a fraction that passes through a 325-mesh screen, but is retained on a 400-mesh screen, would be classified as "-325, +400", the implication being that the particles of this fraction range in size between 44 and 37 μ. The average particle diameter of this fraction would be then 40.5 μ.

A detailed discussion of sieving errors has been outlined by Herdon (32), and consequently only the most important ones will be outlined here. Particularly, in sieving, measurement by geometric property can be considerably influenced by particle shape, especially by extreme shapes. This technique is likely to measure the large dimension of flat particles and the small dimension of needles or rod-like particles (34). In the former case, the material retained on a sieve will have a smaller volume than that predicted on the basis of an ideal sphere, and in the latter case, the volume of the retained fraction will be larger than predicted.

Roberts and Beddow (44) studied some of the effects of particle shape and size upon blinding during sieving.

It was shown that the level of "hard blinding" was markedly dependent upon mesh aperture below about 100 μ. The "hard blinding" term describes the material which is jammed in the mesh interstices; it reduces sieving efficiency and is very difficult to remove. It was suggested that for a given size, irregular particles did not hard blind as much as do spherical particles because they were more able to rotate and dislodge from the aperture.

The greatest disadvantage of sieving is that it has no end point. Different times of sieving will give different results. Different sieve load will also give different results. The use of the smaller sieve apertures will magnify the effect of overloading and the discrepancies between results for different loadings (32, 33).

When there is a preponderance of particles smaller than 40 μ, severe agglomeration may occur on dry shaking. Breakdown of these agglomerates is usually secured after shaking the sieve for a sufficient time. However, prolonged agitation of the powder often leads to attrition by a grinding action, resulting in a gradual decrease in particle size. The technique of wet sieving is usually more effective than dry sieving for such samples. This method is similar to dry sieving with the exception that the passage of material through the sieves is obtained by a stream of liquid (36). Wet sieving has been success-

fully used for sizing diameters in the range of 6-150 μ (36). One disadvantage in wet sieving is the problem of determining the weight of dry material retained on the sieve; (i.e., additional time is required to dry a sieve cut prior to weighing) (35). However, for sub-sieve size powders (when most or all of a sample is -325 mesh), this method, if done manually, is often time consuming and tedious, and consequently sedimentation is usually the preferred method for powders having particles in the size range 2-50 μ.

Sedimentation methods utilize the dependence of the falling velocities of particles on their size (35). This phenomenon is essentially that of the resistance to motion encountered by a body falling in a fluid.

When a spherical body is left undisturbed in a liquid in a gravitational field, it will first sink with increasing velocity, but when the resistance the fluid offers to the movement of sphere ($= 6 \pi rnv$) equals the total force acting downward, the particle will maintain a constant velocity. This force is the difference between the force of gravity acting downward, $4/3\ \pi r^3 \rho_1 g$, and the buoyant force, $4/3\ \pi r^3 \rho_2 g$, given by Archimedes' principle, and acting upward (45). At equilibrium, the situation is described by

$$6\pi r \eta v = \frac{4}{3} \pi r^3 (\rho_1 - \rho_2)g,$$

where ρ_1 = density of the particle; ρ_2 = density of the medium; g = acceleration due to gravity; r = radius of the particle; v = velocity of the particle; and η = viscosity of the medium. Hence,

$$v = \frac{2}{9} \frac{(\rho_1 - \rho_2)gr^2}{\eta} \qquad (34)$$

and

$$r = \left[\frac{9}{2} \frac{v \eta}{(\rho_1 - \rho_2)g} \right]^{\frac{1}{2}} \qquad (35)$$

If all the quantities are in cgs units, r will be obtained from equation (35) given above, in centimeters. If the particle has fallen from the surface of liquid, h, in time t, equation (34) can be coupled with the relationship v = h/t, and rearranged to give the particle diameter, in microns, as

$$d = 10^4 \left[\frac{18 \eta h}{(\rho_1 - \rho_2)gt} \right]^{\frac{1}{2}} \qquad (36)$$

Although Stokes' law assumes sphericity of particles, it has been shown experimentally that the law does hold reasonably well for most systems encountered in practice (32).

Stokes' law also assumes streamline flow, so that in order to determine whether the law is valid for a parti-

cular system, the nature of the fluid flow around the settling particles must be assessed. This is done by means of the Reynolds number, R_e, a dimensionless ratio defined as $R_e = vd/\nu$, where ν is the kinematic viscosity ($= \eta/\rho_2$) of the fluid in cgs units, and the other symbols have the same meaning as previously. It is considered that, with the value of R_e up to 0.2, streamline flow occurs, and Stokes' law is strictly applicable. However, Herdan (32) is of the opinion that Stokes' law can be used, without introducing significant error, up to $R_e = 1$, and Amstein and Scott (46) reported that even up to $R_e \equiv 4.0$, the deviation is not very great.

The "neighbour" effect of many particles reduces the drag on an individual particle. Thus, a cloud of particles settles faster than individual particles of the same size as those in the cloud, provided the cloud is small, compared with the container dimensions (32). On the other hand, if the cloud spreads horizontally across the container, its settling rate will be less than that of the individual particles (32). To prevent this happening the sedimentation sample must be small, usually no more than about 0.2 - 0.5 % of the total volume of liquid (35), furthermore, dispersion of the particulate matter is imperative. Often, dispersing agents have to be employed to lower the surface tension of the liquid and, therefore,

enhance the wetability of the particle surface. Amstein and Scott (46) reported that, provided dispersion is complete, a 16-fold change in the concentration of solids has no detectable influence on the results up to a concentration of 2% by volume.

The diameters (or radii) of irregular particles obtained by calculation from Stokes' law are commonly designated as "equivalent" or "equivalent spherical" diameters (radii). This diameter is defined as having the same numerical value as the diameter of a perfect sphere of the same material which sinks through the fluid at the same average rate as the particle in question. Hence, if not specified, it is always understood that the diameter obtained by sedimentation analysis is the "equivalent spherical diameter".

The Andreasen pipette method of sedimentation requires the preparation of a well-dispersed suspension of test material, and the withdrawl of small samples of suspension at known depth and fixed time-intervals (32, 46). The first sample is pipetted as soon as possible after initial dispersion of the material in the liquid and other samples are withdrawn at suitable time intervals. The concentration of particulate matter in the samples is determined either analytically or by evaporating an aliquot to dryness and weighing the resulting solid.

Each sample drawn has a smaller particle size than that corresponding to the falling velocity given by Stokes'law, because all particles of a larger size will have fallen below the level of the pipette tip. After evaporation and drying, the weight of the first sample gives the initial concentration of the powder, while subsequent samples give the cumulative weight undersize corresponding to the particular Stokes' diameter in question (32, 46).

THE PRESENTATION OF PARTICLE-SIZE DISTRIBUTIONS

The size distribution of a sample containing particles of different sizes may be represented by the fraction of particles in a specific size range (the frequency distribution), or above or below a certain size (the cumulative distribution). The frequency of occurrence of particles within a particular size range may be specified using one of several bases. It may be determined on a number basis, a weight basis, a length basis or on the basis of the total surface exposed (34,35,47).

It is theoretically possible to convert from one basis to another (34,47) although the measurement basis may influence the precision of the conversion. For example a few large particles may be overlooked in a number distribution based on count. The large particles may negligibly affect the number distribution, but they may markedly influence a mass distribution. Consequently, if a mass distribution is calculated from the count distribution, the precision will be poor because of the overlooked large particles (34). Furthermore, if shape varies with size, conversion between bases requires a knowledge of the shape factor and how it varies with size and this is not always easy to determine (34). Heywood (47) lists shape coefficients for various kind of powders.

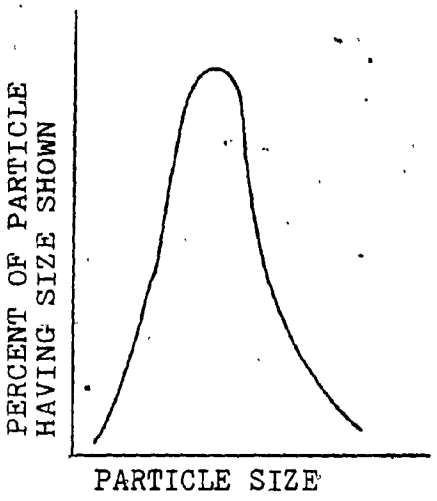

Figure 1. Schematic Frequency Distribution.

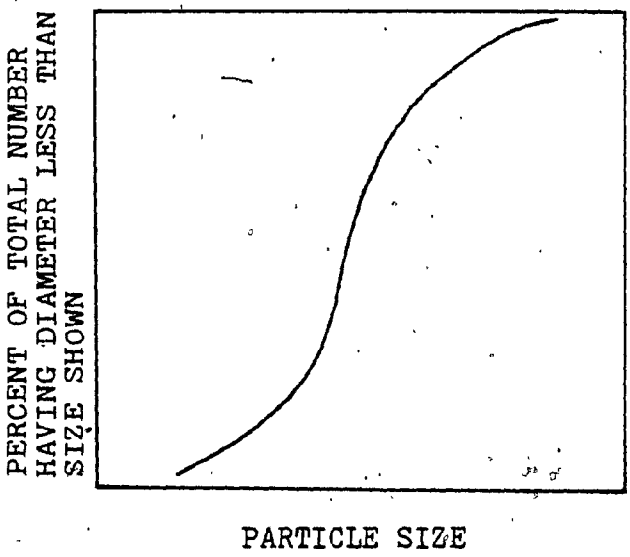

Figure 2. Schematic Cumulative Distribution.

A frequency size distribution is schematically illustrated in Figure 1. The curve resembles a probability curve, but is slightly skewed, rather than symmetrical, as is the normal probability curve. Skewed distributions are frequently encountered in particle sizing. Figure 2 schematically illustrates a cumulative distribution curve. This curve is the integral of the frequency curve. For the particle size, the equation for the normal distribution has the form (32,48),

$$y = \frac{1}{\sigma\sqrt{2\pi}} \exp\left[-\frac{1}{2}\left(\frac{x - \bar{x}}{\sigma}\right)^2\right],$$

where y is the probability density, x the diameter of the particle, $\bar{x}$ the arithmetic mean diameter, and σ the standard deviation. The number of particles, n_i, with diameter between x_1 and x_2, or the number distribution, is (32):

$$n_i = \frac{\Sigma n_i}{\sqrt{2\pi}} \int_{x_1}^{x_2} \exp\left[-\frac{1}{2}\left(\frac{x - \bar{x}}{\sigma}\right)^2\right] dx.$$

The arithmetic mean and standard deviation are, of course, defined (32) as:

$$\left[\bar{x} = \frac{\Sigma n_i x_i}{\Sigma n_i} \quad \text{and} \quad \sigma = \left[\Sigma \frac{\left[n_i (x_i - \bar{x})^2 \right]}{\Sigma n_i} \right]^{\frac{1}{2}} \right],$$

respectively. Normal distributions of particle size have been observed for some substances produced by chemical processes such as condensation and precipitation (32), in which the particles tend to a uniform size.

Many powder systems, especially those obtained by comminution, are not satisfactorily defined by the normal distribution law, because the distributions of these systems are slightly skewed. It is often found, however, that plotting the frequencies against the logarithm of the size results in a normal curve, symmetrical about the geometric mean particle size. Such systems are said to have a log-normal distribution.

The log-normal distribution is given (32) by

$$y = \frac{1}{\log \sigma_g \sqrt{2\pi}} \exp \left[-\frac{1}{2} \left(\frac{\log x - \log x_g}{\log \sigma_g} \right)^2 \right],$$

where x_g is the geometric mean diameter, defined as,

$$\log x_g = \frac{\Sigma n_i \log x_i}{\Sigma n_i}$$

and σ_g is the geometric standard deviation. This is the standard deviation of the distribution of ratios around the geometric mean and its logarithm is the standard deviation of log x (32). It is defined as:

$$\log \sigma_g = \left[\frac{\Sigma \left[n_i (\log x_i - \log x_g)^2 \right]}{\Sigma n_i} \right]^{\frac{1}{2}}$$

The number of particles between x_1 and x_2 is then (32):

$$n_i = \frac{\Sigma n_i}{\log \sigma_g \sqrt{2\pi}} \int_{x_1/\log \sigma_g}^{x_2/\log \sigma_g} \exp\left[-\frac{1}{2} \left(\frac{\log x - \log x_g}{\log \sigma_g} \right)^2 \right] d \log x.$$

All the foregoing relationships are based on frequency measurements by count; similar relationships have been derived for the weight distributions (32).

Because many experimental techniques directly yield data for cumulative distributions, cumulative curves are used more extensively than frequency plots, and furthermore, more information can be derived from the cumulative distribution (48). These curves are produced by plotting

the percentage particles having particle size greater than (oversize) or less than (undersize) a given size against particle size.

If the cumulative curve can be transformed into a straight line, then the interpretation of cumulative data can most efficiently be done. While algebraic transforms exist to linearize normal cumulative distributions, it is common practice to use probability graph paper, which is available commercially. The cumulative percentage scale is so set up in this graph paper that plotting the cumulative frequency vs. the linear size yields a straight line (48). Similarly, the log normal cumulative distribution is linearized on log probability paper by a plot of cumulative percentage vs. size on a logarithmic scale (or else on probability paper, against the logarithm of the size). The plots obtained in this manner are called "probability" plots. Once a straight line has been obtained, the median and standard deviation are readily determined.

In some cases, the particle size distribution plot on log probability paper may superficially not appear to be log-normally distributed, as Figure 3 illustrates (49). Examination of the probability scale reveals that a 1% unit around 95% probability is about four times as great as that around 50% probability, and the same holds true for the corresponding units at the low probabilities (35).

The units are therefore increasingly exaggerated in both directions from the 50% point, and thus any deviations from a straight line are exaggerated at both ends of the distribution.

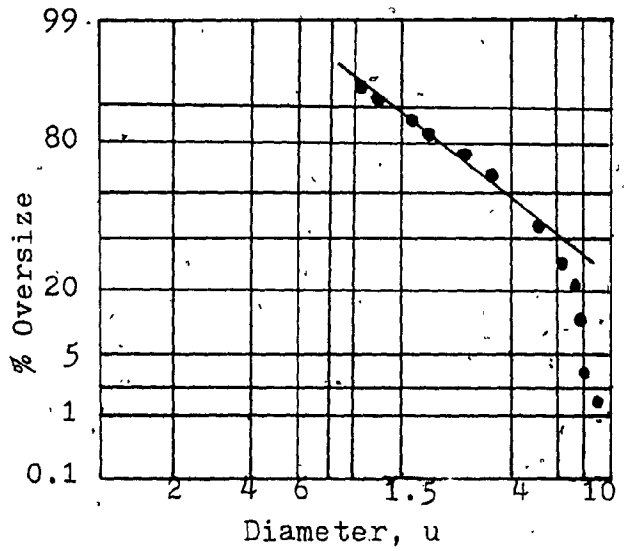

Figure 3. Log Probability plot of cumulative weight fraction data (49), demonstrating irregular curvature.

If insufficient data are taken at either end, the deviation would be further exaggerated, and these artificial exaggerations might make the distribution appear curved at the end in question (35,49). A straight line is still considered the best representation for these data points, as these deviations are of little practical significance (34,35,49).

The median diameter, corresponding to the 50% cumulative size, and the standard deviation, are readily obtained from the probability plot. The median is simply the value of the diameter at the 50% point (for normal distributions, the 50% point represents both the median and mean). The difference in particle size between diameters at 50% and the size corresponding to 84.13% or 15.87% is the standard deviation. In a log-normal probability plot, the log of the median is obtained at the 50% point. The geometric standard deviation is the ratio of the size at 84.13% and 50%, or 50% and 15.87%, i.e., log σ_g is the difference between the logarithms of the sizes at 84.13% and 50%, or 50% and 15.87%. Since the geometric standard deviation is a measure of the degree of uniformity, a completely uniform material would have a geometric standard deviation of 1, whereas a material containing varying particle sizes would have larger geometric standard deviation (34). Most particulate materials have geometric standard deviations in the range of 2 to 3.

SCOPE AND PURPOSE OF THE INVESTIGATION

Ufford (2) was the first to study the disproportionation reaction,

$$Cu + Cu^{2+} \underset{\text{cold}}{\overset{\text{hot}}{\rightleftharpoons}} 2\,Cu^{+}, \qquad (1)$$

in a dynamic system, in which the hot solution was continuously removed from contact with the massive metal in order that the latter would have no effect on crystals formed by the reverse reaction. The driving force for the circulation of liquid was the difference in densities between hot and cold solution. The main purpose of Ufford's was to study the variation in crystal habit with changing variables. The effects of these variables on the rate of production of crystals and their size and shape distributions were only of secondary concern to him. He found the crystals produced by this method to be very pure, regardless of the purity of the starting material.

The reaction (1) was also studied in a dynamic system by deGa (3). The yield and size of copper crystals produced by redox reaction in continuously circulating aqueous cupric sulphate-sulphuric acid solutions were studied as functions of solution flow rate, duration of run and

acid concentration.

This investigation was undertaken to study reaction (1) in a greater detail in a dynamic system and a semi-pilot plant approach to investigate the reaction was undertaken in order to determine the feasibility of industrial application of this method for the preparation of metals of high purity from ores and impure mixtures.

It was decided that a new apparatus was to be designed and a semi-pilot plant approach to the problem was to be attempted. The amount of copper powder produced would therefore be large enough to investigate physical properties such as apparent density and tensile strength. The usefulness of copper powder produced by this technique in metallurgical industry could then be investigated.

The solutions chosen to be circulated were mixtures of cupric sulphate in sulphuric acid. The variables chosen to be investigated were, amount of copper wire, flow rate and duration of experiment. During the investigation, it was felt that the effect of the crystallizing temperature on the yield and size of the powder had to be investigated. The modified Andreasen pipette method was used for the particle-size analysis, as the powders produced were mainly of sub-sieve size.

During the investigation it was realized that the effect of crystallizing temperature on the particle size

could be explained on the basis of correlation of all trends observed, and by nucleation and growth kinetics. It was also decided that the effect of the apparent density and particle size on the tensile strength of the sintered specimens from the copper powder produced by this method would be studied. In order to establish the importance of copper powder produced by this method, its tensile properties would be compared with that of commercially available copper powder.

MATERIAL

Cupric Sulphate. Cupric sulphate pentahydrate (crystal), $CuSO_4 \cdot 5H_2O$, described as meeting A.C.S. specification, was purchased from Fisher Scientific Company Ltd.

Copper Wire. Copper wire was obtained from two sources: (a). In the early part of the work, wire was purchased from Pascal Hardware Company Ltd., in rolls sold commercially as "copper handy wire".

(b). In the latter part of the work, a convenient source of wire was discovered to be used electrical cabling, with a #14 gauge of wire. The plastic sheath was removed from the wire, and the base wire, after inspection, was used directly.

Regardless of its origin, all wire used in this work was cleaned thoroughly, as described later in this thesis. In the several series of experiments conducted no discernible differences were observed that could be attributed to the origin of the wire.

Copper Powder Used for Particle-Size Analysis. A 200-g sample of copper powder, of -325 mesh, was used as a standard in a series of experiments designed to test the reproducibility of the Andreasen pipette method.

Electrolytic copper powder, purchased from Fisher Scientific (their #791317) was ground, and sieved, with

the -325 mesh sample being retained. The sieve used was manufactured by Spex Industries Ltd, Chicago, and had a plastic mesh that could be replaced if necessary. It was of the type customarily used in routine X-ray analysis experiments. A 100-g sample of this -325 mesh powder was added to an equal amount of copper powder produced by the cyclone process, and obtained from The Canada Metal Company Ltd, Oakville, Ontario. As reported by the Company, the analysis of this latter powder was

+ 325 mesh	2.3%
- 325 mesh	97.7%.

This 200-g sample of powder was thoroughly mixed by a preliminary tumbling. In addition, before withdrawing a sample for an experiment, the sample was tumbled for two hours.

Water. Demineralized water, obtained by passing tap water through a Barnstead column, was subsequently distilled in a Corning Ag-1b distilling apparatus, and was used in the preparation of all solutions.

Dispersing Agent. Calgon, used as a dispersing agent, was purchased retail. A 0.05% solution (weight/volume) of Calgon in water was used as the dispersing medium in the sedimentation experiments.

Copper Powder Used for the Determination of Apparent Density. Copper powder produced by the cyclone process at The Canadian Metal Company Ltd (Oakville, Ontario), having

an apparent density of 2.75 g/cm^3, was used as a standard in a series of experiments to test the reproducibility of all density cups, used in this work.

EXPERIMENTAL PROCEDURES

Copper powder was produced in three types of circulation apparatuses. Apparatus 1 used the principle of natural convection while apparatuses 2, 3 utilized the principle of forced circulation.

Size determinations of powders produced under various conditions in apparatus 3 were subsequently determined using a modified Andreasen pipette method.

Natural-Convection Apparatus (Apparatus 1). This apparatus was employed primarily to verify the results which Ufford (2) and de Ga (3) obtained using natural convection. The apparatus was constructed after the design of de Ga's apparatus and is shown in Figure 4.

A 250-ml flat-bottom flask A was used as a reaction vessel. A small water condenser, H, was placed in the neck of the reaction vessel A, and this served to prevent the escape of vapour from the boiling solution in the reaction vessel. Any solution that might inadvertently have "bumped" out of the reaction vessel A and through the top of the condenser, would have been collected in a 500-ml Erlenmeyer flask, J, which was connected through an extension to the top of condenser H.

A little more than halfway down on the right-hand side of the reaction vessel, a side-arm of 8 mm O.D. tubing

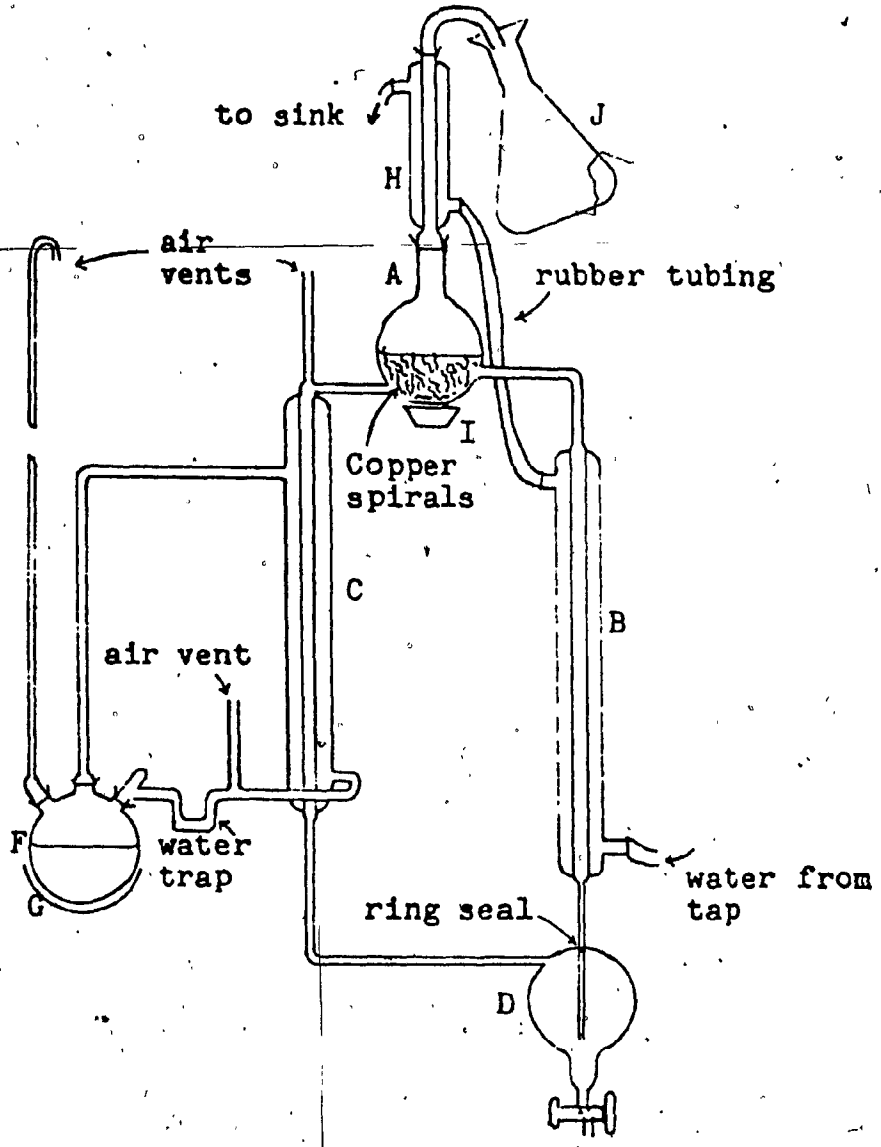

Figure 4. Natural-Convection Apparatus (Apparatus 1).

was added. This side-arm, connected to a water condenser, B, had an inner diameter of 1 cm. The lower end of the condenser was connected to the top of an inverted 250-ml round bottom flask, D, by a piece of 6 mm O.D. tubing, 7,5 cm long. An oblique-bore stopcock was attached to the neck of flask D. This round-bottom flask served as the collection vessel.

On the left-hand side of flask D, about 1 cm from the bottom, a piece of tubing, 25 cm long and 8 mm O.D., was attached. This tubing was connected to a second condenser, C, of similar dimensions to condenser B. This condenser was placed about 15 cm above the point of attachment of side-arm to flask D. The top of condenser C was connected to the reaction vessel A by 8 mm O.D. tubing. This tubing was attached tangentially at a point 1 cm from the bottom of the reaction vessel. Into this connecting tubing, an air vent was inserted.

The liquid circulated through the apparatus due to the difference in densities between hot and cold solutions. The solution, in the condenser C, was heated from room temperature to about 70°C by circulation of steam through the condenser jacket. A 250-ml three-necked flask, F, partially filled with water and heated by a heating mantle, G, was used to generate the steam. A ground-glass joint in the middle neck of the flask was attached to the top out-

let of condenser C with 8 mm O.D. tubing. The bottom outlet of condenser C was connected to a standard-taper joint in the right-hand neck of flask F by a piece of 8 mm O.D. tubing, containing an upright air vent and a water trap. A piece of 6 mm O.D. tubing, about 4 ft long, was connected to a ground-glass joint in the third neck of the flask. This tubing served as an air condenser and air vent. The steam circulated through condenser C and the condensed steam returned to flask F through the water trap. Therefore, this arrangement served for the continuous generation of steam without the need for constant refilling of the boiler.

Copper wire, in the form of small coils, was cleaned in nitric acid, rinsed thoroughly with tap and distilled water, and then placed in the reaction vessel A. The solution which was to react with the metal was poured into the apparatus until it covered the copper coils, and the experiment was begun by heating the reaction vessel A. A natural-convection current between the cold condenser B and the hot condenser C resulted in the circulation of solution throughout the system. The chemical reaction occuring in the reaction vessel A was reversed in condenser B, and the copper powder that precipitated out of solution was gathered in collection vessel D.

From collector D, whenever it was desired, copper

powder was withdrawn through the stopcock with the circulating liquid. The mixture was then filtered on a Buchner funnel and the powder was washed with distilled water and methanol. Following this, the powder was dried with acetone over suction and weighed on an analytical balance.

The copper coils were removed from the reaction vessel A at the end of every run, and then the apparatus was cleaned with nitric acid, and then flushed thoroughly with tap and distilled water. The copper coils from one run were often re-used for another run, after they had been recleaned with nitric acid, as described previously.

Forced-Circulation Apparatus (Apparatus 2). Apparatus 2 is based on the design of de Ga (3). The flow speed of the solution through the system was controlled by a peristaltic pump. The incorporation of a peristaltic pump into apparatus 2 ensured that the circulation of liquid was no longer dependent on natural-convection currents. The constant temperature in the cold condenser was maintained by the circulation of water from a thermostated water bath through the condenser jacket.

Apparatus 2 is illustrated in Figure 5, the differences between its design and that of apparatus 1 as follows. A 250-ml round-bottom flask, D, was added, which served as a secondary collection vessel. The heating condenser, C, had a coiled inner tube and was 19 cm in length

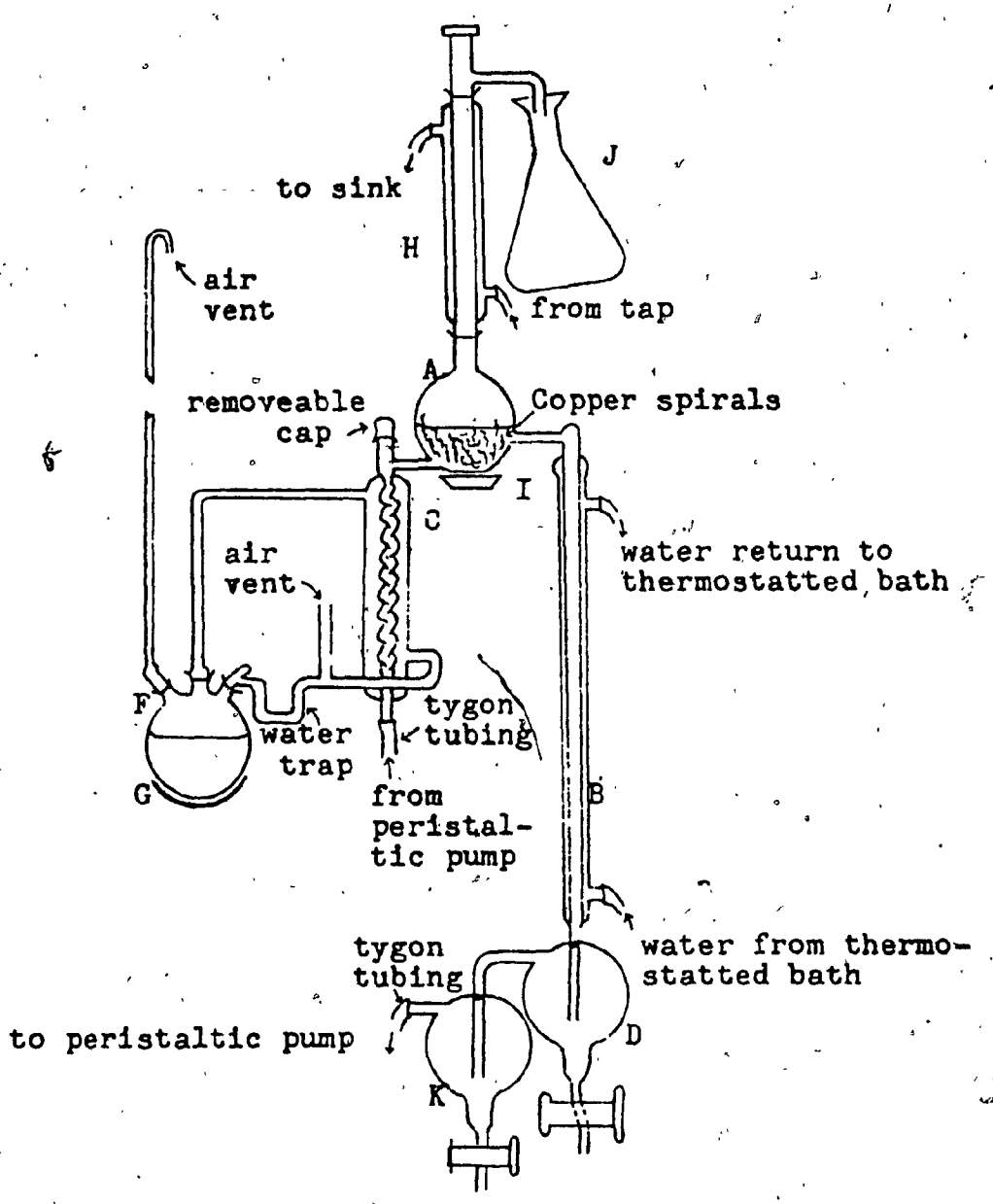

Figure 5. Forced-Circulation Apparatus (Apparatus 2).

and 4 cm in outer diameter. At the top of the condenser C, the air vent with removable cap was added. This cap was kept on during the runs. The bottom of the condenser was connected to flask K by some 2½ to 3 ft ¼-in I.D. tygon tubing, fed through the peristaltic pump. The cooling condenser, B, was 40 cm long and 2 cm outer diameter.

The peristaltic pump, used to control the flow rate of the solutions through the system, was a model 10E 400 Zeromax, with a fine vernier adjustment, manufactured by Sigmamotor. All runs done on apparatus 2, were carried out at a flow rate of 15.0 cc/min. The rate of flow of solution through apparatus 2 was calibrated as per deGa (3).

A Bronwill Constant Temperature Regulator , Model "Thermomix II" was placed in water, in an insulated cylindrical jar of 12 in long and 9 in wide, to set up the thermostated bath. The jar also contained an appropriate-sized cooling coil. The condenser H was cooled by tap water.

The methods used for cleaning the apparatus and collecting powder, in each forced-circulation experiment, were the same as those followed for natural-circulation runs. New tygon tubing was put into the apparatus prior to each run.

Forced-Circulation Apparatus (Apparatus 3). This particular apparatus was designed in the hope that the re-

sults obtained might be of some use if the process under study were ever to be evaluated in an industrial context. Therefore, the main purpose for designing and constructing apparatus 3 was to increase the rate of production of copper powder so that its powder metallurgical properties could be studied. The apparatus 3 was assembled from the following main unit operations - the reaction vessel and cooling condenser, flow control unit, filtration unit, constant-level device, overflow collector and temperature control. The apparatus was disassembled, after each run for cleaning purpose and was reassembled for the next run.

This apparatus is illustrated in Figure 6, and was assembled from the sequence of the unit operations as follows. The reaction vessel, C, was a 2000-ml three-necked flask, which was heated by means of gas burners. The water condenser, K, placed into the central neck of the reaction vessel, served to prevent the escape of vapour from the solution boiling in the reaction vessel. The outer wall of condenser, K, was covered with asbestos in order to ensure that the water running through the condenser did not get heated by the flames of the burners.

Nitrogen gas was bubbled through the solution, to promote smooth boiling. A piece of 8 mm O.D. tubing, 25 cm long, J, with a nozzle at one end, was inserted into a standard joint L, in such a way that the nozzle end of the

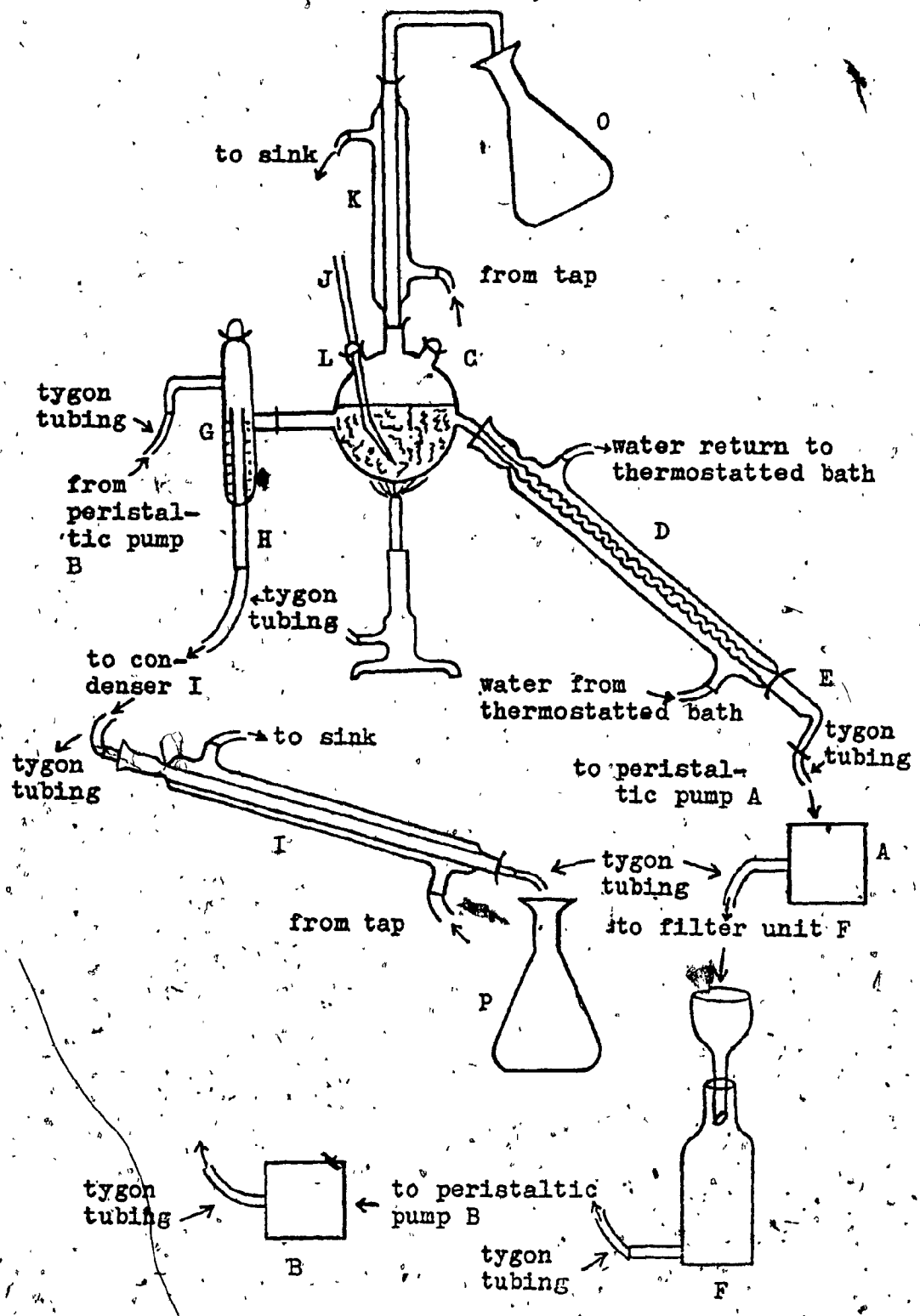

Figure 6. Forced-Circulation Apparatus (Apparatus 3).

tubing was at a point little more than 15 cm down from the joint L. At about 4 cm down from the joint L, the tubing was bent slightly, so that when the joint L was placed in the right-hand neck of the reaction vessel, the nozzle end of the tubing reached a point about ½ in from the bottom of the reaction vessel. The other end of the tubing, J, was connected to the nitrogen gas tank by some 10 ft of ¼-in O.D. tygon tubing. The nitrogen gas was bubbled through the solution in the reaction vessel, via tubing J, at a pressure of 6 lb/in^2 during the run, in order to eliminate the violent "bumping" in the reaction vessel (possibly due to localized superheating). In the top of condenser K was placed an extension, leading into a 500-ml Erlenmyer flask, O. This flask was used merely as a precautionary measure, to catch any solution that might have conceivably "bumped" out of the reaction vessel C and through the top of condenser K.

On the right-hand side of the reaction vessel C, and halfway down, a standard 24/40 male joint was added at an angle as shown in the Figure 6. This joint was fitted into the standard 24/40 male joint of the cooling condenser, D. The cooling condenser used had a coiled inner tube and was 56 cm long and 4 cm in outer diameter. The female joint of the condenser was fitted with a removable adapter E. This adapter was a standard 24/40 male joint to which a piece

of tubing, 8 mm O.D. and 7 cm long, was connected (the adapter attached to 7 cm long piece of 10 mm O.D. tubing, was used for higher flow rates). The solution running out from the cooling condenser and adapter E was led to the filtration unit by 1½ ft to 2 ft of ¼-in I.D. tygon tubing (5/16 - in I.D. tygon tubing for higher flow rates), fed through peristaltic pump A. Peristaltic pump A controlled the flow rate of solution through the system.

The Büchner funnel in conjunction with an aspirator bottle, of 3000-ml capacity, was used as a filtration unit, F. A piece of 10 mm O.D. tubing, 5 cm long, was added to the bottom of the aspirator bottle as shown in Figure 6. The main purpose of the filtration unit was to separate the copper powder from the circulating solution in apparatus 3. This ensured that the copper powder was not being carried past the Büchner funnel along the circulating solution, as was observed in the case of apparatuses 1 and 2. The bottom outlet of the filtration unit was connected to the side-arm of the constant-level device G, by about 5 ft of ¼-in I.D. tygon tubing (5/10 - in I.D. tygon tubing for higher flow rates), fed through peristaltic pump B.

A piece of glass tubing G, 4 cm O.D. and 25 cm long, was used to construct the constant-level device as follows. The bottom end of the tubing G was sealed. On the left-

hand side of tubing G, about 10 cm down from its top, a side-arm of 8 mm O.D. tubing was added. This side-arm was used for the entrance of the solution, being pumped from the bottom outlet of the filtration unit to the constant-level device, by peristaltic pump B, during the run. A standard 24/40 female joint was attached to the top of tubing G. The joint had a removable cap which was kept on during the run. On the right-hand side of tubing G, about 15 cm down from its top, a standard 24/40 female joint was added. By fitting this joint to the male joint on the left-hand side of the reaction vessel C, the constant-level device was assembled to the reaction vessel during the run.

From the centre of the bottom of tubing G, a piece of tubing H of 10 mm O.D. and 15 cm long was inserted. The top end of tubing H was placed about 10 cm above the point of its attachment to the tubing G. Thus, the standard 24/40 female joint, connected to right-side of tubing G, and the top of the tubing H, were at the same level. This tubing H, kept the level of the solution in the constant-level device and the reaction vessel constant, as the excess of solution overflowed from the top of the tubing H.

A 500-ml Erlenmeyer flask, P, was used as a overflow collector. Any excess solution from the top of tubing H,

was led through a piece of tygon tubing, ¼-in I.D. and 2 ft long, to a water condenser, I, of 3 cm O.D. and 45 cm long. The solution coming from the condenser I was collected in flask P.

The peristaltic pumps A and B were both model 10E 400 Zero-Max, with a fine vernier adjustment, manufactured by Sigmamotor. The capacity of the peristaltic pumps used was a function of both the diameter of the tygon tubing and speed, and the flow rate of the solution was calibrated as will be described on page 75.

The cooling condenser D, was cooled by circulating water from the thermostated bath. Thus, the temperature of the solution entering the filtration unit was controlled, and a series of runs were carried out at three different temperature, i.e. 25 ± 3°C, 33 ± 3°C and 44 ± 3°C (the temperature at the filtration unit is indicated, together with the other conditions for each run, further along in this thesis). The thermostated bath was set up by the placement of a Haake Constant Temperature Regulator, Model "Ed 66524", in water in an insulated cylindrical jar, 10 cm wide and 12 cm long. The water from the thermostated bath was circulated through an appropriate-sized cooling coil, placed in ice cold water in a plastic basket. During all the runs, condensers I and K were cooled by tap water.

After assembling apparatus 3 as illustrated in Figure 6, about 500 ml of the solution which was to react with the metal, was poured into the reaction vessel C. Copper wire, in the form of small coils, and cleaned as described previously, was placed in the reaction vessel C. About 2000 ml of the reaction solution was poured into the aspirator bottle, used in the filtration unit. The flow of the solution through the system was obtained by switching on the peristaltic pumps A and B, and the experiment was begun by heating the reaction vessel C by gas burners. At the end of the experiment, the Büchner funnel of the filtration unit, containing the reacting solution and copper powder, was removed from the apparatus. Any copper powder that had lodged in the condenser was swept out and collected, and then all the powder was washed, dried and weighed, as described previously.

After the run, the apparatus was disassembled and cleaned with nitric acid and then flushed thoroughly with tap water and distilled water. The Büchner funnel and aspirator bottle, along with the tygon tubing, the filtration unit, the overflow collector P were cleaned with soap and then flushed with tap and distilled water. The coils from one run were used for another run, after they had been re-cleaned with nitric acid, as described previously.

Calibration of Flow Rate. The flow rate of water through apparatus 3 was measured at various settings of the vernier control of the peristaltic pump A. (As described before, tygon tubing of 5/16 - in I.D. was used to obtain higher flow rates). The vernier control of peristaltic pump B, was adjusted to give the same flow rate, as was given by pump A, during the run. Copper coils were placed in the reaction vessel during the calibration, to ensure that the liquid encountered the same resistance to flow as it would during a normal run. During the measurement of flow rate, water was collected at the filtration unit as the flow rate of the solution through the system was controlled by pump A. The rate of flow of water, at each setting of the vernier control of peristaltic pump A, was determined over a period of 4 to 6 hours. The average values of flow rate obtained at various setting of the vernier control of the peristaltic pump A, are presented in Table 2. These various vernier adjustments of pump A were utilized to keep flow rate constant, for various runs carried out on Apparatus 3. Prior to each run, new tygon tubing, connecting the precipitating condenser D to the filtration unit, was put into the apparatus. The tygon tubing, used to connect the bottom of filtration unit to the constant level device, was changed after five runs.

Table 2

Calibration of Flow Rate

I. Tygon tubing of ¼-in I.D. was used

Pump A's Setting RPM	Flow Rate cc/min
300	10.0
350	13.5
400	18.0
450	24.0
500	28.0
600	36.0
700	43.0
800	50.0
900	62.0
1000	76.0

II. Tygon tubing of 5/16-in I.D. was used

Pump A's Setting RPM	Flow Rate cc/min
600	92.0
660	112.0
690	122.0
700	138.0
730	152.0
760	164.0

Control of Temperature in Reaction Vessel. The temperature of the solution in the reaction vessel was always kept at boiling during an experiment. This was done by increasing the number of Meeker-type gas burners used to heat the reaction vessel. For example, three gas burners, at full flame, were used to heat the reaction vessel during the experiments made at a flow rate of 164.0 cc/min, to achieve a constant value of temperature in the reaction vessel. At higher flow rates it was found very hazardous to maintain the solution at boiling in the reaction vessel, and this was the main limiting factor in the experiments. During the experiments, at higher flow rates, it was observed that clamps (made of aluminium) used for assembling the apparatus on the rack as shown in the Figure 6, were loosening due to the excess of heat from the flames of the burners. There was always a danger of the apparatus breaking due to strain caused by its own weight.

Particle-Size Analysis. It had already been investigated by de Ga (3), that dry and wet sieving was not suitable as a method for sizing the copper powder. It was reported that some 10-20% of the material was lost during the dry sieving process, using standard 8-in metal sieves, and such a material loss would considerably affect the accuracy of the sieving. When a set of plastic sieves was used, the tendency of copper powder to form agglomerates,

by interlocking of fine particles, was observed. Thus, the material was not properly sieved, and as a consequence, the sieving process yielded discordant and non-reproducible results. The same author also concluded that wet sieving was unsuitable for routine analysis, because of the inordinate amount of time required for each sample.

Since the particle size of copper powder produced on apparatus 2 appeared to be subsieve size, de Ga (3) attempted to obtain the size analysis by means of the Andreasen pipette method. It was assumed that Stokes'law was applicable for copper particles sedimenting in water, used as the sedimentation medium. However, because of difficulty in withdrawing the suspension medium smoothly and rapidly through the pipette at the recommended rate of 10-ml in twenty seconds, this method of size-analysis was rejected by de Ga (3).

Particle size determinations of the copper powder produced on apparatus 3, were obtained using a modified Andreasen pipette technique. The assembly of this modified pipette, depicted in Figure 7, consisted of 3 main parts i.e., sedimentation vessel C, filling cannula B and dispensette A. A 500-ml graduated cylinder C, 32 cm high and 5 cm in outer diameter, was used as a sedimentation column. At the top of the cylinder, a narrow neck finished with a screw thread, of SVL 30 type was added. This narrow neck

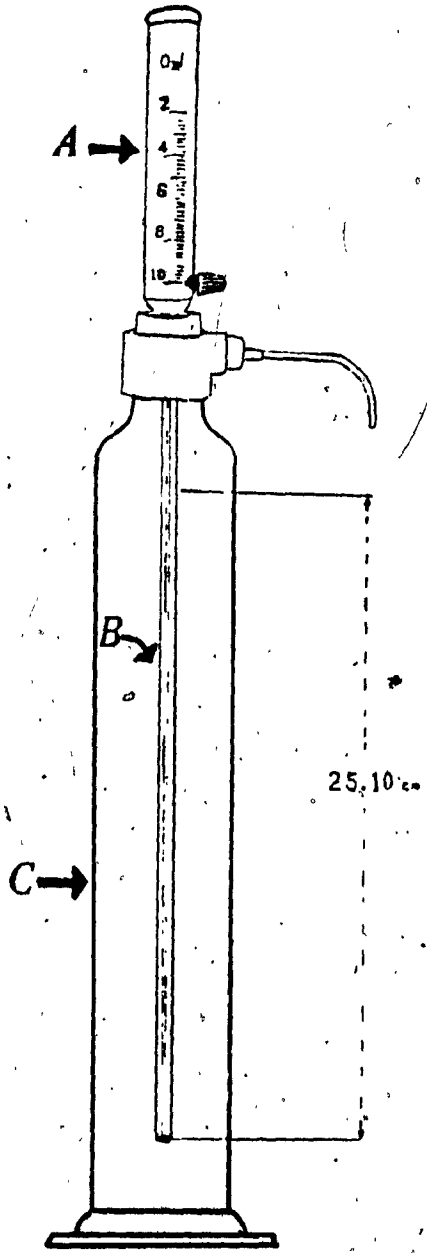

Figure 7. Modified Andreasen Pipette.

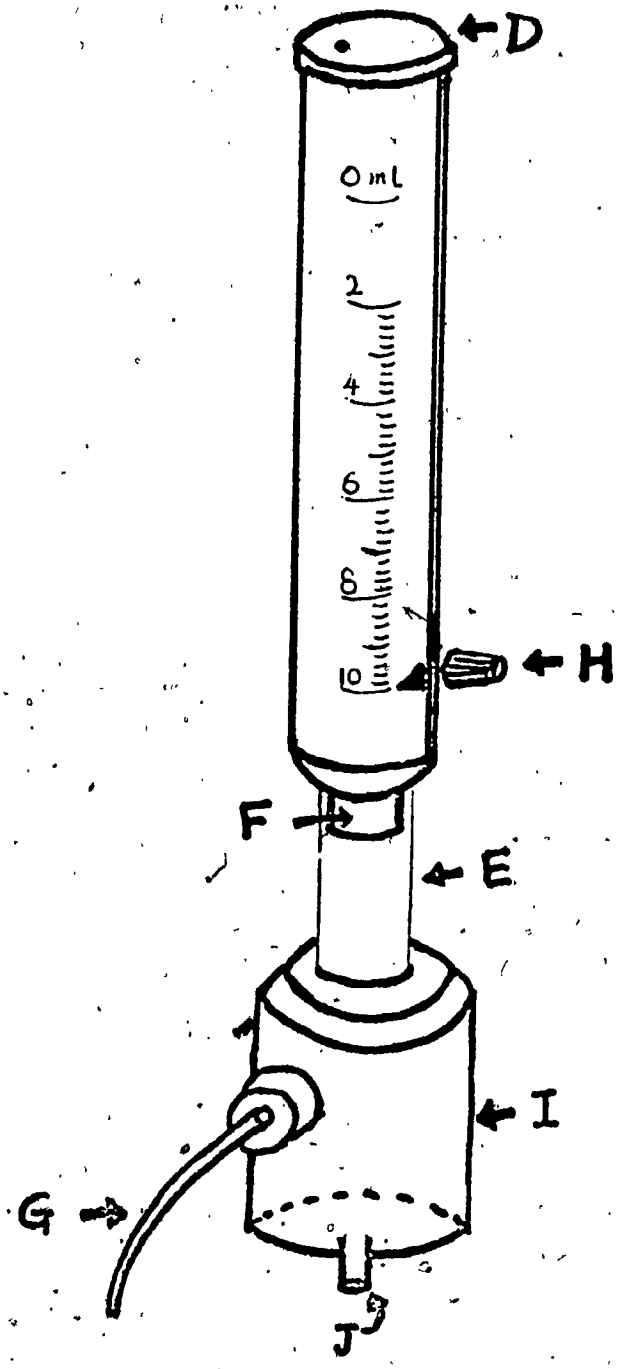

Figure 8. Brinkmann Dispensette

of the sedimentation vessel could take the plastic sorew cap of the size 33-430. Brinkmann Dispensette A, purchased from Brinkmann Instruments (Rexdale, Ontario), and used as a dispenser for rapid and exact dispensing of the suspension medium at the recommended rate of 10-ml in 20 seconds. A piece of capillary tubing B, 1 mm I.D. and 32 cm long, was used as a filling cannula.

The basic components of Dispensette A are shown in Figure 8. The volume of the samples to be withdrawn was adjusted by the arrestment screw H, which was kept at the 10-ml mark of the scale graduation located on the polypropylene sleeve. The valve block I, fabricated from Tefzel, supported the glass cylinder E. The discharge cannula G was inserted by pressing it into the valve cap attached to valve block I. The filling cannula was attached into filling valve cap J, through a piece of Teflon tubing, 5.5 mm I.D. and 3 cm long. The valve block I of the Dispensette was screwed directly onto the top narrow neck of the sedimentation vessel C, as shown in Figure 7. When the plunger mount, D, of the plunger F was lifted, a 10-ml sample of the suspension medium was drawn into the cylinder E via filling cannula and valve. When the plunger F was depressed, the filling valve would close, and the sample flowed out through the discharging cannula G; (plunger mount D, plunger F and glass cylinder E are shown

in Figure 8). The reproducibility of withdrawing 10-ml sample for the dispensette was 0.2%.

A lengthy series of experiments showed that water, used as a sedimentation medium, gave unsatisfactory results and a dispersing agent was required to give good dispersion. After many trials, it was found that Calgon would serve satisfactorily as a dispersing agent. Hence the dispersing medium used in the sedimentation experiments was 0.05% solution (weight/volume) of Calgon in water, a fresh solution being prepared for each run. All the runs were done at room temperature, approximately 25° C. It was decided that a correction for density and viscosity of dispersion-medium water was not necessary, since the concentration of dispersion agent was only 0.05%.

Prior to each analysis, the copper powder was thoroughly mixed on a ball-mill roller. For all runs, the time allowed for tumbling was 30 minutes. A 8.92 g sample was removed from the total lot, to give a concentration of 0.2% by volume on dilution with dispersion medium to 500 ml. This sample was then spatulated with a concentrated solution of dispersing agent before it was put in water. This involved putting the powder and a weighed amount of dispersing agent, (250 mg) Calgon, on a flat glass plate, water being added drop-wise. The paste was vigorously agitated with a stainless steel, flexible-bladed spatula.

This manipulation of the paste was carried out until paste flowed from the spatula in long syrupy threads, thus ensuring a good dispersion (46). The paste was transferred to the sedimentation cylinder and was diluted with water to the 500-ml mark on sedimentation vessel. The narrow mouth of the sedimentation vessel was closed with a plastic cap and the vessel was shaken manually for 15 minutes. The plastic cap was removed and the Dispensette was screwed directly onto the narrow mouth of the sedimentation vessel, as shown in Figure 7. The first 10-ml sample of the suspension medium was removed as soon as possible by withdrawal of the plunger of the Dispensette, and the timer was started simultaneously. The remaining samples were withdrawn at different times. The depth at which the first sample was taken was corrected for the rise in level caused by the insertion of capillary tubing into the sedimentation vessel. This depth corresponded to 25.10 cm as indicated in Figure 7. Similarly, the depth for all other samples were corrected for the fall in level caused by sample withdrawal.

Small flat-bottomed aluminium dishes 6x2.5 cm were used for the collection and evaporation of the samples. After the evaporation, the samples were weighed. The weight of the first sample, after deduction of the blank due to dispersing agent, gave the initial concentration of

the powder. Subsequent samples gave the cumulative weight undersize distribution corresponding to the particular Stokes' diameter in question. The distribution was then plotted graphically, and the median particle diameter was obtained for the sample.

The pipette apparatus was disassembled between runs, and the Dispensette and sedimentation vessel were cleaned and thoroughly rinsed with tap and distilled water. The copper powder sample used in each run was recovered by filtration and stored separately.

Reproducibility Runs. As described previously, a 200-g sample of copper powder, -325 mesh, was used to test the reproducibility of this modified Andreasen pipette. This standard was tumbled on the ball-mill roller for 30 minutes prior to the start of each reproducibility run, following which 8.92 g was removed for size analysis. The procedure for dispersing this sample in dispersing medium, and then withdrawal of 10-ml samples of suspension medium, from sedimentation vessel with the help of the Dispensette, were the same as that described above.

The raw Andreasen pipette data, and resulting size analysis, for four runs, ST1 to ST4, testing reproducibility, are detailed in Tables A21 to A24. The median diameter corresponding to 50% cumulative distribution, and standard deviation for these four reproducibility runs were ob-

tained from probability plots, shown in Figure A21 to A24.

Table 3 lists the value of the median diameter of each reproducibility run, as obtained from the graph of its cumulative distribution. A 25-g sample of standard copper powder was sent to the Aluminium Company of Canada for size analysis*. This sample was analyzed using Micro-mesh Sieves and also by the "Electrozone/Celloscope". The results reported from this analysis are indicated as runs ST5 and ST6 in Table 3. The "Electrozone/Celloscope" uses the so-called Coulter Principle, which measures the particle volume. The particle size determined by this technique, as indicated in Table 3, was found to be lower than that of the size analysis. It is quite likely that the Celloscope was not reading the "true volume" due to the irregular shape of the particles. However, the results tabulated in Table 3 show that the values obtained from the modified Andreasen Pipette method were reproducible, and certainly sufficiently accurate for the purposes of this thesis.

*This work was done through the courtesy of Dr.J.D. Zwicker of the Aluminum Company of Canada, in Arvida, Quebec.

Table 3

Value of the Median Diameter and Standard Deviation for Each Sample in the Reproducibility Runs*

Run Number	Median Diameter, u	Std. Dev.
ST1	15.67	2.07[c]
ST2	15.23	2.03[d]
ST3	15.31	1.99[d]
ST4	15.40	1.89[d]
ST5[a]	16.00	1.84[d]
ST6[b]	13.75	1.91[e]

*All data used to estimate these median diameters, and standard deviations are tabulated in appendix A.

[a]Sample Analyzed using Micromesh Sieves.

[b]Sample Analyzed by Electrozone/Celloscope.

[c]Reported as the mean of the two values: (Size at 84%/Size at 50%) and (Size at 50% / Size at 16%).

[d]Reported as the value: (Size at 84% / Size at 50%).

[e]Reported as the value (Size at 50% / Size at 16%).

Size Determinations of Copper Powder Produced in Forced Circulation Apparatus 3. The samples of copper powder produced in apparatus 3 were tumbled on the ball-mill roller for 30 minutes, following which 8.92-g sample was removed for analysis. The remainder of the procedure was similar to that followed for the reproducibility runs. The particle size analysis was done for the following series of experiments D,G,I,K,M,N,O,P,QI,QK,QM,QR,QS,TK,TM, TN,TO,TP and TR.

Determination of Apparent Density of Copper Powder. The apparent density of copper powder was determined by the use of three different density cups. The density cup X, having a capacity of 25 $\pm$ 0.05 cm^3, was purchased from Alcan Metal Powder, Inc. (Elizabeth, N.J.), as a part of the Hall Flow Meter (ASTM B212-48). The material obtained in the series of experiments done on apparatus 3, was not enough to fill the density cup X, and it was found necessary to use a density cup of smaller capacity, so that the apparent density of copper powder could be determined. Therefore, two density cups Y and Z were machined, from solid brass rod, having approximate volumes of 2.00 cm^3 and 3.00 cm^3 respectively (at Science Technical Centre of S.G.W. Campus, Concordia University). The volumes of cups Y and Z had to be corrected.

Determination of Apparent Density of Copper Powder using Any Density Cup. The standard copper powder was thoroughly mixed by tumbling on a ball-roller mill for one hour, following which an 80-g sample was removed for analysis. This powder was poured carefully into the density cup by means of a spatula, until the powder filled and overflowed the periphery of the cup. The top of the powder was leveled by using the spatula. After the leveling operation, the side of the density cup was tapped lightly to settle the powder in order to avoid spilling in transfer. The cup and contents were then transferred to an analytical balance and weighed. This weight of powder in the density cup, after suitable mathematical treatment, was reported as the apparent density in grams per cubic centimeter.

Reproducibility Runs for Apparent Density using Density Cup X. The procedure followed for the reproducibility runs was the same as described above. Table 4 lists the value of the apparent density of standard powder as determined by the use of density cup X. The value of apparent density of standard powder, from six reproducibility runs, was found to be 2.73 $\pm$ 0.01 g/cm^3, and had an error of 0.73% when compared with the quoted value, 2.75 g/cm^3. From Table 8 it would appear that the experimental technique was suitably reproducible, and

Table 4

Value of the Apparent Density and Standard Deviation for Standard Copper Powder Sample in the Reproducibility Run

Using Density Cup X having a Capacity of 25 $\pm$0.05 cm^3

Run No.	Weight of Copper Powder, g	Apparent Density g/cm^3
X1	68.3170	2.73
X2	67.8339	2.71
X3	68.4764	2.74
X4	68.2033	2.73
X5	68.6038	2.74
X6	68.1954	2.73

Average Apparent Density = 2.73 g/cm^3

Standard Deviation = 0.01

that cup X produced reliable results.

Determination of Apparent Density of Copper Powder using Density Cup Y and Z. The procedure for the determination of the apparent density of copper powder was the same as described previously. The volumes of cups Y and Z were determined using the standard cyclone powder that had been used to study the reproducibility of Cup X. The average weight of the ten different weights of copper powder (Cyclone powder) required to fill each of density cups Y, Z was determined. This average weight was divided by the apparent density of copper powder, as determined by using cup X, to give the corrected volumes of cups Y and Z, and the corrected volumes of cups Y and Z were found to be 1.99^{7} cm^3 and 3.03^{8} cm^3 respectively.

Following the determination of these volumes, for cups Y and Z, it was decided to make a quick set of experiments to ensure that the reproducibility of these cups was as good as the data obtained for cup X. The data obtained are listed in Tables C23 and C24. The mean apparent density of standard copper powder, using cups Y and Z, was found to be 2.73 ± 0.01 and 2.74 ± 0.01 g/cm^3 respectively, as compared to the quoted value of the apparent density of 2.75 g/cm^3. Therefore, it was concluded that density cups Y and Z could be used to determine the apparent density of copper powder.

Determination of Apparent Density of Copper Powder Produced in Apparatus 3. The samples of copper powder produced in apparatus 3 were initially tumbled on the ball-roller mill for one hour. The remainder of the procedure was similar to that followed for the reproducibility runs.

The apparent density analysis was done for the following series of experiments, D,G,I,K,M,N,O,P,QI,QK,QM,QR, QS,TK,TM,TN,TO,TP, and TR.

Tensile Strength. The tensile specimens of copper powders produced in runs M,QS,TR, and as well of powder produced by the cyclone method at the Canada Metal Company Ltd., Oakville, Ontario, were made by compacting in standard MPIF dies (Metal Powder Industries Federation), and by subsequent sintering. The processes of compacting and sintering were carried out at Ontario Research Foundation, Mississauga, Ontario. The powders in the die were compacted at a pressure of 30 T.S.I., and the weights of the powder were adjusted for each sample to produce specimens of approximately 0.250" thickness and 4" in length. The specimens were sintered at 1750°F for ½ hour in a dissociated ammonia atmosphere. This experimental procedure is a standard technique in the metal powder industry and simulates the commercial conditions for the compaction and sintering of copper powders. The shape of the sintered

specimens is shown in Figure 9.

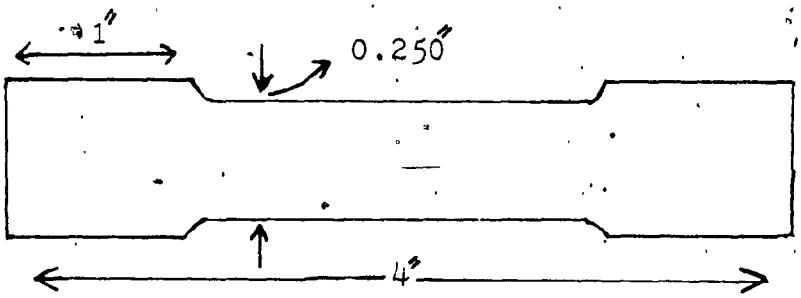

Figure 9. Shape of the Sintered Specimen.

Tensile tests on these specimens were carried out on the Tinius Olsen Tensile Testing Machine*, which has been certified as being to ASTM standards. Load was applied to the specimen until it broke. Tensile strength of the specimen was obtained by dividing the maximum load applied by the original cross-sectional area of the specimen.

*in the Department of Civil Engineering at Concordia University.

RESULTS AND DISCUSSION

Apparatus 1 (Natural Convection). The effect of duration of run on the copper powder yield was investigated on this apparatus. This investigation was carried out to determine whether results similar to those of Ufford (2) and de Ga (3) could be obtained using a similar type of apparatus.

Commercial-grade copper wire was used in all natural-convection run.

Yield. The circulating liquid for natural-convection run NC-1 was a solution of 0.5 M cupric sulphate in 1N sulphuric acid. The yields of copper powder obtained are shown in Table D1, and graphically depicted in Figure 10, together with the results obtained by Ufford (2) and de Ga (3) under the same chemical conditions.

The yields obtained on apparatus 1 were reproducible. The data obtained from run NC-1 verified the results of de Ga (3) and were qualitatively in agreement with those of Ufford (2).

Apparatus 2 (Forced Circulation). Copper powder yield was obtained as a function of duration of run and salt concentration. All runs on apparatus 2 were done at a flow rate of 15.0 cc/min. Commercial-grade copper wire was used in all forced-circulation runs done on apparatus 2.

Figure 10

Comparison of Natural Convection Yields with Those Obtained by Ufford(2) and deGa(3).

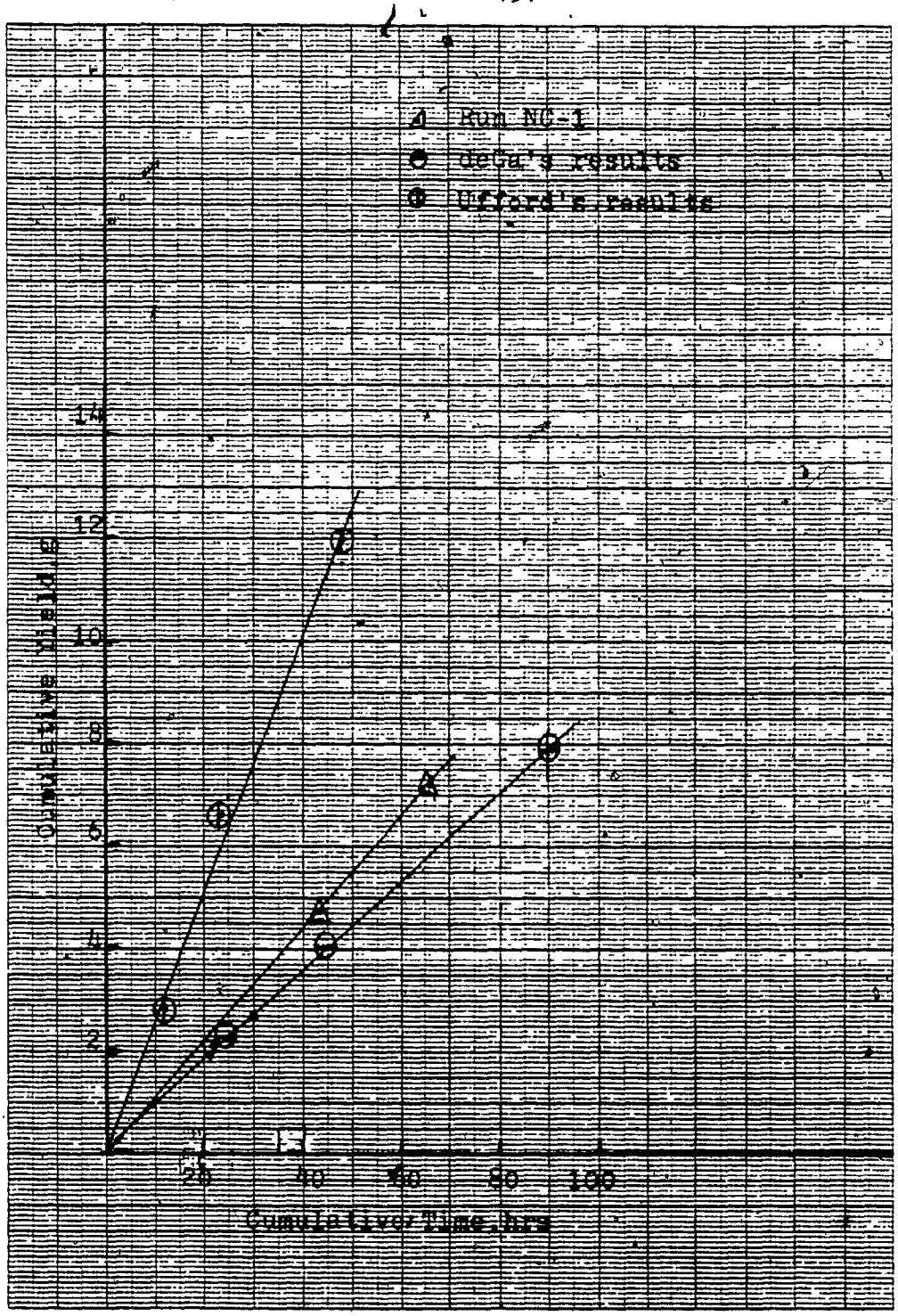

Effect of Duration. The yield as a function of duration of run, at a flow rate of 15.0 cc/min., is shown in Figure 11, which is based on the data presented in Table D2. A solution of 0.5 M cupric sulphate in 1N sulphuric acid was used as a circulating liquid for all runs in this series of experiments. The yield obtained in each run refers to an individual experiment and not to a cumulative yield obtained from a series of experiments.

The results obtained by de Ga (3), under similar chemical and flow rate conditions, are also shown in Figure 11. It would appear that the results obtained on the apparatus 2 were reproducible.

Effect of Salt Concentration. The effect of varying the cupric sulphate concentration at fixed concentration of the sulphuric acid on the yield of copper is demonstrated by the data in Table D29. The duration of the run was arbitrarily fixed at twenty-two hours in all experiments having a constant duration. Run 3A could not be carried out as the salt precipitated out in the cooling condenser of apparatus 2, thus blocking the circulation of the liquid in the apparatus.

Apparatus 3 (Forced Circulation). Yield. Copper powder yield was obtained as a function of duration of run, temperature at the filtration unit and the amount of copper wire used. Unless otherwise indicated, copper cable

Figure 11
Comparison of Forced Circulation Yields with Those Obtained by deGa (3).

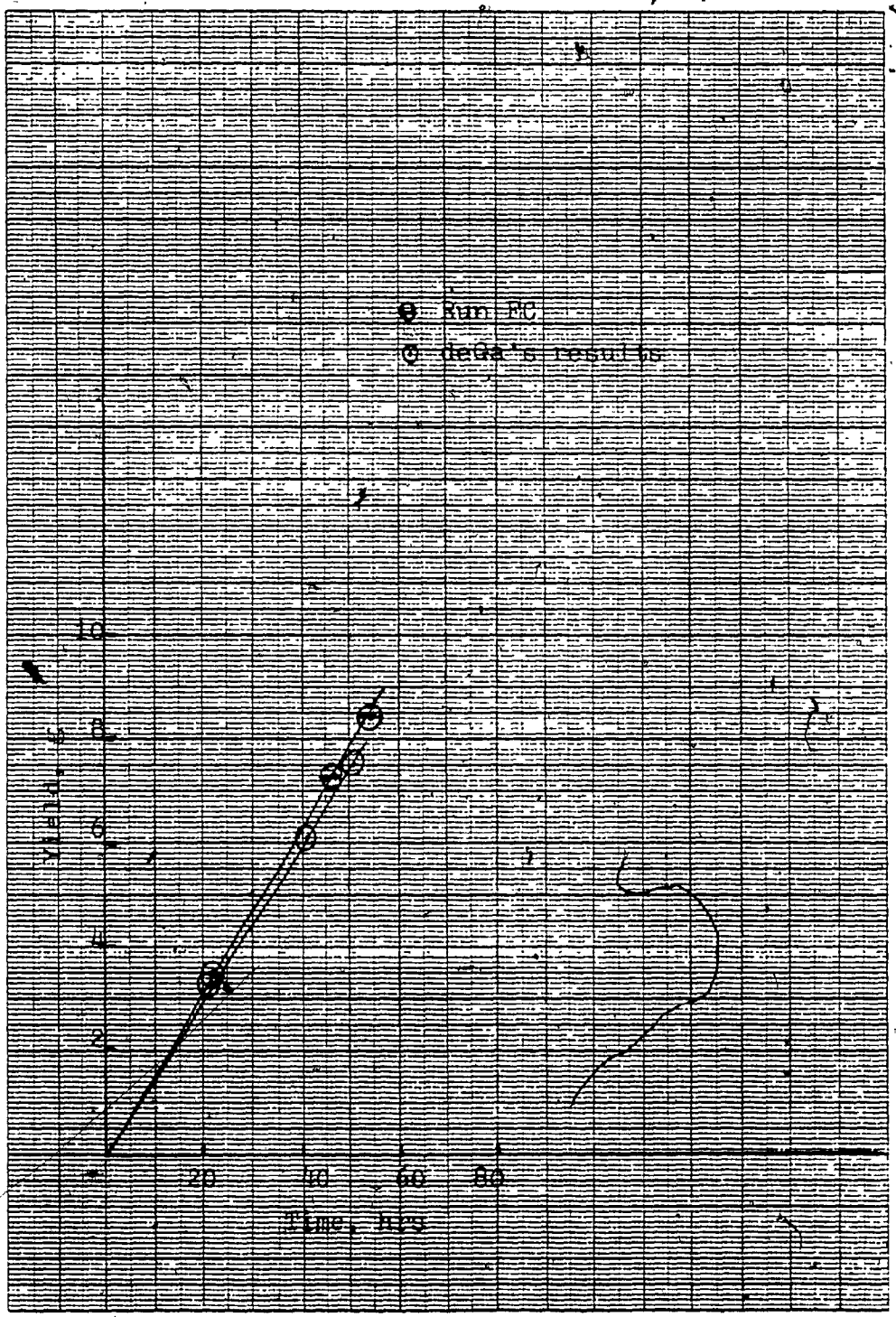

wire, was used in all forced circulation runs done on apparatus 3. The circulating liquid in all these runs was a solution of 0.5 M cupric sulphate in 1N sulphuric acid.

Effect of Amount of Copper Wire used. The effect of varying the amount of copper wire on the yield of copper powder obtained is shown for runs 1B, 2B, 3B, 4B, 5B and 6B in Table D3. On the basis of this data, yield/hour values are graphically depicted in Figure 12. From this figure it was concluded that the amount of copper wire to be used in the remainder of all runs done on apparatus 3 would be 800 g. This weight of copper wire represents the weight of wire before treatment with nitric acid.

Effect of the Solution Flow Rate, and Temperature at the Filtration Unit. Copper powder yield as a function of duration and flow rate, keeping the temperature at the filtration unit at 25 ± 3 °C, is shown in Tables D4 to D17. The average yield/hour obtained from these data (Table D18) is graphically depicted, as a function of flow rate, in Figure 13. Similarly, Tables D19 to D24 and Table D25 represent the yield of copper powder obtained at different flow rates when the temperature at the filtration unit was maintained at 33 ± 3 °C and 44 ± 3 °C respectively. The effects of solution flow rate on the yield for runs done at temperatures of 33 ± 3 °C and 44 ± 3 °C are shown in Figure 14 and 15 respectively. The conditions under which

Figure 12
Variation of Copper Powder Yield with Weight of Copper Wire at the Flow Rate 36.0 cc/min.

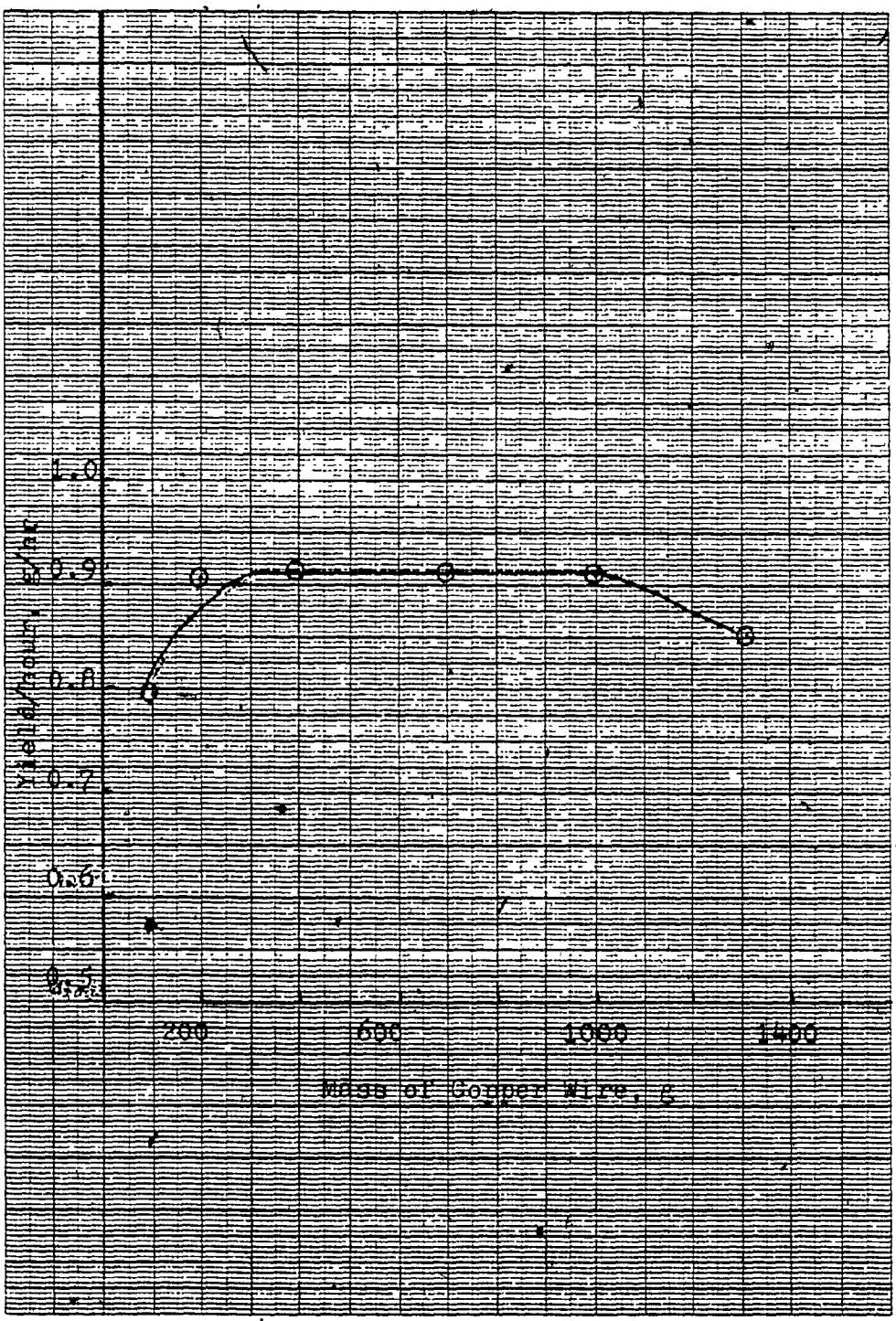

Figure 13

Effect of Liquid Flow Rate on Yield of Copper Powder

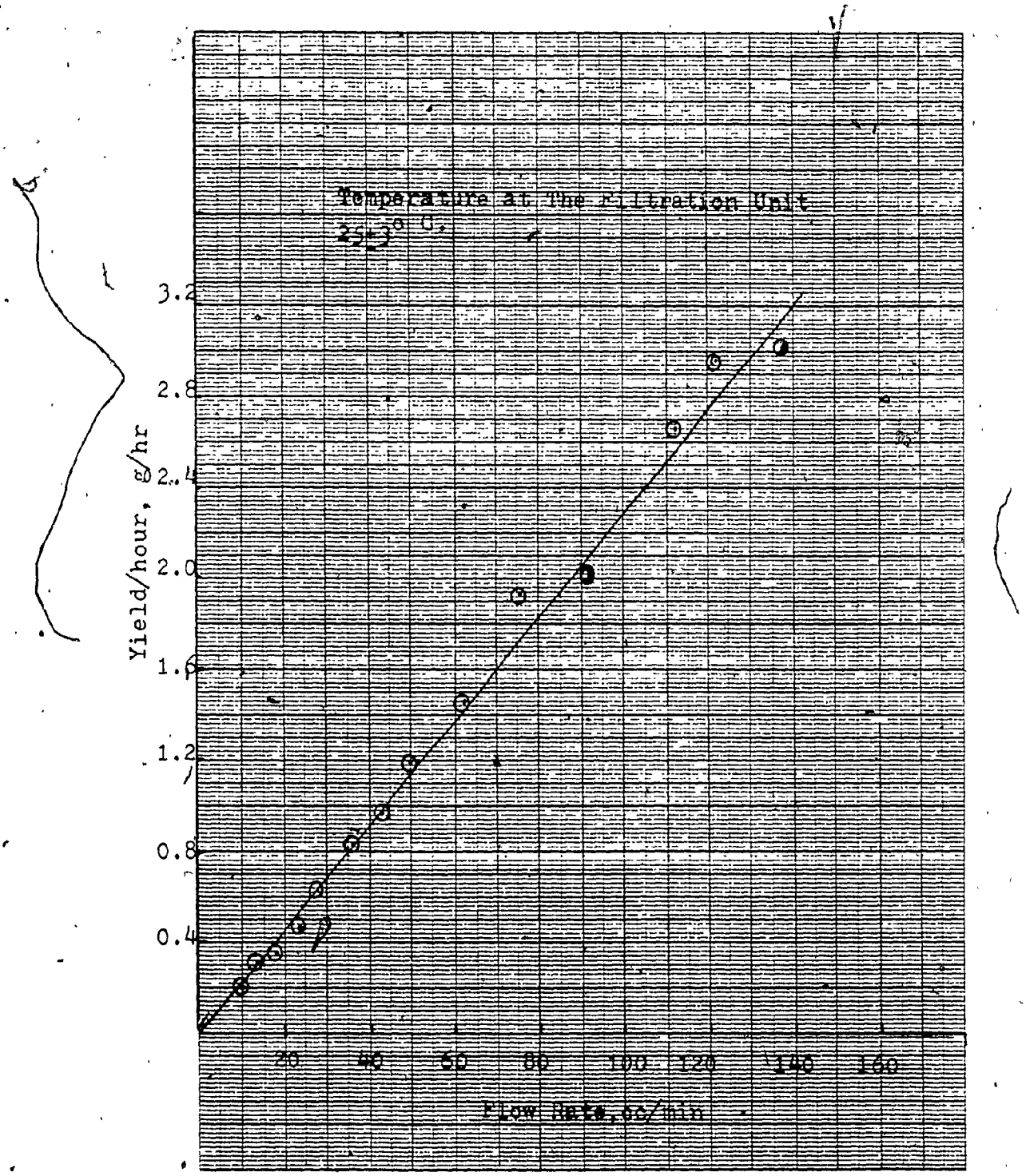

Figure 14
Effect of Liquid Flow Rate on Yield of Copper Powder

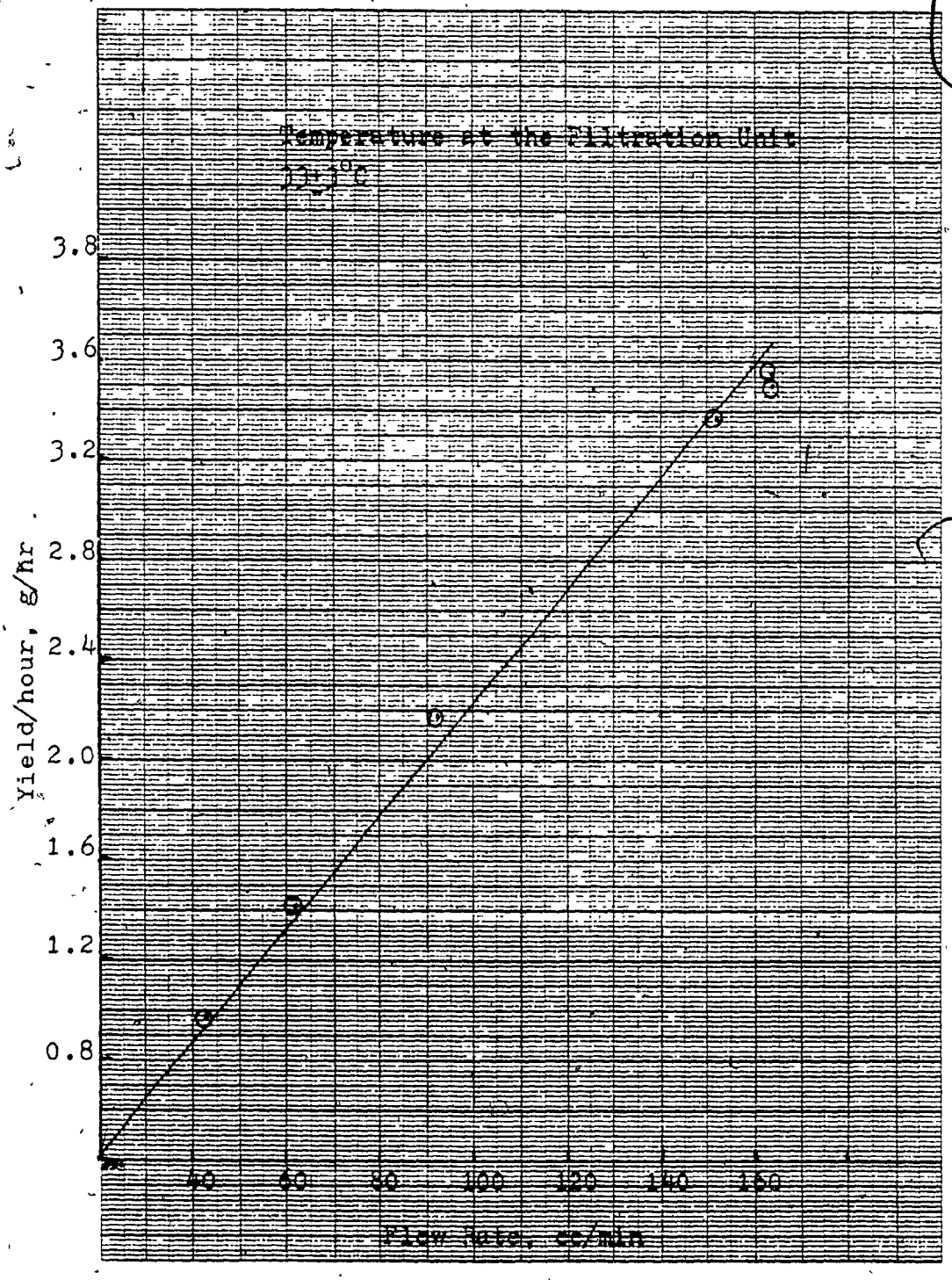

Figure 15

Effect of Liquid Flow Rate on Yield of Copper Powder

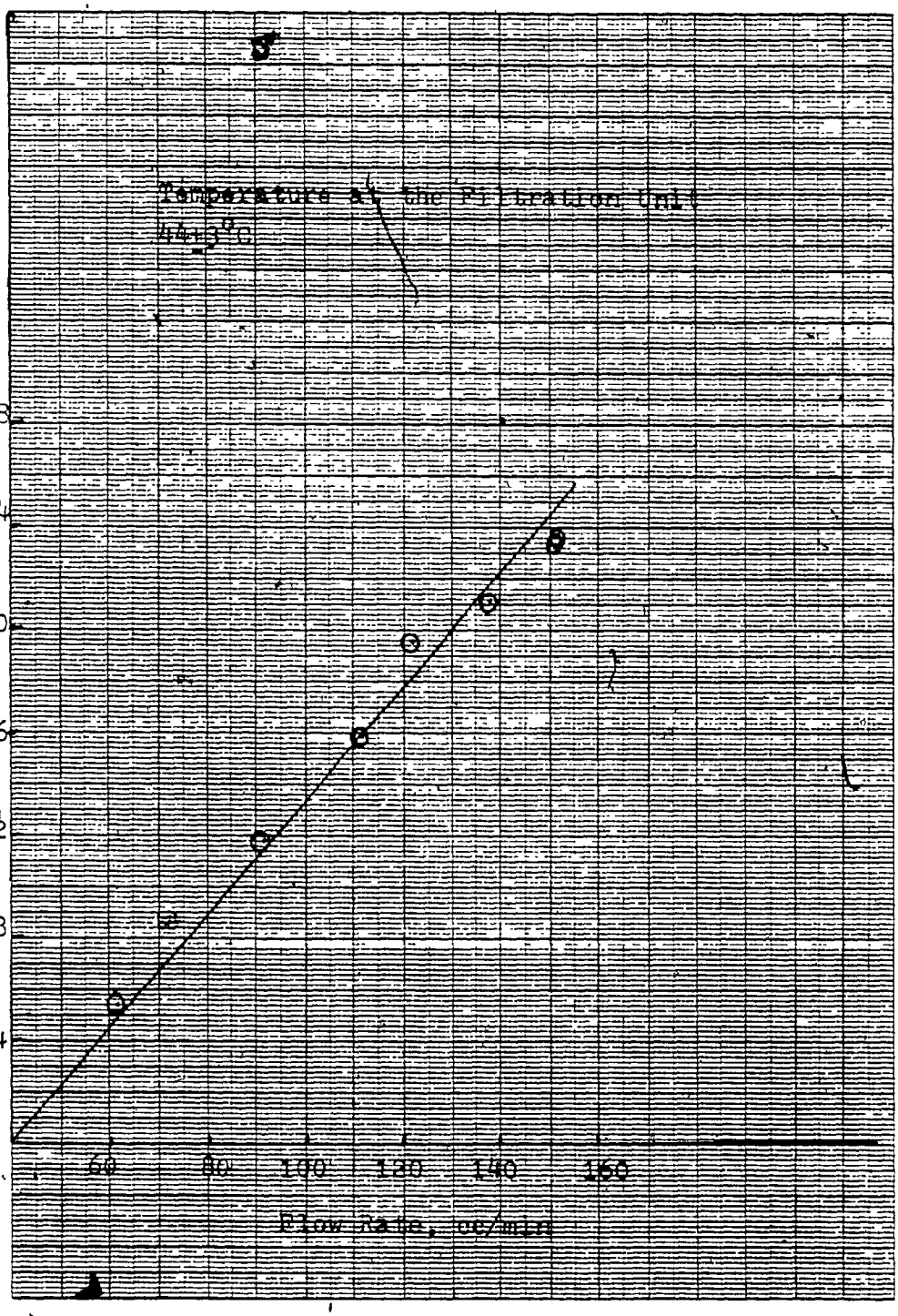

copper powder was obtained are also stated further along in this section of the thesis. Copper powder obtained in the various runs listed in Tables D26 to D28 would be used for the sintering process, but the data from these Tables have been incorporated into the appropriate graphs.

Each run listed in Tables D3 to D28 corresponds to an individual experiment and not to a cumulative yield obtained from a series of experiments. The duration of run was arbitrarily fixed and could vary, in case of series of runs C, from 3 to 10 hours. Furthermore, as stated in the section on experimental procedures and indicated in Table 2, the flow rate during a run was maintained constant by setting the vernier control of the peristaltic pump and using tygon tubing of different sizes. The amount of copper wire used in each run was 800 g.

Particle Size. The raw sedimentation data and the calculated particle-size distributions of copper powder obtained with different flow rates and temperatures at the filtration unit, along with geometric standard deviations, is outlined in Tables A1 to A20. Tables A1 to A20 and Figures A1 to A20 have been assembled in Appendix A.

The effect of flow rates studied on the median diameter of copper powder, when the temperature at the filtration unit was maintained at 25 $\pm$ 3 ^{o}C, is presented in Table E1, and is graphically depicted in Figure 16.

Figure 16

Effect of Liquid Flow Rate on Median Diameter

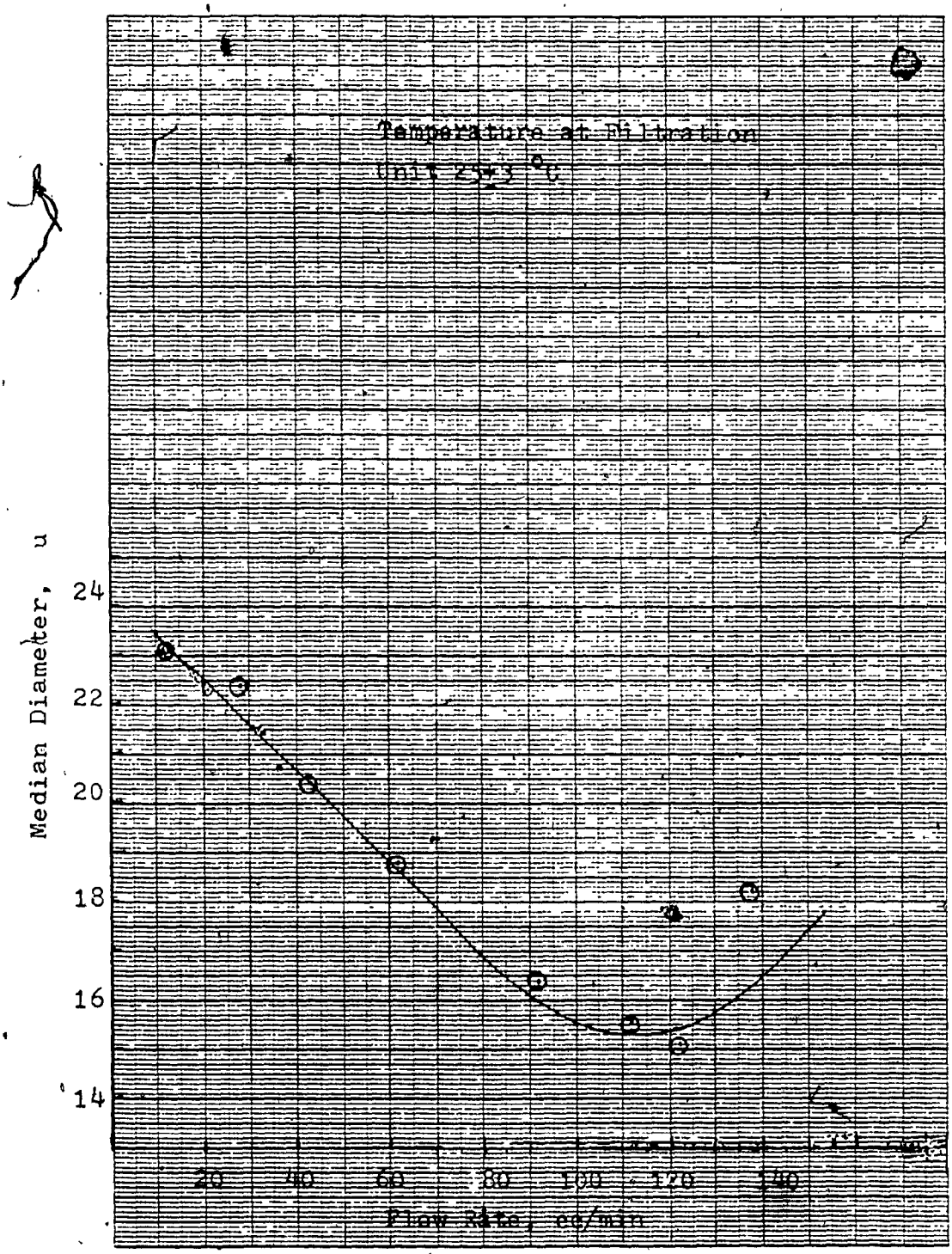

Tables E2 and E3 list the median diameters of powder obtained as a function of flow rate, for temperatures at the filtration unit of 33 ± 3 °C and 44 ± 3 °C respectively. On the basis of these data, the median diameters as a function of the flow rate are shown in Figures 17 and 18.

The effect of these two variables (i.e. flow rate and the temperature at the filtration unit) on the median diameter of the powder is summarized in Table 5, and graphically depicted in Figure 19. The geometric standard deviation for each powder is also listed in Table 5 . The size distributions of the powder produced in all the forced circulation runs were not obtained, when the temperature at the filtration unit was kept at 25 ± 3 °C. It was considered sufficient to size the particles from such runs as would serve to indicate the trends in the sizes of copper powder produced at different flow rates. The particle sizes in the powders analyzed appear to be reasonably well represented by the log-normal distributions.

Apparent Density. Raw data and calculated apparent densities of various copper powders produced on apparatus 3, have been assembled in Appendix C (Tables C1 to C22). The effect of median diameter of copper powder produced at different flow rates and temperature at the filtration unit is summarized in Tables C25 to C27. The standard deviations for the values of apparent densities are also

Figure 17

Effect of Liquid Flow Rate on Median Diameter

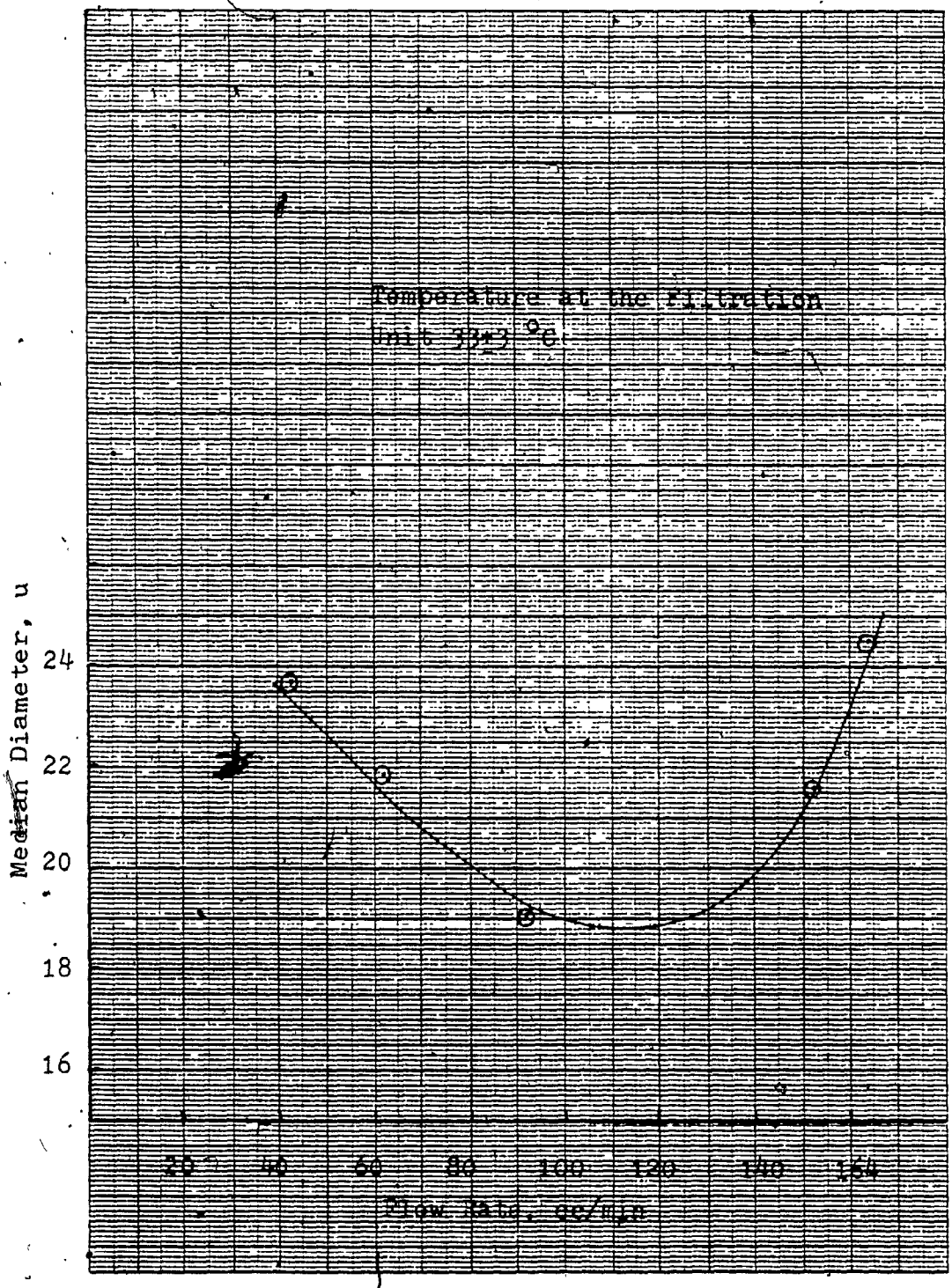

Figure 18
Effect of Liquid Flow Rate on Median Diameter

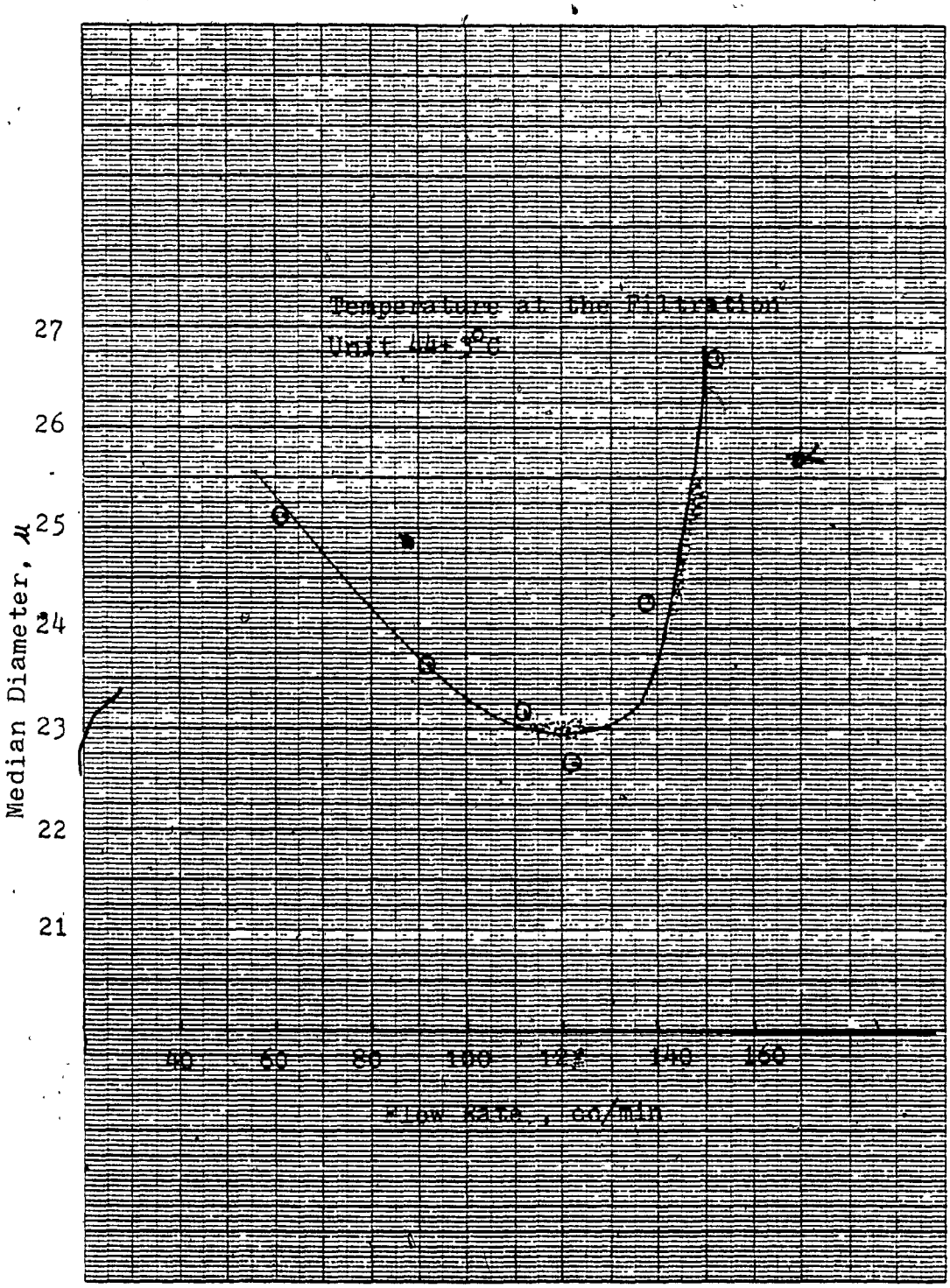

Table 5

Summary of the Effect of Temperature at the Filtration Unit for various Flow Rates on Median Diameter.

Run No.	Flow Rate cc/min	Temperature °C	Median Diameter micron	G.S.D.
I	43.0	25±3	20.42	2.17
QI	43.0	33±3	23.71	1.75
K	62.0	25±3	18.84	2.06
QK	62.0	33±3	21.88	1.74
TK	62.0	44±3	25.12	1.94
M	92.0	25±3	16.41	1.84
QM	92.0	33±3	19.05	1.80
TM	92.0	44±3	23.66	1.86
N	112.0	25±3	15.56	1.92
TN	112.0	44±3	23.17	1.84
O	122.0	25±3	15.14	1.85
TO	122.0	44±3	22.65	1.79
P	138.0	25±3	18.20	1.77
TP	138.0	44±3	24.27	1.91
QR	152.0	33±3	21.63	1.64
TR	152.0	44±3	26.61	2.07

Figure 19
Effect of Temperature at the Filtration Unit and Flow Rate on Median Diameter

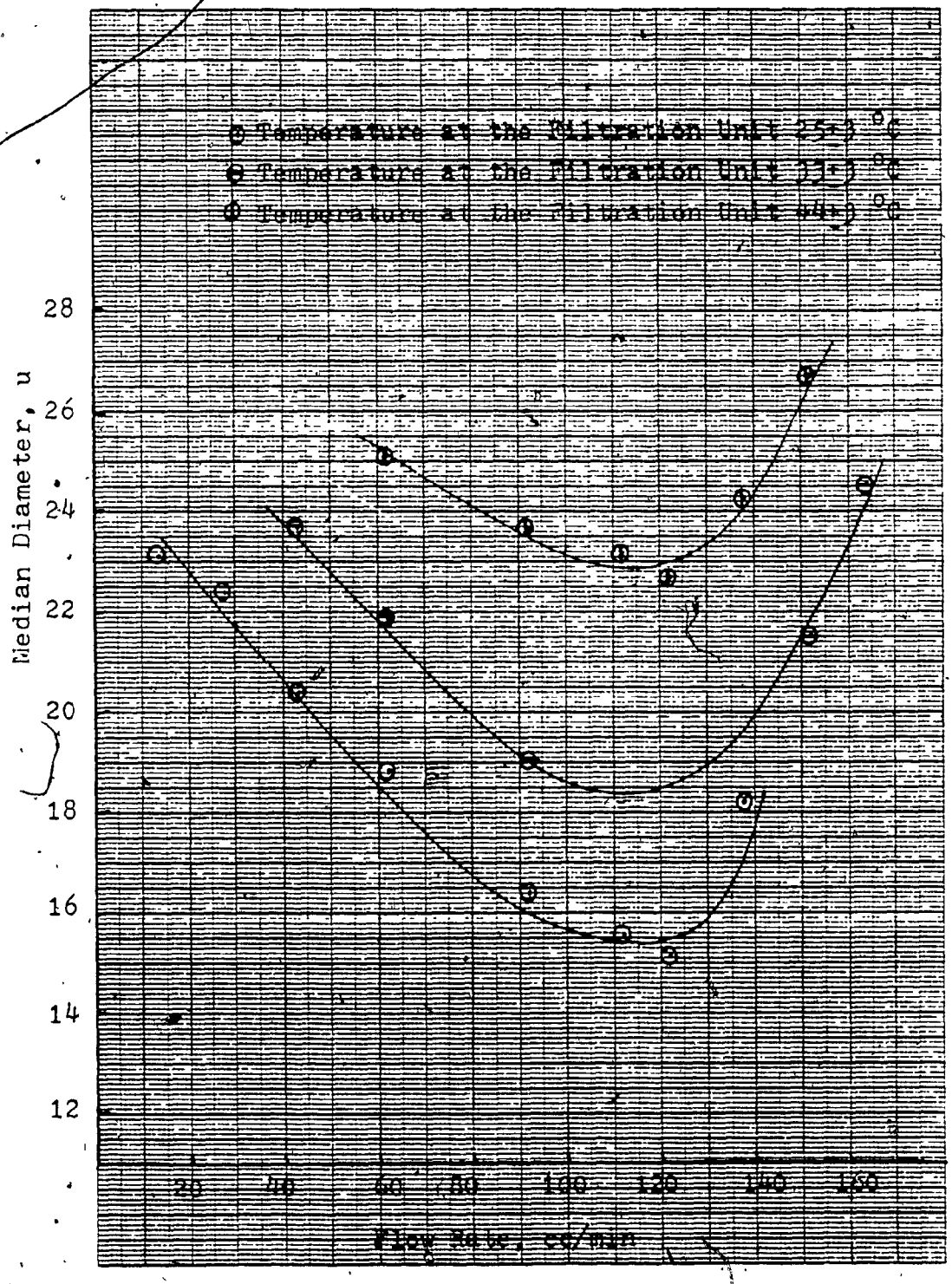

listed in the Tables C25 to C27.

Nucleation and Growth kinetics. The particle size distribution data, which were used for the calculation of nuclei population density n, along with the plots of the population density versus particle size of equation 23 have been assembled in Appendix B (Tables B1 to B17 and Figures B1 to B17). The values of the slope and intercept for each plot depicted in Figure B1 to B17 were determined by a linear least squares method. Thus, the nuclei population density n^{o} and the growth rate G were calculated. The nucleation rate then was calculated as defined by equation 28.

Tables 13 to 15 list values of the nuclei population density, the nucleation rate and the growth rate for the various runs done at different flow rates, when the temperature at the filtration unit was kept at 25 ± 3 °C, 33 ± 3 °C and 44 ± 3 °C respectively. The effect of the nucleation rate and the growth rate on median diameter of the copper powder is presented in Table 6. The geometric standard deviation for the particle size, and temperature at the filtration unit are also listed in Table 6. The data shown in Tables 13 to 15* and Table 6, are graphically depicted in Figures 20 to 26. The plot of nuclei population density versus flow rate for various runs done at 25 ± 3 °C, 33 ± 3 °C and 44 ± 3 °C is shown in Figure

*These tables are on pages 137, 138 and 139 of the thesis.

Table 6

Summary of Tables 13 to 15, Effects of Growth Rate and Nucleation Rate on Median Diameter

Run No.	Flow Rate cc/min	Temperature $^{o}C \pm 3$	N.P.Density $x10^{-7}$ no. μ^{-1}	G.Rate $x10^{3}$ μ sec^{-1}	N.Rate $x10^{-4}$ no. sec^{-1}	M.Diameter microns	G.S.D.
G	28.0	25	5.15	0.91	4.68	22.39	1.79
I	43.0	25	5.39	1.41	7.59	20.42	2.17
QI	43.0	33	1.78	1.64	2.91	23.71	1.75
K	62.0	25	6.09	2.03	12.34	18.81	2.06
QK	62.0	33	3.14	2.28	7.17	21.88	1.74
TK	62.0	44	2.41	2.27	5.48	25.12	1.94
M	92.0	25	6.31	3.00	18.94	16.41	1.84
QM	92.0	33	4.67	3.13	14.60	19.05	1.80
TM	92.0	44	2.61	3.36	8.77	23.66	1.86
N	112.0	25	7.69	3.52	27.10	15.56	1.92
TN	112.0	44	2.48	4.05	10.04	23.17	1.84
O	122.0	25	8.34	3.82	31.90	15.14	1.85
TO	122.0	44	2.31	4.50	10.39	22.65	1.79
TP	138.0	44	2.71	5.07	13.75	24.27	1.91
QR	152.0	33	2.53	5.92	14.98	21.63	1.64
TR	152.0	44	2.21	5.56	12.28	26.61	2.07
QS	164.0	33	1.24	7.08	8.77	24.55	1.69

Figure 20

Plot of Nuclei Population Density versus Flow Rate for various Runs done at 25±3, 33±3, and 44±3 °C

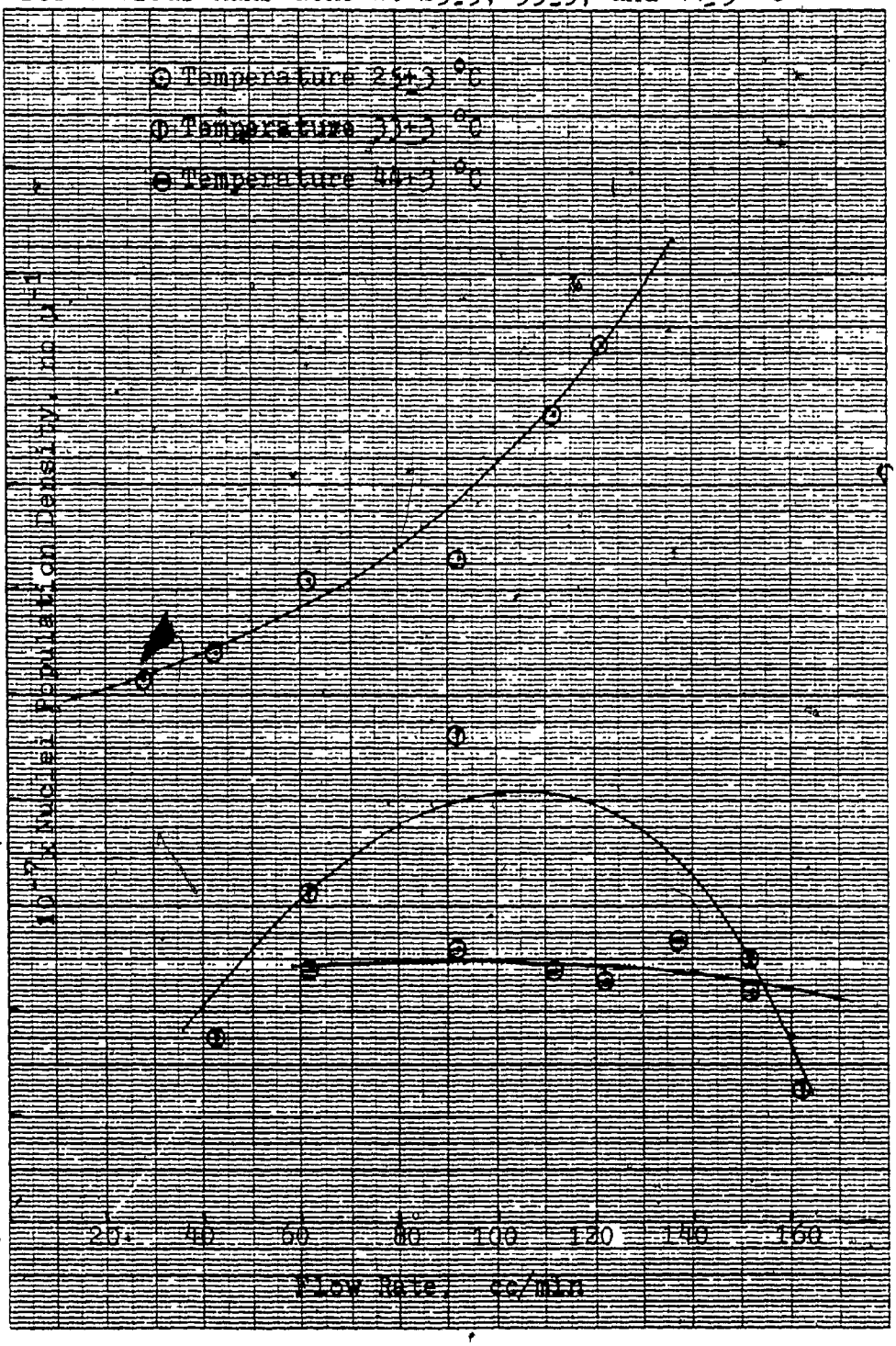

20. Figures 21 to 23 depict the effect of flow rate on the growth rate for the various runs done at the temperatures of 25 ± 3 °C, 33 ± 3 °C and 44 ± 3 °C respectively. Similarly, Figures 28 to 30 show the dependence of nucleation rate on the flow rate of the runs done at the three different temperatures at the filtration unit. The effect of temperature on the nucleation rate and the growth rate for runs K, QK and TK done at the flow rate of 62.00 cc/min, is shown in Figure 27. Figure 28 represents the effect of temperature on the nucleation rate and the growth rate for runs M, QM and TM done at the flow rate of 92.00 cc/min.

Tensile Strength. Tensile strengths of sintered specimens from copper powder produced in runs M, QS, TR, as well as of powder produced by the Cyclone technique, are presented in Tables F1 to F4. The values of the maximum force applied to the cross-sectional area of each specimen are also listed in Tables F1 to F4. The effect of median diameter and apparent density of copper powder on the tensile strength is demonstrated in Table 7 . The average deviations of the tensile strengths are also listed in the Tables F1 to F4 and Table 7.

Natural Convection. From Table D1, it is apparent that, for the natural convection apparatus, yields obtained for the same time periods were quite reproducible.

Figure 21

Plot of Growth Rate versus Flow Rate for Runs done at 25 ± 3 °C

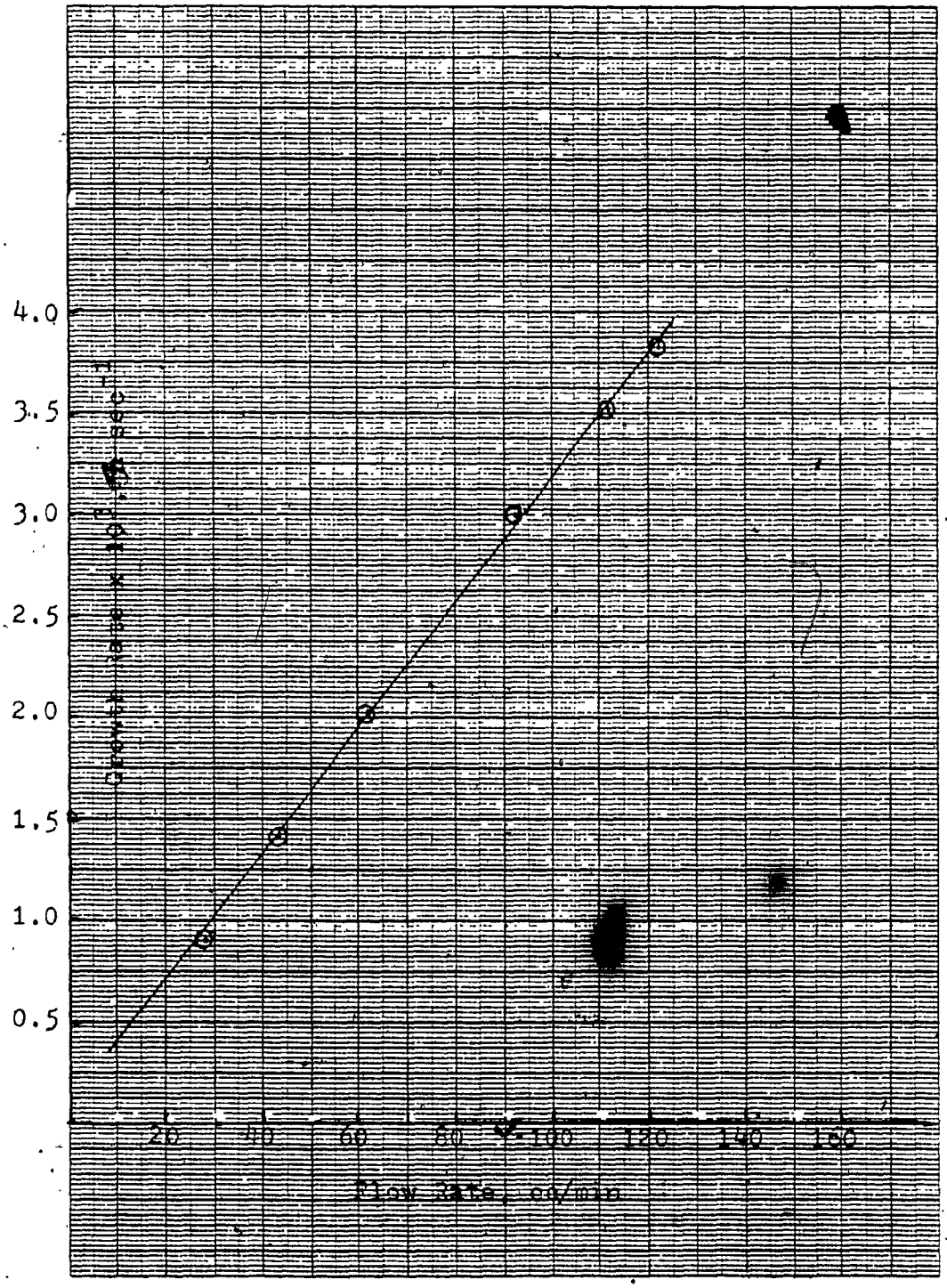

Figure 22
Plot of Growth Rate versus Flow Rate for Runs done at 33±3 °C

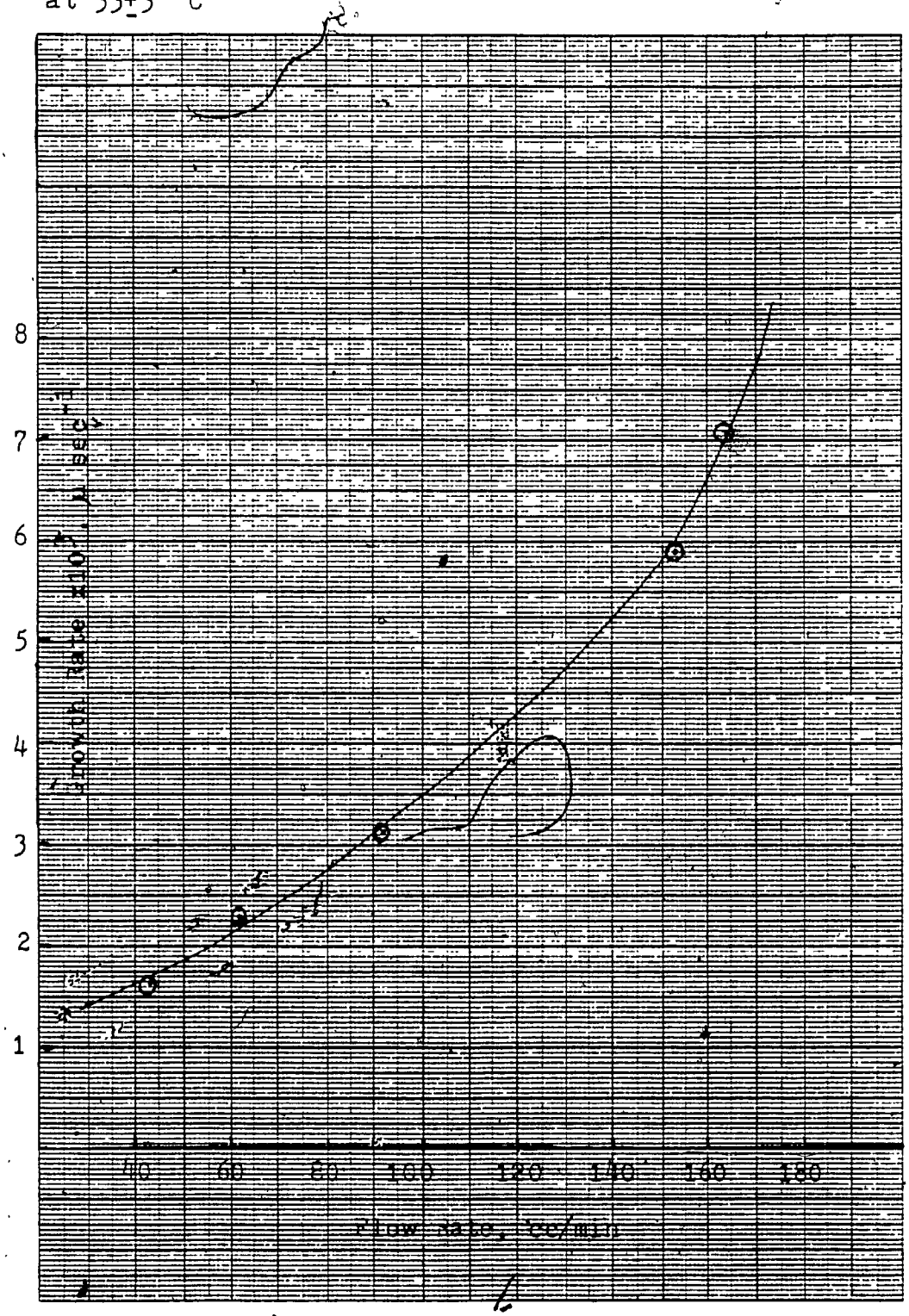

Figure 23
Plot of Growth Rate versus Flow Rate for Runs done at 44±3 °C

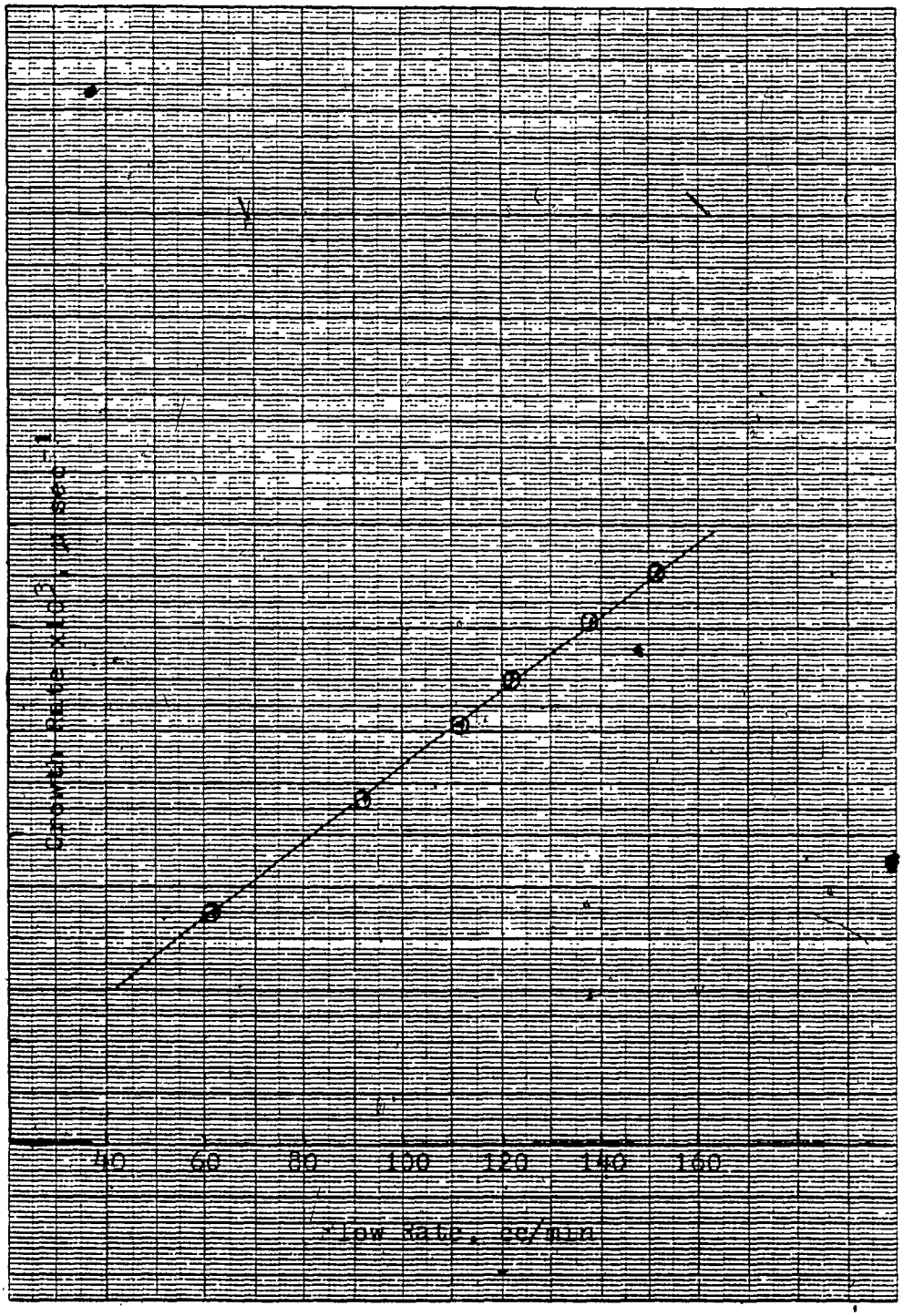

Figure 24
Plot of Nucleation Rate versus Flow Rate for Runs done at 25±3 °C

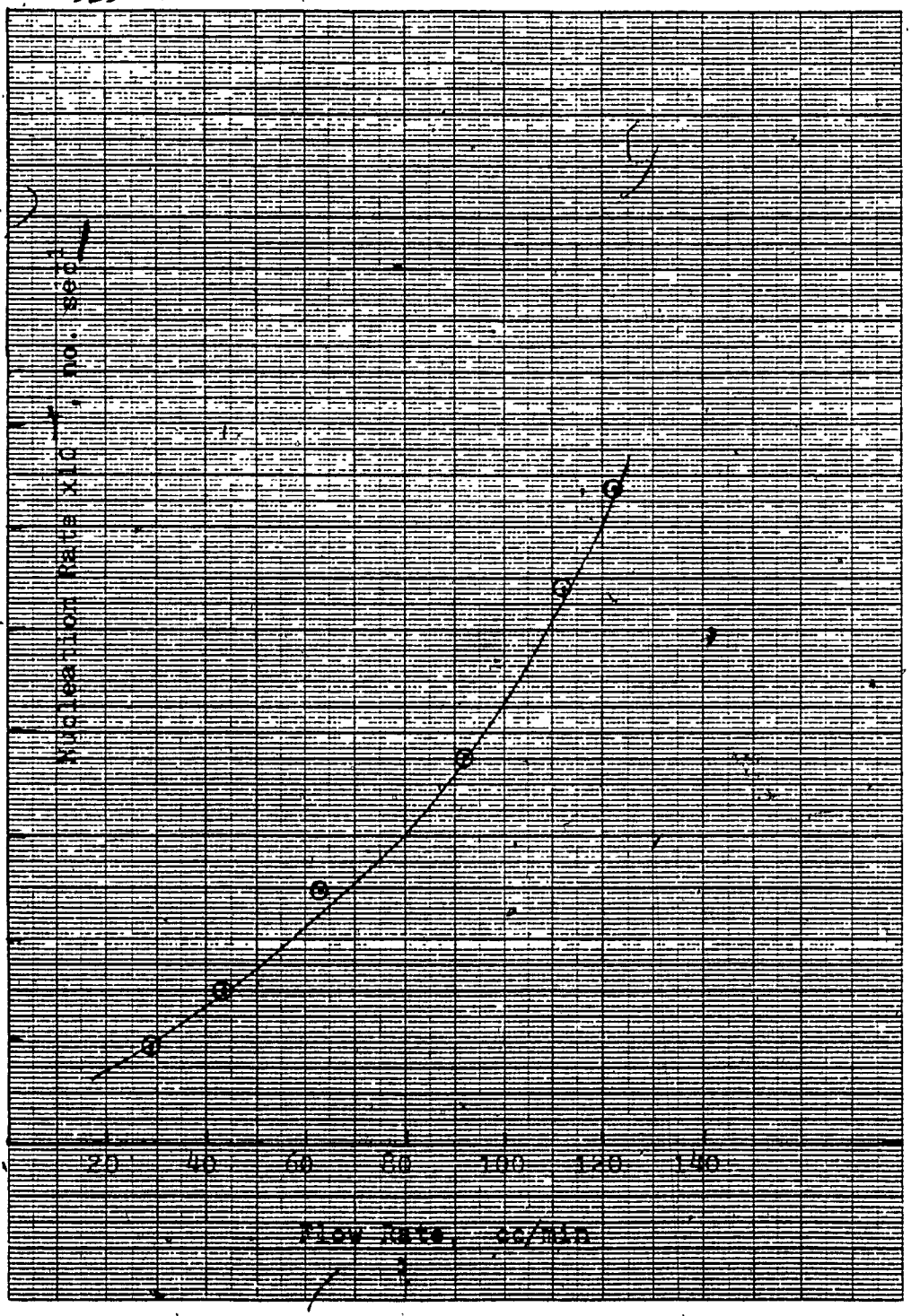

Figure 25
Plot of Nucleation Rate versus Flow Rate for Runs done at 33±3 °C

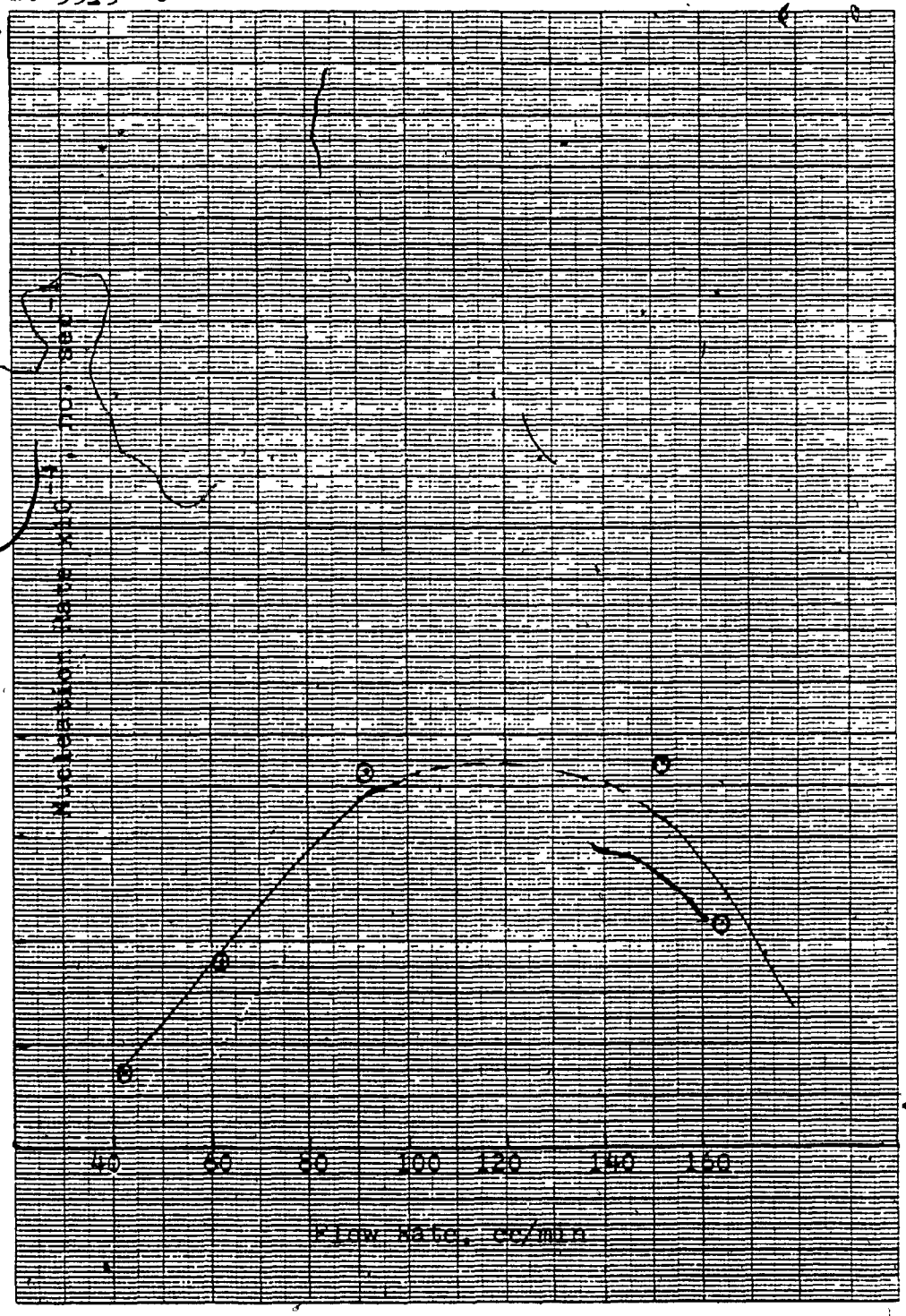

Figure 26

Plot of Nucleation Rate versus Flow Rate for Runs done at 44±3 °C

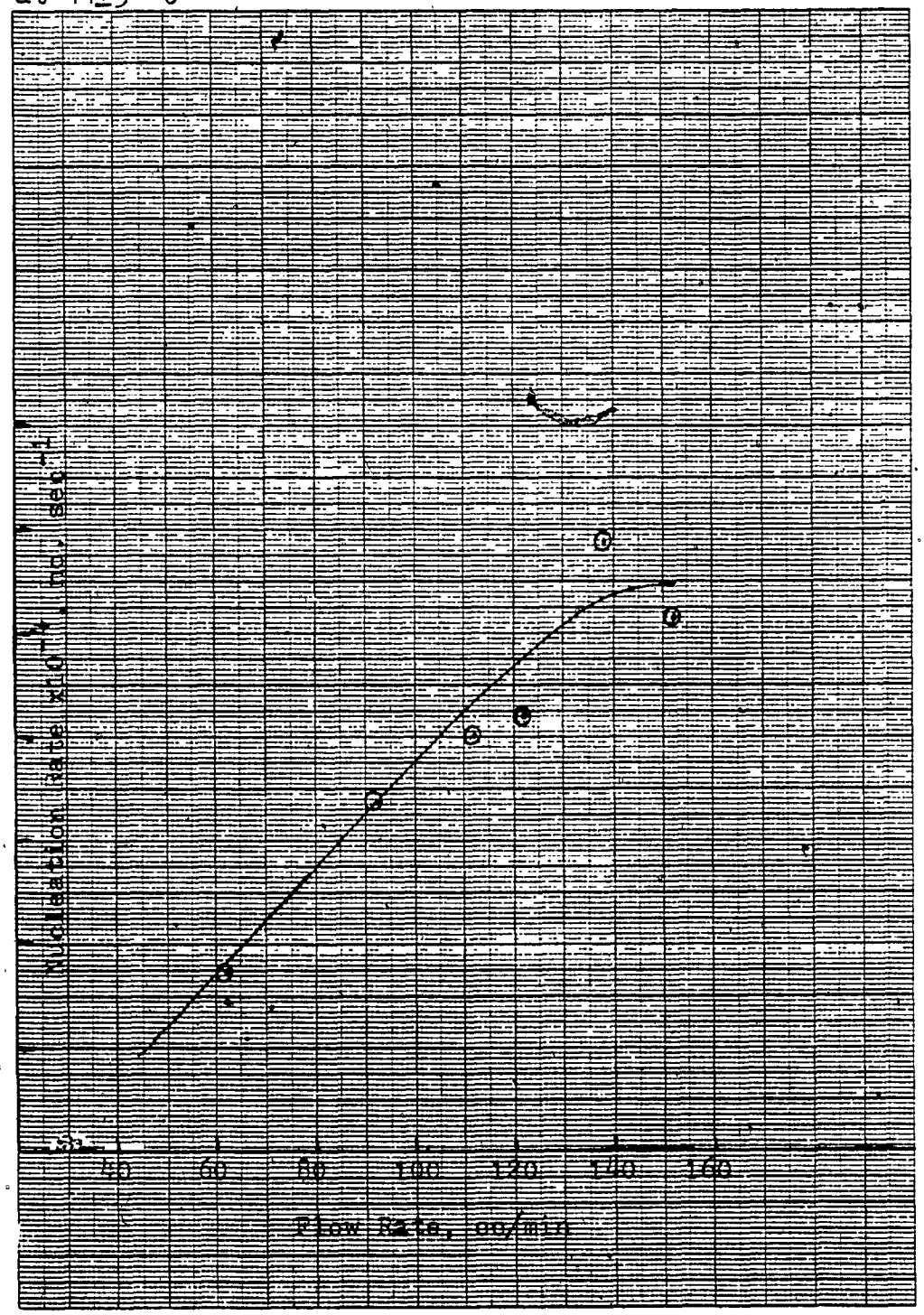

Figure 27
Plot of Growth Rate and Nucleation Rate versus Temperature for Runs K,QK,and TK at Flow Rate 62.0 cc/min.

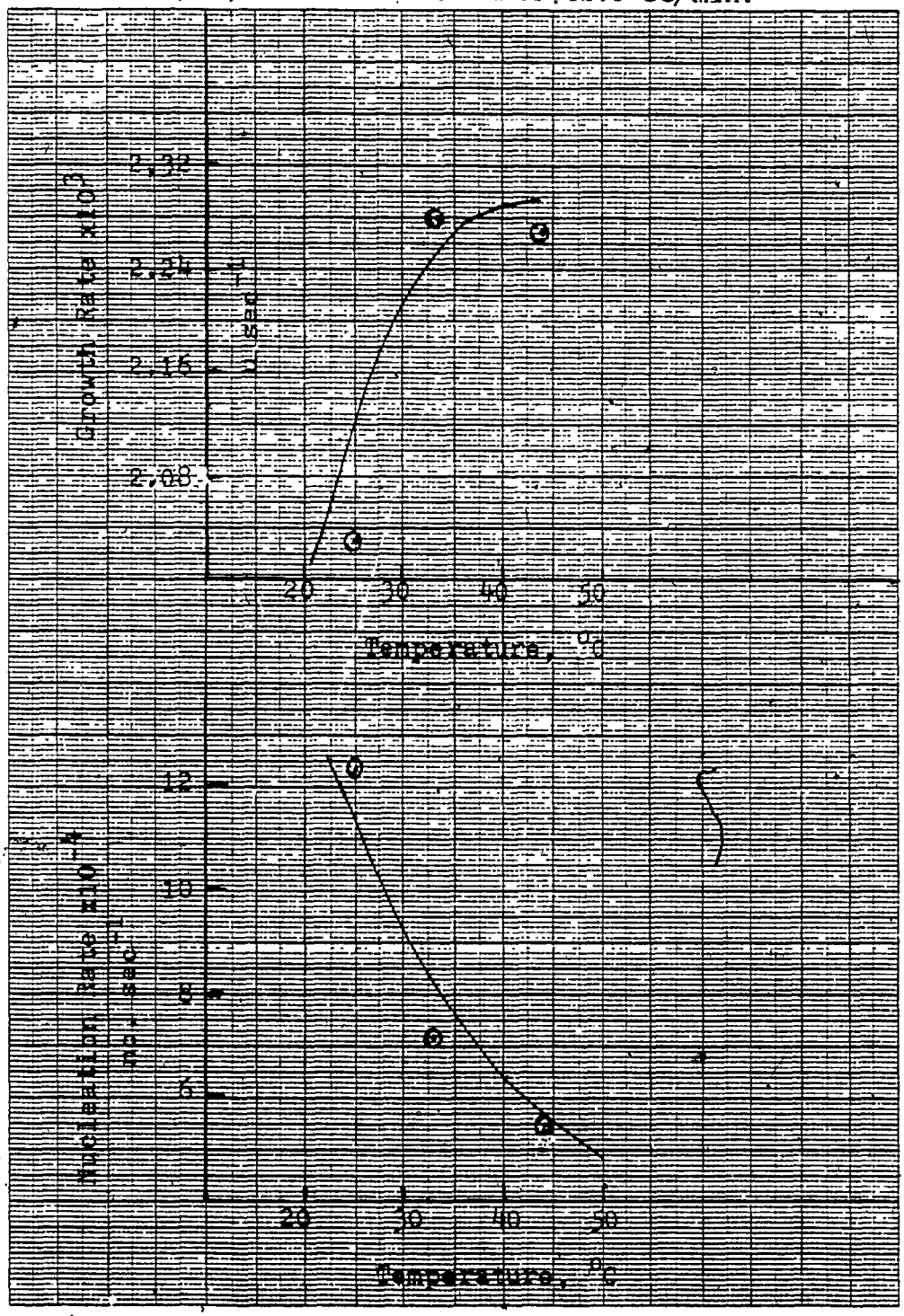

Figure 28
Plot of Growth Rate and Nucleation Rate versus Temperature for Runs M, QM, and TM done at Flow Rate 92.0 cc/min.

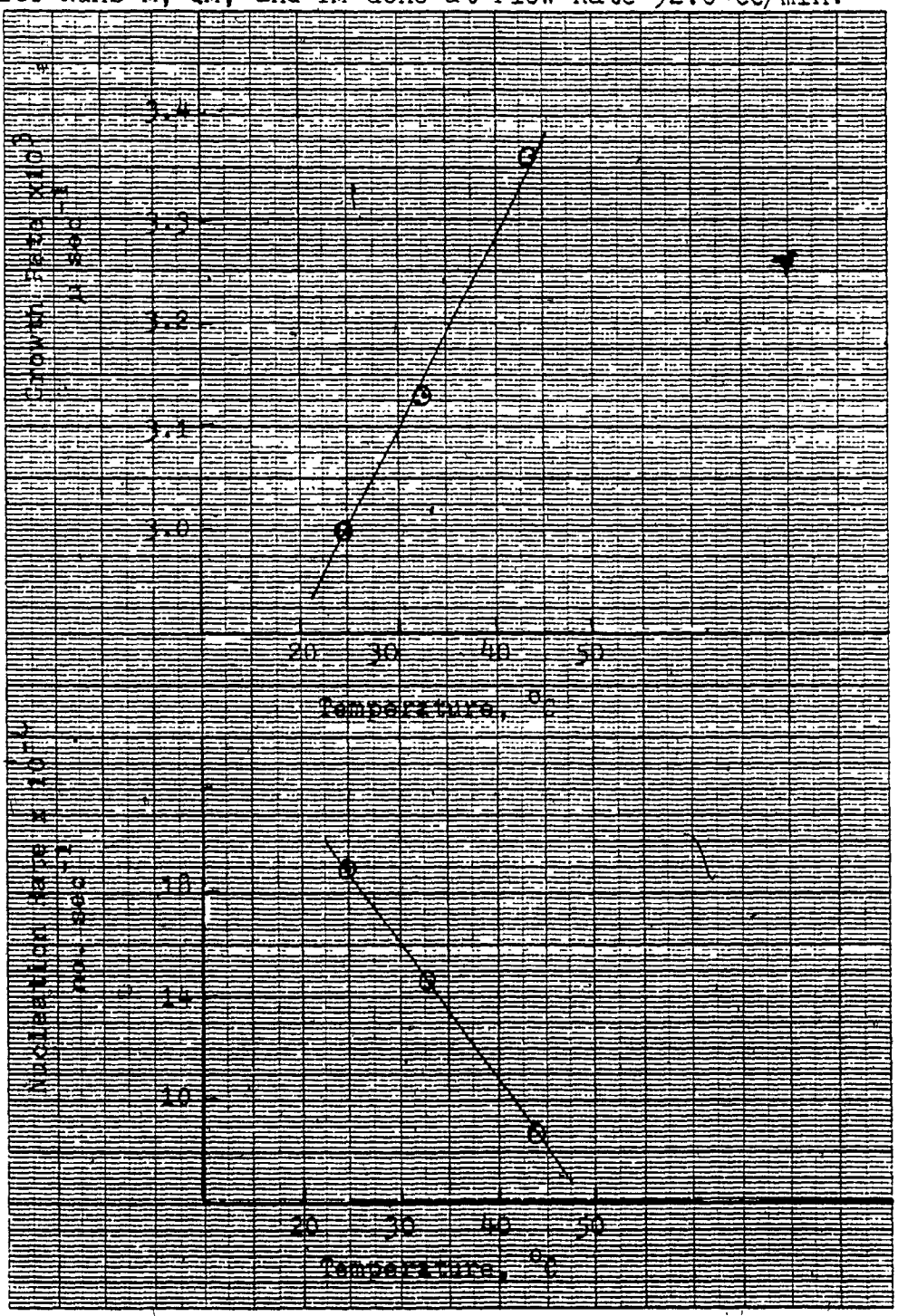

Table 7

Effect of Median Diameter of Powder on the Tensile Strength*

Powder Sample, No.	Median Diameter microns	G.S.D.	Tensile Strength psi	Ave. Dev.
TSD	29.51	1.86	18596	336
TSTR	26.61	2.07	24375	197
TSQS	24.55	1.69	23797	179
TSM	16.41	1.84	26290	89

*Summary of tables F1 to F4 (in appendix F).

A comparison of the cumulative yields obtained in this work, with those previously reported, i.e. de Ga (3) and Ufford (2), is presented in Figure 10. Over the time range plotted, all the yields vary linearly with time, and this suggests that, in these natural convection experiments, the amount of cuprous ion formed in the boiler, by the disproportionation reaction

$$Cu + Cu^{2+} \rightleftharpoons 2Cu^{+}$$

was constant, over the periods of time during which these experiments were performed. This in turn suggests that the solution in the boiler had reached thermodynamic equilibrium, at 100°C, before exiting the boiler.

Both Ufford (2) and de Ga (3) reported that after long time durations (seventy-five hours in the case of Ufford and ninety hours in the case of de Ga), the cumulative yield began to increase as the experiment proceeded. Ufford suggested that this increase in the yield was due to the increased attack of acid on the wire to form cupric ion, whereas this was ascribed by de Ga to the formation of cuprous ion, from the copper wire reaction, above the solution in the reaction vessel, with the refluxing $CuSO_4$-H_2SO_4 solution. The effect might also be due to the slow introduction into the solution of impurities,

which could act as preferential complexing agents, and hence modify the equilibrium of the disproportionation reaction.

In this work, the yield of copper powder, for run NC-1, corroborated the results reported by de Ga (3), for a similar type of apparatus, and with similar dimensions, although the yield was somewhat less than that reported by Ufford (2). As has been suggested by de Ga, the actual yield, in an apparatus working solely by natural convection, is probably considerably dependent upon the dimensions of the apparatus. Also, in this work, it was observed that copper crystals were carried past the collection flask of apparatus one, and many of these crystals were flushed back into the boiler, and hence lost because of re-oxidation. In the work reported by Ufford, these latter crystals were mostly recovered, using a secondary collection flask.

Forced Circulation (Apparatus 2). It will be recalled that apparatus 2 was equivalent in almost all respects to that used by de Ga. Copper powder yields, using this apparatus, are depicted in Figure 11 , and, as in the case of the apparatus employing natural convection, agree well with those reported by de Ga (3). Again a straight line relationship exists between the cumulative yield and the time duration of the experiment.

Effect of Salt Concentration on Yield. The data in Table D29, although limited by experimental conditions, indicate that the yield of copper powder increased by a factor of 1.7, when the copper sulphate concentration was doubled, while the sulphuric acid concentration was maintained constant. De Ga (3), using the same apparatus, found a factor of 1.8. Considering the circumstances involved in attempting to recover every last trace of powder, the slight difference in these two factors is only to be expected.

Under conditions of natural convection, Ufford (2) observed a factor of 3.2.

From the expression for the equilibrium constant of reaction (1), doubling the cupric ion concentration would suggest an increase in the cuprous ion concentration, assuming that the expression can be written in terms of concentrations, of about 1.4. Therefore, since the amount of metallic copper produced should vary directly with the cuprous ion concentration, it would be expected to change by the same factor, i.e. 1.4. But all of the investigations as indicated above, have yielded factors greater than 1.4.

The very large factor observed by Ufford was attributed to increased attack upon the copper wire by the sulphuric acid present in the solution. This would have produced the observed effect, if the attack had been sufficiently strong. Also it will be remembered that, in experiments involving natural convection, the rate of powder yield increased markedly after an intial constant rate

of production. It is conceivable that, if the rate of production were not constant, then the variation in rate of production might have inadvertently affected the calculation of the factor involved.

There is also the possibility that changing the concentration of the solution might so modify the activity coefficients of the ions involved that the factor of 1.4 could no longer be expected. Thus, with the activity coefficients[1] of the ions taken into consideration, the equilibrium constant, K, for reaction (1), for a concentration of cupric ion of 0.5M, would be given by

$$K = \frac{\left[0.062\ Cu^{+}\right]_1^2}{0.062\ Cu^{2+}} = \frac{\left[0.062\ Cu^{+}\right]_1^2}{0.5}$$

and if the cupric ion concentration is doubled from 0.5M to 1.0M, the equilibrium constant K would be

$$K = \frac{\left[0.042\ Cu^{+}\right]_2^2}{0.042\ Cu^{2+}} = 0.042\left[Cu^{+}\right]_2^2 .$$

The factor by which the cuprous ion content will increase when the cupric ion concentration is doubled can be obtained from the above expression for the equilibrium constant, for the reaction (1), as

$$\frac{\left[Cu^{+}\right]_2}{\left[Cu^{+}\right]_1} = 1.7 .$$

Hence, if the concentration is doubled, the cuprous ion content would increase by a factor of 1.7. And therefore the

[1] activity coefficients values for the solutions were taken from "Electrolyte Solutions" by Robinson and Stokes (54).

amount of metallic copper produced would change by the same factor.

Thus, it might be suggested that a factor of 1.7, for the particular ratio being calculated, is a very distinct possibility, rather than the indicated factor of 1.4 that could be expected, and that this possibility is a direct consequence of the change of activity of the ions involved as the concentrations change.

Forced circulation (Apparatus 3). Effect of Amount of Copper Wire on Yield. The effect of varying the amount of copper wire in the boiler upon the yield of powder is detailed in Table D3. At both the low and high ends of the range covered, there were slight decreases in the yield, otherwise the yield was constant within the experimental error. With only 100 grams of wire in the boiler, the decreased yield is presumably due to the lesser availability of surface area of copper metal, thereby decreasing the rate of dissolution of copper metal (50). With 1310 grams of wire in the boiler, the slight decrease in yield is presumably due to somewhat reduced flow rate of solution because of the massive bulk of the wire.

Effect of Solution Flow Rate, and of Crystallizing (Filtration) Temperature, upon Powder Yield. The effect of varying the flow rate of the solution upon the yield of copper powder can be seen in Tables D18, D24 and D25, which are themselves summaries of several other tables. The data

are also plotted, in Figures 13, 14 and 15. For all flow rates studied, other factors being constant, the powder yield appears linearly related to the solution flow rate, implies that even faster rates of flow could be tolerated by the reaction going on in the boiler. At a flow rate of 160 cc/min., the dwell time in the boiler was approximately 4.36 minutes; one wonders at what flow rate the yield would begin to deviate from linearity. Unfortunately equipment limitations set an upper limit to the flow rate at which the reaction could be studied; even at 160 cc/min the entire apparatus shook, and the danger of an inadvertent break in the glass, and the subsequent spraying of hot corrosive solution throughout the immediate neighbourhood, was somewhat daunting.

It can also be inferred, from the data of Tables D18, D24 and D25, that the powder yield is independent of the temperature in the crystallizing condenser, at least within the temperature range 25°C - 44°C. This is apparent from Figures 13, 14 and 15, since the regression coefficients of the three lines are almost identical. This point can also be seen from Table 8 , where several representative experiments are compared; and it is immediately apparent that within experimental error, the yield is unaffected by the temperature within the crystallizer. This result was somewhat surprising; but it might well be

Table 8

Effect of Temperature on the Copper Powder Yield

Run No.	Flow Rate cc/min.	Temperature °C	Yield g/hr
I	43.0	25±3	0.9756
QI	43.0	33±3	0.9867
K	62.0	25±3	1.4666
QK	62.0	33±3	1.4187
TK	62.0	44±3	1.5439
M	92.0	25±3	2.1154
QM	92.0	33±3	2.1857
TM	92.0	44±3	2.1815
QR	152.0	33±3	3.3774
1TR	152.0	44±3	3.3602

extremely useful, if the process were ever to be developed commercially.

Effect of Solution Flow Rate, and of Crystallizing Temperature upon Average Particle Size. The effect of varying the flow rate of the solution upon the average particle size is detailed in Tables E1, E2 and E3, and summarized in Table 5. The data are also shown, ultimately, in Figure 19. It is apparent that the particle size, for any given crystallizing temperature, decreases with an increase in solution flow rate, until a flow rate of approximately 115 cc/min. is reached. This decrease is to be expected, because the faster the flow rate the smaller the time allowed for a given nucleus to grow, within the cooling condenser, before it was removed from solution via the filter paper. This type of behaviour could be said to have been anticipated in this work, on the basis of data previously reported by de Ga (3).

But what was not at all expected was the behaviour, that set in at solution flow rates above 115-120 cc/min. As shown in Figure 19, above this roughly constant flow rate of solution, the particle size began to increase as the solution flow rate increased. This also can be seen from the Tables 9 , 10 and 11, that the progressive shift in particle size becomes positive as the flow rate of the solution increased above 115-120 cc/min. As may be seen

Table 9

Progressive Shift in Particle Size as Flow Rate Increases

(Temperature at the filtration unit 25±3°C)

Run No.	Flow Rate cc/min	Median Diameter microns	Progressive Shift ± %
D	13.5	23.11	—
G	28.0	22.39	-3.12
I	43.0	20.42	-11.64
K	62.0	18.84	-18.48
M	92.0	16.41	-29.00
N	112.0	15.56	-32.70
O	122.0	15.14	-34.50
P	138.0	18.20	+20.21*

* Progressive shift in particle size calculated from the base value of particle size 15.14 μ .

Table 10

Progressive Shift in Particle Size as Flow Rate Increases

(Temperature at the filtration unit 33±3°C)

Run No.	Flow Rate cc/min	Median Diameter microns	Progressive Shift ± %
QI	43.0	23.71	
QK	62.0	21.88	-7.72
QM	92.0	19.05	-19.65
QR	152.0	21.55	+13.54*
QS	164.0	24.55	+28.90*

*Progressive shift in the particle size calculated from base value of particle size 19.05 μ .

Table 11

Progressive Shift in Particle Size as Flow Rate Increases

(Temperature at the filtration unit 44±3 °C)

Run No.	Flow Rate cc/min	Median Diameter microns	Progressive Shift ± %
TK	62.0	25.12	—
TM	92.0	23.66	-5.81
TN	112.0	23.17	-7.76
TO	122.0	22.65	-9.83
TP	138.0	24.27	+7.15*
TR	152.0	26.61	+17.48*

*Progressive shift in the particle size calculated from the base value of particle size 22.65 μ .

from Figure 19, this behaviour was observed at all three condenser temperatures at which data were collected, and, as may be seen from Tables 9, 10 and 11, the percentage increases in particle size were approximately the same.

Regardless of the flow rate of solution, Figure 19 and Table 12 show clearly that the average particle size of the copper powder increased, as the temperature of the cooling condenser was increased, other conditions being held constant. In general, crystals subject to supersaturation will grow more rapidly as the temperature is increased, and consequently the behaviour observed in Figure 19 was to have been expected. This behaviour was evident in the work reported in this thesis. In all the experiments it was noted that the larger crystals tended to grow at the top of the cooling condenser, where the hot solution entered from the reaction vessel.

For solution flow rates of above 116-120 cc/min., it is possible that the increase in particle size is due to the particular design chosen for the apparatus. And it is possible that the cooling condenser was not being operated at a sufficiently fast flow rate of cooling water to ensure an almost constant temperature within the condenser. As an example, for one series of experiments with the cooling condenser at 25 $\pm$ 3°C, the temperature, as measured at the filtration unit, could be maintained at 23°C,

Table 12

Progressive Shift in the Particle Size as Temperature at the Filtration Unit Increases

Run No.	Flow Rate cc/min	Temperature °C	Median Diameter microns	Progressive Shift, %
I	43.0	25±3	20.42	—
QI	43.0	33±3	23.71	+16.11
K	62.0	25±3	18.84	—
QK	62.0	33±3	21.88	+16.32
TK	62.0	44±3	25.12	+33.54
M	92.0	25±3	16.41	—
QM	92.0	33±3	19.05	+16.09
TM	92.0	44±3	23.66	+44.18
N	112.0	25±3	15.56	—
TN	112.0	44±3	23.17	+48.91
O	122.0	25±3	15.14	—
TO	122.0	44±3	22.65	+49.60
P	138.0	25±3	18.20	—
TP	138.0	44±3	24.27	+33.35

below a solution flow rate of 92 cc/min. Above this flow rate however, the average temperature at the filtration unit began to rise, and, at a solution flow rate of 122 cc/min., was about 27°C. At a solution flow rate of 138 cc/min., the temperature was about 28°C.

A similar type of behaviour was observed for the other two temperatures at which the cooling condenser was operated. Thus, for an average temperature of 44 ± 3°C, the temperature at the filtration unit was about 41°C, when the solution flow rate was at or below 92 cc/min. However, for the solution flow rate range 122-152 cc/min., the temperature at the filtration unit was about 47°C.

All these numbers can serve only to show that the temperature of the cooling condenser was somewhat variable during the series of experiments. But it is very possible that the increased particle size above about 115-120 cc/min. can be attributed to this fact. It also suggests strongly that if any further work is done in this system, then a considerably better cooling system should be used, if precise control of the particle size of the powder is to be achieved.

The overall variation in powder particle size, as the temperature of the precipitating condenser, and the solution flow rate, were varied, can also at least in part, be attributed to the physical behaviour of the system

under study, and this aspect of the problem will be discussed in the next section.

Effects of Nucleation Rate and Growth Rate on Average Particle Size. The effect of nucleation rate and growth rate on the particle size can be seen in Tables 13, 14 and 15. On the basis of the data in these tables, the effect of progressive shift in growth rate and nucleation rate on the progressive shift of particle size is shown in Table 16. As shown in Table 13, when the temperature is kept constant, growth rate and nucleation rate increase with increasing flow rate. This trend of increasing growth rate and nucleation rate with increasing flow rate is graphically depicted in Figures 21 and 24 respectively. The data in Tables 14 and 15 show that the growth rate increases with the increasing flow rate, while the nucleation rate also increases except at the higher values of the flow rate where the nucleation rate starts decreasing, and the particle size increasing. The data in Table 14 and 15 are also plotted in Figures 22, 23, 25 and 26. Figures 22 and 23 show the increases in the growth rate with increasing flow rate, for all the flow rates studied, keeping other conditions constant. The variations of nucleation rate with increasing flow rate, at two other temperatures, are depicted in Figures 25 and 26.

The trend of decrease in the particle size with the

Table 13

Nuclei Population Density, Growth Rate and Nucleation Rate at various Flow Rates

(Temperature at the filtration unit 25±3°C)

Run No.	Flow Rate cc/min	Nuclei Population Density $x10^{-7}$ no. μ^{-1}	Growth Rate $x10^{3}$ μ sec^{-1}	Nucleation Rate $x10^{-4}$ no. sec^{-1}
G	28.0	5.15	0.91	4.68
I	43.0	5.39	1.41	7.59
K	62.0	6.09	2.03	12.34
M	92.0	6.31	3.00	18.94
N	112.0	7.69	3.52	27.10
O	122.0	8.34	3.82	31.90

Table 14

Nuclei Population Density, Growth Rate and Nucleation Rate at various Flow Rate

(Temperature at the filtration unit 33±3°C)

Run No.	Flow Rate cc/min	Nuclei Population Density $x10^{-7}$ no. μ^{-1}	Growth Rate $x10^{3}$ μ sec^{-1}	Nucleation Rate $x10^{-4}$ no. sec^{-1}
QI	43.0	1.78	1.64	2.91
QK	62.0	3.14	2.28	7.17
QM	92.0	4.67	3.13	14.60
QR	152.0	2.53	5.92	14.98
QS	164.0	1.24	7.08	8.77

Table 15

Nuclei Population Density, Growth Rate and Nucleation Rate at various Flow Rates

(Temperature at the filtration unit 44±3°C)

Run No.	Flow rate cc/min	Nuclei Population Density $x10^{-7}$ no. μ^{-1}	Growth Rate $x10^{3}$ μ sec^{-1}	Nucleation Rate $x10^{-4}$ no. sec^{-1}
TK	62.0	2.41	2.27	5.48
TM	92.0	2.61	3.36	8.77
TN	112.0	2.48	4.05	10.04
TO	122.0	2.31	4.50	10.39
TP	138.0	2.71	5.07	13.75
TR	152.0	2.21	5.56	12.28

Table 16

Comparison of Progressive Shift of Particle Size and that of Growth Rate and Nucleation Rate

Run No.	Flow Rate cc/min	Temperature °C±3	Progressive Shift G.Rate ±%	Progressive Shift N.Rate ±%	Median Diameter micron	Progressive Shift Particle Size ±%
I	43.0	25	—	—	20.42	—
QI	43.0	33	+16.31	-61.66	23.71	+16.11
K	62.0	25	—	—	18.81	—
QK	62.0	33	+12.31	-41.90	21.88	+16.32
TK	62.0	44	+11.82	-55.60	25.12	+33.54
M	92.0	25	—	—	16.41	—
QM	92.0	33	+4.30	-22.91	19.05	+16.09
TM	92.0	44	+12.00	-53.70	23.66	+44.18
N	112.0	25	—	—	15.56	—
TN	112.0	44	+15.06	-62.95	23.17	+48.91
O	122.0	25	—	—	15.14	—
TO	122.0	44	+17.80	-67.43	22.65	+49.60
QR	152.0	33	—	—	21.63	—
TR	152.0	44	-6.08	-18.02	26.61	+23.02

increases in the flow rate is shown in Tables 13, 14 and 15. Increases in both the nucleation and growth rates were observed. But it is probable that the increase in the nucleation rate overshadowed the increase in the growth rate, and this would explain the decrease in particle size. This is apparent from Table 13, because when the flow rate was increased from 28 cc/min. to 92 cc/min., while other conditions were held constant, the growth rate increased by a factor of 3.30, while the nucleation rate was increased 4.05 times. Similarly, for a temperature at the filtration unit of $33\pm3^{o}C$ (Table 14), when the flow rate was increased from 43 cc/min. to 92 cc/min., the growth rate increased by a factor of about 2, whereas the nucleation rate increased by 5 times.

At the highest flow rate, i.e. above 150 cc/min., (Tables 14, 15) the growth rate increases while the nucleation rate decreases, and hence the particle size increases. This is because a decrease in the nucleation rate would result in an easier growth of the already existing nuclei, rather than further nucleation and hence the particle size would increase. The effect is shown in Tables 14 and 15.

The effect of nucleation and growth rate on the average particle size, as the temperature of the crystallization

increased, other conditions being held constant, can be seen in Table 6 . The effect of progressive shift in growth rate and nucleation rate on the particle size is presented in Table 16. Thus, it can be seen from Table 16, for the experiment done at 62 cc/min., that when the temperature was increased from 25±3 °C to 33±3 °C, progressive shifts of about +12% and about -41% took place in growth rate and nucleation rate respectively; and a progressive shift of the particle size was about +16%.

At the same flow rate, when the temperature was raised to 44±3 °C, progressive shifts of about +12% and -55% took place in the growth rate and nucleation rate respectively, while a progressive shift of about +33% took place in the particle size. A similar type of behaviour was observed for the other experiments, and also, as may be seen from Table 16, the progressive shifts in the particle sizes were approximately the same.

Furthermore, it is evident from Figure 27 that at 62 cc/min., as the temperature of crystallization is increased, increases in the growth rate take place. A similar type of behaviour can also be observed in Figure 28 , which represents the plot of growth rate and nucleation rate versus the temperature, for runs done at 92 cc/min.. Again decreases in the nucleation rate as the temperature increases, and the increases in the particle size, are

attributed to the increases in the growth rate. Decreases in the nucleation rate would lead to the growth of the already-existing nuclei more easily than further nucleation and hence to increased particle size.

Effect of Median Diameter of Copper Powder on Apparent Density. Tables C25, C26 and C27, show the effect of the median diameter of the copper powder upon the apparent density of the powder, and the data in these tables are summarized in Table 17. It can be seen from Table C25 that decreasing the particle size about 1.54 times (from 23.31 to 15.14 μ) results in the apparent density increasing only about 1.07 times. Similarly, small increases in the apparent density can be observed from Table C26. When the particle size decreased from 24.55 to 19.05 μ, the apparent density increased by a factor of 1.04. The data in Table C27 that the apparent density increased only about 1.03 times, when the particle size decreased by a factor of 1.17, i.e., a particle size decreases from 26.61 to 22.65 μ. It can be also seen from Table 17, that no significant changes in the apparent density took place, when the particle size was varied.

In general, with metal powders, apparent density decreases (significantly) with decreasing particle size, since a smaller particle will reduce the

Table 17

Summary of Tables C25 to C27, Effect of Median Diameter of Powder on Apparent Density

Run No.	Flow Rate cc/min	Temperature °C+3	Median Diameter microns	Apparent Density, g/cm³ a	b	c
D	13.5	25	23.31	3.34+0.01	3.35+0.01	
G	28.0	25	22.39	3.37+0.01	3.38+0.01	
I	43.0	25	20.42	3.38+0.01	3.40+0.01	
QI	43.0	33	23.71	3.34+0.01		
K	62.0	25	18.84	3.45+0.01		
QK	62.0	33	21.88	3.39+0.01		
TK	62.0	44	25.12	3.31+0.01		
M	92.0	25	16.41	3.46+0.01	3.46+0.01	3.45+0.01
QM	92.0	33	19.05	3.45+0.01		
TM	92.0	44	23.66	3.33+0.01	3.34+0.01	
N	112.0	25	15.56	3.51+0.02	3.51+0.01	
TN	112.0	44	23.17	3.34+0.01		
O	122.0	25	15.14	3.56+0.01	3.58+0.02	
TO	122.0	44	22.65	3.37+0.01		
P	138.0	25	18.20	3.45+0.02	3.44+0.01	
TP	138.0	44	24.27	3.32+0.01	3.31+0.01	
QR	152.0	33	21.63	3.38+0.01	3.41+0.01	
TR	152.0	44	26.60	3.29+0.02	3.29+0.02	3.25+0.01
QS	164.0	33	24.55	3.31+0.01	3.31+0.01	3.29+0.02

[a]Apparent Density determined using Density Cup Number Y.

[b]Apparent Density determined using Density Cup Number Z.

[c]Apparent Density determined using Density Cup Number X.

ability of the particle to settle efficiently (51). But there were no significant changes in the apparent density observed in the work reported in this thesis. However, the differences in the particle sizes of the powders were probably not large enough to reflect any significant changes in the value of the apparent density (52).

Effect of Median Diameter of Copper Powder on Tensile Strength. The effect of median diameter on tensile strength is shown in Table 7 , which is summary of Tables F1 to F4. Percentage increases in the tensile strength of sintered specimens of copper powder produced as compared with that of commercially available powder (Cyclone technique) are presented in Table 18. It can be seen, from Tables 7 and 18, that decreasing the particle size from 29.51 to 26.61 μ results in an increase in the tensile strength of about 31% . Further decrease in the particle size, from 26.61 to 24.55 μ , results in an insignificant change in the tensile strength. The data in Table 7 show that when the particle size decreases from 24.55 to 16.41 μ, the tensile strength increases about 10%. It can also be seen from Table 18 that a higher tensile strength of powder, produced in the work reported in this thesis, was obtained when compared with that of the sample of commercial powder.

Table 7 shows that for the powder obtained in this work, the tensile strengths of the sinter specimens

Table 18

Percentage Increases in the Tensile Strength of Sintered Specimen from Copper Powders Produced and that of Cyclone Technique

Tensile Specimen Series No.	Median Diameter, μ	Tensile Strength psi	Average Deviation	Percentage Increases
TSD(Cyclone)	29.51	18596	336	—
TSTR	26.61	24375	197	31.08
TSQS	24.55	23797	179	27.97
TSM	16.41	26290	89	41.37

increased with decreasing particle size, all the samples being subject to the same sintering conditions. These results can be corroborated to some extent by the work of Nyce and Shafer (53), who published some data, using copper powder, which indicated that the tensile strength of a sinter specimen increased as the particle size decreased. But their data are quite incomplete, and can not be compared directly with the work reported in this thesis.

Increases in the tensile strengths of the specimens with decreasing particle size, other conditions being held constant, are logical, as a decreasing particle size would suggest a greater driving force for sintering, because of the possibility of more pore-solid interfacial area in the sinter mass. Furthermore, with a smaller particle size there would be greater interparticle contact i.e. number of necks and hence more path for volume diffusion. A small particle size may also correspond to smaller internal grain size, thus promoting grain boundary diffusion transport (55). Consequently, reducing the particle size should result in an increased tensile strength. From Table 7 it can be seen that a smaller difference in the particle size probably led to the insignificant change in the tensile strength, as the particle size decreased from 26.61 to 24.55 μ.

A further factor that could contribute to higher tensile strength obtained in the cases of TSTR TSQS and TSM powders as compared with TSD powder (Table 18), is the

oxide layer observed on the TSD powder. This oxide layer would hinder the interparticle contact and neck growth during the compactation and sintering.

Copper powder, in pure form or preblended with other elements, has been used industrially for many years. Its most significant commercial application has been in self-lubricating bearings and this application accounts for approximately 75% of granular copper powder consumed. Other important applications include pure copper for the electrical and electronics industry, P/M friction materials, structural parts, brushes and filters. It can be seen from Table 18, that the copper powder produced by the technique reported in this thesis, shows higher physical properties, when compared to the commercial powder. Because of the unique properties of pure copper powder produced by this technique, due to the absence of an oxide layer, it is conceivable that electrical and mechanical parts could be made by P/M methods which would have higher mechanical, electrical and thermal properties than are available at present.

SUMMARY AND CONTRIBUTION TO KNOWLEDGE

1. The yield and size of copper powder produced by a disproportionation reaction in continuously circulating aqueous cupric sulphte - sulphuric acid solutions were studied as a function of flow rate of solution, duration of run, salt concentration, mass of copper wire and temperature of crystallization.

2. Size analysis of the powder was done using the Andreasen pipette method. The apparatus as purchased was modified, to give a much more easily handled device, and tests showed the modified pipette to have an error of less than 2%.

3. Powder yield increased linearly with increasing flow rate, and showed no deviation from linearity even at the highest flow rate studied (160 cc/min.). This was to be expected, since more cupric ions would come into contact with copper wire as the flow rate was increased, and hence the yield would increase.

4. The increase in the yield with increasing cupric sulphate concentration was due to the direct dependence of the rate of production on the equilibrium constant for the reaction. The rate production was found to increase by a factor as predicted from the equilibrium ratio of cuprous to cupric ion when the activity coefficents of the cupric

ions were taken into consideration.

5. A slight decrease in the yield, at both the low and high ends of the range covered, was observed, when the effect of mass of copper on the yield was studied. This was explained in terms of lesser availability of surface area of copper metal and reduced flow rate of solution because of the massive bulk of the wire respectively.

6. The crystallization of the copper powder was studied at temperatures of 25±3 °C, 33±3 °C and 44±3 °C. At these three temperatures, the powder yield was independent of temperature.

7. The particle size of the powder was found to be dependent upon the temperature of crystallization, in that increasing the temperature of crystallization, at a given flow rate, increased the particle size. This was explained on the basis that the growth of already existing nuclei becomes easier than further nucleation, as the temperature increases. This was shown by a mathematical analysis of growth and nucleation kinetics, since it could be calculated that as the nucleation rate decreased, the growth rate increased, and hence an increased particle size would result.

8. Increases in the flow rate led to decreases in the particle size, until a flow rate of approximately 115 cc/min. was reached. This was explained in terms of the residence time allowed for a given nucleus to grow. But

above a flow rate of approximately 115-120 cc/min., the particle size began to increase, as the flow rate was increased. This was explained on the basis that at these large flow rates, the temperature of crystallization would increase somewhat, because of the limitations of the apparatus.

9. The effect of particle size on the apparent density was not significant, as the differences in the particle sizes of the powder were not large enough to reflect any significant changes in the values of the apparent density.

10. The tensile strengths of sintered specimens increased as the particle size decreased. This was explained in terms of interparticle contact and number of necks during the processes of compactation and sintering. Higher tensile strengths were obtained with powder produced in this investigation, as compared with powder produced commercially, and this was attributed to the smaller size of particle, and the absence of an oxide layer.

SUGGESTIONS FOR FURTHER WORK

Listed below are topics that can be investigated by extensions of the techniques used in this research.

1. The crystal habits of the copper crystals obtained in this research could be studied and compared with Ufford's results (2), which were obtained in the absence of controlled flow speed and cooling temperature.

2. Ufford (2) has grown silver and gold crystals by the dynamic method. An extension of this technique to the precipitation of other metal crystals might well prove interesting.

3. This technique might now be attempted to extract copper from its ore as copper powder: it might also be useful in the recovery of copper from scrap metal.

4. To obtain yield at higher flow rates it would be easier to heat the circulating solution, if two reaction vessels in series are used between constant level and cooling condenser units. Thus the warm circulating solution entering the second reaction vessel would not need so many meeker type gas burners to boil the solution and therefor it would lessen the danger of any breakage of the apparatus as was a possibility in this research.

5. For higher flow rate, it was observed the variation in the temperature of the cooling condenser. In order to investigate the effect of higher flow rate

(> 120 cc/min.) on the particle size, new cooling system should be designed.

6. The effect of additives (organic molecules or inorganic ions) on the particle size would also be an interesting topic of research.

7. It would be interesting to compare the size distributions of other metals, prepared under conditions similar to those detailed in this thesis, with the size distributions of copper powder studied.

REFERENCES

1. Berzelius J. J., Ann. Chim. Phys. 2 (2), 228 (1816); as given in reference 2.
2. Ufford J. R., Ph. D. Thesis, McGill University, Montreal, 1960.
3. de Ga C. F., M. Sc. Thesis, Sir George Williams University, Montreal, 1972.
4. Hiller F., Liebig Ann. 85, 253 (1853); Mallet J., Ann. J. Sc. 30, 253 (1860); Forster F. and Seidel O., Zeit. anorg. Chem. 14, 106 (1897); all quoted in reference 2.
5. Recoura A., Comp. Rend. 148, 1105 (1909); quoted in reference 2.
6. Geneslay G., Bull. soc. chim. France 4 (5), 111-14 (1937); as quoted in Sneed M., Maynard J. and Brasted R., "Comperhensive Inorganic Chemistry", Vol. II, D. Van Nostrand Co., Inc., Princeton, New Jersey, 1954, p 85.
7. Abel E., Zeit. anorg. Chem. 26, 386 (1901), quoted in reference 2.
8. Luther R., Zeit. fur Phys. Chem. 34, 448 (1900), ibid. 36, 396 (1901); reported in reference 2.
9. Fenwick F., J. Am . Chem. Soc. 48, 860-70 (1926).
10. Bodlander and Storebeck, Z. anorg. chem. 31, 458 (1902); quoted in reference 2.
11. Heinerth E., Z. Elecktrochem. 37, 61-76 (1931); as quoted in reference 2 and C. A. 25, 2646 (1931).
12. Latimer W. M., "Oxidation Potentials", 2nd ed.,

Prentice-Hall, New York, 1952, p 185.

13. Taube H., Adv. Inorg. Chem. and Radiochem. 1, 1-53 (1953).

14. Basolo F. and Pearson R. G., "Mechanisms of Inorganic Reaction", 2nd ed., John Wiley and Sons, Inc., New York, 1967, pp 454-525.

15. Taube H., Myers H. and Rick R. L., J. Am. Chem. Soc. 75, 4118-4119 (1953).

16. Cotton F. A. and Wilkinson G., "Advanced Inorganic Chemistry" 3rd ed., John Willey and Sons, New York, 1972, pp 672-680.

17. Sutin N., Accts. Chem. Res. 1 (8), 225-31 (1968).

18. Haim A., Accts. Chem. Res. 8 (8), 264-72 (1975).

19. Egli P. H. and Zerfass S., Faraday Discussion No. 5, 61 (1949).

20. Mullin J. W., "Crystallization", Butterworths Publishers Ltd., London, England, 2nd ed., 1972, pp 136-173.

21. Walton A. G., Science, 148, 601 (1965).

22. Nyvlt J., J. Cryst. Growth 3 (4), 377-383 (1968).

23. Brien R. P., Ed., "Crystal Growth", Pergamon Press, New York, 1975, 1st. Ed., pp 289-325.

24. Mullin J. W., Chakabarty M., and Mehta K., J. App. Chem., 20, 367-371 (1970).

25. Larson M. A. and Randolph A. D., Chem. Eng. Prog. Sym. series, 65 (95), 1-13 (1969).

26. Larson M. A. and Randolph A. D., "Theory of Particulate Process", Academic Press, New York (1971),

pp 64-78.

27. Mullin J. W., "Crystallization", 2nd ed. Butterworths Publishers Ltd; London, England, (1972), pp 335-371.

28. McCabe W. L., Ind. Eng. Chem. 21, 30-33 (1929), ibid. 21, 112-119 (1929).

29. Robinson J. N. and Roberts J. E., Can. J. Chem. Eng. 35, 105-112 (1957).

30. Larson M. A. and Gench W. J., Chem. Eng. Prog. Sym. series, 68 (121), 57-66 (1972).

31. Singh G., Chem. Eng. Prog. Sym. series, 72 (153), 100-109 (1976).

32. Herdan G., "Small Particle Statistics", 2nd ed., revised, Butterworths, London, 1960.

33. Terence A., "Particle Size Measurements", Champman and Hall Ltd., London, 1968.

34. Lapple C. E., Chem. Eng. 75 (11), 149-56 (1968).

35. Irani R. R. and Callis C. F., "Particle Size: Measurement, Interpretation and Application", John Wiley and Sons, Inc., New York, 1963.

36. Daeschner H. W., Powder Tech. 2, 349-55 (1968/69).

37. Orr C. Jr. and Dalla Valle J. M., "Fine Particle Measurements", The Macmillan Co., New York, 1959.

38. Girgis B.S. and Girgis L.G., Powder Tech. 7, 85-91 (1973).

39. Hausner H. H., "Handbook of Powder Metallurgy", Chemical Publishing Co., Inc., New York, 1973.

40. Zwicker J. D., Powder Tech. 6, 133-138 (1972).

41. Non-Hai Hu, John, Env. Sci. and Tech. 5, 251-254 (1971).

42. Bakker W. T. and Bartok D., Ceramic Bullenten 45, 582-85 (1966).

43. Hausner H. H., "Handbook of Metal Powder", ed. Porter A. R., Reinhold Publishing Corporation, New York, 1966.

44. Roberts T. A. and Beddow J. K., Powder Tech. 2, 121-24 (1968/69).

45. Krumbein W. C. and Pettijohn F. J., "Manual of Sedimentary Petrography", D. Appleton-Century Co., Inc., 1938, pp 91-165.

46. Amstein E. H. and Scott B. A., J. Appl. Chem. 1, Supplementary Issue No. 1, S10-20 (1951).

47. Heywood H., Rudy 18 (3-4), 75-81 (1970).

48. Cadle R. D., "Particle Size: Theory and Industrial Applications", Reinhold Publishing Co., New York, 1965.

49. Grandillo A. D., Int. J. Powder Met. 6 (1), 3-14 (1970).

50. Lu B. C.-Y. and Graydon W. F., Can. J. Chem. 32, 153-63 (1954).

51. Hirschbarn J. S., "Introduction to Powder Metallurgy", American Powder Metallurgy Institute, Princeton, New Jersey, 2nd ed., 1976, pp 72-81.

52. Dick J. G., Concordia University, Sir George Williams Campus, Personal Communication, 1978.

53. Nyce A. C. and Shafer W. M., Int. J. Powder Met. 8

(N4), 171-180 (1972).

54. Robinxon R.A. and Stokes R.H., " Electrolyte Solutions ", 2nd ed. Butterworth Scientific Publication, London, 1959.

55. Hirschbarn J. S. , "Introduction to Powder Metallurgy", 2nd ed., American Powder Metallurgy Institute, Princeton, New Jersy, 1976, pp 200-01.

56. Gibbs J.W., "Collected Works" Longmans Green, London, 1928.

APPENDIX A

Experimental data obtained in the particle-size analysis experiments

Table A1

Calculation of Particle Size Distribution for Copper Powder Produced by Cyclone Technique

Samples No.	Weight g	Time sec	Height cm	CPU	Size micron	Log of Size
1	0.1183	—	25.10	—	—	—
2	0.0958	20	24.50	80.98	50.27	1.7010
3	0.0733	40	23.90	61.96	35.11	1.5451
4	0.0568	60	23.30	48.01	28.30	1.4515
5	0.0449	80	22.70	37.95	24.19	1.3833
6	0.0343	100	22.10	28.99	21.35	1.3291
7	0.0296	120	21.50	25.02	19.22	1.2835
8	0.0237	140	20.90	20.03	17.55	1.2440
9	0.0204	160	20.30	17.24	16.18	1.2087
10	0.0167	180	19.70	14.11	15.02	1.1764
11	0.0137	200	19.10	11.58	14.04	1.1471
12	0.0086	260	18.50	7.27	12.12	1.0833
13	0.0060	320	17.90	5.07	10.74	1.0308
14	0.0045	380	17.30	3.80	9.69	0.9861
15	0.0033	440	16.70	2.79	8.85	0.9467
16	0.0027	500	16.10	2.28	8.15	0.9109
17	0.0022	560	15.50	1.86	7.56	0.8783
18	0.0021	620	14.90	1.77	7.04	0.8476
19	0.0018	740	14.30	1.52	6.31	0.8000
20	0.0017	860	13.70	1.44	5.73	0.7587

Median Diameter at 50% = 29.51 μ

Standard Deviation[a] = 1.86

[a]Reported as the value: (Size at 50% / Size at 16%).

Figure A1

Cumulative Particle Size Distribution Plot for Cyclone Powder

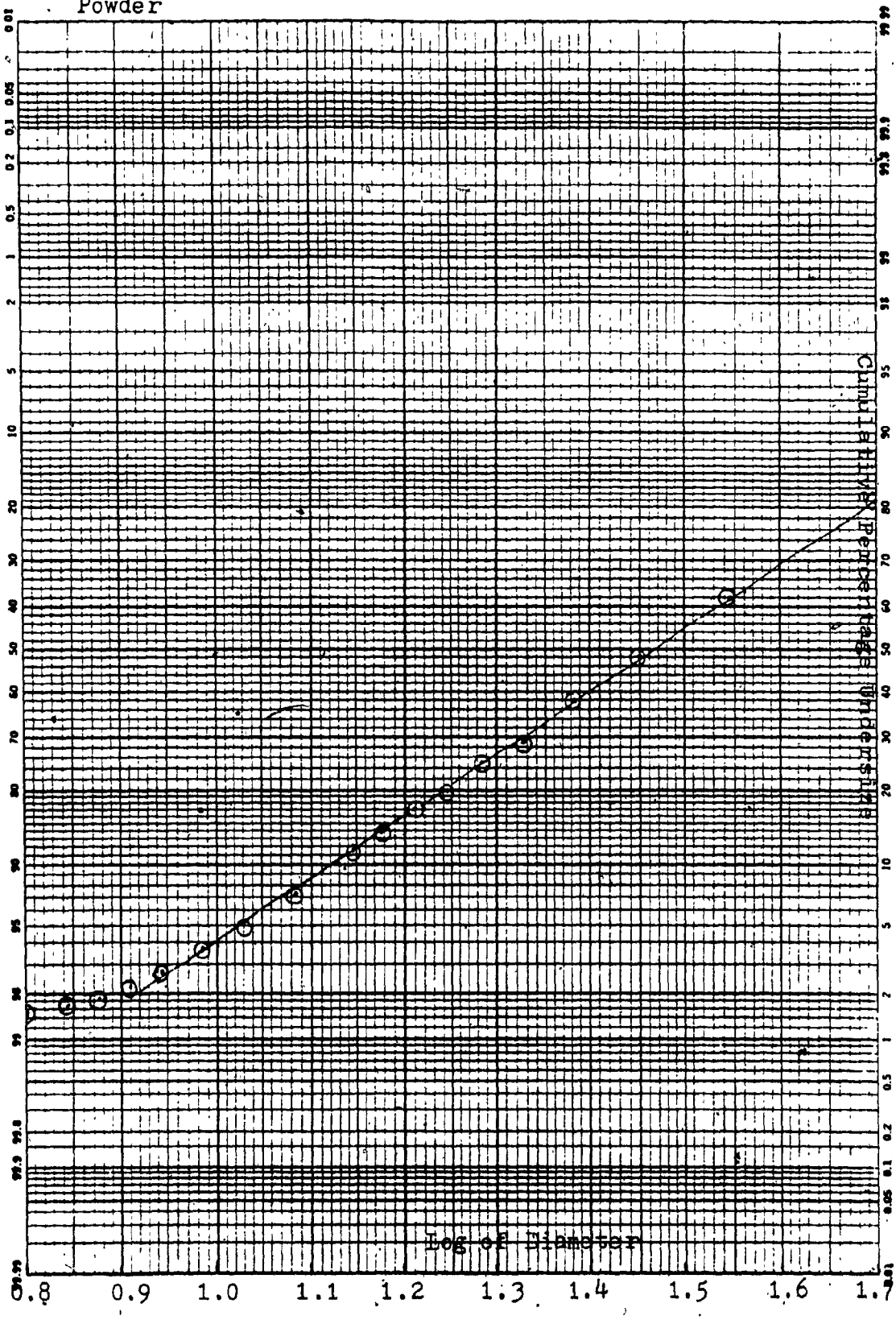

Table A2

Calculation of Particale Size Distribution for Series of Experiment from Run D (Table D5)

Samples No.	Weight g	Time sec	Height cm	CPU	Size micron	Log of Size
1	0.0851	—	25.10	—	—	—
2	0.0742	20	24.50	87.19	50.27	1.7010
3	0.0634	40	23.90	74.50	35.11	1.5451
4	0.0520	60	23.30	61.10	28.30	1.4515
5	0.0428	80	22.70	50.29	24.19	1.3833
6	0.0367	100	22.10	43.13	21.35	1.3291
7	0.0319	120	21.50	37.49	19.22	1.2835
8	0.0288	140	20.90	33.84	17.55	1.2440
9	0.0246	160	20.30	28.91	16.18	1.2087
10	0.0225	180	19.70	26.44	15.02	1.1764
11	0.0183	200	19.10	21.51	14.04	1.1471
12	0.0149	260	18.50	17.50	12.12	1.0833
13	0.0129	320	17.90	15.22	10.74	1.0308
14	0.0125	380	17.30	14.69	9.69	0.9861
15	0.0114	440	16.70	13.40	8.85	0.9467
16	0.0106	500	16.10	12.52	8.15	0.9109
17	0.0091	560	15.50	10.69	7.56	0.8783

Median Diameter at 50% = 23.31 μ

Standard Deviation[a] = 1.87

[a]Reported as the value: (Size at 84% / Size at 50%).

Figure A2

Cumulative Particle Size Distribution Plot for Run D

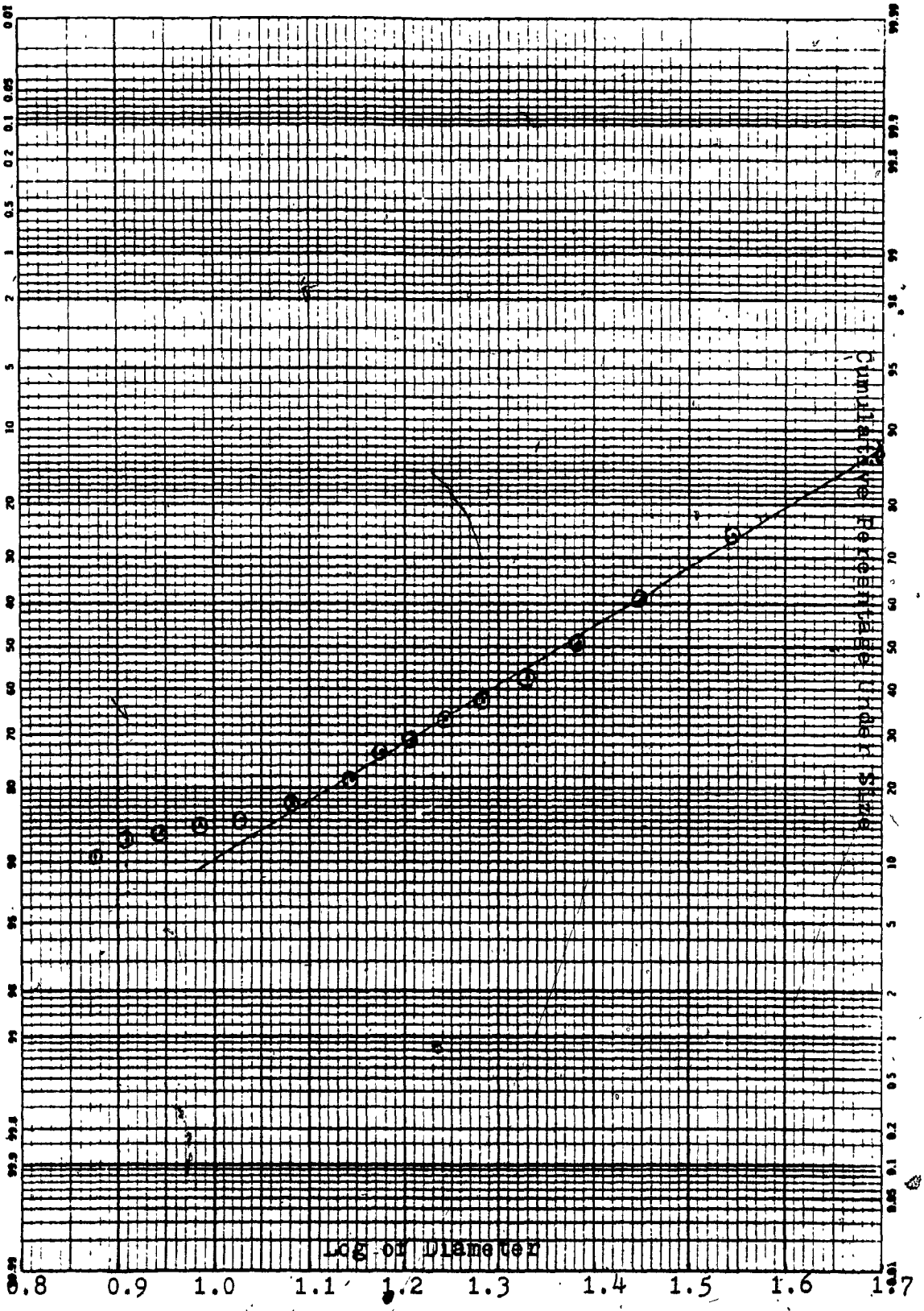

Table A3

Calculation of Particle Size Distribution for Series of Experiment from Run G (Table D8)

Samples No.	Weight g	Time sec	Height cm	CPU	Size micron	Log of Size
1	0.1263	—	25.10	—	—	—
2	0.1023	20	24.50	80.99	50.27	1.7010
3	0.0876	40	23.90	69.55	35.11	1.5451
4	0.0785	60	23.30	62.15	28.30	1.4515
5	0.0671	80	22.70	53.13	24.19	1.3833
6	0.0617	100	22.10	48.85	21.35	1.3291
7	0.0561	120	21.50	44.42	19.22	1.2835
8	0.0499	140	20.90	39.51	17.55	1.2440
9	0.0463	160	20.30	36.66	16.18	1.2087
10	0.0408	180	19.70	32.30	15.02	1.1764
11	0.0384	200	19.10	30.40	14.04	1.1471
12	0.0341	260	18.50	27.10	12.12	1.0833
13	0.0266	320	17.90	21.06	10.74	1.0308
14	0.0230	380	17.30	18.21	9.69	0.9861
15	0.0203	440	16.70	16.07	8.85	0.9467
16	0.0181	500	16.10	14.33	8.15	0.9109
17	0.0165	560	15.50	13.06	7.56	0.8783
18	0.0145	620	14.90	11.48	7.04	0.8476

Median Diameter at 50% = 22.39 μ

Standard Deviation[a] = 1.79

[a]Reported as the value: (Size at 50% / Size at 16%).

Figure A3

Cumulative Particle Size Distribution Plot for Run G

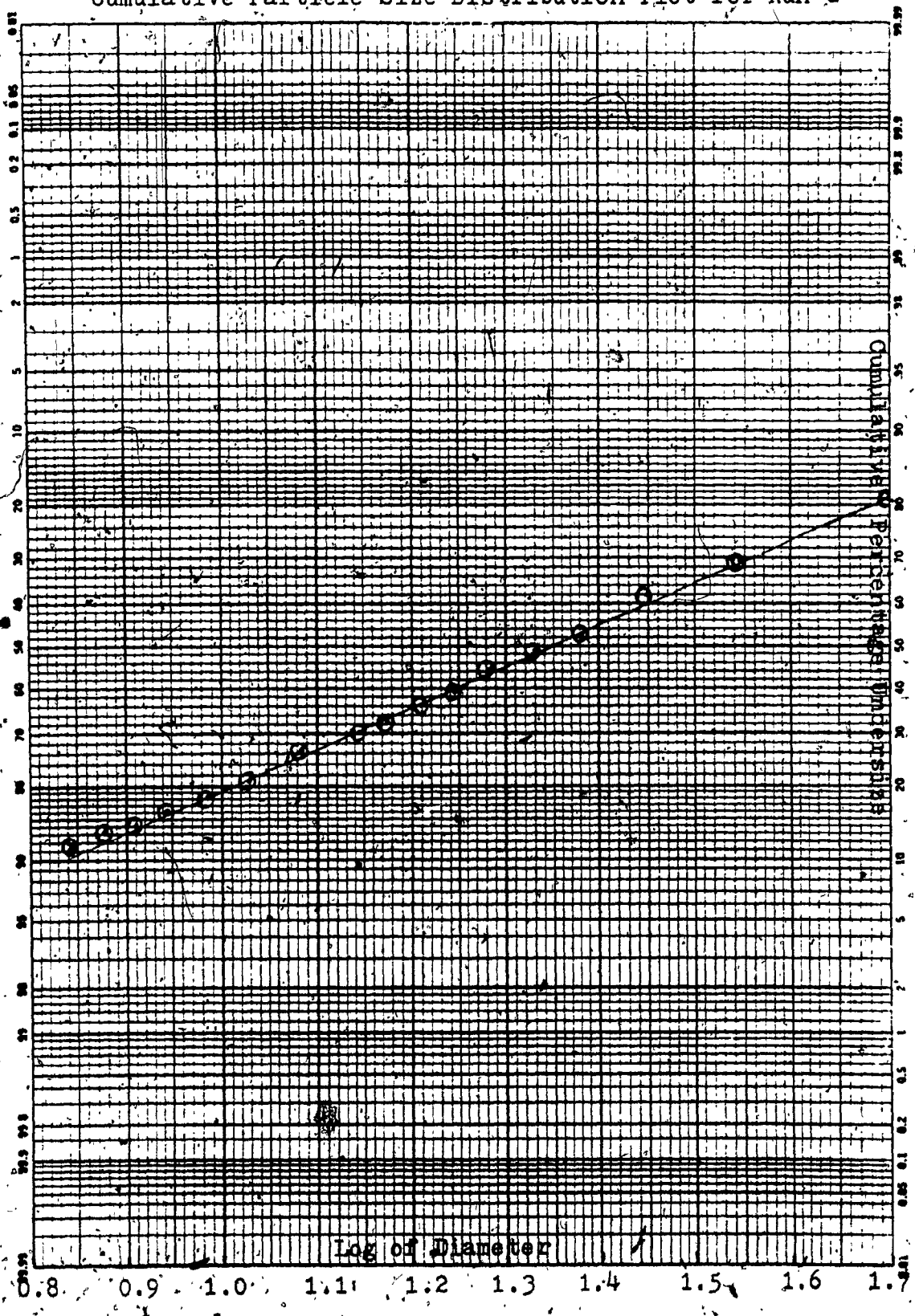

Table A4

Calculation of Particle Size Distribution for Series of Experiment for Run I (Table D10)

Samples No.	Weight g	Time sec	Height cm	CPU	Size micron	Log of Size
1	0.1269	—	25.10	—	—	—
2	0.1120	20	24.50	88.26	50.27	1.7010
3	0.0978	40	23.90	77.06	35.11	1.5451
4	0.0837	60	23.30	65.96	28.30	1.4515
5	0.0747	80	22.70	58.86	24.19	1.3833
6	0.0666	100	22.10	52.48	21.35	1.3291
7	0.0594	120	21.50	46.80	19.22	1.2835
8	0.0534	140	20.90	42.08	17.55	1.2440
9	0.0496	160	20.30	39.08	16.18	1.2087
10	0.0447	180	19.70	35.23	15.02	1.1764
11	0.0404	200	19.10	31.83	14.04	1.1471
12	0.0315	260	18.50	24.82	12.12	1.0833
13	0.0267	320	17.90	21.04	10.74	1.0308
14	0.0217	380	17.30	17.10	9.69	0.9861
15	0.0197	440	16.70	15.53	8.85	0.9467
16	0.0173	500	16.10	13.63	8.15	0.9109
17	0.0168	560	15.50	13.23	7.56	0.8783

Median Diameter at 50% = 20.42 μ

Standard Deviation[a] = 2.17

[a]Reported as the average of the two values: (Size at 84% / Size at 50%) and (Size at 50% / Size at 16%).

Figure A4

Cumulative Particle Size Distribution Plot for Run I

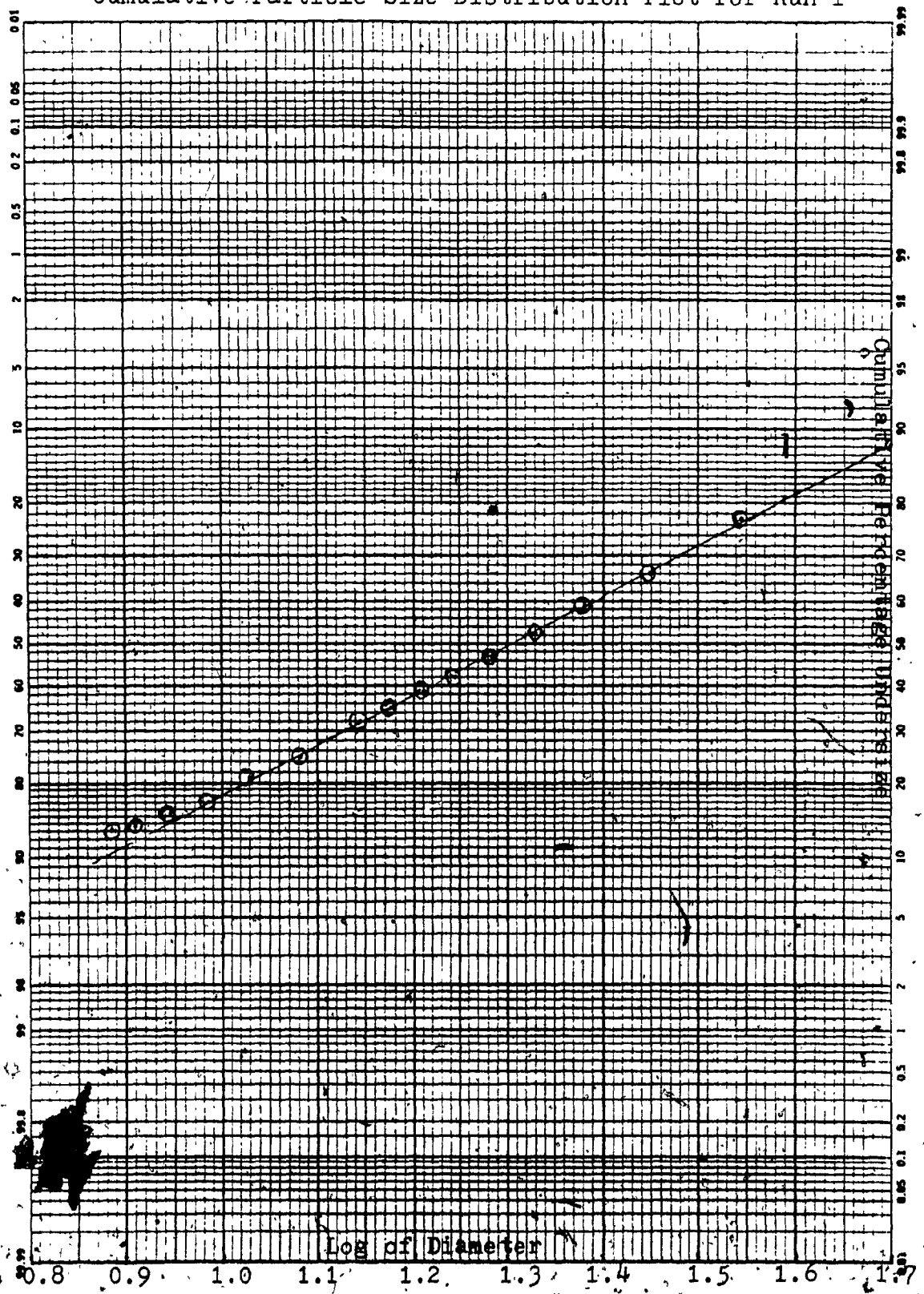

Table A5

Calculation of Particle Size Distribution for Series of Experiment from Run K (Table D12)

Samples No.	Weight g	Time sec	Height cm	CPU	Size micron	Log of Size
1	0.1298	—	25.10	—	—	—
2	0.1094	20	24.50	84.24	50.27	1.7010
3	0.1026	40	23.90	79.04	35.11	1.5451
4	0.0953	60	23.30	73.42	28.30	1.4515
5	0.0829	80	22.70	63.86	24.19	1.3833
6	0.0743	100	22.10	57.24	21.35	1.3291
7	0.0668	120	21.50	51.24	19.22	1.2835
8	0.0597	140	20.90	45.99	17.55	1.2440
9	0.0533	160	20.30	41.06	16.18	1.2087
10	0.0492	180	19.70	37.90	15.02	1.1764
11	0.0425	200	19.10	32.74	14.04	1.1471
12	0.0358	260	18.50	27.58	12.12	1.0833
13	0.0291	320	17.90	22.42	10.74	1.0308
14	0.0234	380	17.30	18.03	9.69	0.9861
15	0.0211	440	16.70	16.70	8.85	0.9467
16	0.0187	500	16.10	14.41	8.15	0.9109
17	0.0163	560	15.50	12.56	7.56	0.8783
18	0.0158	620	14.90	12.17	7.04	0.8476
19	0.0147	740	14.30	11.33	6.31	0.8000
20	0.0125	860	13.70	9.63	5.73	0.7587

Median Diameter at 50% = 18.84 μ

Standard Deviation[a] = 2.06

[a]Reported as the average of the two values: (Size at 84% / Size at 50%) and (Size at 50% / Size at 16%).

Figure A5

Cumulative Particle Size Distribution Plot for Run K

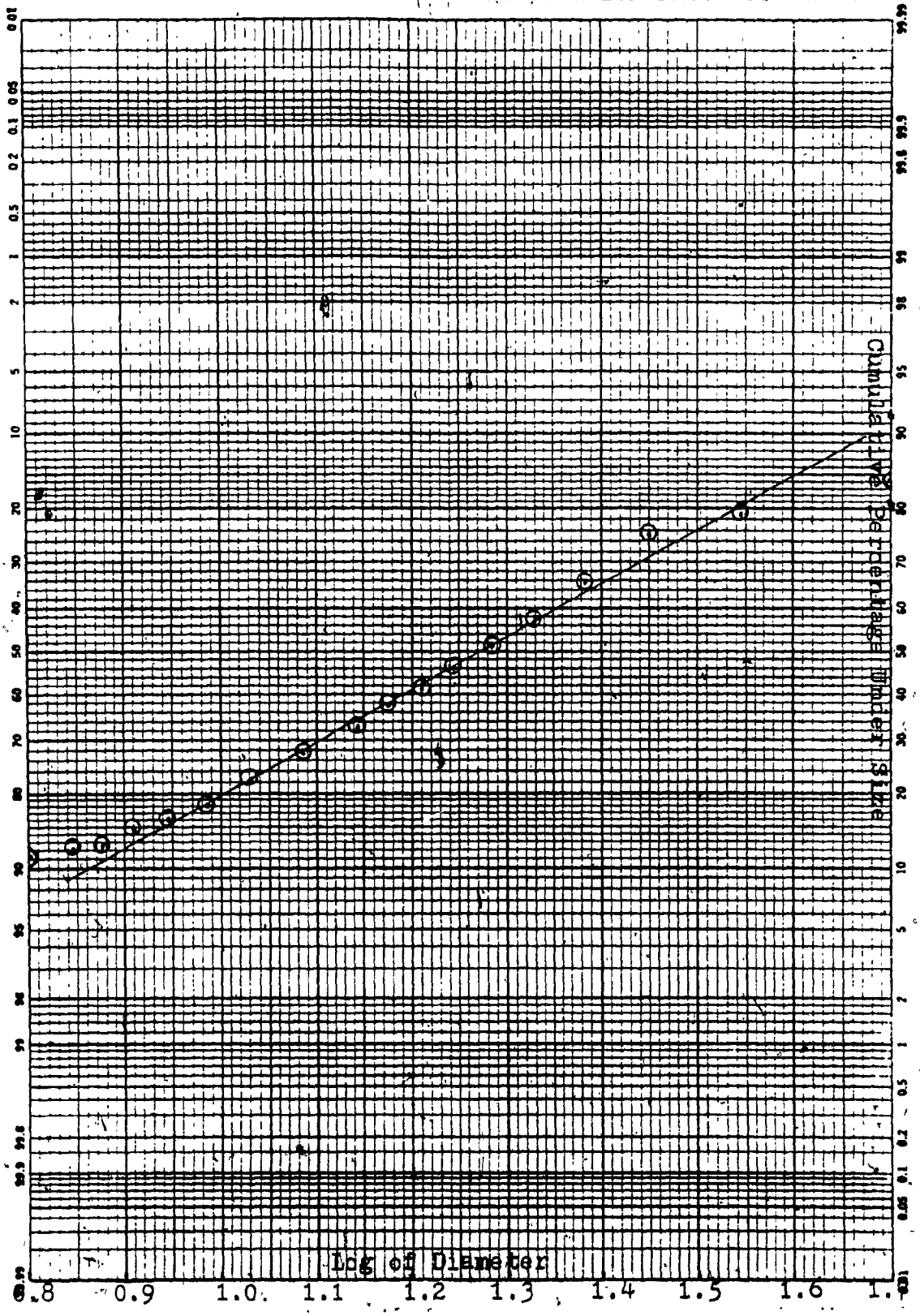

Table A6

Calculation of Particle Size Distribution for Series of Experiment from Run M (Table D14)

Samples No.	Weight g	Time sec	Height cm	CPU	Size micron	Log of Size
1	0.1124	—	25.10	—	—	—
2	0.1110	20	24.50	98.75	50.27	1.7010
3	0.1064	40	23.90	94.66	35.11	1.5451
4	0.0933	60	23.30	83.01	28.30	1.4515
5	0.0840	80	22.70	74.73	24.19	1.3833
6	0.0746	100	22.10	66.37	21.35	1.3291
7	0.0677	120	21.50	60.77	19.22	1.2835
8	0.0629	140	20.90	55.96	17.55	1.2440
9	0.0552	160	20.30	49.11	16.18	1.2087
10	0.0492	180	19.70	43.77	15.02	1.1764
11	0.0447	200	19.10	39.77	14.04	1.1471
12	0.0338	260	18.50	30.07	12.12	1.0833
13	0.0276	320	17.90	24.55	10.74	1.0308
14	0.0236	380	17.30	20.99	9.69	0.9861
15	0.0204	440	16.70	18.15	8.85	0.9467
16	0.0171	500	16.10	15.21	8.15	0.9109
17	0.0153	560	15.50	14.15	7.56	0.8783
18	0.0136	620	14.90	12.10	7.04	0.8476
19	0.0116	740	14.30	10.32	6.31	0.8000
20		860	13.70	8.90	5.73	0.7587

Median Diameter at 50% = 16.41 μ

Standard Deviation[a] = 1.84

[a]Reported as the value: (Size at 84% / Size at 50%).

Figure A6

Cumulative Particle Size Distribution Plot for Run M

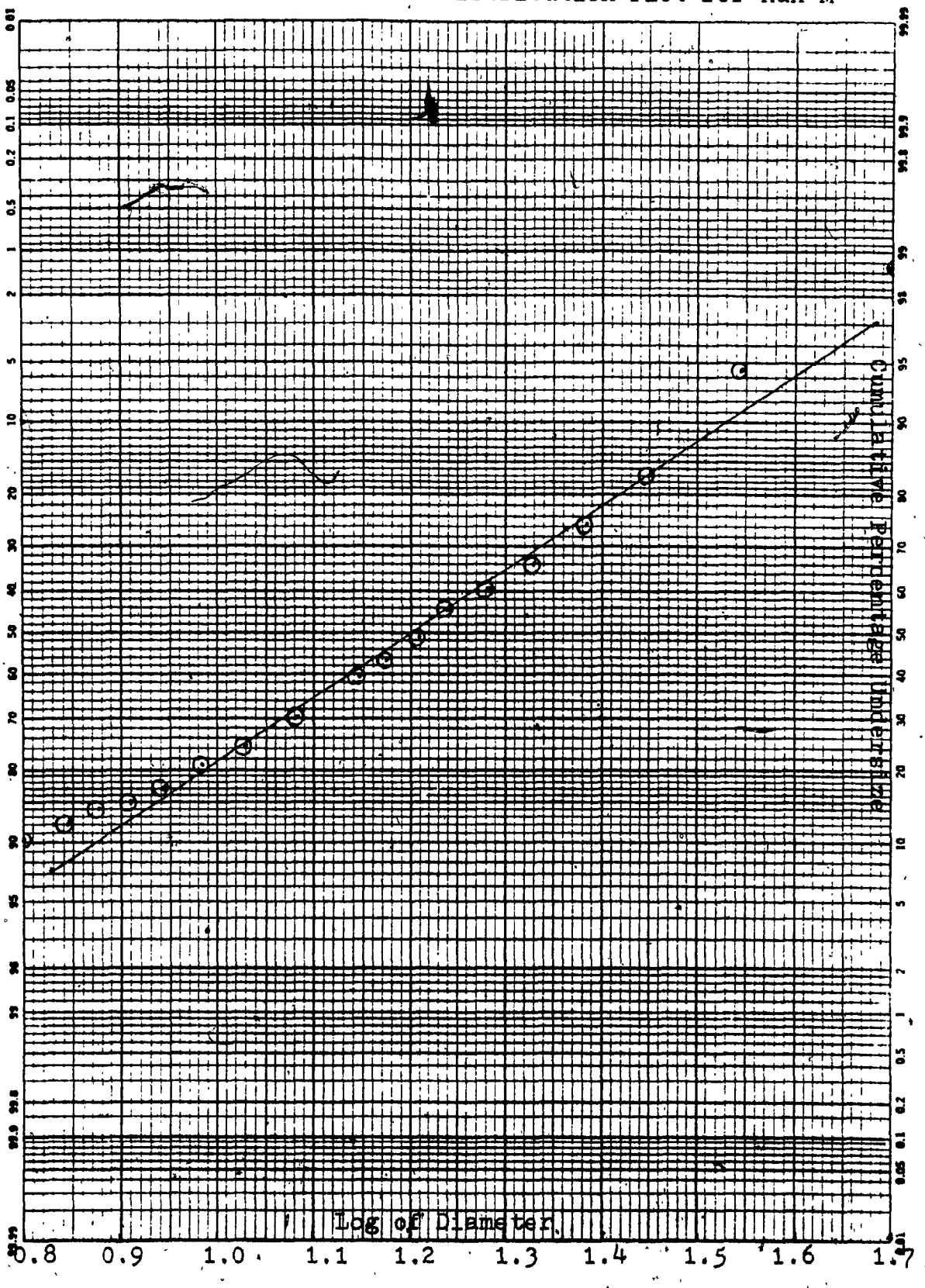

Table A7

Calculation of Particle Size Distribution for Series of Experiment Run N (Table D15)

Samples No.	Weight g.	Time sec	Height cm	CPU	Size micron	Log of Size
1	0.1145	—	25.10	—	—	—
2	0.1094	20	24.50	95.55	50.27	1.7010
3	0.1031	40	23.90	90.04	35.11	1.5451
4	0.0927	60	23.30	80.96	28.30	1.4515
5	0.0851	80	22.70	74.32	24.19	1.3833
6	0.0790	100	22.10	68.99	21.35	1.3291
7	0.0704	120	21.50	61.48	19.22	1.2835
8	0.0653	140	20.90	57.03	17.55	1.2440
9	0.0607	160	20.30	53.00	16.18	1.2087
10	0.0545	180	19.70	47.00	15.02	1.1764
11	0.0492	200	19.10	42.97	14.04	1.1471
12	0.0411	260	18.50	35.90	12.12	1.0833
13	0.0340	320	17.90	29.69	10.74	1.0308
14	0.0253	380	17.30	22.10	9.69	0.9861
15	0.0212	440	16.70	18.50	8.85	0.9467
16	0.0189	500	16.10	16.51	8.15	0.9109
17	0.0171	560	15.50	14.93	7.56	0.8783
18	0.0161	620	14.90	14.06	7.04	0.8476
19	0.0149	740	14.30	13.01	6.31	0.8000
20	0.0146	860	13.70	12.75	5.73	0.7587

Median Diameter at 50% = 15.56 μ

Standard Deviation[a] = 1.92

[a]Reported as the average of the two values: (Size at 84% / Size at 50%) and (Size at 50% / Size at 16%).

Figure A7

Cumulative Particle Size Distribution Plot for Run N

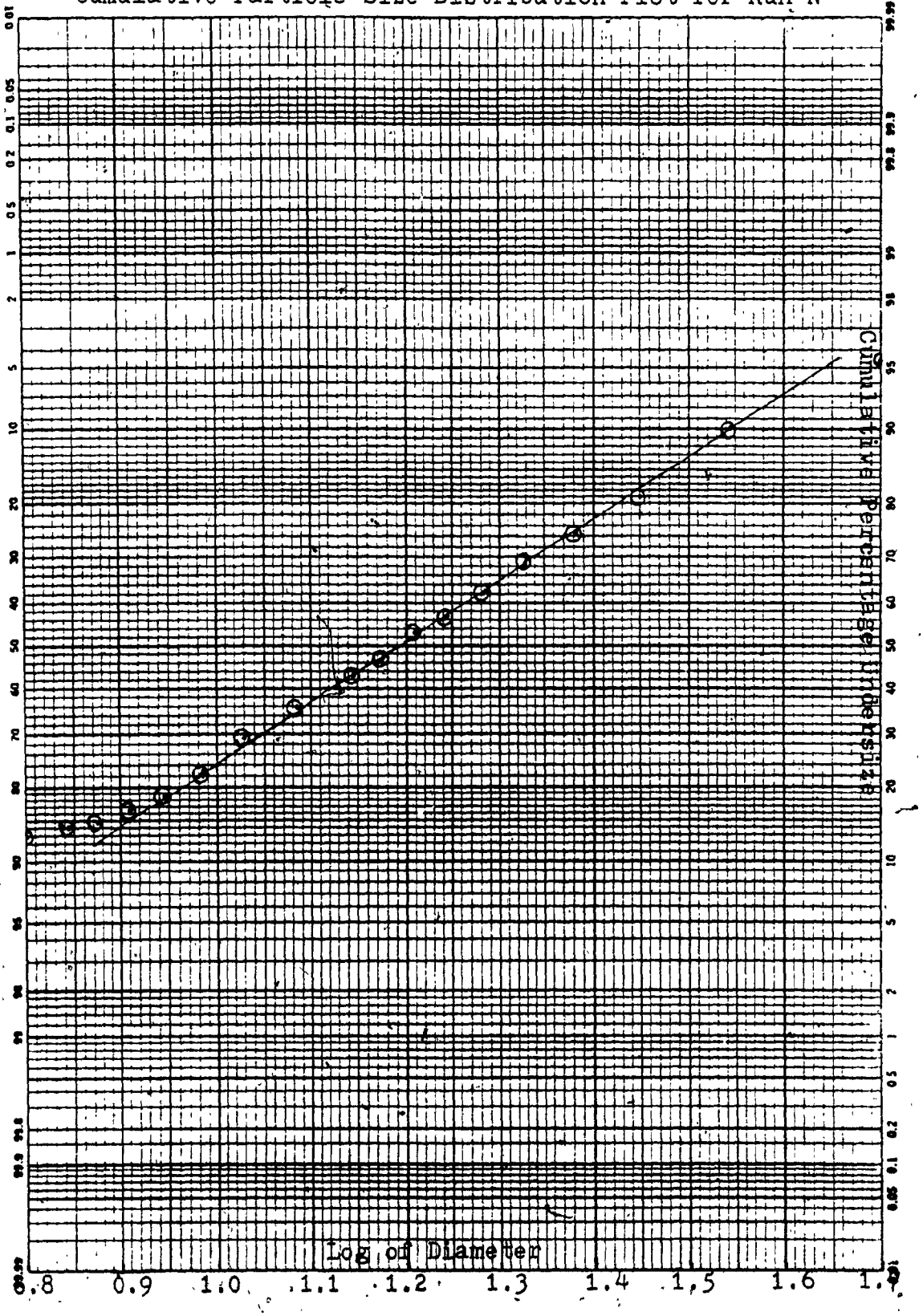

Table A8

Calculation of Particle Size Distribution for Series of Experiment from Run 0 (Table D16)

Samples No.	Weight g	Time sec	Height cm	CPU	Size micron	Log of Size
1	0.1187	—	25.10	—	—	—
2	0.1129	20	24.50	95.11	50.27	1.7010
3	0.1086	40	23.90	91.49	35.11	1.5451
4	0.1009	60	23.30	85.00	28.30	1.4515
5	0.0929	80	22.70	78.26	24.19	1.3833
6	0.0825	100	22.10	71.78	21.35	1.3291
7	0.0772	120	21.50	65.04	19.22	1.2835
8	0.0711	140	20.90	59.90	17.55	1.2440
9	0.0641	160	20.30	54.00	16.18	1.2087
10	0.0587	180	19.70	49.45	15.02	1.1764
11	0.0527	200	19.10	44.40	14.04	1.1471
12	0.0422	260	18.50	35.35	12.12	1.0833
13	0.0332	320	17.90	27.97	10.74	1.0308
14	0.0275	380	17.30	23.17	9.69	0.9861
15	0.0231	440	16.70	19.46	8.85	0.9467
16	0.0196	500	16.10	16.51	8.15	0.9109
17	0.0175	560	15.50	14.75	7.56	0.8783
18	0.0160	620	14.90	13.48	7.04	0.8476
19	0.0153	740	14.30	12.89	6.31	0.8000
20	0.0128	860	13.70	10.78	5.73	0.7587

Median Diameter at 50% = 15.14 μ

Standard Deviation[a] = 1.85

[a]Reported as the average of the two values: (Size at 84% / Size at 50%) and (Size at 50% / Size at 16%).

Figure A8

Cumulative Particle Size Distribution Plot for Run 0

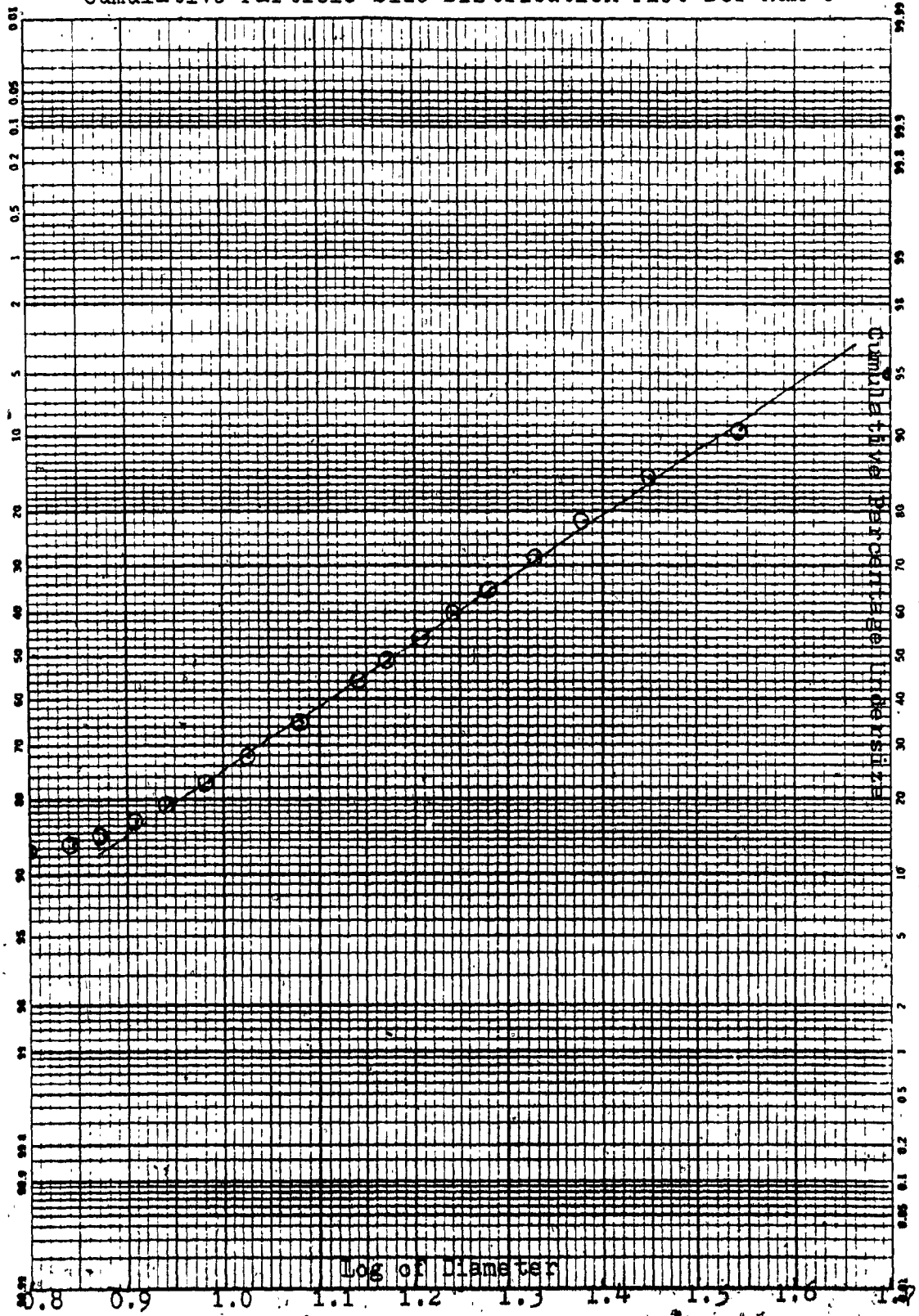

Table A9

Calculation of Particle Size Distribution for Series of Experiment from Run P (Table D17)

Samples No.	Weight g	Time sec	Height cm	CPU	Size micron	Log of Size
1	0.1218	—	25.10	—	—	—
2	0.1127	20	24.50	92.53	50.27	1.7010
3	0.1054	40	23.90	86.54	35.11	1.5451
4	0.0938	60	23.30	77.01	28.30	1.4515
5	0.0827	80	22.70	67.90	24.19	1.3833
6	0.0719	100	22.10	59.03	21.35	1.3291
7	0.0635	120	21.50	52.13	19.22	1.2835
8	0.0572	140	20.90	46.96	17.55	1.2440
9	0.0499	160	20.30	40.97	16.18	1.2087
10	0.0447	180	19.70	36.70	15.02	1.1764
11	0.0390	200	19.10	32.02	14.04	1.1471
12	0.0292	260	18.50	23.97	12.12	1.0833
13	0.0213	320	17.90	17.49	10.74	1.0308
14	0.0162	380	17.30	13.30	9.69	0.9861
15	0.0137	440	16.70	11.25	8.85	0.9467
16	0.0122	500	16.10	10.02	8.15	0.9109
17	0.0109	560	15.50	8.95	7.56	0.8783
18	0.0094	620	14.90	8.12	7.04	0.8476
19	0.0088	740	14.30	7.22	6.31	0.8000
20	0.0081	860	13.70	6.65	5.73	0.7587

Median Diameter at 50% = 18.20 μ

Standard Deviation[a] = 1.77

[a]Reported as the average of the two values: (Size at 84% / Size at 50%) and (Size at 50% / Size at 16%).

Figure A9

Cumulative Particle Size Distribution Plot for Run P

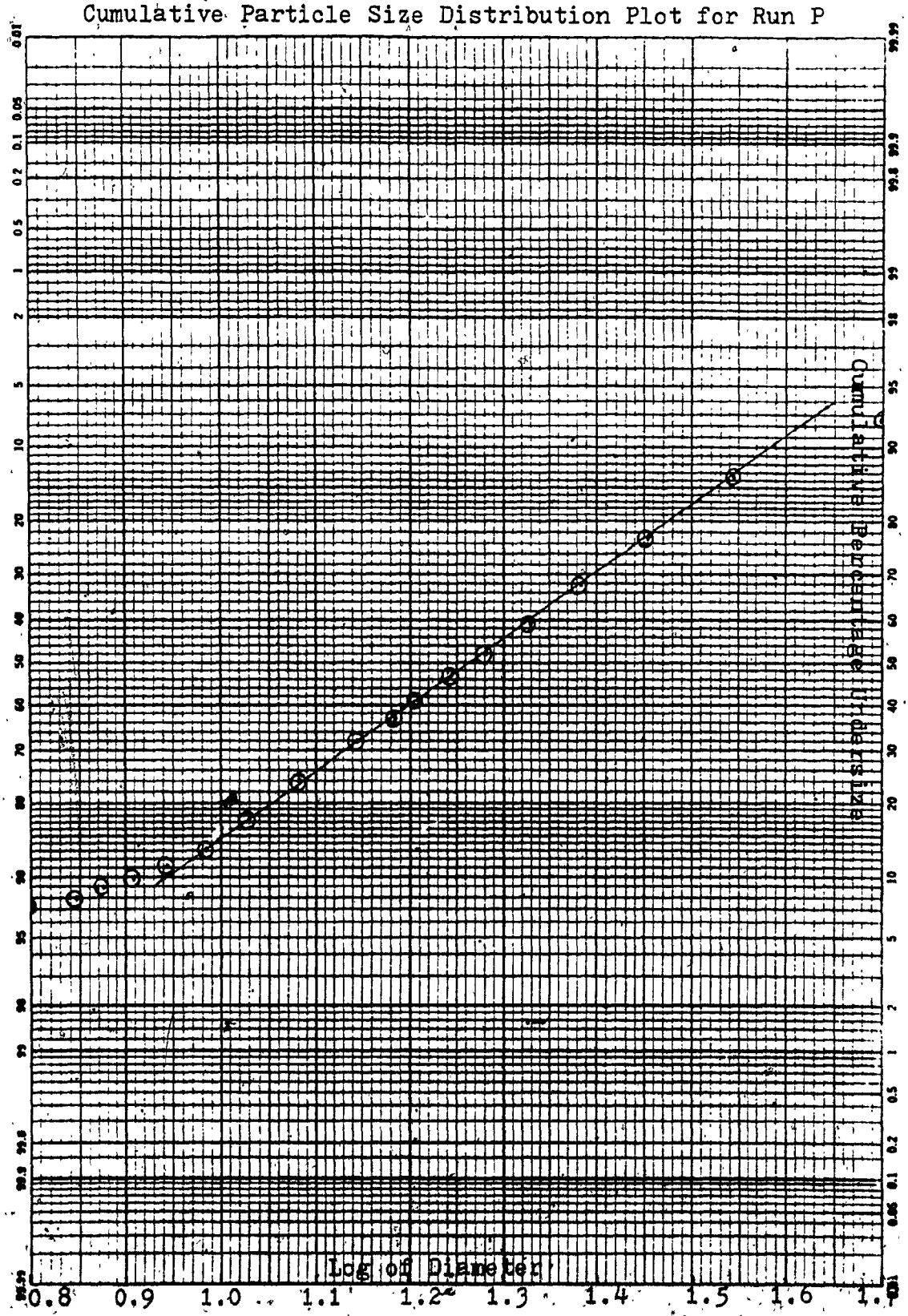

Table A10

Calculation of Particle Size Distribution for Run QI (Table D19)

Samples No.	Weight g	Time sec	Height cm	CPU	Size micron	Log of Size
1	0.0983	—	25.10	—	—	—
2	0.0885	20	24.50	90.03	50.27	1.7010
3	0.0737	40	23.90	74.97	35.11	1.5451
4	0.0599	60	23.30	60.94	28.30	1.4515
5	0.0502	80	22.70	51.07	24.19	1.3833
6	0.0413	100	22.10	42.01	21.35	1.3291
7	0.0353	120	21.50	35.91	19.22	1.2835
8	0.0275	140	20.90	27.98	17.55	1.2440
9	0.0253	160	20.30	25.74	16.18	1.2087
10	0.0197	180	19.70	20.04	15.02	1.1764
11	0.0167	200	19.10	16.99	14.04	1.1471
12	0.0122	260	18.50	12.41	12.12	1.0833
13	0.0088	320	17.90	8.95	10.74	1.0308
14	0.0057	380	17.30	5.75	9.69	0.9861
15	0.0039	440	16.70	3.97	8.85	0.9467
16	0.0031	500	16.10	3.15	8.15	0.9109
17	0.0027	560	15.50	2.75	7.56	0.8783
18	0.0024	620	14.90	2.44	7.04	0.8476
19	0.0021	740	14.30	2.14	6.31	0.8000
20	0.0020	860	13.70	2.03	5.73	0.7587

Median Diameter at 50% = 23.71 μ

Standard Deviation[a] = 1.75

[a]Reported as the average of the two values: (Size at 84% / Size at 50%) and (Size at 50% / Size at 16%).

Figure A10
Cumulative Particle Size Distribution Plot for Run QI

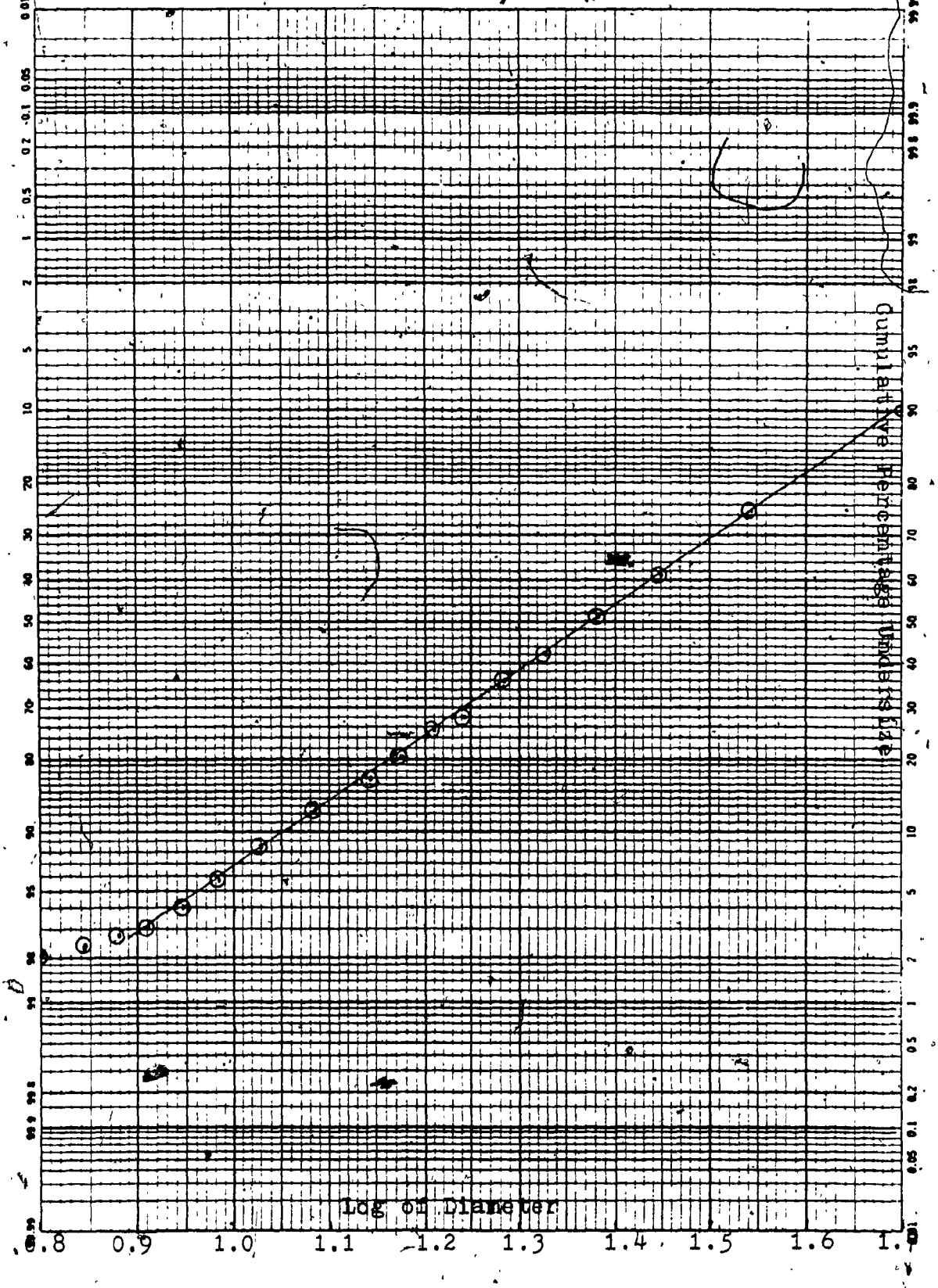

Table A11

Calculation of Particle Size Distribution for Run QK (Table D20)

Samples No.	Weight g	Time sec	Height cm	CPU	Size micron	Log of Size
1	0.1351	—	25.10	—	—	—
2	0.1267	20	24.50	93.78	50.27	1.7010
3	0.1067	40	23.90	78.98	35.11	1.5451
4	0.0905	60	23.30	66.99	28.30	1.4515
5	0.0743	80	22.70	55.00	24.19	1.3833
6	0.0648	100	22.10	47.96	21.35	1.3291
7	0.0540	120	21.50	39.97	19.22	1.2835
8	0.0459	140	20.90	33.96	17.55	1.2440
9	0.0378	160	20.30	27.98	16.18	1.2087
10	0.0338	180	19.70	25.02	15.02	1.1764
11	0.0283	200	19.10	20.98	14.04	1.1471
12	0.0196	260	18.50	14.51	12.12	1.0833
13	0.0146	320	17.90	10.51	10.74	1.0308
14	0.0101	380	17.30	7.48	9.69	0.9861
15	0.0081	440	16.70	6.00	8.85	0.9467
16	0.0065	500	16.10	4.81	8.15	0.9109
17	0.0054	560	15.50	4.00	7.56	0.8783
18	0.0047	620	14.90	3.48	7.04	0.8476
19	0.0040	740	14.30	2.96	6.31	0.8000
20	0.0037	860	13.70	2.74	5.73	0.7587

Median Diameter at 50% = 21.88 μ

Standard Deviation[a] = 1.74

[a]Reported as the average of the two values: (Size at 84% / Size at 50%) and (Size at 50% / Size at 16%).

Figure A11

Cumulative Particle Size Distribution Plot for Run QK

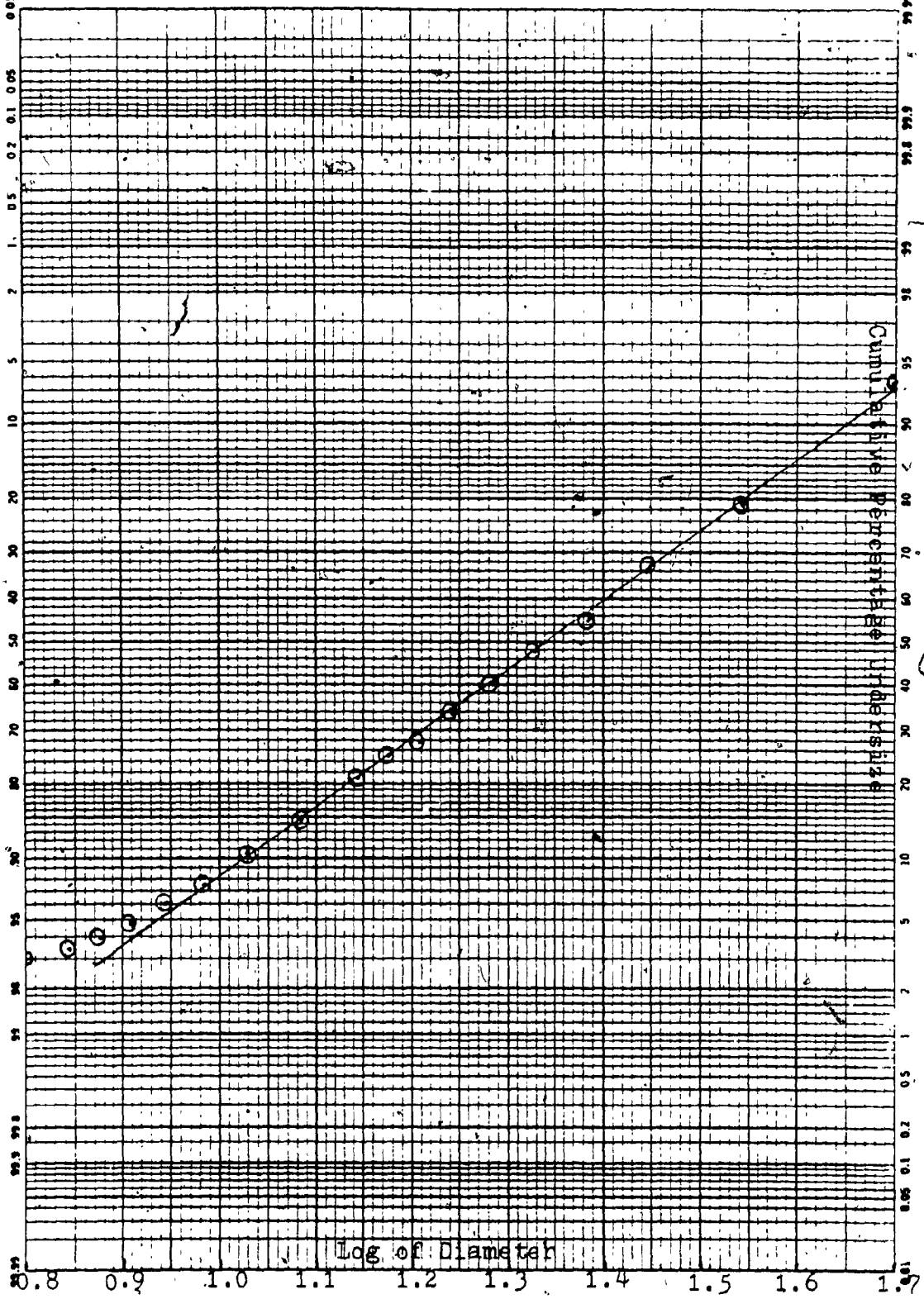

Table A12

Calculation of Particle Size Distribution for Run QM (Table D21)

Samples No.	Weight g	Time sec	Height cm	CPU	Size micron	Log of Size
1	0.1158	—	25.10	—	—	—
2	0.1101	20	24.50	95.08	50.27	1.7010
3	0.0984	40	23.90	84.97	35.11	1.5451
4	0.0852	60	23.30	73.58	28.30	1.4515
5	0.0767	80	22.70	66.23	24.19	1.3833
6	0.0669	100	22.10	57.77	21.35	1.3291
7	0.0576	120	21.50	49.74	19.22	1.2835
8	0.0521	140	20.90	44.99	17.55	1.2440
9	0.0474	160	20.30	40.93	16.18	1.2087
10	0.0393	180	19.70	33.94	15.02	1.1764
11	0.0346	200	19.10	29.88	14.04	1.1471
12	0.0246	260	18.50	21.24	12.12	1.0833
13	0.0185	320	17.90	15.98	10.74	1.0308
14	0.0151	380	17.30	13.04	9.69	0.9861
15	0.0115	440	16.70	9.93	8.85	0.9467
16	0.0092	500	16.10	7.94	8.15	0.9109
17	0.0077	560	15.50	6.65	7.56	0.8783
18	0.0069	620	14.90	5.96	7.04	0.8476
19	0.0063	740	14.30	5.44	6.31	0.8000
20	0.0057	860	13.70	4.92	5.73	0.7587

Median Diameter at 50% = 19.05 μ

Standard Deviation[a] = 1.80

[a]Reported as the average of the two values: (Size at 84% / Size at 50%) and (Size at 50% / Size at 16%).

Figure A12

Cumulative Particle Size Distribution Plot for Run QM

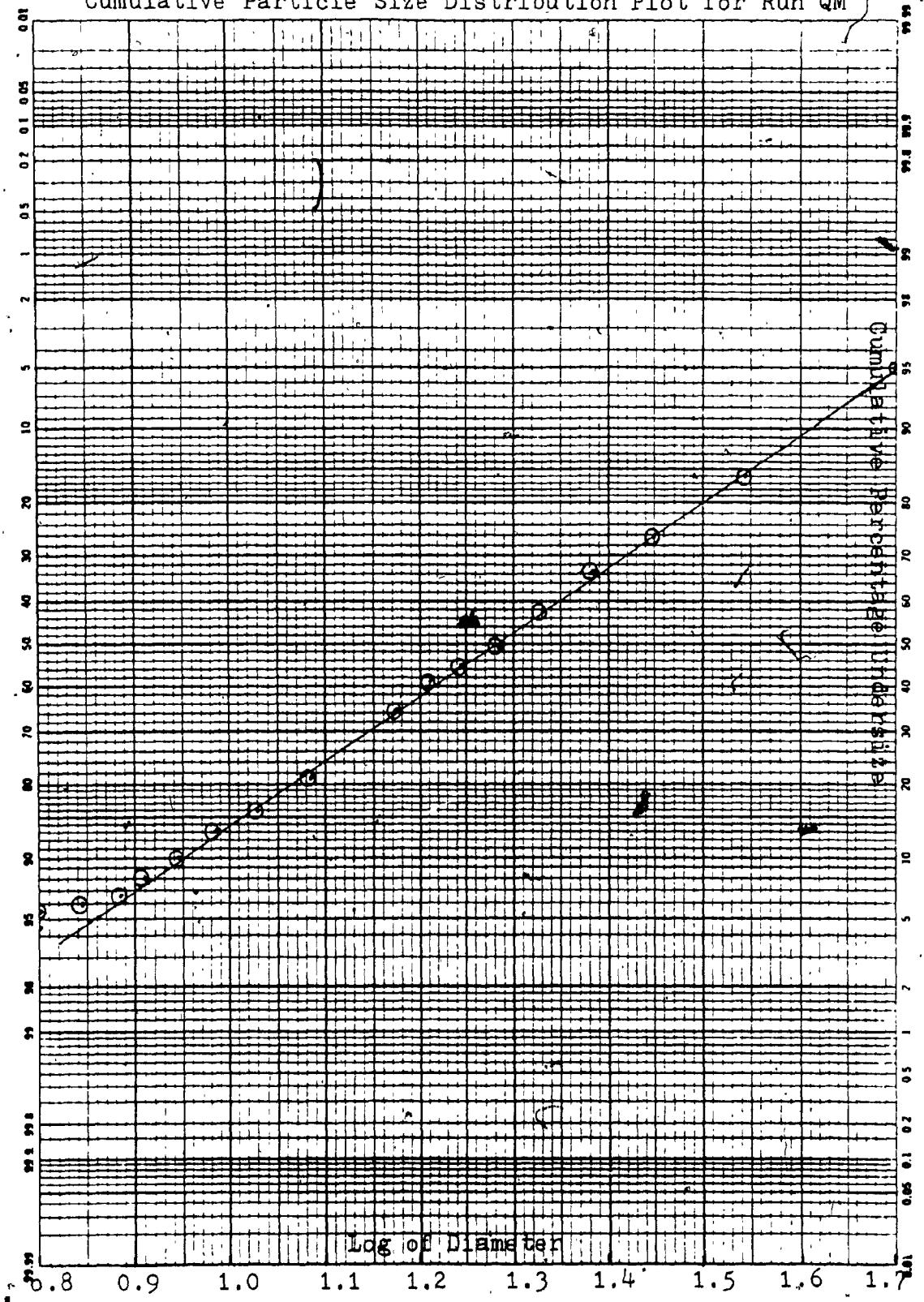

Table A13

Calculation of Particle Size Distribution for Run QR (Table D22)

Samples No.	Weight g	Time sec	Height cm	CPU	Size micron	Log of Size
1	0.1261	—	25.10	—	—	—
2	0.1167	20	24.50	92.55	50.27	1.7010
3	0.1050	40	23.90	83.27	35.11	1.5451
4	0.0902	60	23.30	71.53	28.30	1.4515
5	0.0740	80	22.70	58.68	24.19	1.3833
6	0.0627	100	22.10	49.72	21.35	1.3291
7	0.0518	120	21.50	41.08	19.22	1.2835
8	0.0416	140	20.90	32.99	17.55	1.2440
9	0.0347	160	20.30	28.49	16.18	1.2087
10	0.0281	180	19.70	22.28	15.02	1.1764
11	0.0239	200	19.10	18.95	14.04	1.1471
12	0.0152	260	18.50	12.05	12.12	1.0833
13	0.0102	320	17.90	8.09	10.74	1.0308
14	0.0072	380	17.30	5.71	9.69	0.9861
15	0.0050	440	16.70	3.94	8.85	0.9467
16	0.0046	500	16.10	3.65	8.15	0.9109
17	0.0041	560	15.50	3.25	7.56	0.8783
18	0.0039	620	14.90	3.09	7.04	0.8476
19	0.0038	740	14.30	3.01	6.31	0.8000
20	0.0036	860	13.70	2.85	5.73	0.7587

Median Diameter at 50% = 21.63 μ

Standard Deviation[a] = 1.64

[a]Reported as the average of the two values: (Size at 84% / Size at 50%) and (Size at 50% / Size at 16%).

Figure A13

Cumulative Particle Size Distribution Plot for Run QR

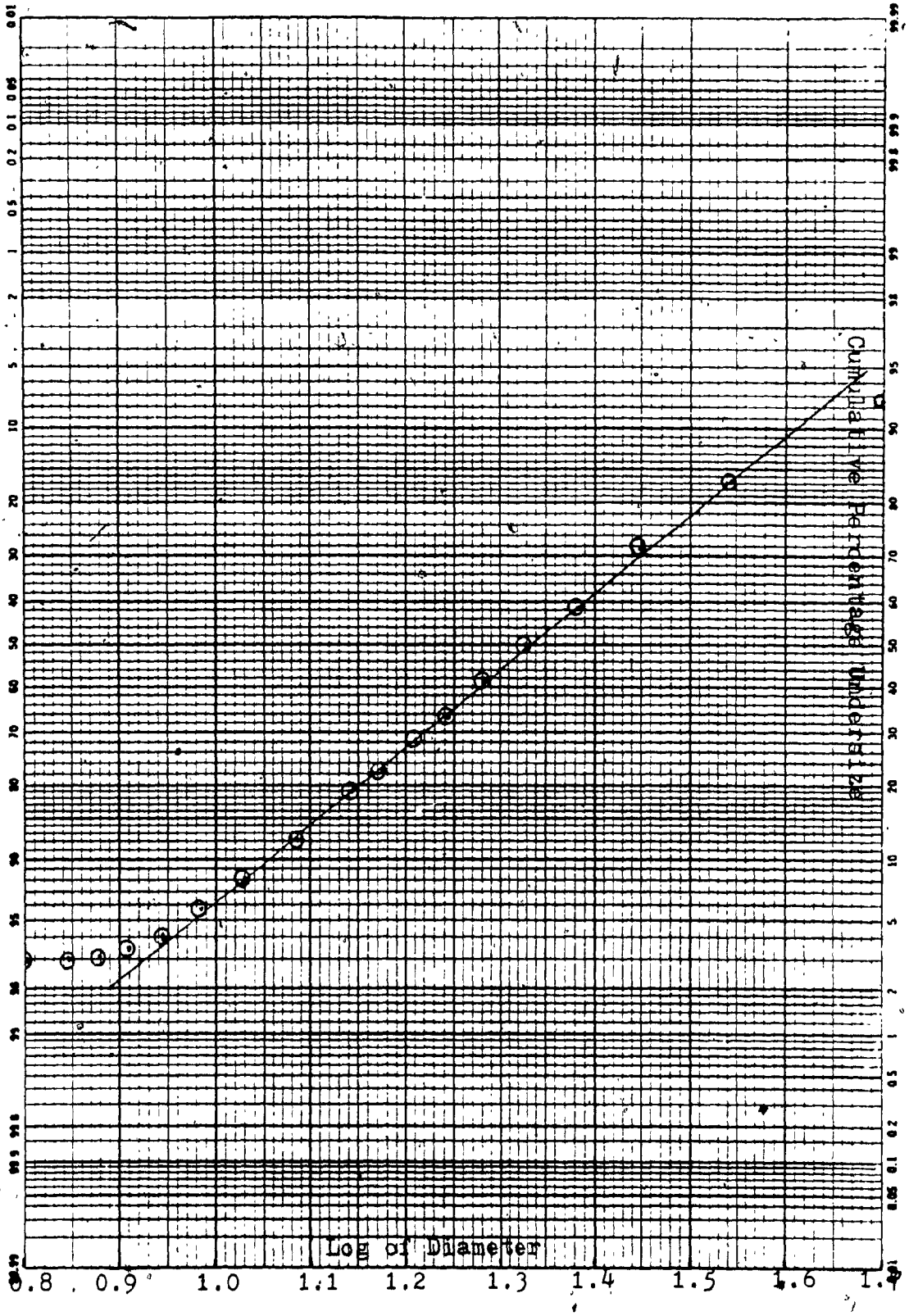

Table A14

Calculation of Particle Size Distribution for Series of Experiment from Run QS(Table D23)

Samples No.	Weight g	Time sec	Height cm	CPU	Size micron	Log of Size
1	0.1120	—	25.10	—	—	—
2	0.1001	20	24.50	89.38	50.27	1.7010
3	0.0857	40	23.90	76.52	35.11	1.5451
4	0.0683	60	23.30	60.98	28.30	1.4515
5	0.0557	80	22.70	49.73	24.19	1.3833
6	0.0432	100	22.10	38.57	21.35	1.3291
7	0.0358	120	21.50	31.96	19.22	1.2835
8	0.0270	140	20.90	24.11	17.55	1.2440
9	0.0218	160	20.30	19.46	16.18	1.2087
10	0.0174	180	19.70	15.54	15.02	1.1764
11	0.0131	200	19.10	11.70	14.04	1.1471
12	0.0080	260	18.50	11.70	12.12	1.0833
13	0.0047	320	17.90	7.14	10.74	1.0308
14	0.0040	380	17.30	4.20	9.69	0.9861
15	0.0036	440	16.70	3.57	8.85	0.9467
16	0.0031	500	16.10	3.21	8.15	0.9109
17	0.0028	560	15.50	2.76	7.56	0.8783
18	0.0026	620	14.90	2.50	7.04	0.8476
19	0.0023	740	14.30	2.32	6.31	0.8000
20	0.0020	860	13.70	1.79	5.73	0.7587

Median Diameter at 50% = 24.55 μ

Standard Deviation[a] = 1.69

[a]Reported as the average of the two values: (Size at 84% / Size at 50%) and (Size at 50% / Size at 16%).

Figure A14

Cumulative Particle Size Distribution Plot for Run QS

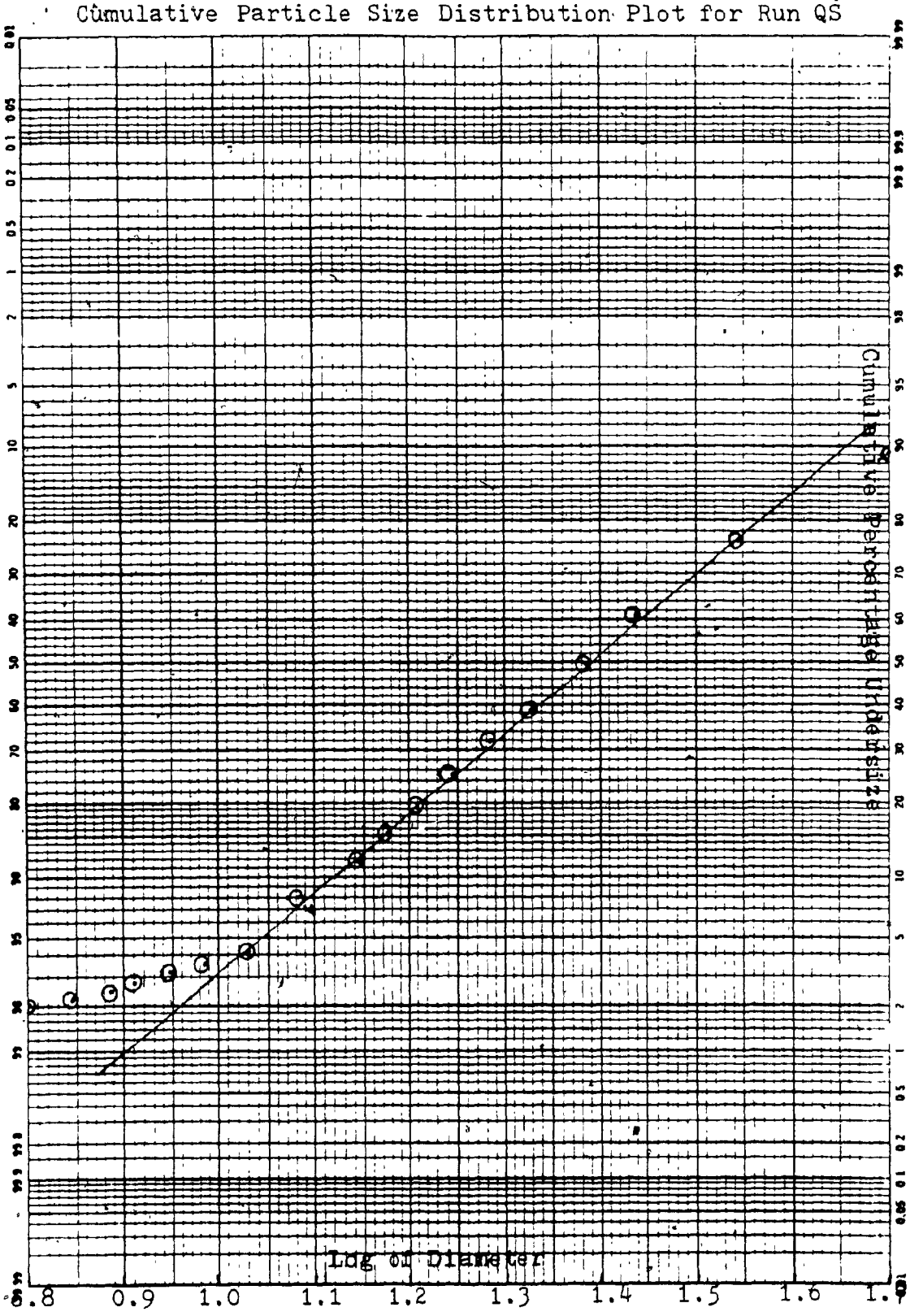

Table A15

Calculation of Particle Size Distribution for Run TK (Table D25)

Samples No.	Weight g	Time sec	Height cm	CPU	Size micron	Log of Size
1	0.1128	—	25.10	—	—	—
2	0.1005	20	24.50	85.31	50.27	1.7010
3	0.0818	40	23.90	69.45	35.11	1.5451
4	0.0648	60	23.30	55.01	28.30	1.4515
5	0.0555	80	22.70	47.11	24.19	1.3833
6	0.0470	100	22.10	39.90	21.35	1.3291
7	0.0402	120	21.50	34.13	19.22	1.2835
8	0.0343	140	20.90	29.12	17.55	1.2440
9	0.0283	160	20.30	24.02	16.18	1.2087
10	0.0256	180	19.70	21.73	15.02	1.1764
11	0.0223	200	19.10	18.93	14.04	1.1471
12	0.0165	260	18.50	14.01	12.12	1.0833
13	0.0118	320	17.90	10.01	10.74	1.0308
14	0.0106	380	17.30	8.99	9.69	0.9861
15	0.0099	440	16.70	8.40	8.85	0.9467
16	0.0085	500	16.10	7.22	8.15	0.9109
17	0.0081	560	15.50	6.87	7.56	0.8783
18	0.0076	620	14.90	6.45	7.04	0.8476
19	0.0070	740	14.30	5.94	6.31	0.8000
20	0.0064	860	13.70		5.73	0.7587

Median Diameter at 50% = 25.12 μ

Standard Deviation[a] = 1.94

[a]Reported as the average of the two values: (Size at 84% / Size at 50%) and (Size at 50% / Size at 16%).

Figure A15

Cumulative Particle Size Distribution Plot for Run TK

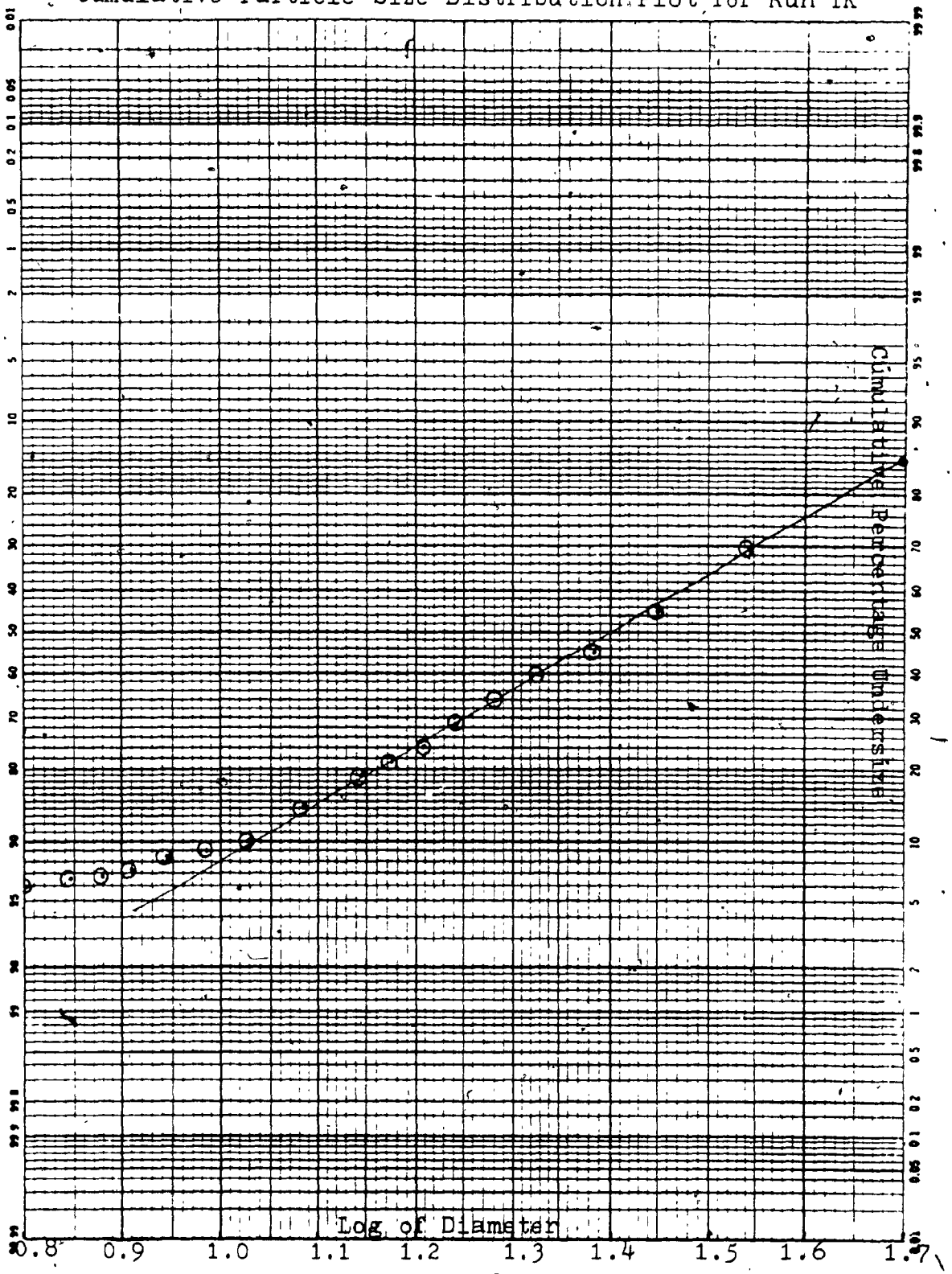

Table A16

Calculation of Particle Size Distribution for Run TM (Table D25)

Samples No.	Weight g	Time sec	Height cm	CPU	Size micron	Log of Size
1	0.1130	—	25.10	—	—	—
2	0.1015	20	24.50	89.82	50.27	1.7010
3	0.0836	40	23.90	73.98	35.11	1.5451
4	0.0700	60	23.30	61.95	28.30	1.4515
5	0.0578	80	22.70	51.15	24.19	1.3833
6	0.0509	100	22.10	45.04	21.35	1.3291
7	0.0445	120	21.50	39.38	19.22	1.2835
8	0.0372	140	20.90	32.92	17.55	1.2440
9	0.0316	160	20.30	27.96	16.18	1.2087
10	0.0259	180	19.70	22.92	15.02	1.1764
11	0.0231	200	19.10	20.44	14.04	1.1471
12	0.0165	260	18.50	14.60	12.12	1.0833
13	0.0118	320	17.90	10.44	10.74	1.0308
14	0.0084	380	17.30	7.43	9.69	0.9861
15	0.0069	440	16.70	6.11	8.85	0.9467
16	0.0052	500	16.10	5.11	8.15	0.9109
17	0.0045	560	15.50	3.98	7.56	0.8783
18	0.0042	620	14.90	3.71	7.04	0.8476
19	0.0037	740	14.30	3.27	6.31	0.8000
20	0.0031	860	13.70	2.74	5.73	0.7587

Median Diameter at 50% = 23.66 μ

Standard Deviation[a] = 1.86

[a]Reported as the average of the two values: (Size at 84% / Size at 50%) and (Size at 50% / Size at 16%).

Figure A16

Cumulative Particle Size Distribution Plot for Run TM

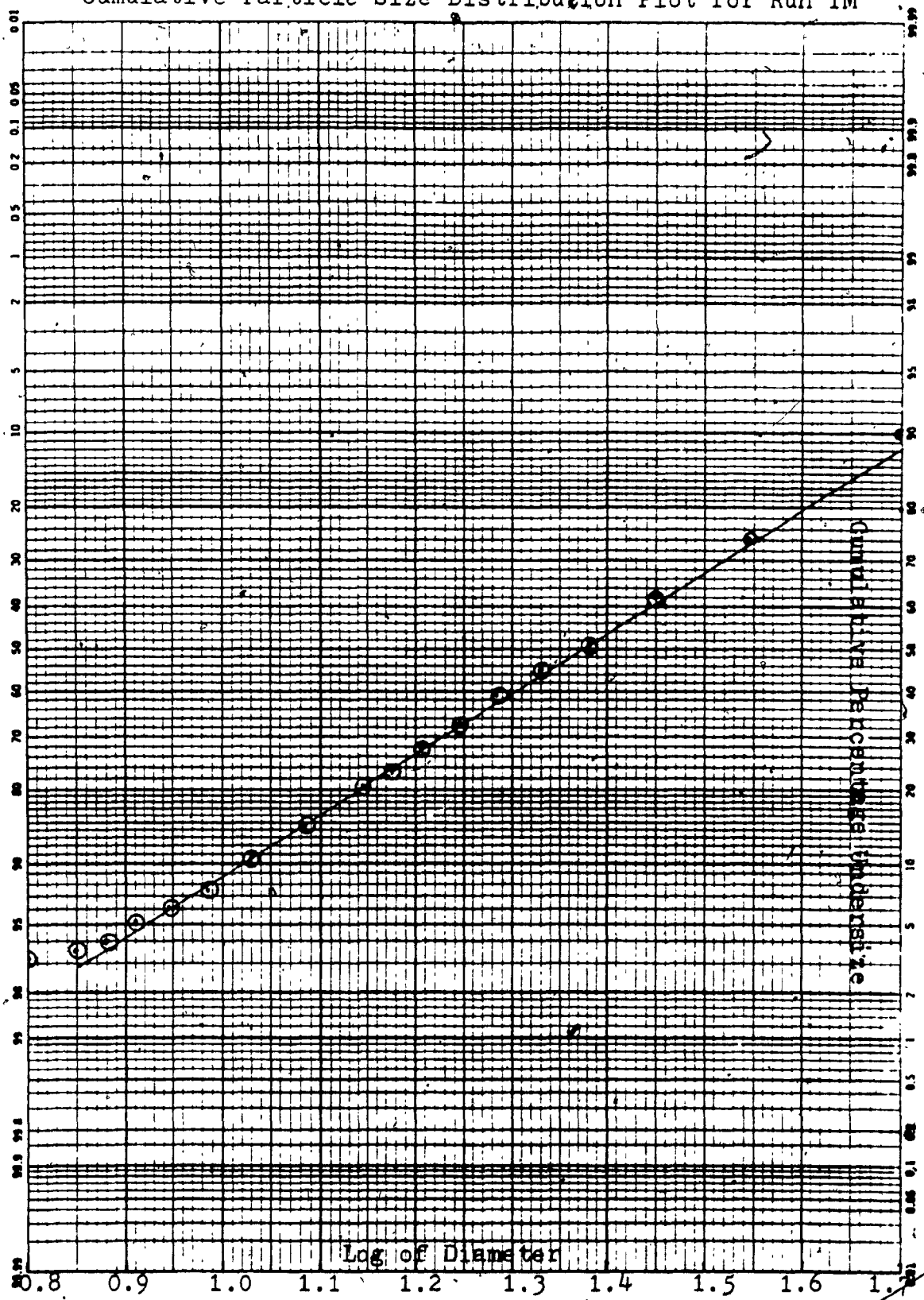

Table A17

Calculation of Particle Size Distribution for Run TN (Table D25)

Samples No.	Weight g	Time sec	Height cm	CPU	Size micron	Log of Size
1	0.1031	—	25.10	—	—	—
2	0.0917	20	24.50	88.94	50.27	1.7010
3	0.0763	40	23.90	74.01	35.11	1.5451
4	0.0639	60	23.30	61.98	28.30	1.4515
5	0.0539	80	22.70	52.28	24.19	1.3833
6	0.0464	100	22.10	45.00	21.35	1.3291
7	0.0383	120	21.50	37.15	19.22	1.2835
8	0.0340	140	20.90	32.98	17.55	1.2440
9	0.0298	160	20.30	28.90	16.18	1.2087
10	0.0247	180	19.70	23.96	15.02	1.1764
11	0.0217	200	19.10	21.05	14.04	1.1471
12	0.0160	260	18.50	15.52	12.12	1.0833
13	0.0117	320	17.90	11.35	10.74	1.0308
14	0.0103	380	17.30	9.99	9.69	0.9861
15	0.0086	440	16.70	8.34	8.85	0.9467
16	0.0078	500	16.10	7.57	8.15	0.9109
17	0.0071	560	15.50	6.89	7.56	0.8783
18	0.0062	620	14.90	6.01	7.04	0.8476
19	0.0055	740	14.30	5.33	6.31	0.8000
20	0.0051	860	13.70	4.95	5.73	0.7587

Median Diameter at 50% = 23.17 μ

Standard Deviation[a] = 1.84

[a]Reported as the average of the two values: (Size at 84% / Size at 50%) and (Size at 50% / Size at 16%).

Figure A17

Cumulative Particle Size Distribution Plot for Run TN

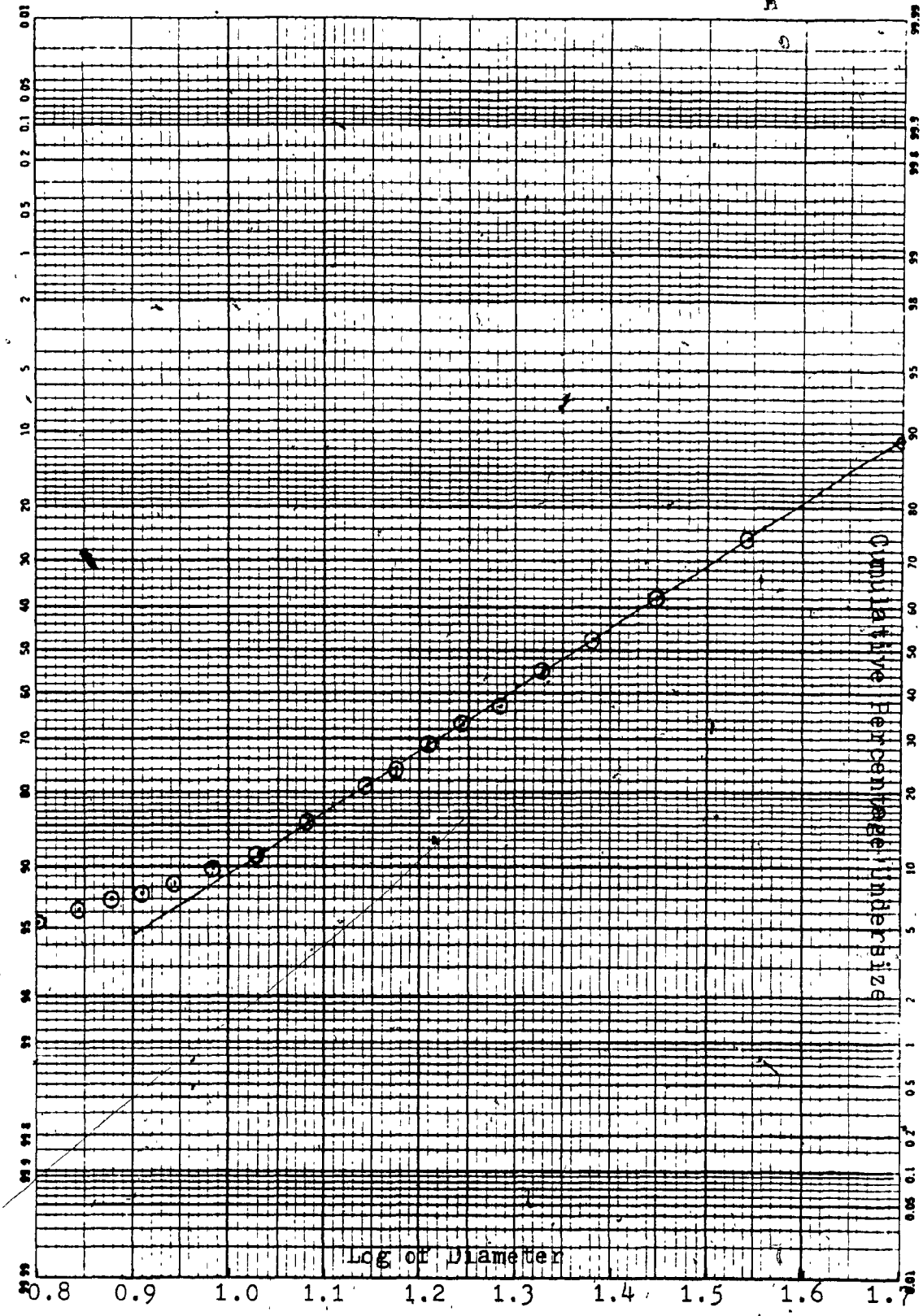

Table A18

Calculation of Particle Size Distribution for Run TO (Table D25)

Samples No.	Weight g	Time sec	Height cm	CPU	Size micron	Log of Size
1	0.1009	—	25.10	—	—	—
2	0.0913	20	24.50	90.49	50.27	1.7010
3	0.0783	40	23.90	77.60	35.11	1.5451
4	0.0656	60	23.30	65.01	28.30	1.4515
5	0.0534	80	22.70	52.92	24.19	1.3833
6	0.0464	100	22.10	45.99	21.35	1.3291
7	0.0383	120	21.50	37.96	19.22	1.2835
8	0.0333	140	20.90	33.00	17.55	1.2440
9	0.0292	160	20.30	28.94	16.18	1.2087
10	0.0242	180	19.70	23.98	15.02	1.1764
11	0.0212	200	19.10	21.01	14.04	1.1471
12	0.0148	260	18.50	14.67	12.12	1.0833
13	0.0101	320	17.90	10.01	10.74	1.0308
14	0.0072	380	17.30	7.14	9.69	0.9861
15	0.0061	440	16.70	6.05	8.85	0.9467
16	0.0051	500	16.10	5.45	8.15	0.9109
17	0.0050	560	15.50	4.96	7.56	0.8783
18	0.0044	620	14.90	4.36	7.04	0.8476
19	0.0040	740	14.30	3.96	6.31	0.8000
20	0.0037	860	13.70	3.67	5.73	0.7587

Median Diameter at 50% = 22.65 μ

Standard Deviation[a] = 1.79

[a]Reported as the average of the two values: (Size at 84% / Size at 50%) and (Size at 50% / Size at 16%).

Figure A18

Cumulative Particle Size Distribution Plot for Run TO

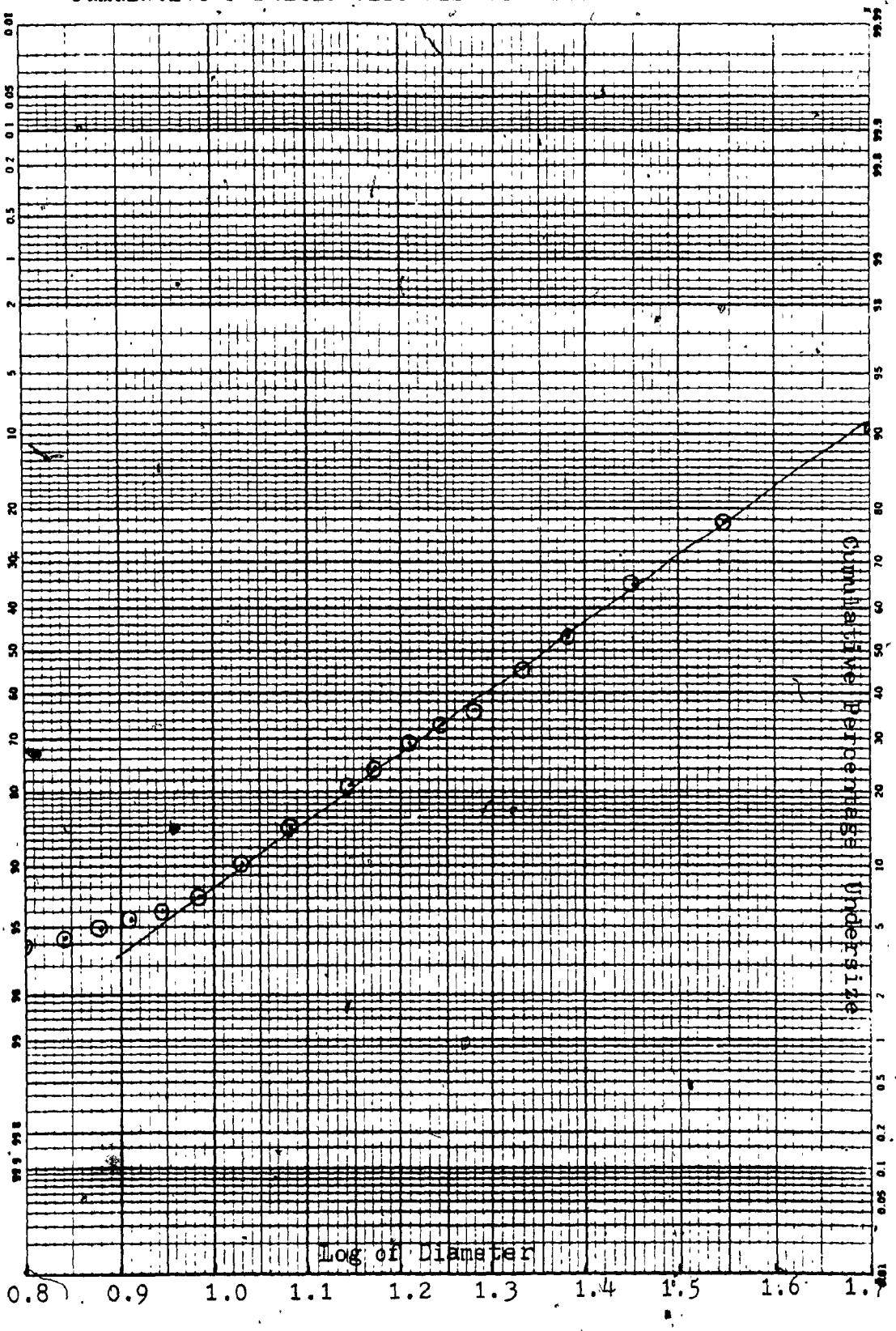

Table A19

Calculation of Particle Size Distribution for Run TP (Table D25)

Samples No.	Weight g	Time sec	Height cm	CPU	Size micron	Log of Size
1	0.1228	—	25.10	—	—	—
2	0.1074	20	24.50	87.46	50.27	1.7010
3	0.0875	40	23.90	71.25	35.11	1.5451
4	0.0769	60	23.30	62.62	28.30	1.4515
5	0.0627	80	22.70	51.06	24.19	1.3833
6	0.0536	100	22.10	43.65	21.35	1.3291
7	0.0448	120	21.50	36.48	19.22	1.2835
8	0.0392	140	20.90	31.92	17.55	1.2440
9	0.0333	160	20.30	27.12	16.18	1.2087
10	0.0272	180	19.70	22.15	15.02	1.1764
11	0.0245	200	19.10	19.95	14.04	1.1471
12	0.0185	260	18.50	15.07	12.12	1.0833
13	0.0136	320	17.90	11.07	10.74	1.0308
14	0.0098	380	17.30	7.98	9.69	0.9861
15	0.0073	440	16.70	5.94	8.85	0.9467
16	0.0056	500	16.10	4.56	8.15	0.9109
17	0.0046	560	15.50	3.75	7.56	0.8783
18	0.0037	620	14.90	3.01	7.04	0.8476
19	0.0032	740	14.30	2.61	6.31	0.8000
20	0.0029	860	13.70	2.36	5.73	0.7587

Median Diameter at 50% = 24.27 μ

Standard Deviation[a] = 1.91

[a]Reported as the average of the two values: (Size at 84% / Size at 50%) and (Size at 50% / Size at 16%).

Figure A19

Cumulative Particle Size Distribution Plot for Run TP

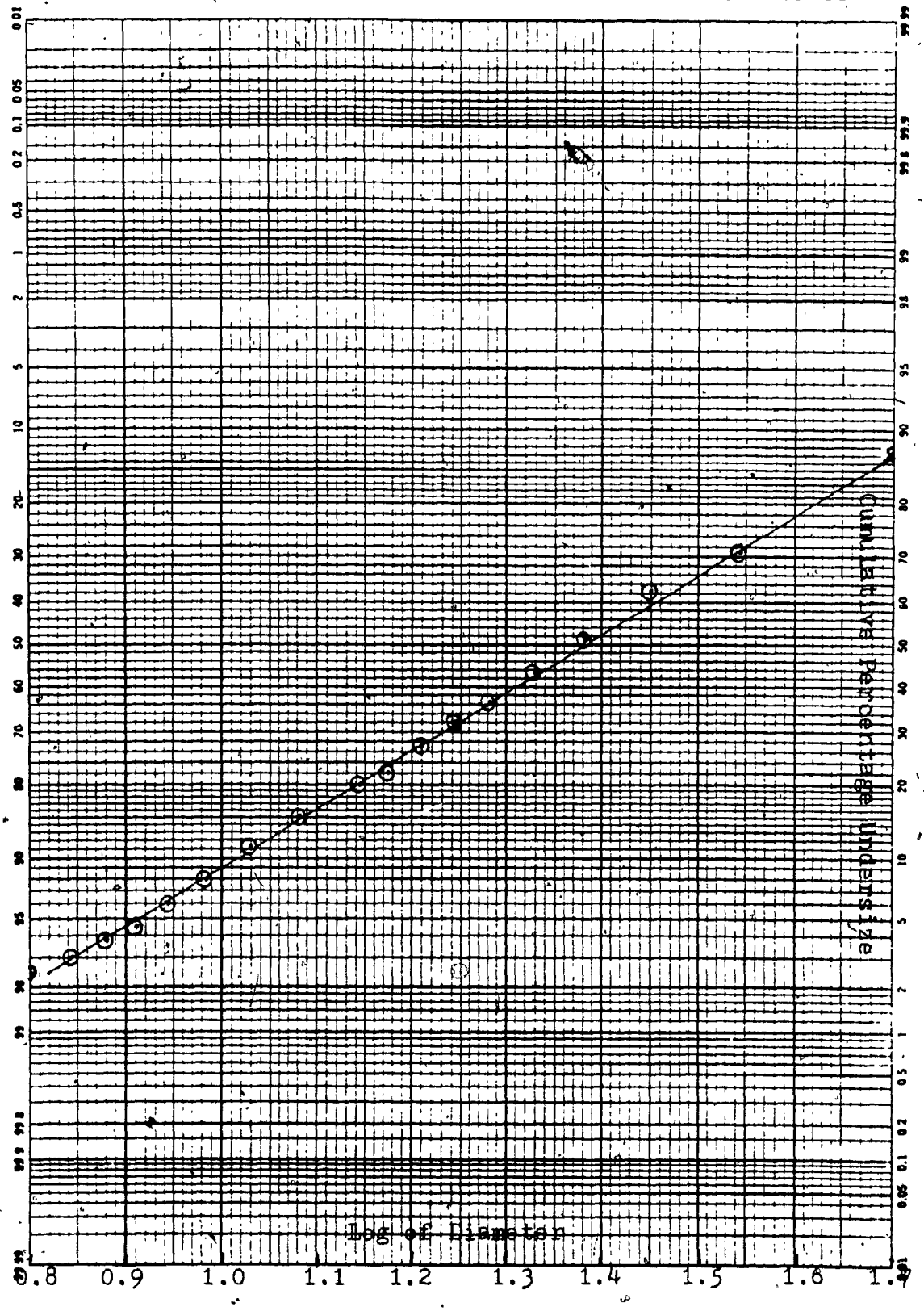

Table A20

Calculation of Particle Size Distribution for Series of Experiment from Run TR (Table 36,39)

Samples No.	Weight g	Time sec	Height cm	CPU	Size micron	Log of Size
1	0.1077	—	25.10	—	—	—
2	0.0878	20	24.30	81.52	50.27	1.7010
3	0.0690	40	23.90	64.07	35.11	1.5451
4	0.0571	60	23.30	53.02	28.30	1.4515
5	0.0474	80	22.70	44.01	24.19	1.3833
6	0.0409	100	22.10	37.98	21.35	1.3291
7	0.0346	120	21.50	32.13	19.22	1.2835
8	0.0312	140	20.90	28.97	17.55	1.2440
9	0.0254	160	20.30	23.58	16.18	1.2087
10	0.0226	180	19.70	20.98	15.02	1.1764
11	0.0199	200	19.10	18.48	14.04	1.1471
12	0.0151	260	18.50	14.02	12.12	1.0832
13	0.0113	320	17.90	10.49	10.74	1.0308
14	0.0086	380	17.30	7.99	9.69	0.9861
15	0.0070	440	16.70	6.50	8.85	0.9467
16	0.0059	500	16.10	5.49	8.15	0.9109
17	0.0051	560	15.50	4.74	7.56	0.8783
18	0.0045	620	14.90	4.18	7.04	0.8476
19	0.0041	740	14.30	3.71	6.31	0.8000
20	0.0037	860	13.70	3.44	5.73	0.7587

Median Diameter at 50% = 26.61 μ

Standard Deviation[a] = 2.07

[a]Reported as the value: (Size at 50% / Size at 16%).

Figure A20

Cumulative Particle Size Distribution Plot for Run TR

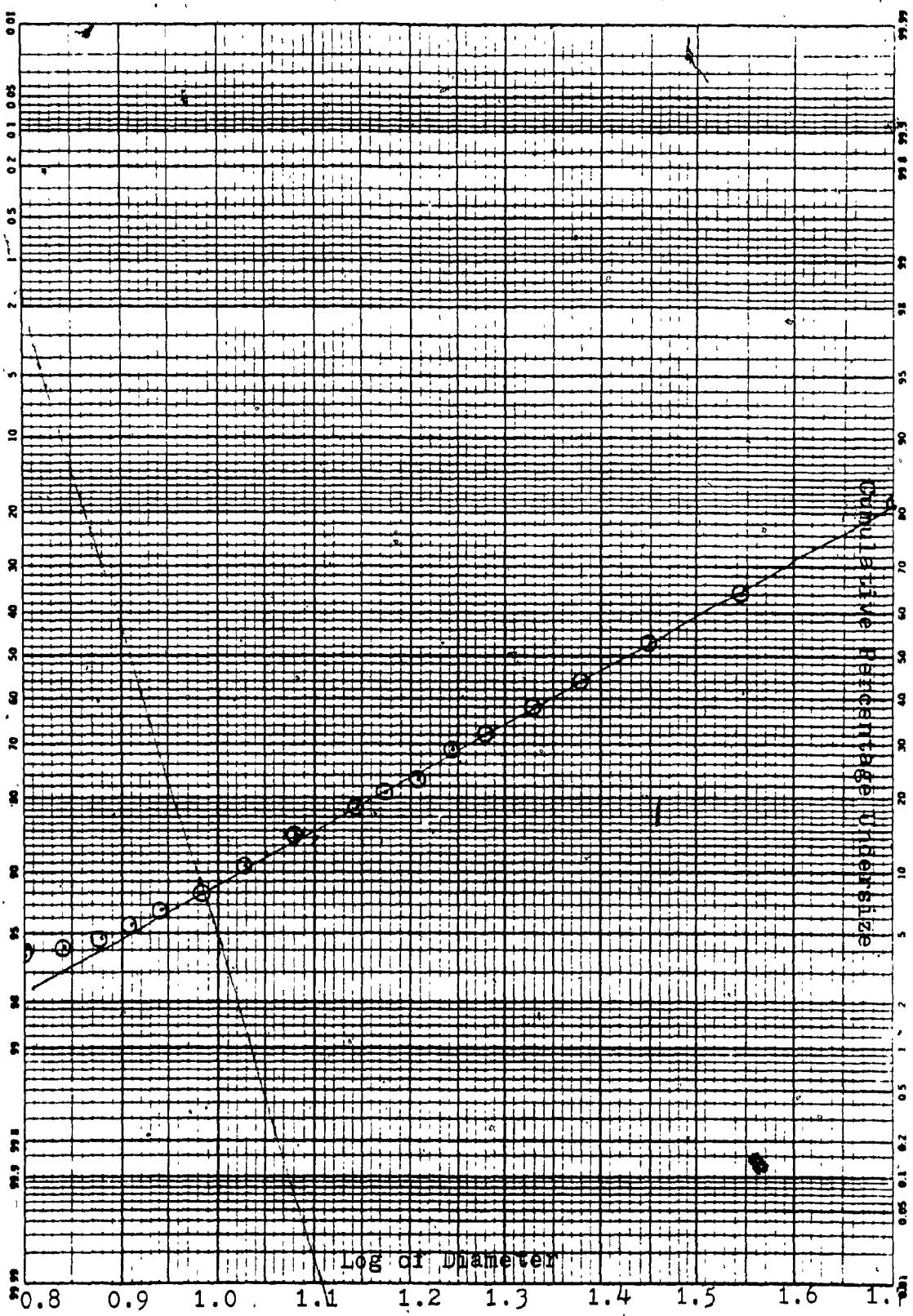

Table A21

Calculation of Particle Size Distribution for Run ST1

Samples No.	Weight g	Time sec	Height cm	CPU	Size micron	Log of Size
1	0.1121	—	25.10	—	—	—
2	0.1054	20	24.50	94.02	50.27	1.7010
3	0.0975	40	23.90	86.98	35.11	1.5451
4	0.0886	60	23.30	79.04	28.30	1.4515
5	0.0799	80	22.70	71.28	24.19	1.3833
6	0.0741	100	22.10	66.10	21.35	1.3291
7	0.0691	120	21.50	61.64	19.22	1.2835
8	0.0628	140	20.90	56.02	17.55	1.2440
9	0.0583	160	20.30	52.01	16.18	1.2087
10	0.0545	180	19.70	48.62	15.02	1.1764
11	0.0488	200	19.10	43.53	14.04	1.1471
12	0.0401	260	18.50	35.77	12.12	1.0833
13	0.0338	320	17.90	30.15	10.74	1.0308
14	0.0271	380	17.30	24.17	9.69	0.9861
15	0.0242	440	16.70	21.59	8.85	0.9467
16	0.0202	500	16.10	18.02	8.15	0.9109
17	0.0157	560	15.50	14.00	7.56	0.8783
18	0.0126	620	14.90	11.24	7.04	0.8476
19	0.0097	740	14.30	8.65	6.31	0.8000
20	0.0086	860	13.70	7.67	5.73	0.7587

Median Diameter at 50% = 15.67 μ

Standard Deviation[a] = 2.07

[a]Reported as the average of the two values: (Size at 84% / Size at 50%) and (Size at 50% / Size at 16%).

Figure A21 :
Cumulative Particle-Size Distribution Plot for Run ST1

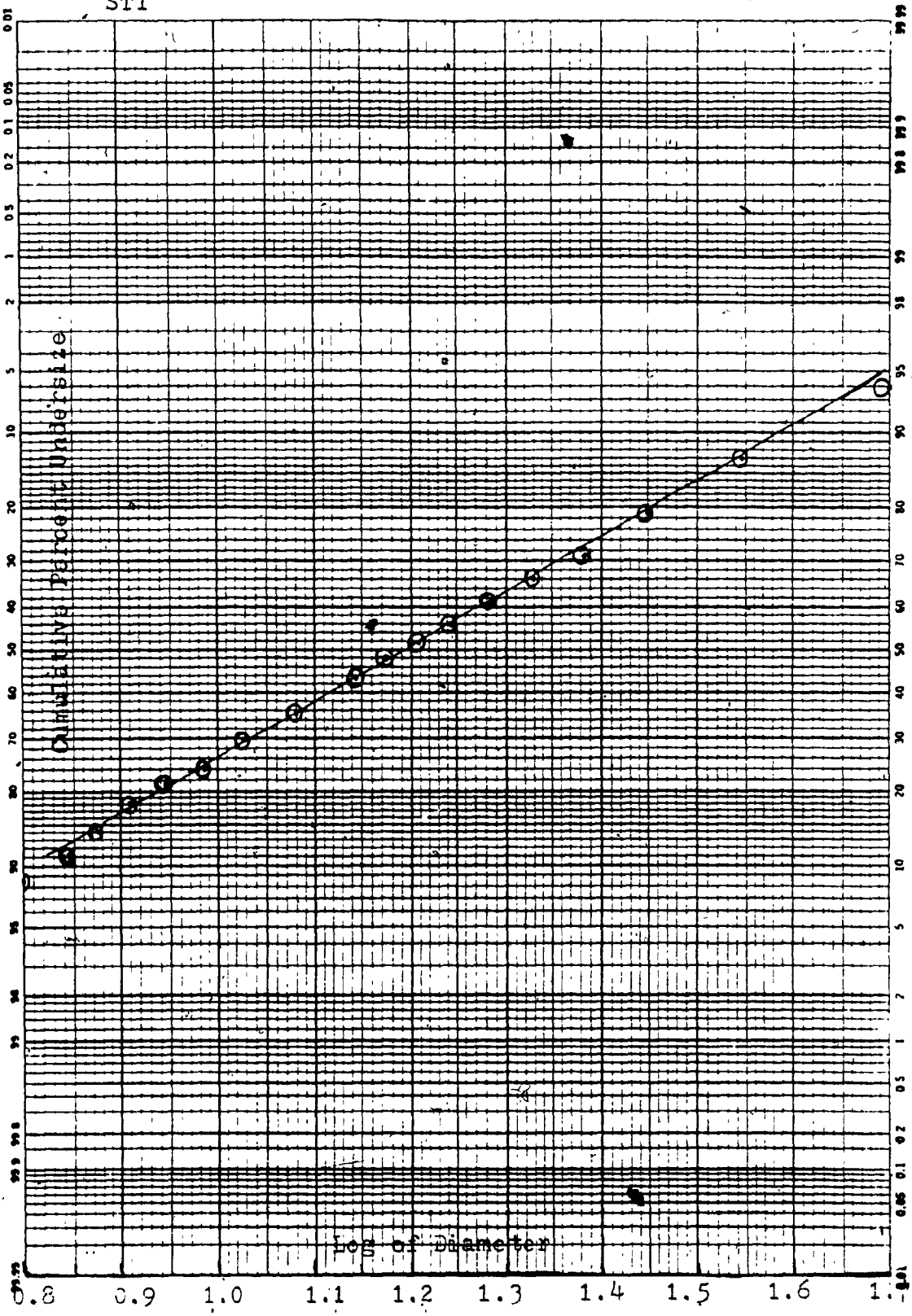

Table A22

Calculation of Particle Size Distribution for Run ST2

Samples No.	Weight g	Time sec	Height cm	CPU	Size micron	Log of Size
1	0.1529	—	25.10	—	—	—
2	0.1430	20	24.50	93.52	50.27	1.7010
3	0.1371	40	23.90	89.67	35.11	1.5451
4	0.1220	60	23.30	79.79	28.30	1.4515
5	0.1142	80	22.70	74.69	24.19	1.3833
6	0.1023	100	22.10	66.91	21.35	1.3291
7	0.0955	120	21.50	62.42	19.22	1.2835
8	0.0887	140	20.90	58.01	17.55	1.2440
9	0.0813	160	20.30	53.17	16.18	1.2087
10	0.0748	180	19.70	48.92	15.02	1.1764
11	0.0685	200	19.10	44.80	14.04	1.1471
12	0.0562	260	18.50	36.76	12.12	1.0833
13	0.0483	320	17.90	31.59	10.74	1.0308
14	0.0426	380	17.30	27.86	9.69	0.9861
15	0.0370	440	16.70	24.00	8.85	0.9467
16	0.0360	500	16.10	23.54	8.15	0.9109
17	0.0327	560	15.50	21.38	7.56	0.8783
18	0.0315	620	14.90	20.60	7.04	0.8476
19	0.0276	740	14.30	18.05	6.31	0.8000
20	0.0231	860	13.70	15.11	5.73	0.7587

Median Diameter at 50% = 15.23 μ

Standard Deviation[a] = 2.03

[a]Reported as the value: (Size at 84% / Size at 50%).

Figure A22

Cumulative Particle Size Distribution Plot for Run ST2

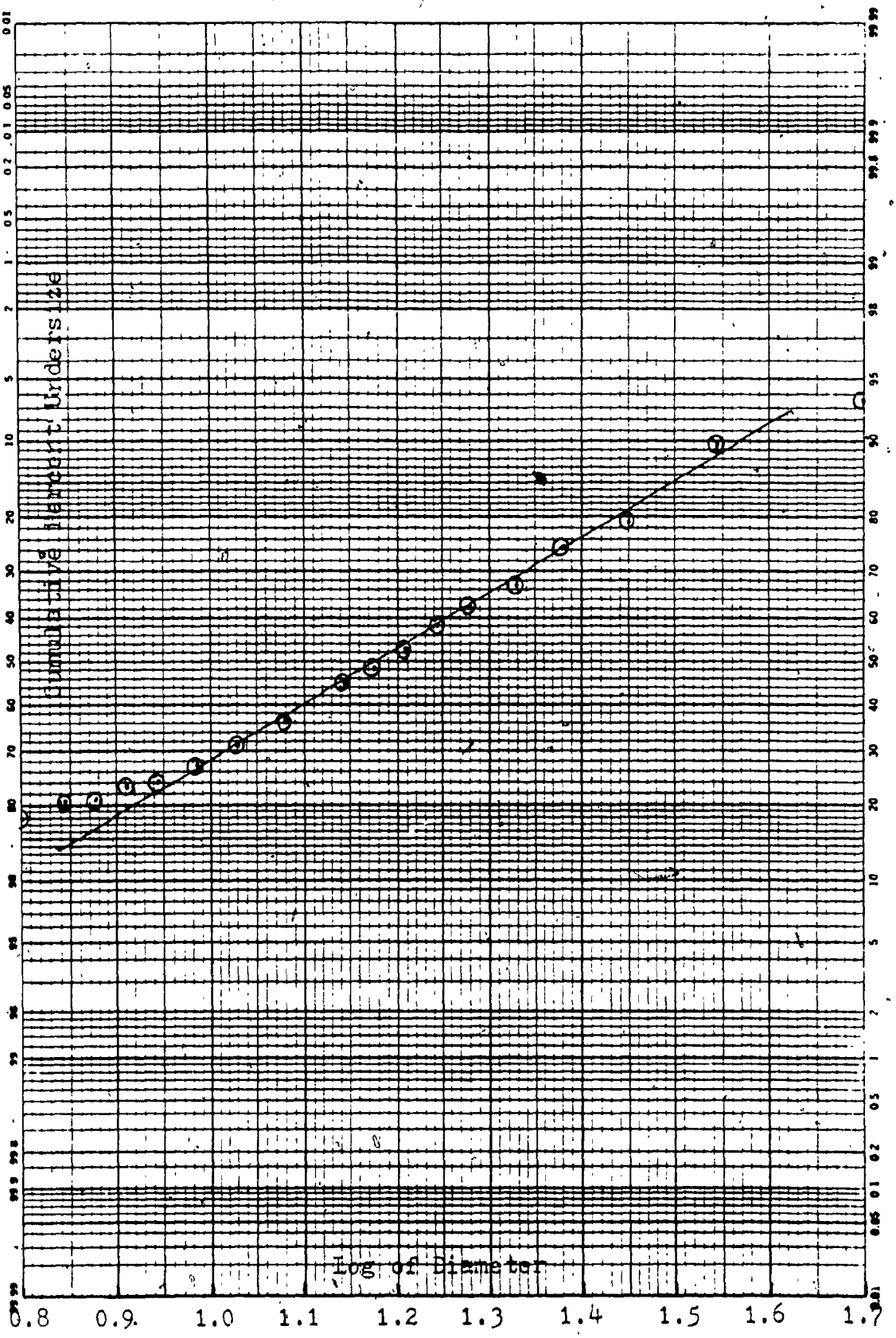

Table A23

Calculation of Particle Size Distribution for Run ST3

Samples No.	Weight g	Time sec	Height cm	CPU	Size micron	Log of Size
1	0.1513	—	25.10	—	—	—
2	0.1443	20	24.50	95.37	50.27	1.7010
3	0.1396	40	23.90	92.27	35.11	1.5451
4	0.1239	60	23.30	81.89	28.30	1.4515
5	0.1159	80	22.70	76.60	24.19	1.3833
6	0.1045	100	22.10	69.07	21.35	1.3291
7	0.0972	120	21.50	64.24	19.22	1.2835
8	0.0897	140	20.90	59.29	17.55	1.2440
9	0.0828	160	20.30	54.73	16.18	1.2087
10	0.0748	180	19.70	49.44	15.02	1.1764
11	0.0663	200	19.10	43.82	14.04	1.1471
12	0.0556	260	18.50	36.75	12.12	1.0833
13	0.0489	320	17.90	32.32	10.74	1.0308
14	0.0433	380	17.30	28.62	9.69	0.9861
15	0.0378	440	16.70	24.98	8.85	0.9467
16	0.0358	500	16.10	23.66	8.15	0.9109
17	0.0324	560	15.50	21.41	7.56	0.8783
18	0.0291	620	14.90	19.23	7.04	0.8476
19	0.0251	740	14.30	16.59	6.31	0.8000
20	0.0236	860	13.70	15.60	5.73	0.7587

Median Diameter at 50% = 15.31 μ

Standard Deviation[a] = 1.99

[a]Reported as the value: (Size at 84% / Size at 50%).

Figure A23

Cumulative Particle Size Distribution Plot for Run ST3

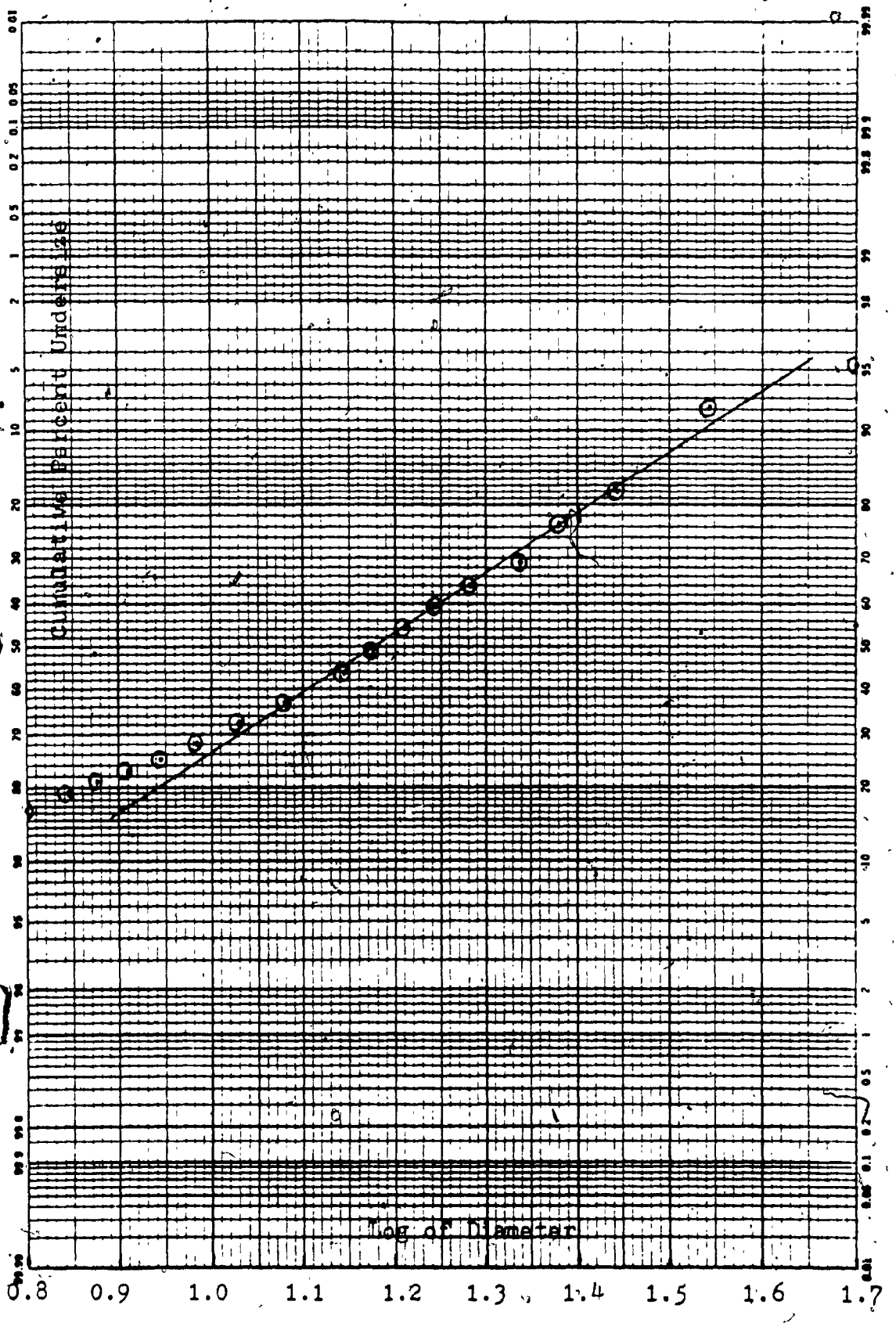

Table A24

Calculation of Particle Size Distribution for Run ST4

Samples No.	Weight g	Time sec	Height cm	CPU	Size micron	Log of Size
1	0.1517	—	25.10	—	—	—
2	0.1480	20	24.50	97.56	50.27	1.7010
3	0.1379	40	23.90	90.90	35.11	1.5451
4	0.1283	60	23.30	84.57	28.30	1.4515
5	0.1145	80	22.70	75.48	24.19	1.3833
6	0.1073	100	22.10	70.73	21.35	1.3291
7	0.0954	120	21.50	62.89	19.22	1.2835
8	0.0871	140	20.90	57.41	17.55	1.2440
9	0.0794	160	20.30	52.34	16.18	1.2087
10	0.0727	180	19.70	47.92	15.02	1.1764
11	0.0687	200	19.10	45.29	14.04	1.1471
12	0.0552	260	18.50	36.39	12.12	1.0833
13	0.0465	320	17.90	30.65	10.74	1.0308
14	0.0410	380	17.30	27.03	9.69	0.9861
15	0.0372	440	16.70	24.52	8.85	0.9467
16	0.0323	500	16.10	21.19	8.15	0.9109
17	0.0293	560	15.50	19.31	7.56	0.8783
18	0.0284	620	14.90	18.72	7.04	0.8476
19	0.0258	740	14.30	17.00	6.31	0.8000
20		860	13.70		5.73	0.7587

Median Diameter at 50% = 15.40 μ

Standard Deviation[a] = 1.89

[a]Reported as the value: (Size at 84% / Size at 50%).

Figure A24

Cumulative Particle Size Distribution Plot for Run ST4

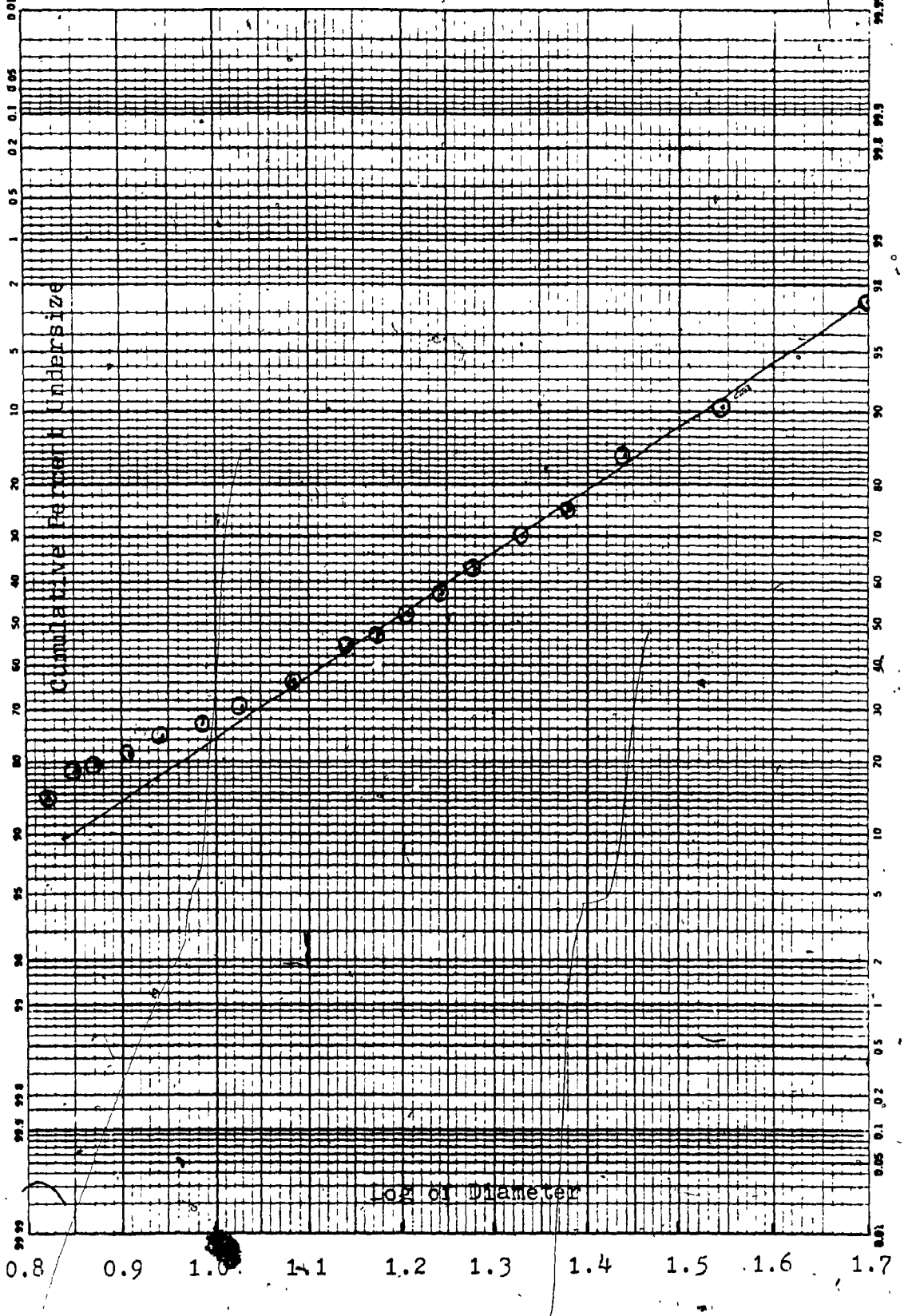

APPENDIX B

Tabulated nuclei population density, nucleation rate and growth rate data obtained from particle-size analysis.

The particle-size distribution obtained from the particle size analysis were used to obtain $\bar{L}$, ΔL, and the weight of fraction of powder of the given size fraction $\bar{L}$, dW, $\bar{L}$ is the mean size of the particle sizes having a ΔL difference in the sizes. The specific gravity of crystal, 8.92 g/cm^3 was taken. The α, the volume shape factor of the particle was the factor by which particle volume will differ from the Stokes' sphere whose diameter was obtained in the particle size analysis.

The population density n (number u^{-1}) was calculated by dividing dW by $\alpha\rho\bar{L}^3\Delta L$. The data obtained are plotted as Log n versus $\bar{L}$. The values of the slope and intercept for each plot were determined by a linear least squares method. The growth rate was determined from the slope i.e. $1/2.303\ Gt$, where t is the residence time of the crystal in the crystallizer. The nuclei population density, n^o, was determined from the intercept i.e. Log n, and equation 29 was used to determine the nucleation rate.

Table B1

Determination of Population Density, Nucleation Rate and Growth Rate for Run G *

Size μ	ΔL μ	$\bar{L}$ μ	$\bar{L}^3$ μ^3	$\alpha \rho \bar{L}^3 \Delta L$ g μ	Weight, dW g	P. Density, n. no. μ^{-1}	Log n
50.27-35.11	15.16	42.69	7.78×10^4	5.51×10^{-6}	0.1023	1.86×10^4	4.27
35.11-28.30	6.81	31.70	3.19×10^4	1.01×10^{-7}	0.0876	8.67×10^4	4.94
28.30-24.19	4.11	26.25	1.81×10^4	3.47×10^{-7}	0.0785	2.26×10^5	5.35
24.19-21.35	2.84	22.77	1.18×10^3	1.57×10^{-8}	0.0671	4.27×10^5	5.63
21.35-19.22	2.13	20.28	8.34×10^3	8.30×10^{-8}	0.0617	7.43×10^5	5.87
19.22-17.55	1.67	18.38	6.21×10^3	4.85×10^{-8}	0.0561	1.16×10^6	6.06
17.55-16.18	1.37	16.87	4.80×10^3	3.07×10^{-8}	0.0499	1.62×10^6	6.21
16.88-15.02	1.16	15.60	3.80×10^3	2.06×10^{-8}	0.0463	2.25×10^6	6.35
15.02-14.04	0.98**	14.50	3.05×10^3	1.40×10^{-8}	0.0408	2.91×10^6	6.46
14.04-12.12	0.64**	13.08	2.24×10^3	6.69×10^{-9}	0.0384	5.71×10^6	6.71
12.12-10.74	0.46**	11.43	1.49×10^3	3.21×10^{-9}	0.0341	1.06×10^7	7.03
<10.74	—	—	—	—	—	—	—

Nuclei Population Density, n^o = 5.15×10^7 no./μ

Nucleation Rate = 4.68×10^4 no./sec

Growth Rate = 0.91×10^{-3} μ/sec

*Withdraw down time = [redacted]49 h.

**Δ L corrected for time interval.

Figure B1

Plot of Logarithm of Population Density Versus Mean Diameter for Run G.

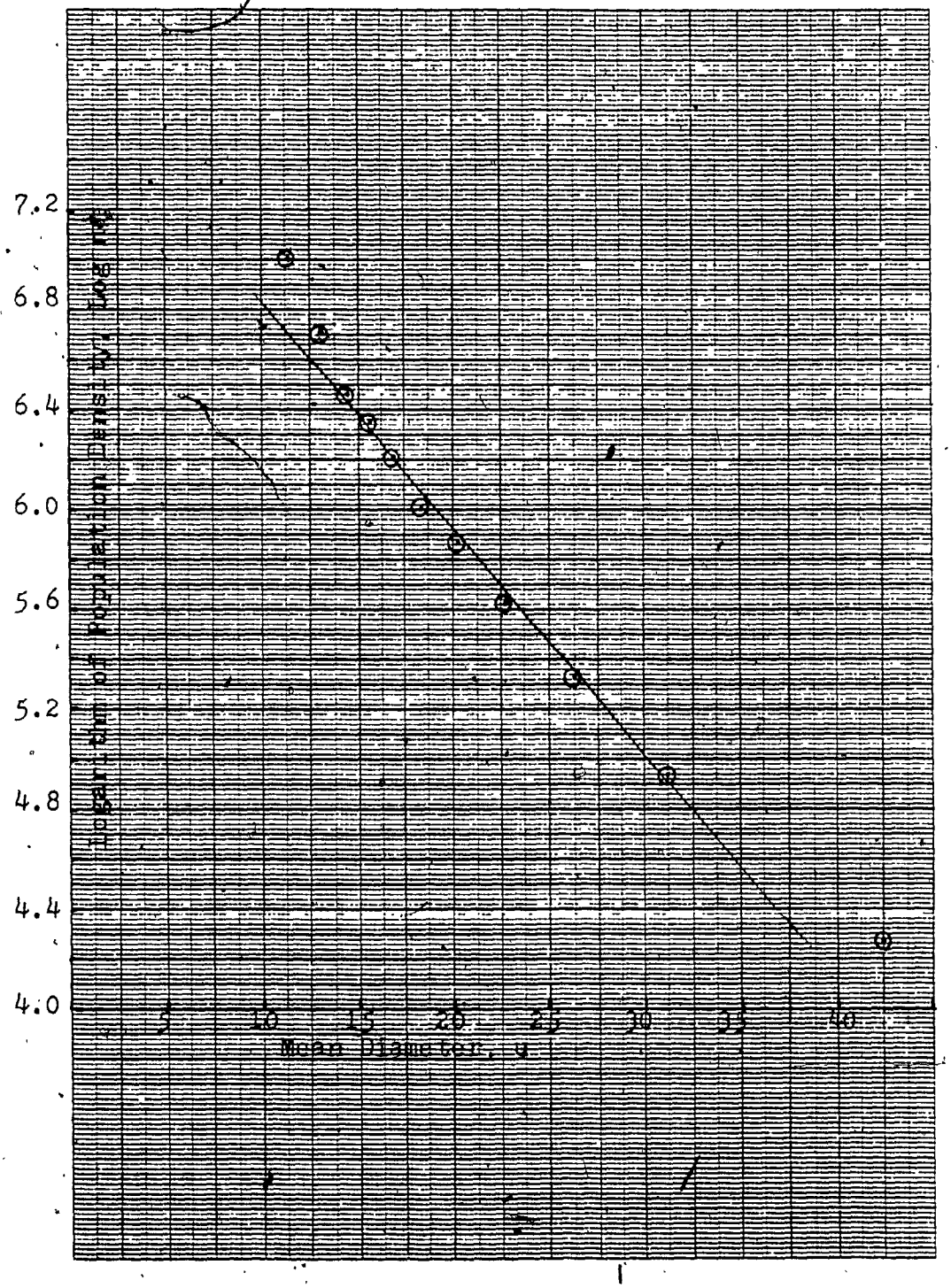

Table B2

Determination of Population Density, Nucleation Rate and Growth Rate for Run I*

Size μ	ΔL μ	$\bar{L}$ μ	$\bar{L}^3$ μ^3	$\alpha \rho \bar{L}^3 \Delta L$ g μ	Weight, dW g	P.Density, n. no. μ^{-1}	Log n
50.27-35.11	15.16	42.69	7.78×10^4	5.51×10^{-6}	0.1120	2.03×10^4	4.31
35.11-28.30	6.81	31.70	3.19×10^4	1.01×10^{-7}	0.0978	9.68×10^4	4.99
28.30-24.19	4.11	26.25	1.81×10^4	3.47×10^{-7}	0.0837	2.41×10^5	5.38
24.19-21.35	2.84	22.77	1.18×10^4	1.57×10^{-8}	0.0747	4.76×10^5	5.68
21.35-19.22	2.13	20.28	8.34×10^3	8.30×10^{-8}	0.0666	8.02×10^5	5.90
19.22-17.55	1.67	18.38	6.21×10^3	4.85×10^{-8}	0.0594	1.22×10^6	6.09
17.55-16.18	1.37	16.87	4.80×10^3	3.07×10^{-8}	0.0534	1.74×10^6	6.24
16.88-15.02	1.16	15.60	3.80×10^3	2.06×10^{-8}	0.0496	2.41×10^6	6.38
15.02-14.04	0.98**	14.50	3.05×10^3	1.40×10^{-8}	0.0447	3.19×10^6	6.50
14.04-12.12	0.64**	13.08	2.24×10^3	6.69×10^{-9}	0.0404	6.04×10^6	6.78
12.12-10.74	0.46	11.43	1.49×10^3	3.21×10^{-9}	0.0315	9.81×10^6	6.99
<10.74	—	—	—	—	—	—	—

Nuclei Population Density, n^o = 5.39×10^7 no./μ

Nucleation Rate = 7.59×10^4 no./sec

Growth Rate = 1.41×10^{-3} μ/sec

*Withdraw down time = 0.97 h.

**Δ L corrected for time interval.

Figure B2

Plot of Logrithm of Population Density Versus Mean Diameter for Run I.

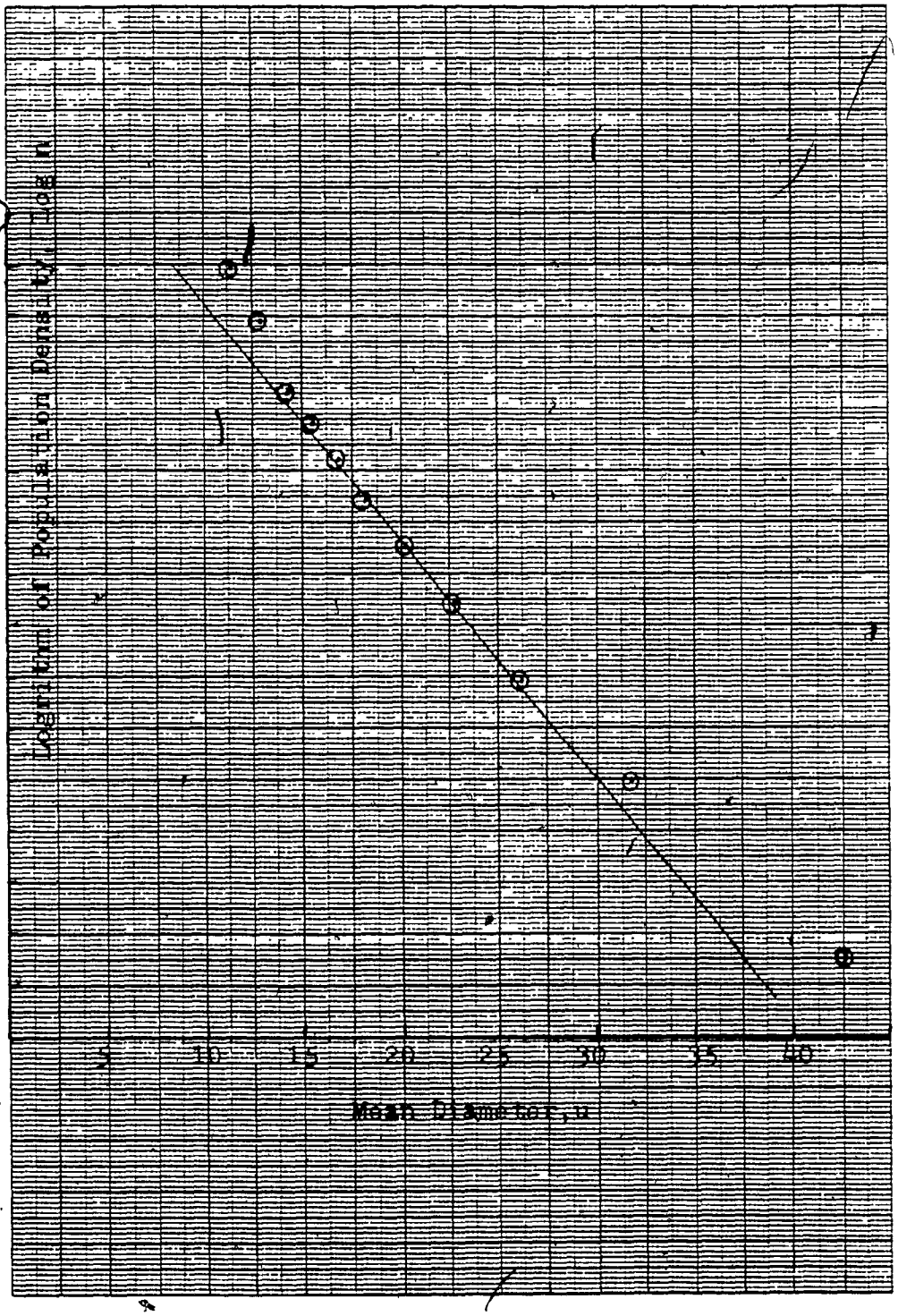

Table B3

Determination of Population Density, Nucleation Rate and Growth Rate for Run QI *

Size μ	ΔL μ	$\bar{L}$ μ	$\bar{L}^3$ μ^3	$\alpha \rho \bar{L}^3 \Delta L$ g μ	Weight, dW g	P.Density, n. no. μ^{-1}	Log n
50.27-35.11	15.16	42.69	7.78×10^4	5.51×10^{-6}	0.0885	1.61×10^4	4.21
35.11-28.30	6.81	31.70	3.19×10^4	1.01×10^{-7}	0.0737	7.30×10^5	4.86
28.30-24.19	4.11	26.25	1.81×10^4	3.47×10^{-7}	0.0599	1.73×10^5	5.24
24.19-21.35	2.84	22.77	1.18×10^3	1.57×10^{-8}	0.0502	3.20×10^5	5.50
21.35-19.22	2.13	20.28	8.34×10^3	8.30×10^{-8}	0.0413	4.97×10^5	5.70
19.22-17.55	1.67	18.38	6.21×10^3	4.85×10^{-8}	0.0353	7.28×10^5	5.86
17.55-16.18	1.37	16.87	4.80×10^3	3.07×10^{-8}	0.0275	8.96×10^5	5.95
16.88-15.02	1.16	15.60	3.80×10^3	2.06×10^{-8}	0.0253	1.23×10^6	6.09
15.02-14.04	0.98**	14.50	3.05×10^3	1.40×10^{-9}	0.0197	1.41×10^6	6.15
14.04-12.12	0.64**	13.08	2.24×10^3	6.69×10^{-9}	0.0167	2.50×10^6	6.40
12.12-10.74	0.46**	11.43	1.49×10^3	3.21×10^{-9}	0.0122	3.80×10^6	6.57
<10.74	—	—	—	—	—	—	—

Nuclei Population Density, n^σ = 1.78×10^7 no./μ

Nucleation Rate = 2.91×10^4 no./sec

Growth Rate = 1.64×10^{-3} μ/sec

*Withdraw down time = 0.97 h.

**Δ L corrected for time interval.

Figure B3

Plot of Logarithm of Population Density Versus Mean Diameter for Run QI.

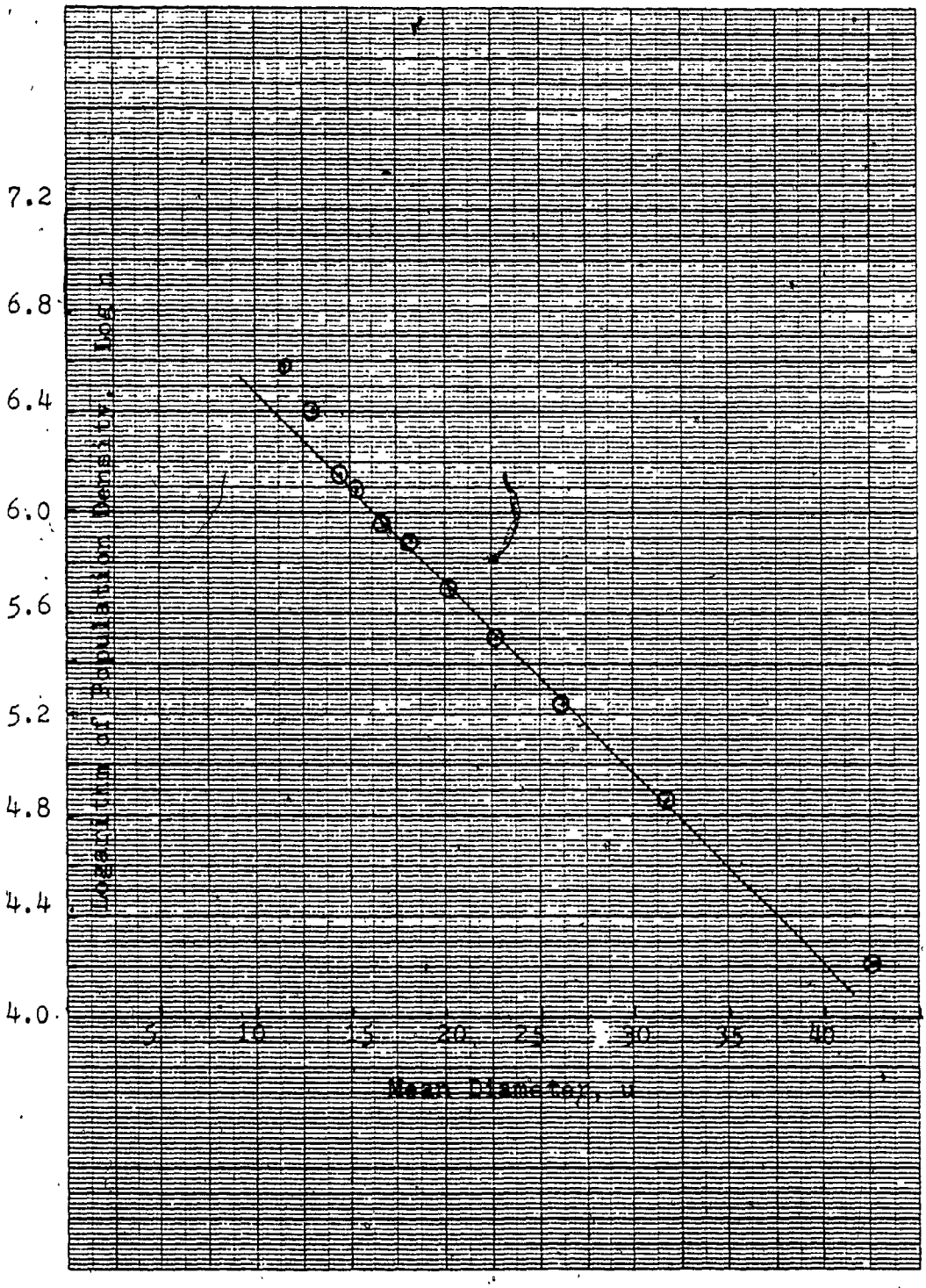

Table B4

Determination of Population Density, Nucleation Rate and Growth Rate for Run K*

Size μ	ΔL μ	$\bar{L}$ μ	$\bar{L}^3$ μ^3	$\alpha \rho \bar{L}^3 \Delta L$ g μ	Weight, dW g	P.Density, n. no. μ^{-1}	Log n
50.27-35.11	15.16	42.69	7.78×10^4	5.51×10^{-6}	0.1094	1.98×10^4	4.30
35.11-28.30	6.81	31.70	3.19×10^4	1.01×10^{-6}	0.1026	1.01×10^5	5.01
28.30-24.19	4.11	26.25	1.81×10^4	3.47×10^{-7}	0.0953	2.75×10^5	5.44
24.19-21.35	2.84	22.77	1.18×10^4	1.57×10^{-7}	0.0829	5.28×10^5	5.72
21.35-19.22	2.13	20.28	8.34×10^3	8.30×10^{-8}	0.0743	8.95×10^5	5.95
19.22-17.55	1.67	18.38	6.21×10^3	4.85×10^{-8}	0.0668	1.38×10^6	6.14
17.55-16.18	1.37	16.87	4.80×10^3	3.07×10^{-8}	0.0597	1.94×10^6	6.29
16.88-15.02	1.16	15.60	3.80×10^3	2.06×10^{-8}	0.0533	2.59×10^6	6.41
15.02-14.04	0.98**	14.50	3.05×10^3	1.40×10^{-9}	0.0492	3.51×10^6	6.54
14.04-12.12	0.64**	13.08	2.24×10^3	6.69×10^{-9}	0.0425	6.35×10^6	6.80
12.12-10.74	0.46	11.43	1.49×10^3	3.21×10^{-9}	0.0358	1.11×10^7	7.05
<10.74	—	—	—	—	—	—	—

Nuclei Population Density, n^o = 6.09×10^7 no./μ

Nucleation Rate = 12.34×10^4 no./sec

Growth Rate = 2.03×10^{-3} μ /sec

*Withdraw down time = 0.67 h.

**Δ L corrected for time interval.

Figure B4

Plot of Logarithm of Population Density Versus Mean Diameter for Run K.

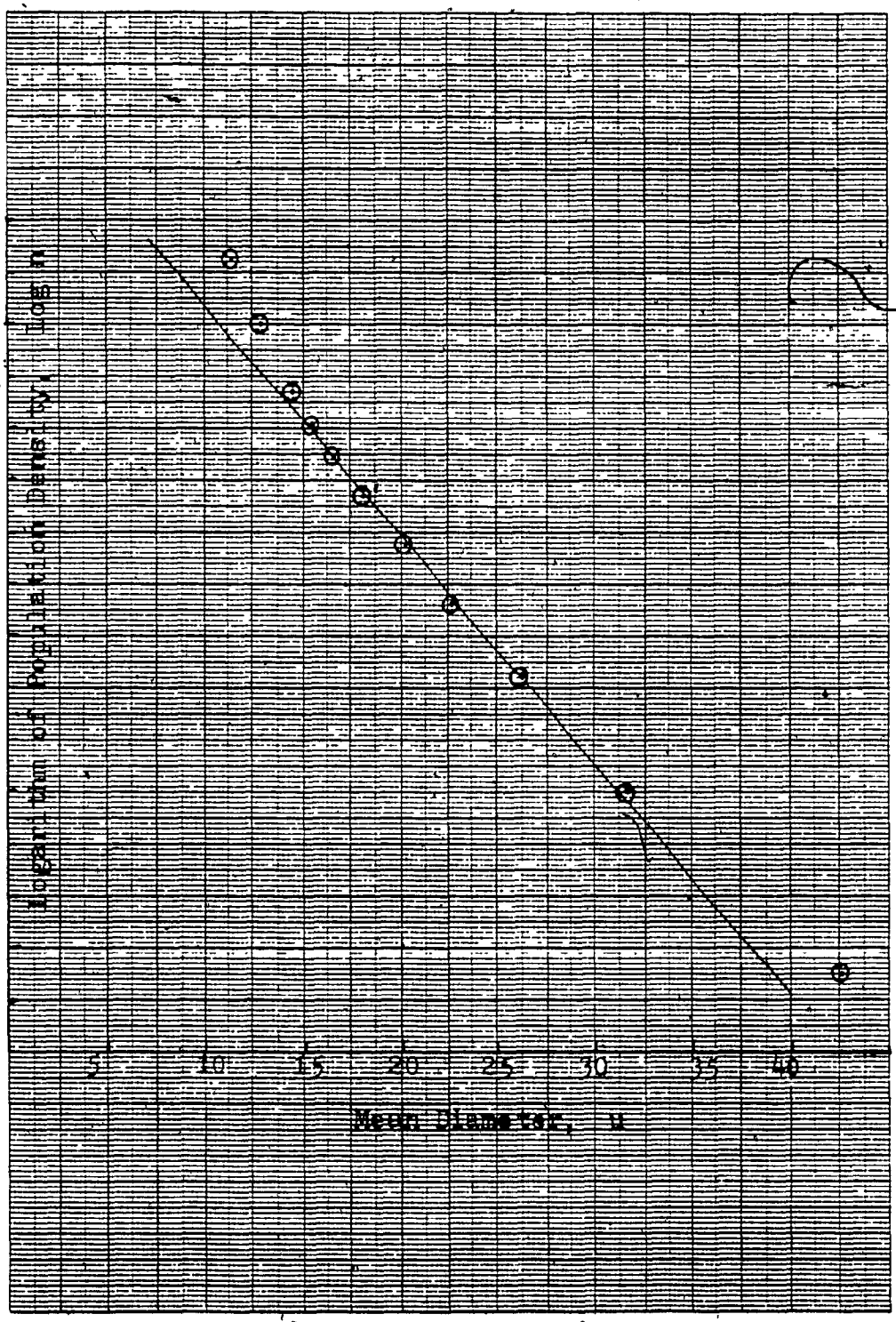

Table B5

Determination of Population Density, Nucleation Rate and Growth Rate for Run QK*

Size μ	ΔL μ	$\bar{L}$ μ	$\bar{L}^3$ μ^3	$\alpha \rho \bar{L}^3 \Delta L$ g μ	Weight, dW g	P. Density, n. no. μ^{-1}	Log n
50.27-35.11	15.16	42.69	7.78×10^4	5.51×10^{-6}	0.1267	2.30×10^4	4.36
35.11-28.30	6.81	31.70	3.19×10^4	1.01×10^{-6}	0.1067	1.06×10^5	5.02
28.30-24.19	4.11	26.25	1.81×10^4	3.47×10^{-7}	0.0905	2.61×10^5	5.42
24.19-21.35	2.84	22.77	1.18×10^4	1.57×10^{-7}	0.0743	4.73×10^5	5.67
21.35-19.22	2.13	20.28	8.34×10^3	8.30×10^{-8}	0.0648	7.81×10^5	5.89
19.22-17.55	1.67	18.38	6.21×10^3	4.85×10^{-8}	0.0540	1.11×10^6	6.05
17.55-16.18	1.37	16.87	4.80×10^3	3.07×10^{-8}	0.0459	1.49×10^6	6.17
16.88-15.02	1.16	15.60	3.80×10^3	2.06×10^{-8}	0.0378	1.83×10^6	6.26
15.02-14.04	0.98**	14.50	3.05×10^3	1.40×10^{-9}	0.0338	2.41×10^6	6.38
14.04-12.12	0.64**	13.08	2.24×10^3	6.69×10^{-9}	0.0283	4.23×10^6	6.63
12.12-10.74	0.46	11.43	1.49×10^3	3.21×10^{-9}	0.0196	6.11×10^6	6.78
<10.74	—	—	—	—	—	—	—

Nuclei Population Density, n^o = 3.14×10^7 no./μ

Nucleation Rate = 7.17×10^4 no./sec

Growth Rate = 2.28×10^{-3} μ/sec

*Withdraw down time = 0.67 h

**Δ L corrected for time interval.

Figure B5

Plot of Logarithm of Population Density Versus Mean Diameter for Run QK.

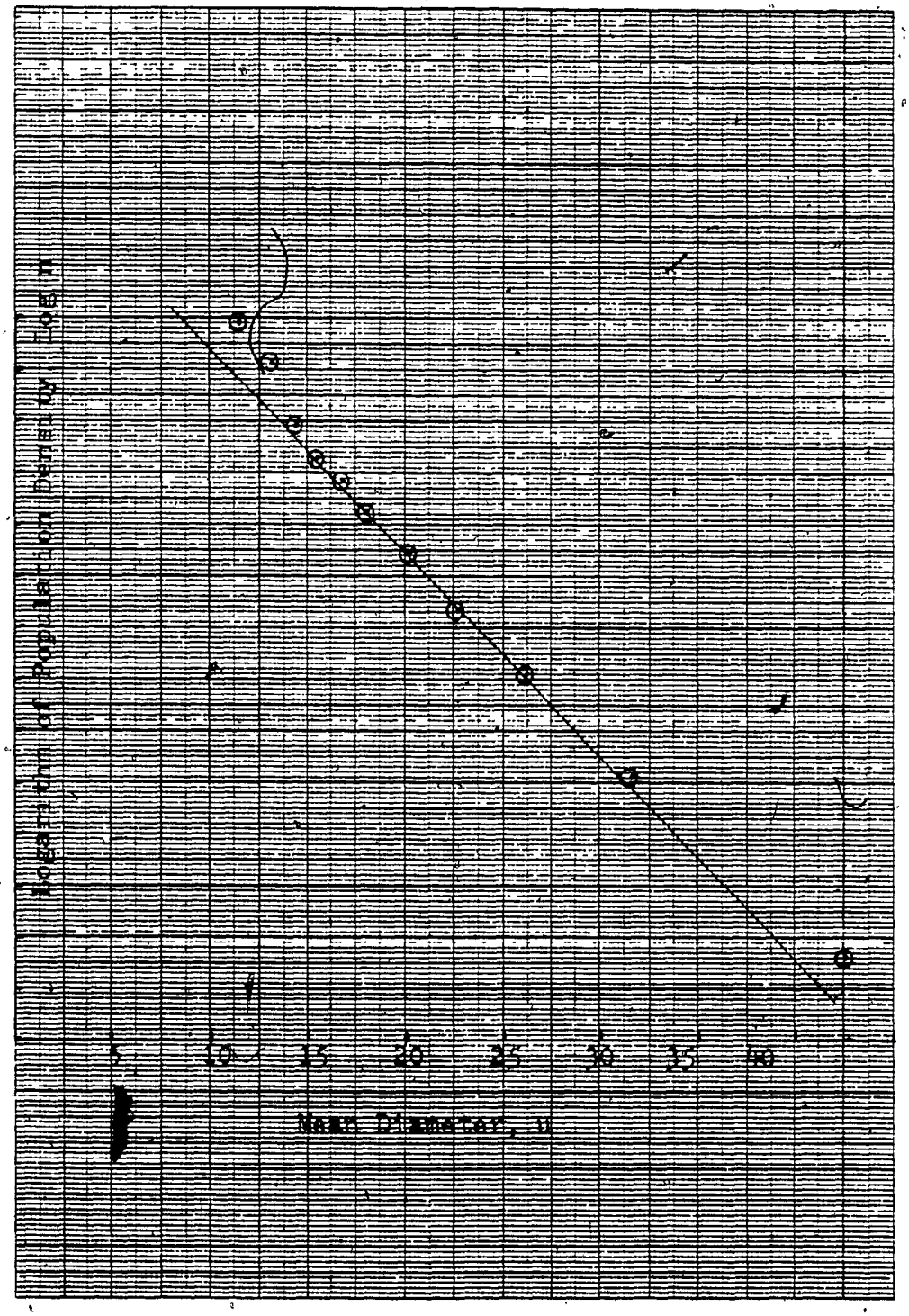

Table B6

Determination of Population Density, Nucleation Rate and Growth Rate for Run TK *

Size μ	ΔL μ	$\bar{L}$ μ	$\bar{L}^3$ μ^3	$\alpha \rho \bar{L}^3 \Delta L$ g μ	Weight, dW g	P.Density, n. no. μ^{-1}	Log n
50.27-35.11	15.16	42.69	7.78×10^4	5.51×10^{-6}	0.1005	1.82×10^4	4.26
35.11-28.30	6.81	31.70	3.19×10^4	1.01×10^{-7}	0.0818	8.10×10^4	4.91
28.30-24.19	4.11	26.25	1.81×10^4	3.47×10^{-7}	0.0648	1.87×10^5	5.27
24.19-21.35	2.84	22.77	1.18×10^4	1.57×10^{-8}	0.0555	3.53×10^5	5.56
21.35-19.22	2.13	20.28	8.34×10^3	8.30×10^{-8}	0.0470	5.66×10^5	5.75
19.22-17.55	1.67	18.38	6.21×10^3	4.85×10^{-8}	0.0402	8.29×10^5	5.92
17.55-16.18	1.37	16.87	4.80×10^3	3.07×10^{-8}	0.0343	1.12×10^6	6.05
16.88-15.02	1.16	15.60	3.80×10^3	2.06×10^{-8}	0.0283	1.37×10^6	6.14
15.02-14.04	0.98**	14.50	3.05×10^3	1.40×10^{-9}	0.0256	1.83×10^6	6.26
14.04-12.12	0.64**	13.08	2.24×10^3	6.69×10^{-9}	0.0223	3.33×10^6	6.52
12.12-10.74	0.46	11.43	1.49×10^3	3.21×10^{-9}	0.0165	5.14×10^6	6.71
<10.74	—	—	—	—	—	—	—

Nuclei Population Density, n^o = 2.41×10^7 no./μ

Nucleation Rate = 5.48×10^3 no./sec

Growth Rate = 2.27×10^{-3} μ/sec

*Withdraw down time = 0.67 h.

**Δ L corrected for time interval.

Figure B6

Plot of Logrithm of Population Density Versus Mean Diameter for Run TK.

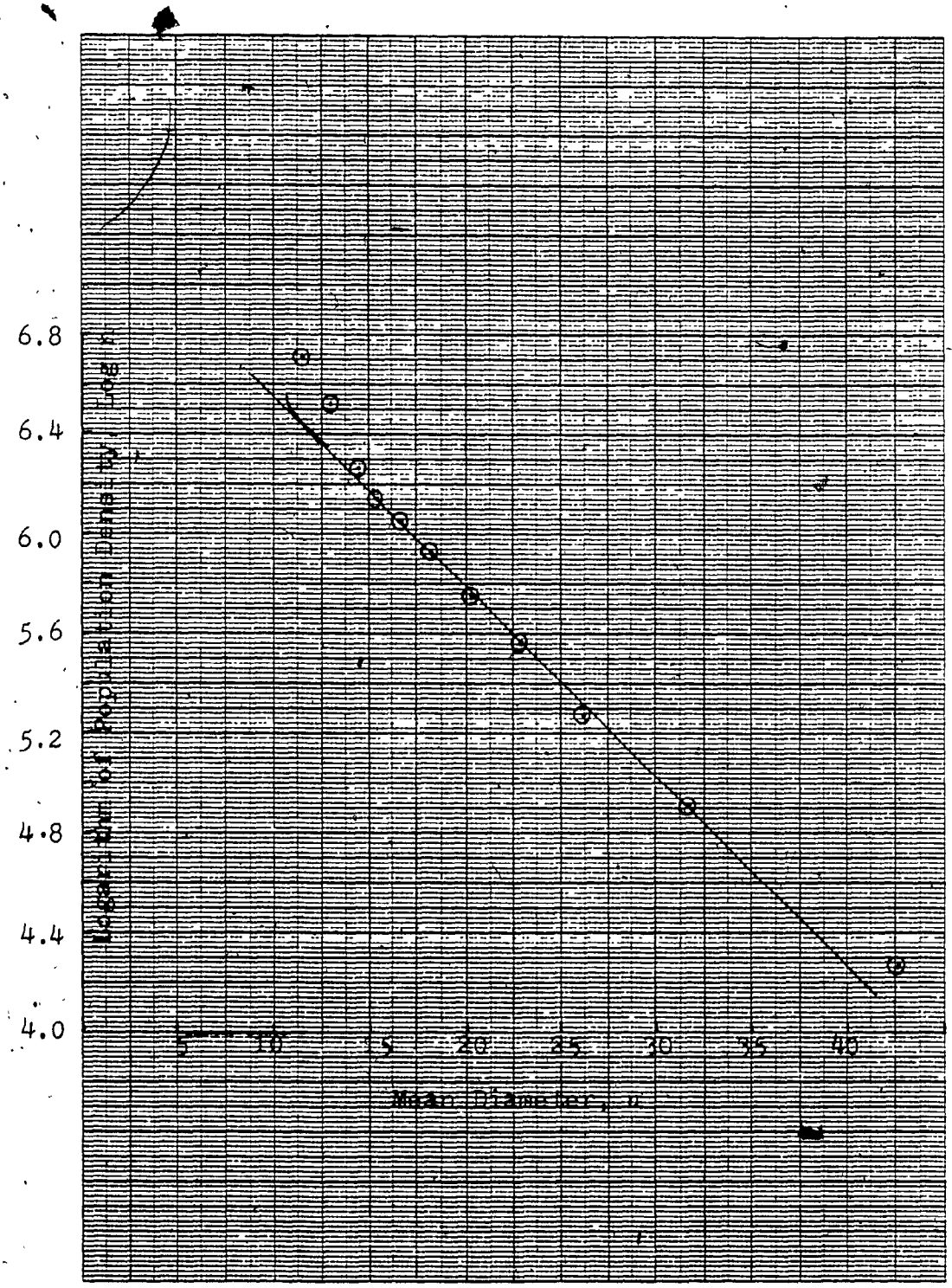

Table B7

Determination of Population Density, Nucleation Rate and Growth Rate for Run M*

Size μ	ΔL μ	$\bar{L}$ μ	$\bar{L}^3$ μ^3	$\alpha \rho \bar{L}^3 \Delta L$ g μ	Weight, dW g	P.Density, n. no. μ^{-1}	Log n
50.27-35.11	* 15.16	42.69	7.78×10^4	5.51×10^{-6}	0.1110	2.01×10^4	4.30
35.11-28.30	6.81	31.70	3.19×10^4	1.01×10^{-6}	0.1064	1.05×10^5	5.02
28.30-24.19	4.11	26.25	1.81×10^4	3.47×10^{-7}	0.0933	2.69×10^5	5.43
24.19-21.35	2.84	22.77	1.18×10^4	1.57×10^{-8}	0.0840	5.35×10^5	5.73
21.35-19.22	2.13	20.28	8.34×10^3	8.30×10^{-8}	0.0746	8.99×10^5	5.93
19.22-17.55	1.67	18.38	6.21×10^3	4.85×10^{-8}	0.0677	1.39×10^6	6.14
17.55-16.18	1.37	16.87	4.80×10^3	3.07×10^{-8}	0.0629	2.05×10^6	6.31
16.88-15.02	1.16	15.60	3.80×10^3	2.06×10^{-8}	0.0552	2.68×10^6	6.43
15.02-14.04	0.98**	14.50	3.05×10^3	1.40×10^{-8}	0.0492	3.51×10^6	6.54
14.04-12.12	0.64**	13.08	2.24×10^3	6.69×10^{-9}	0.0447	6.68×10^6	6.82
12.12-10.74	0.46	11.43	1.49×10^3	3.21×10^{-9}	0.0338	1.05×10^7	7.02
<10.74	—	—	—	—	—	—	—

Nuclei Population Density, n^0 = 6.31×10^7 no./μ

Nucleation Rate = 18.94×10^4 no./sec

Growth Rate = 3.00×10^{-3} μ/sec

*Withdraw down time = 0.45 h.

**Δ L corrected for time interval.

Figure B7

Plot of Logarithm of Population Density Versus Mean Diameter for Run M.

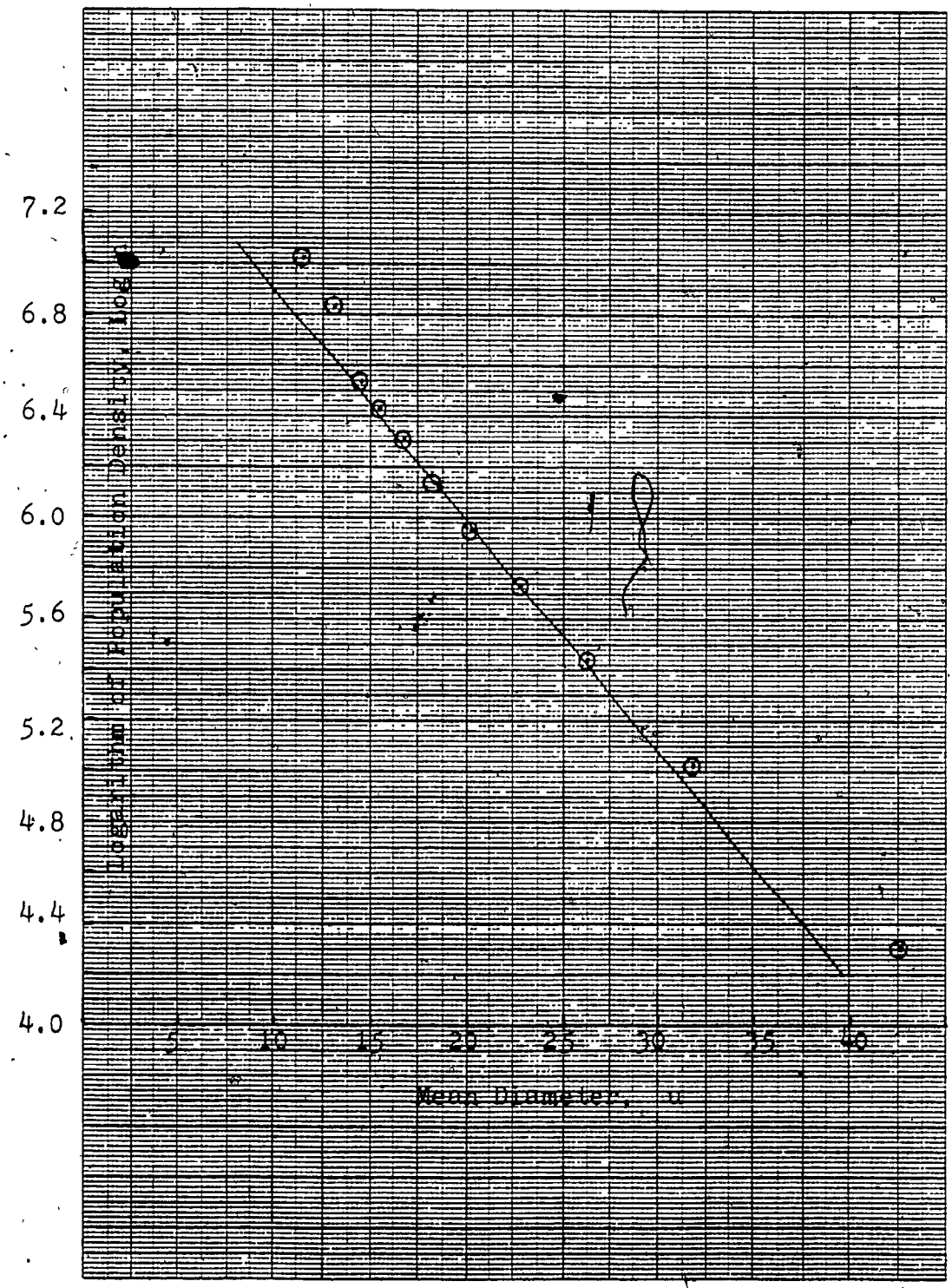

Table B8

Determination of Population Density, Nucleation Rate and Growth Rate for Run QM*

Size μ	ΔL μ	$\bar{L}$ μ	$\bar{L}^3$ μ^3	$\alpha \rho \bar{L}^3 \Delta L$ g μ	Weight, dW g	P.Density, n. no. μ^{-1}	Log n
50.27-35.11	15.16	42.69	7.78×10^4	5.51×10^{-6}	0.1101	2.00×10^4	4.30
35.11-28.30	6.81	31.70	3.19×10^4	1.01×10^{-7}	0.0984	9.74×10^5	4.99
28.30-24.19	4.11	26.25	1.81×10^4	3.47×10^{-7}	0.0852	2.45×10^5	5.40
24.19-21.35	2.84	22.77	1.18×10^3	1.57×10^{-8}	0.0767	4.88×10^5	5.69
21.35-19.22	2.13	20.28	8.34×10^3	8.30×10^{-8}	0.0669	8.06×10^5	5.91
19.22-17.55	1.67	18.38	6.21×10^3	4.85×10^{-8}	0.0576	1.19×10^6	6.07
17.55-16.18	1.37	16.87	4.80×10^3	3.07×10^{-8}	0.0521	1.70×10^6	6.23
16.88-15.02	1.16	15.60	3.80×10^3	2.06×10^{-8}	0.0474	2.30×10^6	6.36
15.02-14.04	0.98**	14.50	3.05×10^3	1.40×10^{-9}	0.0393	2.81×10^6	6.45
14.04-12.12	0.64**	13.08	2.24×10^3	6.69×10^{-9}	0.0346	5.17×10^6	6.71
12.12-10.74	0.46	11.43	1.49×10^3	3.21×10^{-9}	0.0246	7.66×10^6	6.88
<10.74	—	—	—	—	—	—	—

Nuclei Population Density, n^o = 4.67×10^7 no./μ

Nucleation Rate = 14.62×10^4 no./sec

Growth Rate = 3.13×10^{-3} μ/sec

*Withdraw down time = 0.45 h.

**Δ L corrected for time interval.

Figure B8

Plot of Logarithm of Population Density Versus Mean Diameter for Run QM.

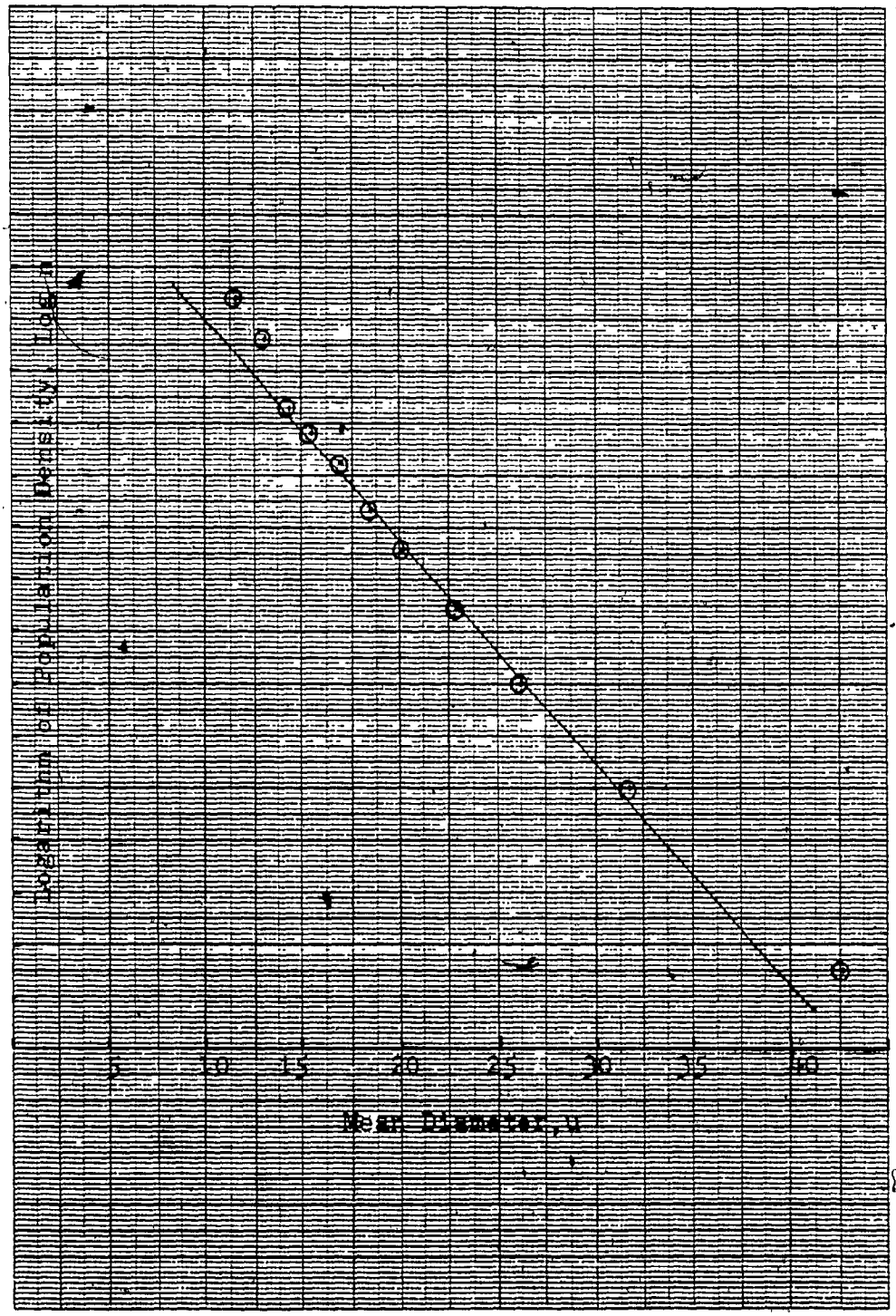

Table B9

Determination of Population Density, Nucleation Rate and Growth Rate for Run TM*

Size μ	ΔL μ	$\bar{L}$ μ	$\bar{L}^3$ μ^3	$\alpha \rho \bar{L}^3 \Delta L$ g μ	Weight, dW g	P.Density, n. no. μ^{-1}	Log n
50.27-35.11	15.16	42.69	7.78×10^4	5.51×10^{-6}	0.1015	1.84×10^4	4.26
35.11-28.30	6.81	31.70	3.19×10^4	1.01×10^{-6}	0.0836	8.27×10^4	4.92
28.30-24.19	4.11	26.25	1.81×10^4	3.47×10^{-7}	0.0700	2.02×10^5	5.30
24.19-21.35	2.84	22.77	1.18×10^4	1.57×10^{-7}	0.0578	3.68×10^5	5.57
21.35-19.22	2.13	20.28	8.34×10^3	8.30×10^{-8}	0.0509	6.13×10^5	5.79
19.22-17.55	1.67	18.38	6.21×10^3	4.85×10^{-8}	0.0445	9.17×10^5	5.96
17.55-16.18	1.37	16.87	4.80×10^3	3.07×10^{-8}	0.0372	1.21×10^6	6.08
16.88-15.02	1.16	15.60	3.80×10^3	2.06×10^{-8}	0.0316	1.53×10^6	6.18
15.02-14.04	0.98**	14.50	3.05×10^3	1.40×10^{-9}	0.0259	1.85×10^6	6.27
14.04-12.12	0.64**	13.08	2.24×10^3	6.69×10^{-9}	0.0231	3.45×10^6	6.54
12.12-10.74	0.46**	11.43	1.49×10^3	3.21×10^{-9}	0.0165	5.14×10^6	6.71
<10.74	—	—	—	—	—	—	—

Nuclei Population Density, n^o = 2.61×10^7 no./μ

Nucleation Rate = 8.77×10^4 no./sec

Growth Rate = 3.36×10^{-3} μ/sec

*Withdraw down time = 0.45 h.

**Δ L corrected for time interval.

Figure B9

Plot of Logarithm of Population Density Versus Mean Diameter for Run TM.

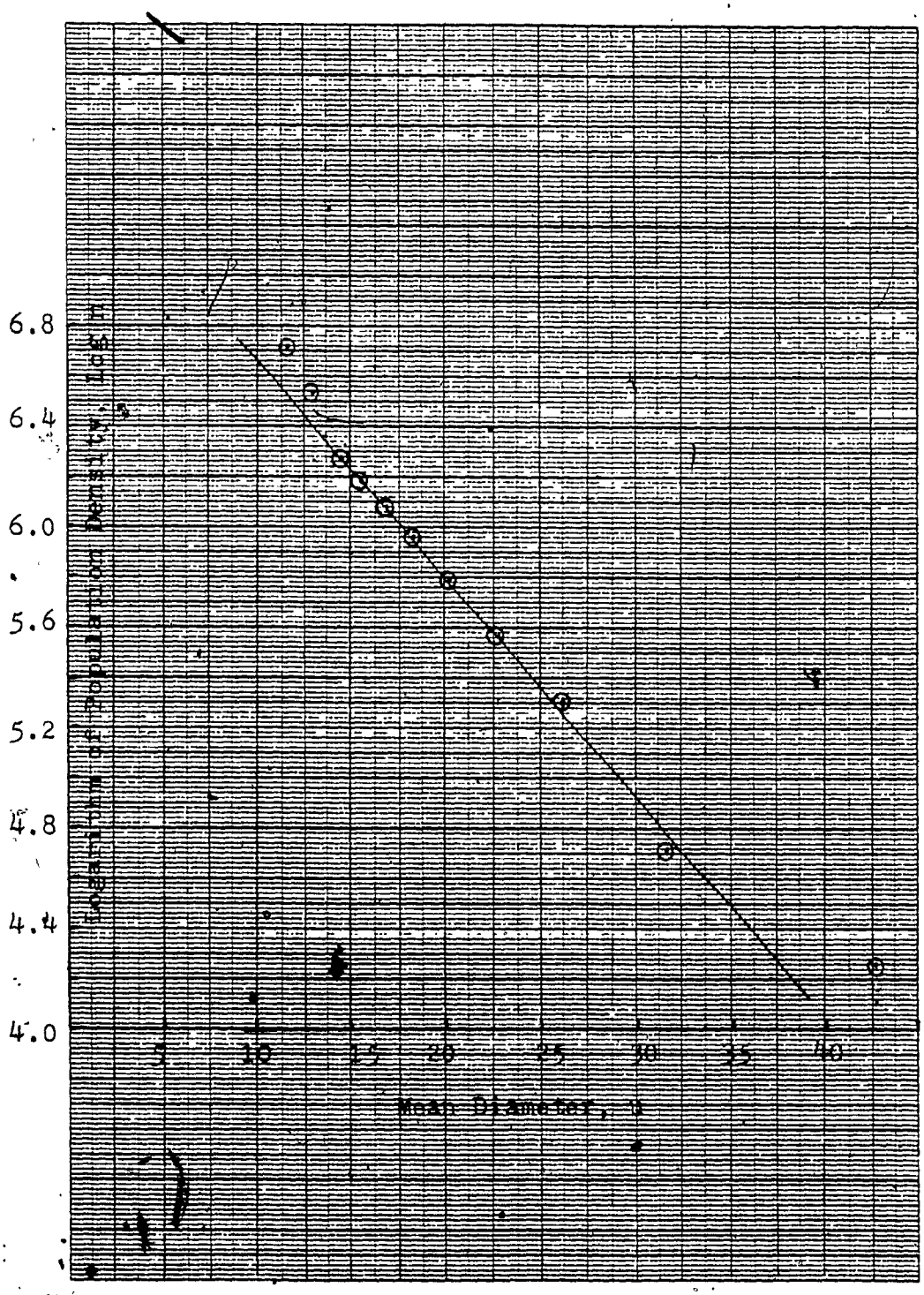

Table B10

Determination of Population Density, Nucleation Rate and Growth Rate for Run N*

Size μ	ΔL μ	$\bar{L}$ μ	$\bar{L}^3$ μ^3	$\alpha \rho \bar{L}^3 \Delta L$ g μ	Weight, dW g	P.Density, n. no. μ^{-1}	Log n
50.27-35.11	15.16	42.69	7.78×10^4	5.51×10^{-6}	0.1094	1.98×10^4	4.30
35.11-28.30	6.81	31.70	3.19×10^4	1.01×10^{-6}	0.1031	1.02×10^5	5.01
28.30-24.19	4.11	26.25	1.81×10^4	3.47×10^{-7}	0.0927	2.67×10^5	5.43
24.19-21.35	2.84	22.77	1.18×10^4	1.57×10^{-8}	0.0851	5.42×10^5	5.73
21.35-19.22	2.13	20.28	8.34×10^3	8.30×10^{-8}	0.0790	9.52×10^5	5.98
19.22-17.55	1.67	18.38	6.21×10^3	4.85×10^{-8}	0.0704	1.45×10^6	6.16
17.55-16.18	1.37	16.87	4.80×10^3	3.07×10^{-8}	0.0653	2.13×10^6	6.33
16.88-15.02	1.16	15.60	3.80×10^3	2.06×10^{-8}	0.0607	2.95×10^6	6.47
15.02-14.04	0.98**	14.50	3.05×10^3	1.40×10^{-9}	0.0545	3.89×10^6	6.59
14.04-12.12	0.64**	13.08	2.24×10^3	6.69×10^{-9}	0.0492	7.35×10^6	6.87
12.12-10.74	0.46	11.43	1.49×10^3	3.21×10^{-9}	0.0411	1.28×10^7	7.12
<10.74	—	—	—	—	—	—	—

Nuclei Population Density, n^o = 7.69×10^7 no./μ

Nucleation Rate = 27.10×10^4 no./sec.

Growth Rate = 3.52×10^{-3} μ/sec

*Withdraw down time = 0.37 h.

**ΔL corrected for time interval.

Figure B10

Plot of Logarithm of Population Density Versus Mean Diameter for Run N.

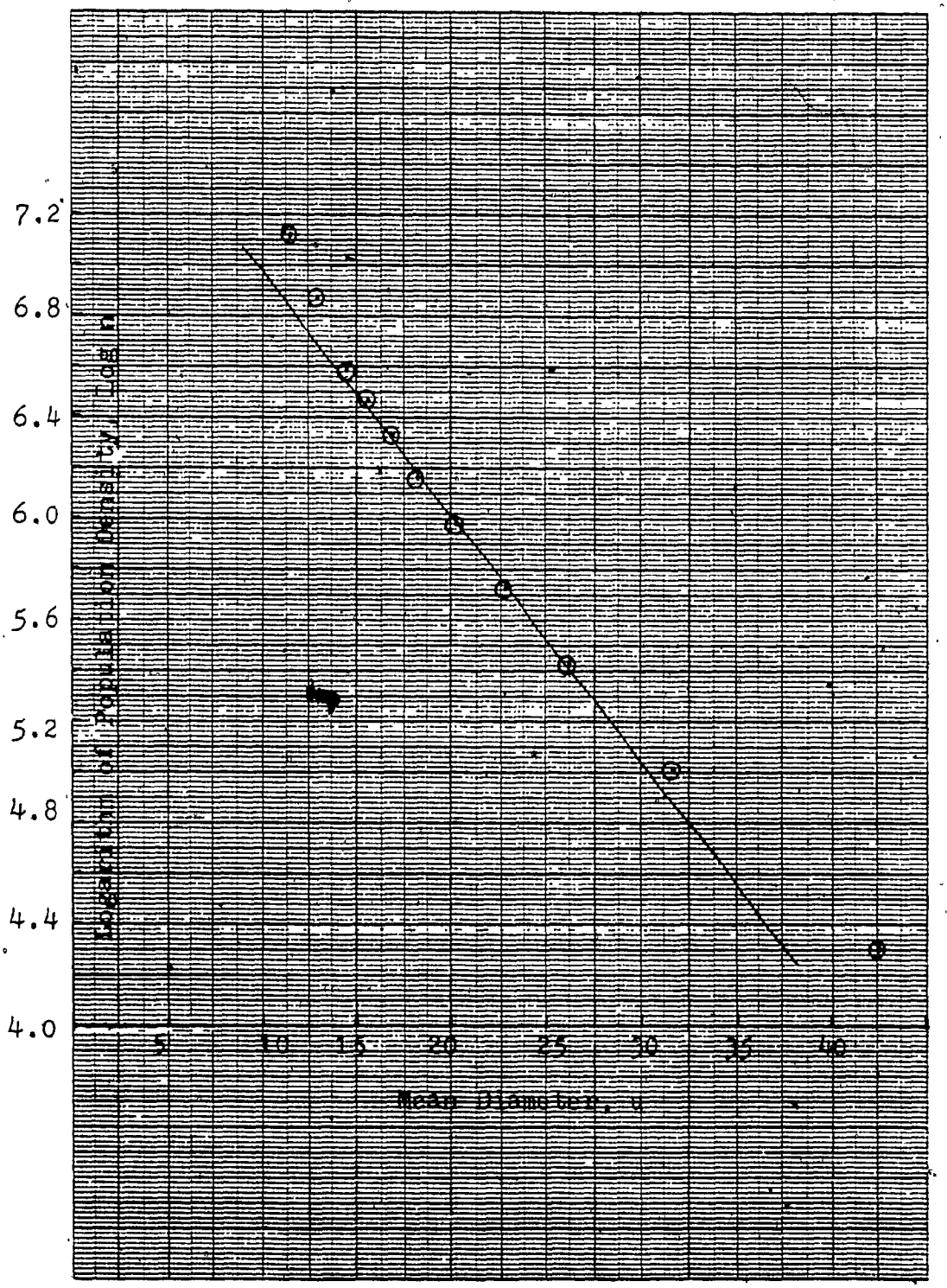

Table B11

Determination of Population Density, Nucleation Rate and Growth Rate for Run TN*

Size μ	ΔL μ	$\bar{L}$ μ	$\bar{L}^3$ μ^3	$\alpha \rho \bar{L}^3 \Delta L$ g μ	Weight, dW g	P.Density, n. no. μ^{-1}	Log n
50.27-35.11	15.16	42.69	7.78×10^4	5.51×10^{-6}	0.0917	1.66×10^4	4.22
35.11-28.30	6.81	31.70	3.19×10^4	1.01×10^{-7}	0.0763	7.55×10^4	4.88
28.30-24.19	4.11	26.25	1.81×10^4	3.47×10^{-7}	0.0639	1.84×10^5	5.26
24.19-21.35	2.84	22.77	1.18×10^4	1.57×10^{-8}	0.0539	3.43×10^5	5.53
21.35-19.22	2.13	20.28	8.34×10^3	8.30×10^{-8}	0.0464	5.59×10^5	5.75
19.22-17.55	1.67	18.38	6.21×10^3	4.85×10^{-8}	0.0383	7.90×10^5	5.90
17.55-16.18	1.37	16.87	4.80×10^3	3.07×10^{-8}	0.0340	1.11×10^6	6.04
16.88-15.02	1.16	15.60	3.80×10^3	2.06×10^{-8}	0.0298	1.45×10^6	6.16
15.02-14.04	0.98**	14.50	3.05×10^3	1.40×10^{-9}	0.0247	1.76×10^6	6.25
14.04-12.12	0.64**	13.08	2.24×10^3	6.69×10^{-9}	0.0217	3.24×10^6	6.51
12.12-10.74	0.46	11.43	1.49×10^3	3.21×10^{-9}	0.0160	4.98×10^6	6.70
<10.74	—	—	—	—			

Nuclei Population Density, n^o = 2.48×10^7 no./μ

Nucleation Rate = 10.14×10^4 no./sec

Growth Rate = 4.05×10^{-3} μ/sec

*Withdraw down time = 0.37 h.

**Δ L corrected for time interval.

Figure B11

Plot of Logarithm of Population Density Versus Mean Diameter for Run TN.

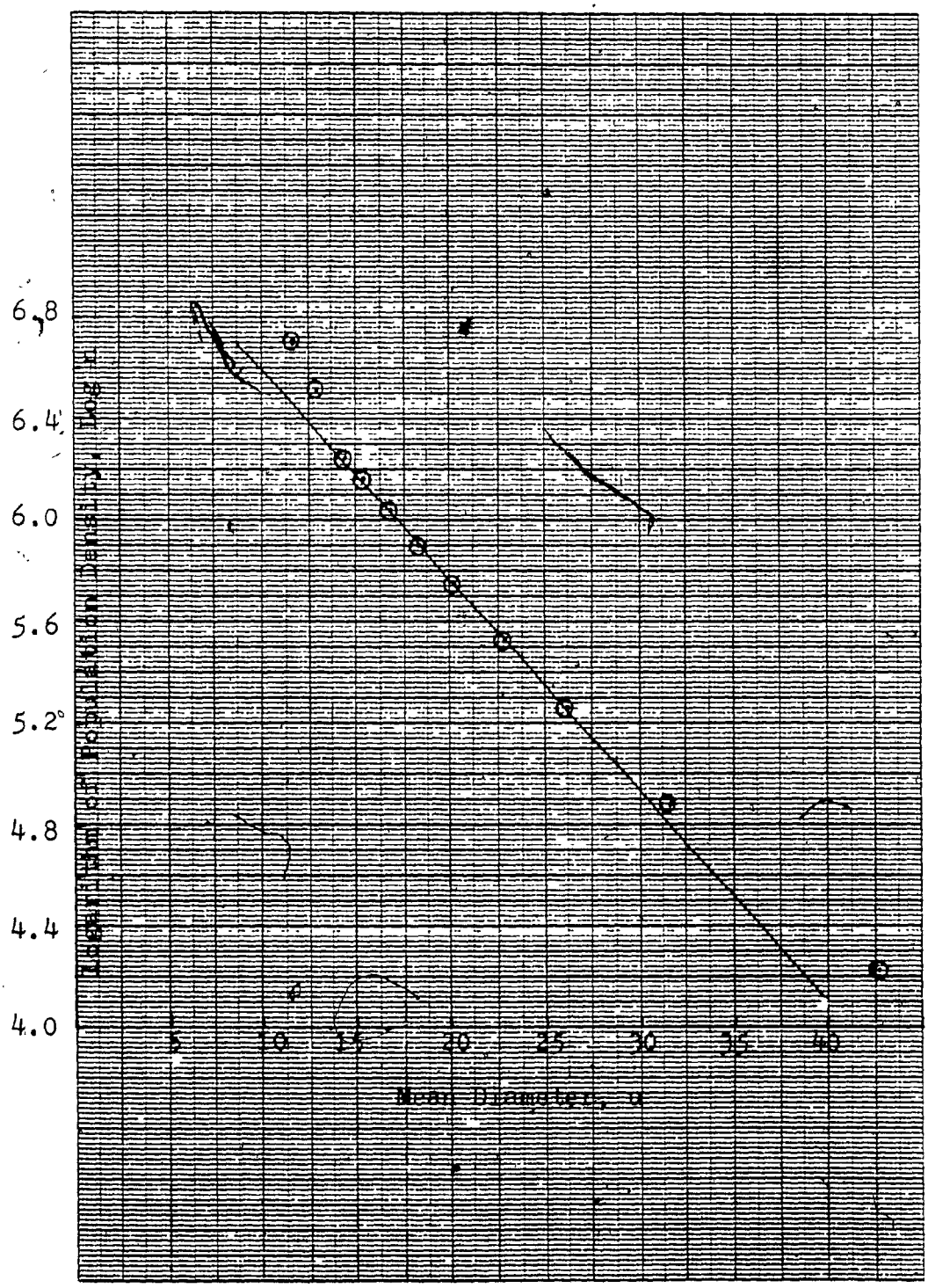

Table B12

Determination of Population Density, Nucleation Rate and Growth Rate for Run 0 *

Size μ	ΔL μ	$\bar{L}$ μ	$\bar{L}^3$ μ^3	$\alpha \rho \bar{L}^3 \Delta L$ g μ	Weight, dW g	P.Density, n. no. μ^{-1}	Log n
50.27-35.11	15.16	42.69	7.78×10^4	5.51×10^{-6}	0.1129	2.05×10^4	4.31
35.11-28.30	6.81	31.70	3.19×10^4	1.01×10^{-6}	0.1086	1.07×10^5	5.03
28.30-24.19	4.11	26.25	1.81×10^4	3.47×10^{-7}	0.1009	2.91×10^5	5.46
24.19-21.35	2.84	22.77	1.18×10^4	1.57×10^{-8}	0.0929	5.92×10^5	5.77
21.35-19.22	2.13	20.28	8.34×10^3	8.30×10^{-8}	0.0852	1.03×10^6	6.01
19.22-17.55	1.67	18.38	6.21×10^3	4.85×10^{-8}	0.0772	1.59×10^6	6.20
17.55-16.18	1.37	16.87	4.80×10^3	3.07×10^{-8}	0.0711	2.32×10^6	6.36
16.88-15.02	1.16	15.60	3.80×10^3	2.06×10^{-8}	0.0641	3.11×10^6	6.49
15.02-14.04	0.98**	14.50	3.05×10^3	1.40×10^{-9}	0.0587	4.19×10^6	6.62
14.04-12.12	0.64**	13.08	2.24×10^3	6.69×10^{-9}	0.0527	7.89×10^6	6.90
12.12-10.74	0.46	11.43	1.49×10^3	3.21×10^{-9}	0.0422	1.31×10^7	7.12
<10.74	—	—	—	—	—	—	—

Nuclei Population Density, n^o = 8.34×10^7 no./μ

Nucleation Rate = 31.90×10^4 no./sec

Growth Rate = 3.82×10^{-3} μ /sec

*Withdraw down time = 0.34 h.

**Δ L corrected for time interval.

Figure B12

Plot of Logarithm of Population Density Versus Mean Diameter for Run 0.

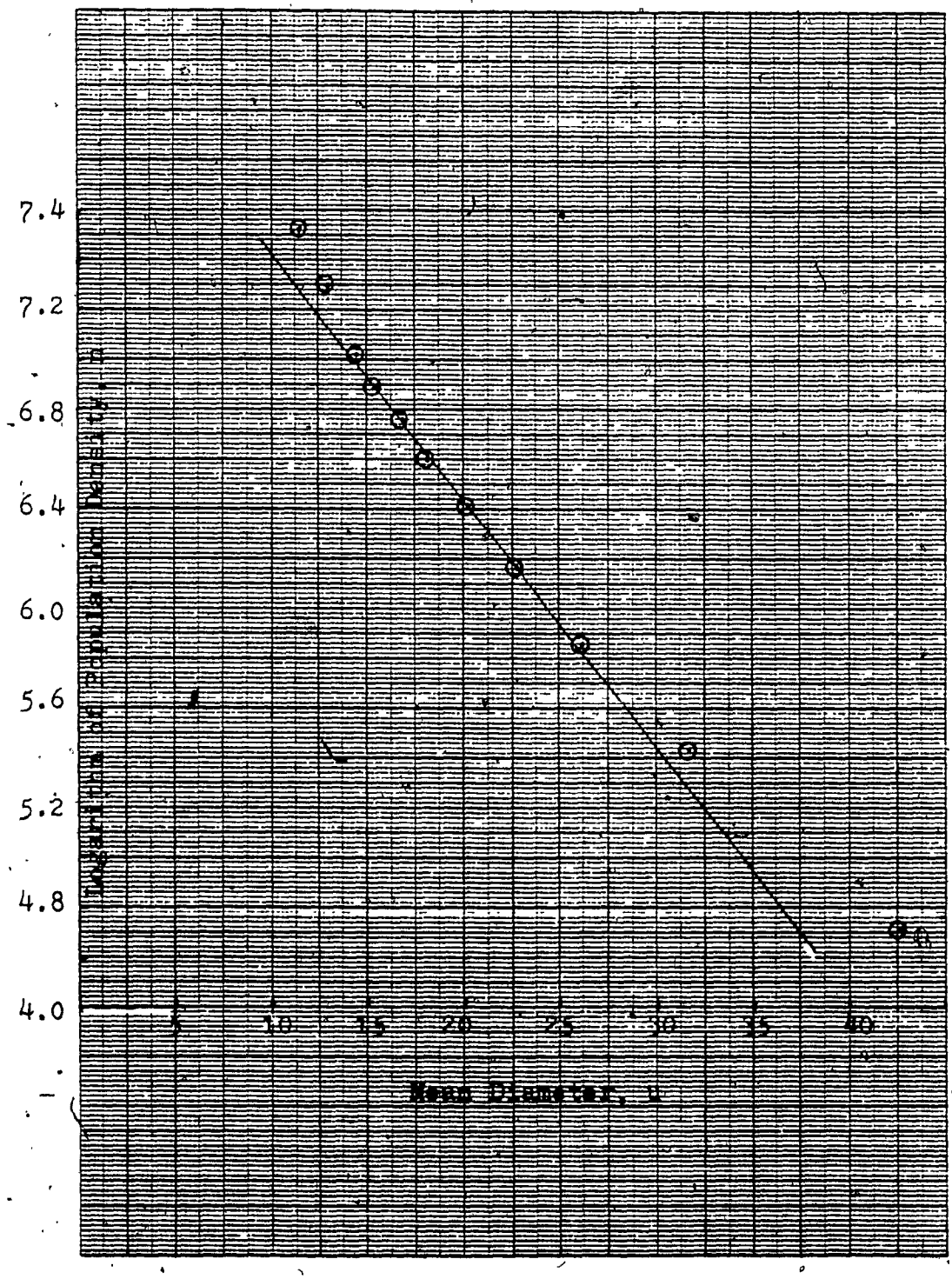

Table B13

Determination of Population Density, Nucleation Rate and Growth Rate for Run T0*

Size μ	ΔL μ	$\bar{L}$ μ	$\bar{L}^3$ μ^3	$\alpha \rho \bar{L}^3 \Delta L$ g μ	Weight, dW g	P.Density, n. no. μ^{-1}	Log n
50.27-35.11	15.16	42.69	7.78×10^4	5.51×10^{-6}	0.0913	1.66×10^4	4.22
35.11-28.30	6.81	31.70	3.19×10^4	1.01×10^{-7}	0.0783	7.75×10^5	4.89
28.30-24.19	4.11	26.25	1.81×10^4	3.47×10^{-7}	0.0656	1.89×10^5	5.28
24.19-21.35	2.84	22.77	1.18×10^3	1.57×10^{-8}	0.0534	3.40×10^5	5.53
21.35-19.22	2.13	20.28	8.34×10^3	8.30×10^{-8}	0.0464	5.59×10^6	5.75
19.22-17.55	1.67	18.38	6.21×10^3	4.85×10^{-8}	0.0383	7.90×10^6	5.90
17.55-16.18	1.37	16.87	4.80×10^3	3.07×10^{-8}	0.0333	1.08×10^6	6.03
16.88-15.02	1.16	15.60	3.80×10^3	2.06×10^{-8}	0.0292	1.42×10^6	6.15
15.02-14.04	0.98**	14.50	3.05×10^3	1.40×10^{-8}	0.0242	1.73×10^6	6.24
14.04-12.12	0.64**	13.08	2.24×10^3	6.69×10^{-9}	0.0212	3.17×10^6	6.50
12.12-10.74	0.46**	11.43	1.49×10^3	3.21×10^{-9}	0.0148	4.61×10^6	6.66
<10.74	—	—	—	—	—	—	—

Nuclei Population Density, n^o = 2.31×10^7 no./μ

Nucleation Rate = 10.39×10^4 no./sec

Growth Rate = 4.50×10^{-3} μ/sec

*Withdraw down time = 0.34 h.

**Δ L corrected for time interval.

Figure B13

Plot of Logarithm of Population Density Versus Mean Diameter for Run T0.

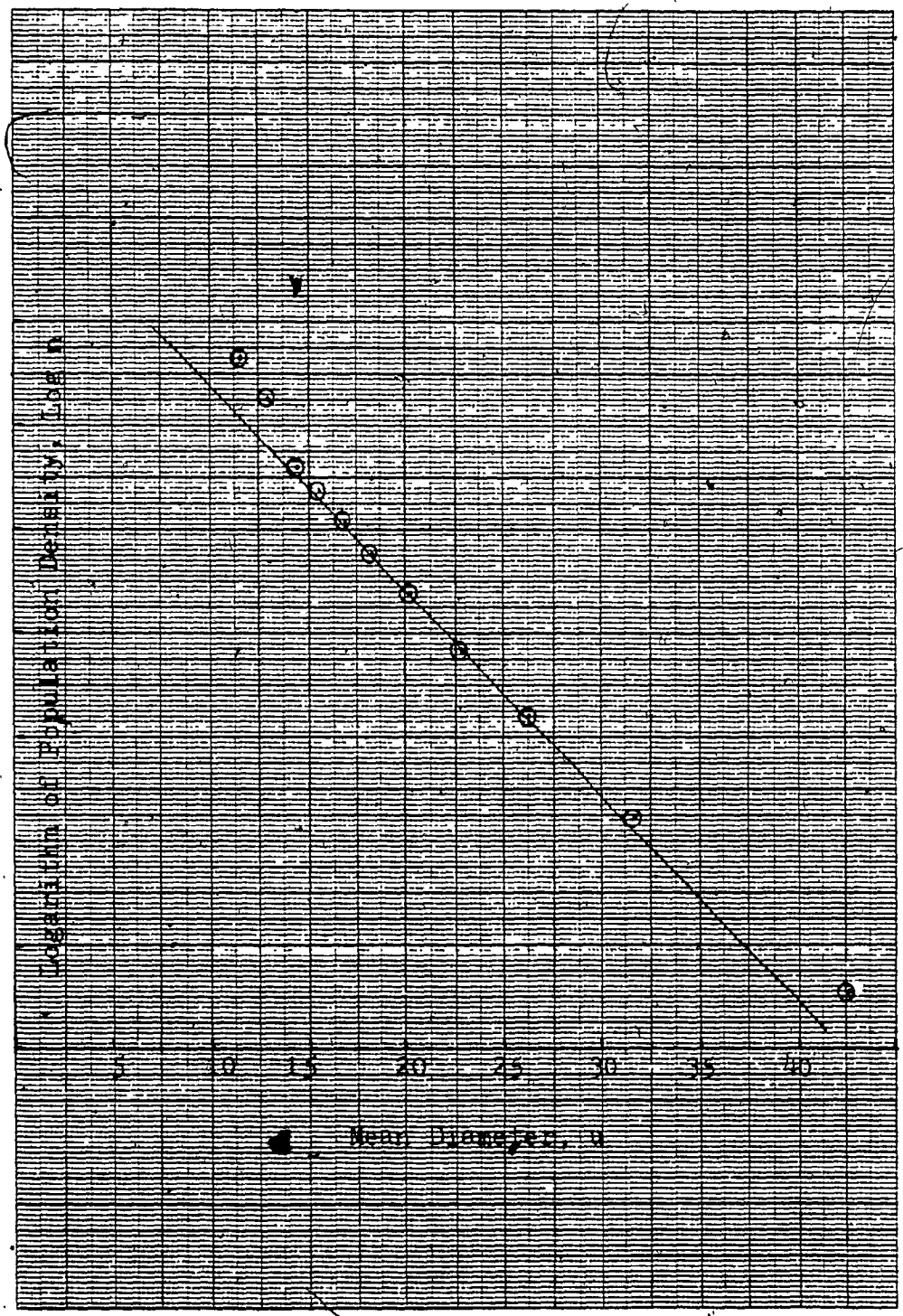

Table B14

Determination of Population Density, Nucleation Rate and Growth Rate for Run TP*.

Size μ	ΔL μ	$\bar{L}$ μ	$\bar{L}^3$ μ^3	$\alpha \rho \bar{L}^3 \Delta L$ g μ	Weight, dW g	P.Density, n. no. μ^{-1}	Log n
50.27-35.11	15.16	42.69	7.78×10^4	5.51×10^{-6}	0.1074	1.95×10^4	4.29
35.11-28.30	6.81	31.70	3.19×10^4	1.01×10^{-6}	0.0875	8.66×10^4	4.94
28.30-24.19	4.11	26.25	1.81×10^4	3.47×10^{-7}	0.0769	2.22×10^5	5.35
24.19-21.35	2.84	22.77	1.18×10^4	1.57×10^{-8}	0.0627	3.99×10^5	5.60
21.35-19.22	2.13	20.28	8.34×10^3	8.30×10^{-8}	0.0536	6.46×10^5	5.81
19.22-17.55	1.67	18.38	6.21×10^3	4.85×10^{-8}	0.0448	9.24×10^5	5.97
17.55-16.18	1.37	16.87	4.80×10^3	3.07×10^{-8}	0.0392	1.28×10^6	6.11
16.88-15.02	1.16	15.60	3.80×10^3	2.06×10^{-8}	0.0333	1.62×10^6	6.21
15.02-14.04	0.98**	14.50	3.05×10^3	1.40×10^{-9}	0.0272	1.94×10^6	6.29
14.04-12.12	0.64**	13.08	2.24×10^3	6.69×10^{-9}	0.0245	3.66×10^6	6.56
12.12-10.74	0.46	11.43	1.49×10^3	3.21×10^{-9}	0.0185	5.76×10^6	6.76
<10.74	—	—	—	—			

Nuclei Population Density, n^o = 2.71×10^7 no./μ

Nucleation Rate = 13.75×10^4 no./sec

Growth Rate = 5.07×10^{-3} μ/sec

*Withdraw down time = 0.30 h.

**Δ L corrected for time interval.

Figure B14

Plot of Logarithm of Population Density Versus Mean Diameter for Run TP.

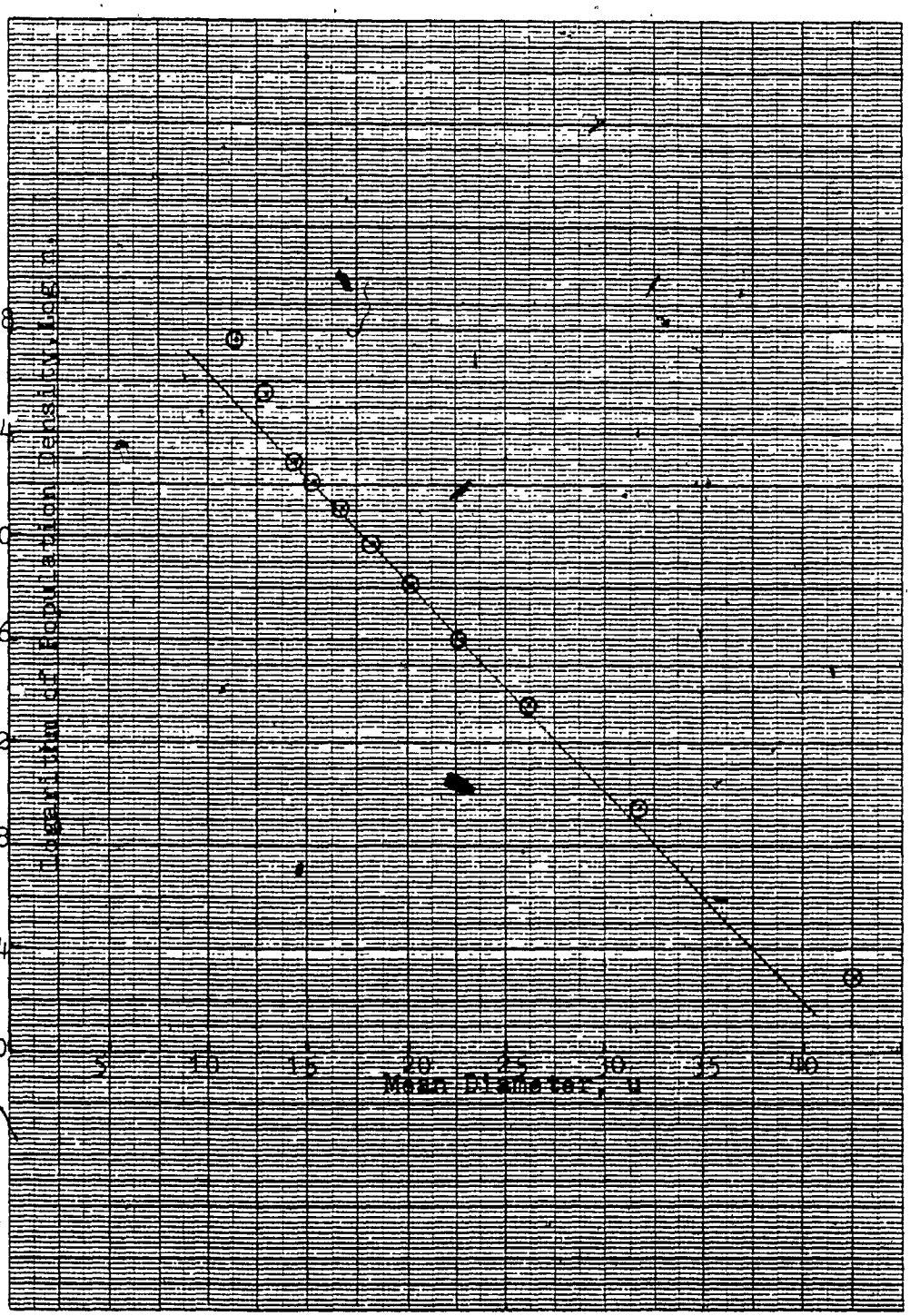

Table B15

Determination of Population Density, Nucleation Rate and Growth Rate for Run QR

Size μ	ΔL μ	$\bar{L}$ μ	$\bar{L}^3$ μ^3	$\alpha \rho \bar{L}^3 \Delta L$ g μ	Weight, dW g	P.Density, n. no. μ^{-1}	Log n
50.27-35.11	15.16	42.69	7.78×10^4	5.51×10^{-6}	0.1167	2.12×10^4	4.32
35.11-28.30	6.81	31.70	3.19×10^4	1.01×10^{-6}	0.1050	1.04×10^5	5.02
28.30-24.19	4.11	26.25	1.81×10^4	3.47×10^{-7}	0.0902	2.60×10^5	5.41
24.19-21.35	2.84	22.77	1.18×10^4	1.57×10^{-7}	0.0740	4.71×10^5	5.67
21.35-19.22	2.13	20.28	8.34×10^3	8.30×10^{-8}	0.0627	7.55×10^5	5.88
19.22-17.55	1.67	18.38	6.21×10^3	4.85×10^{-8}	0.0518	1.07×10^6	6.03
17.55-16.18	1.37	16.87	4.80×10^3	3.07×10^{-8}	0.0416	1.35×10^6	6.13
16.88-15.02	1.16	15.60	3.80×10^3	2.06×10^{-8}	0.0347	1.68×10^6	6.23
15.02-14.04	0.98**	14.50	3.05×10^3	1.40×10^{-8}	0.0281	2.01×10^6	6.30
14.04-12.12	0.64**	13.08	2.24×10^3	6.69×10^{-9}	0.0239	3.57×10^6	6.55
12.12-10.74	0.46**	11.43	1.49×10^3	3.21×10^{-9}	0.0152	4.73×10^6	6.67
<10.74	—	—	—	—	—	—	—

Nuclei Population Density, n^o = 2.53×10^7 no./μ

Nucleation Rate = 14.98×10^4 no./sec

Growth Rate = 5.92×10^{-3} μ /sec

*Withdraw down time = 0.27 h.

**Δ L corrected for time interval.

Figure B15

Plot of Logarithm of Population Density Versus Mean Diameter for Run QR.

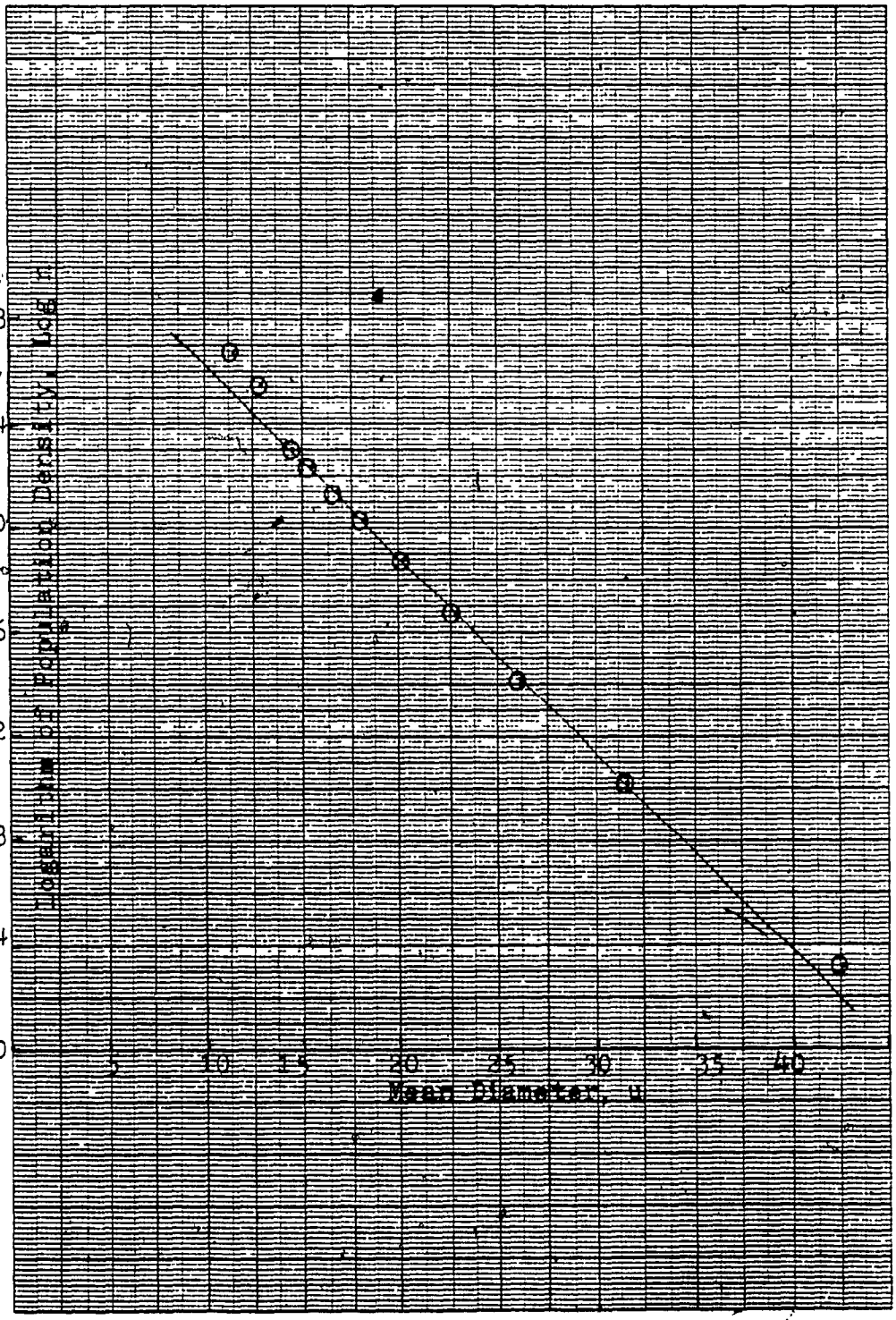

Table B16

Determination of Population Density, Nucleation Rate and Growth Rate for Run TR*

Size μ	ΔL μ	$\bar{L}$ μ	$\bar{L}^3$ μ^3	$\alpha \rho \bar{L}^3 \Delta L$ g μ	Weight, dW g	P.Density, n. no. μ^{-1}	Log n
50.27-35.11	15.16	42.69	7.78×10^4	5.51×10^{-6}	0.0878	1.59×10^4	4.20
35.11-28.30	6.81	31.70	3.19×10^4	1.01×10^{-6}	0.0690	6.83×10^4	4.83
28.30-24.19	4.11	26.25	1.81×10^4	3.47×10^{-7}	0.0571	1.64×10^5	5.22
24.19-21.35	2.84	22.77	1.18×10^4	1.57×10^{-7}	0.0474	3.02×10^5	5.48
21.35-19.22	2.13	20.28	8.34×10^3	8.30×10^{-8}	0.0409	4.93×10^5	5.69
19.22-17.55	1.67	18.38	6.21×10^3	4.85×10^{-8}	0.0346	7.13×10^5	5.85
17.55-16.18	1.37	16.87	4.80×10^3	3.07×10^{-8}	0.0312	1.02×10^6	6.01
16.88-15.02	1.16	15.60	3.80×10^3	2.06×10^{-8}	0.0254	1.23×10^6	6.09
15.02-14.04	0.98**	14.50	3.05×10^3	1.40×10^{-9}	0.0226	1.61×10^6	6.21
14.04-12.12	0.64**	13.08	2.24×10^3	6.69×10^{-9}	0.0199	2.97×10^6	6.47
12.12-10.74	0.46**	11.43	1.49×10^3	3.21×10^{-9}	0.0151	4.70×10^6	6.67
<10.74	—	—	—	—	—	—	—

Nuclei Population Density, n^o = 2.21×10^7 no./μ

Nucleation Rate = 12.28×10^4 no./sec

Growth Rate = 5.56×10^{-3} μ /sec

*Withdraw down time = 0.27 h.

**ΔL corrected for time interval.

Figure B16

Plot of Logarithm of Population Density Versus Mean Diameter for Run TR.

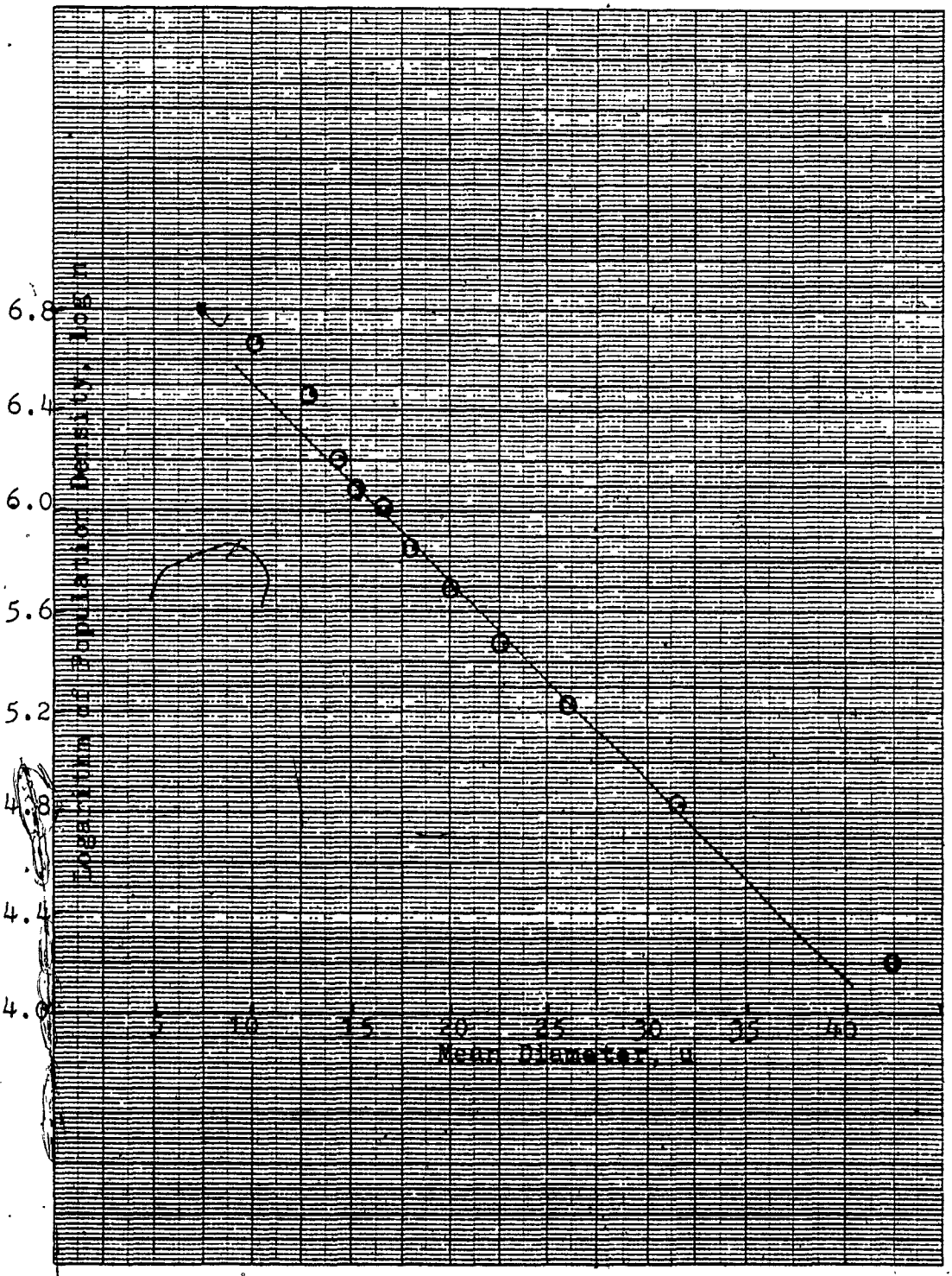

Table B17

Determination of Population Density, Nucleation Rate and Growth Rate for Run QS*

Size μ	ΔL μ	$\bar{L}$ μ	$\bar{L}^3$ μ^3	$\alpha \rho \bar{L}^3 \Delta L$ g μ	Weight, dW g	P.Density, n. no. μ^{-1}	Log n
50.27-35.11	15.16	42.69	7.78×10^4	5.51×10^{-6}	0.1001	1.82×10^4	4.26
35.11-28.30	6.81	31.70	3.19×10^4	1.01×10^{-7}	0.0857	8.48×10^4	4.93
28.30-24.19	4.11	26.25	1.81×10^4	3.47×10^{-7}	0.0683	1.97×10^5	5.29
24.19-21.35	2.84	22.77	1.18×10^3	1.57×10^{-8}	0.0557	3.55×10^5	5.55
21.35-19.22	2.13	20.28	8.34×10^3	8.30×10^{-8}	0.0432	5.20×10^5	5.72
19.22-17.55	1.67	18.38	6.21×10^3	4.85×10^{-8}	0.0358	7.38×10^5	5.87
17.55-16.18	1.37	16.87	4.80×10^3	3.07×10^{-8}	0.0270	8.79×10^5	5.94
16.88-15.02	1.16	15.60	3.80×10^3	2.06×10^{-8}	0.0218	1.06×10^6	6.02
15.02-14.04	0.98**	14.50	3.05×10^3	1.40×10^{-9}	0.0174	1.24×10^6	6.09
14.04-12.12	0.64**	13.08	2.24×10^3	6.69×10^{-9}	0.0131	1.96×10^6	6.29
12.12-10.74	0.46	11.43	1.49×10^3	3.21×10^{-9}	0.0080	2.49×10^6	6.40
<10.74	—	—	—	—	—	—	—

Nuclei Population Density, n^o = 1.24×10^7 no./μ

Nucleation Rate = 8.77×10^4 no./sec

Growth Rate = 7.08×10^{-3} μ/sec

*Withdraw down time = 0.25 h.

**Δ L corrected for time interval.

Figure B17

Plot of Logarithm of Population Density Versus Mean Diameter for Run QS.

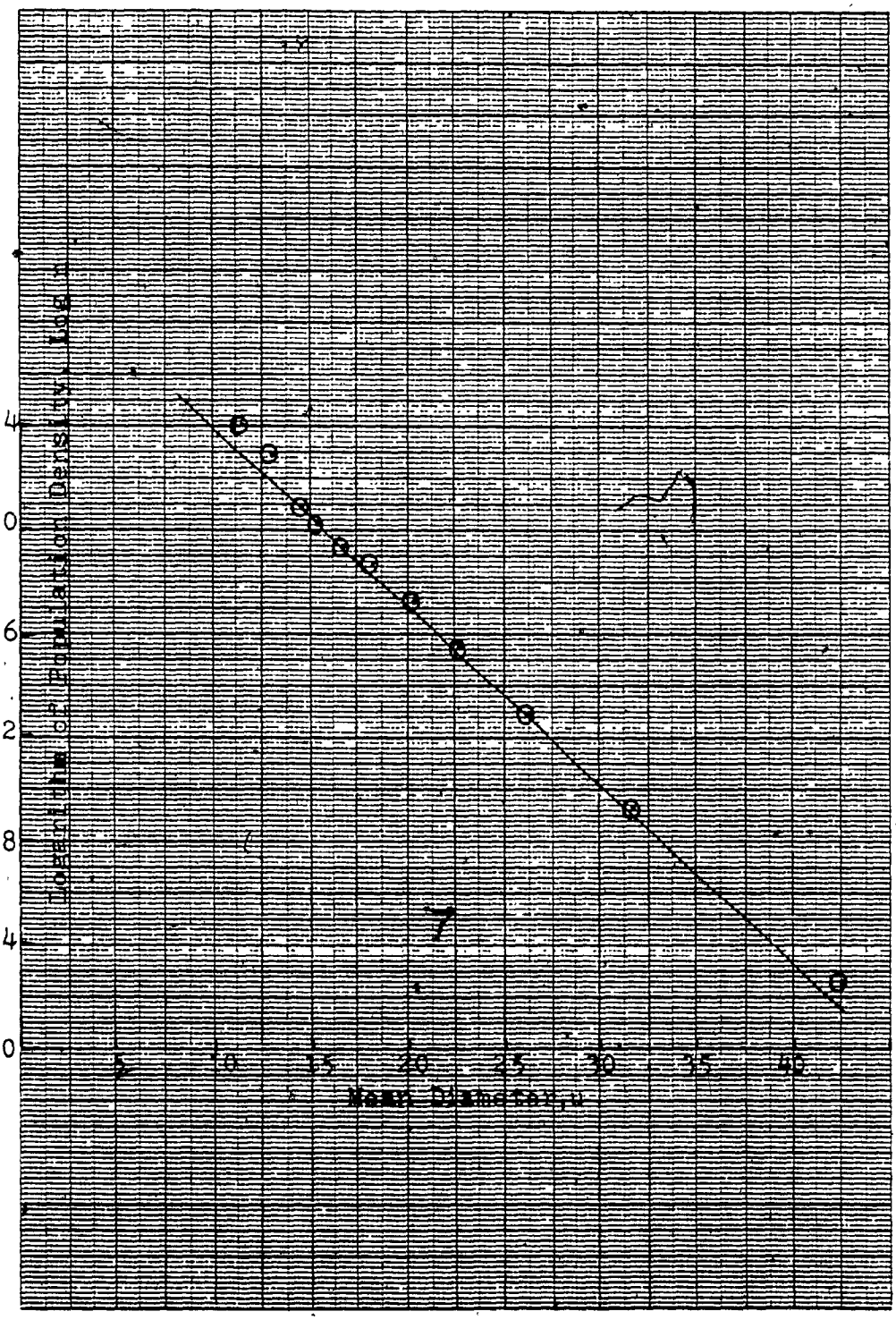

APPENDIX C

Experimental data obtained in the determination of apparent density experiments.

Table C1

Determination of Apparent Density of Copper Powder Produced in Run D (Table D5)

I. Using Density Cup Y having a Capacity of 1.99^7 cm^3

Run No.	Weight of Copper Powder, g	Apparent Density g/cm^3
YD1	6.6809	3.34
YD2	6.6917	3.35
YD3	6.6787	3.34
YD4	6.6681	3.33
YD5	6.6597	3.33
YD6	6.6501	3.33

Mean Apparent Density = 3.34 g/cm^3

Standard Deviation = 0.01

II. Using Density Cup Z having a Capacity of 3.03^8 cm^3

Run No.	Weight of Copper Powder, g	Apparent Density g/cm^3
ZD1	10.1109	3.34
ZD2	10.1089	3.34
ZD3	10.1273	3.34
ZD4	10.1671	3.36
ZD5	10.1409	3.35
ZD6	10.1500	3.35

Mean Apparent Density = 3.35 g/cm^3

Standard Deviation = 0.01

Table C2

Determination of Apparent Density of Copper Powder Produced in Run G (Table D9)

I. Using Density Cup Y having a Capacity of 1.99^{7} cm^3

Run No.	Weight of Copper Powder, g	Apparent Density g/cm^3
YG1	6.7560	3.38
YG2	6.7420	3.37
YG3	6.7809	3.39
YG4	6.7327	3.37
YG5	6.7103	3.36
YG6	6.7431	3.37

Mean Apparent Density = 3.37 g/cm^3

Standard Deviation = 0.01

II. Using Density Cup Z having a Capacity of 3.03^{8} cm^3

Run No.	Weight of Copper Powder, g	Apparent Density g/cm^3
ZG1	10.2139	3.37
ZG2	10.2278	3.38
ZG3	10.2301	3.38
ZG4	10.2089	3.37
ZG5	10.2181	3.37
ZG6	10.2367	3.38

Mean Apparent Density = 3.38 g/cm^3

Standard Deviation = 0.01

Table C3

Determination of Apparent Density of Copper Powder Produced in Run I (Table D10)

I. Using Density Cup Y having a Capacity of 1.997 cm^3

Run No.	Weight of Copper Powder, g	Apparent Density g/cm^3
YI1	6.7803	3.39
YI2	6.7913	3.40
YI3	6.7709	3.39
YI4	6.7387	3.37
YI5	6.7856	3.39
YI6	6.7489	3.37

Average Apparent Density = 3.38 g/cm^3

Standard Deviation = 0.01

II. Using Density Cup Z having a Capacity of 3.03 g/cm^3

Run No.	Weight of Copper Powder, g	Apparent Density g/cm^3
ZI1	10.3198	3.41
ZI2	10.2867	3.39
ZI3	10.3209	3.41
ZI4	10.2710	3.39
ZI5	10.3078	3.40
ZI6	10.3301	3.41

Average Apparent Density = 3.40 g/cm^3

Standard Deviation = 0.01

Table C4

Determination of Apparent Density of Copper Powder Produced in Run K (Table D12)

Using Density Cup Y having a Capacity of 1.997 cm^3

Run No.	Weight of Copper Powder, g	Apparent Density g/cm^3
YK1	6.9089	3.45
YK2	6.9318	3.47
YK3	6.8971	3.47
YK4	6.9203	3.46
YK5	6.8793	3.44
YK6	6.8609	3.43

Average Apparent Density = 3.45 g/cm^3

Standard Deviation = 0.01

Table C5

Determination of Apparent Density of Copper Powder Produced in Run M (Tables D14, D26)

I. Using Density Cup Y having a Capacity of 1.99^7 cm^3

Run No.	Weight of Copper Powder, g	Apparent Density g/cm^3
YM1	6.9179	3.46
YM2	6.9478	3.47
YM3	6.8973	3.45
YM4	6.9307	3.47
YM5	6.9209	3.46
YM6	6.9481	3.47

Average Apparent Density = 3.46 g/cm^3

Standard Deviation = 0.01

II. Using Density Cup Z having a Capacity of 3.03^8 cm^3

Run No.	Weight of Copper Powder, g	Apparent Density g/cm^3
YM1	10.4619	3.45
YM2	10.4809	3.46
YM3	10.4589	3.45
YM4	10.4821	3.46
YM5	10.4701	3.46
YM6	10.4834	3.46

Average Apparent Density = 3.46 g/cm^3

Standard Deviation = 0.01

Table C6

Determination of Apparent Density of Copper Powder Produced in Run N (Table D15)

I. Using Density Cup Y having a Capacity of 1.99^7 cm^3

Run No.	Weight of Copper Powder, g	Apparent Density g/cm^3
YN1	7.0079	3.50
YN2	6.9813	3.49
YN3	7.0871	3.54
YN4	6.9719	3.49
YN5	6.9907	3.50
YN6	7.0385	3.52

Average Apparent Density = 3.51 g/cm^3

Standard Deviation = 0.02

II. Using Density Cup Z having a Capacity of 3.03^8 cm^3

Run No.	Weight of Copper Powder, g	Apparent Density g/cm^3
ZN1	10.6431	3.51
ZN2	10.6609	3.52
ZN3	10.5921	3.49
ZN4	10.6378	3.51
ZN5	10.6527	3.52
ZN6	10.6709	3.52

Average Apparent Density = 3.51 g/cm^3

Standard Deviation = 0.01

Table C7

Determination of Apparent Density of Copper Powder Produced in Run O (Table D16)

I. Using Density Cup Y having a Capacity of 1.99^7 cm^3

Run No.	Weight of Copper Powder, g	Apparent Density g/cm^3
Y01	7.1390	3.57
Y02	7.0987	3.55
Y03	7.0816	3.54
Y04	7.1222	3.56
Y05	7.1439	3.57
Y06	7.1088	3.55

Average Apparent Density = 3.56 g/cm^3

Standard Deviation = 0.01

II. Using Density Cup Z having a Capacity of 3.03^8 cm^3

Run No.	Weight of Copper Powder, g	Apparent Density g/cm^3
Z01	10.8239	3.57
Z02	10.7989	3.56
Z03	10.9231	3.60
Z04	10.9109	3.60
Z05	10.8102	3.57
Z06	10.8009	3.56

Average Apparent Density = 3.58 g/cm^3

Standard Deviation = 0.02

Table C8

Determination of Apparent Density of Copper Powder Produced in Run P (Table D17)

I. Using Density Cup Y having a Capacity 1.99^7 cm^3

Run No.	Weight of Copper Powder, g	Apparent Density g/cm^3
YP1	6.9354	3.47
YP2	6.8871	3.44
YP3	6.9409	3.47
YP4	6.9089	3.45
YP5	6.9183	3.46
YP6	6.8593	3.43

Average Apparent Density = 3.45 g/cm^3

Standard Deviation = 0.02

II. Using Density Cup Z having a Capacity of 3.03^8 cm^3

Run No.	Weight of Copper Powder, g	Apparent Density g/cm^3
ZP1	10.4311	3.44
ZP2	10.4619	3.45
ZP3	10.4327	3.44
ZP4	10.4181	3.44
ZP5	10.4072	3.43
ZP6	10.3621	3.42

Average Apparent Density = 3.44 g/cm^3

Standard Deviation = 0.01

Table C9

Determination of Apparent Density of Copper Powder Produced in Run QI (Table D19)

Using Density Cup Y having a Capacity of 1.997 cm^3

Run No.	Weight of Copper Powder, g	Apparent Density g/cm^3
YQI1	6.6679	3.33
YQI2	6.6709	3.34
YQI3	6.6989	3.35
YQI4	6.6892	3.34
YQI5	6.6487	3.32
YQI6	6.6633	3.33

Average Apparent Density = 3.34 g/cm^3

Standard Deviation = 0.01

Table C10

Determination of Apparent Density of Copper Powder Produced in Run QK (Table D20)

Using Density Cup Y having a Capacity of 1.99^7 cm^3

Run No.	Weight of Copper Powder, g	Apparent Density g/cm^3
YQK1	6.7901	3.40
YQK2	6.7831	3.39
YQK3	6.7712	3.39
YQK4	6.7529	3.38
YQK5	6.7328	3.37
YQK6	6.7610	3.38

Average Apparent Density = 3.39 g/cm^3

Standard Deviation = 0.01

Table C11

Determination of Apparent Density of Copper Powder Produced in Run QM (Table D21)

Using Density Cup Y having a capacity of 1.99^7 cm^3

Run No.	Weight of Copper Powder, g	Apparent Density g/cm^3
YQM1	6.9204	3.46
YQM2	6.9001	3.45
YQM3	6.8794	3.44
YQM4	6.8901	3.45
YQM5	6.8871	3.44
YQM6	6.9109	3.46

Average Apparent Density = 3.45 g/cm^3

Standard Deviation = 0.01

Table C12

Determination of Apparent Density of Copper Powder Produced in Run QR (Table D22)

I. Using Density Cup Y having a Capacity of 1.99^7 cm^3

Run No.	Weight of Copper Powder, g	Apparent Density g/cm^3
YQR1	6.7987	3.40
YQR2	6.7734	3.39
YQR3	6.7649	3.38
YQR4	6.7809	3.39
YQR5	6.7485	3.37
YQR6	6.7343	3.37

Average Apparent Density = 3.38 g/cm^3

Standard Deviation = 0.01

II. Using Density Cup Z having a Capacity of 3.03^8 cm^3

Run No.	Weight of Copper Powder, g	Apparent Density g/cm^3
ZQR1	10.3304	3.41
ZQR2	10.3129	3.40
ZQR3	10.3401	3.41
ZQR4	10.3189	3.41
ZQR5	10.3204	3.41
ZQR6	10.3089	3.40

Average Apparent Density = 3.41 g/cm^3

Standard Deviation = 0.01

Table C13

Determination of Apparent Density of Copper Powder Produced in Run QS (Tables D23, D27)

I. Using Density Cup Y having a capacity of 1.99^7 cm^3

Run No.	Weight of Copper Powder, g	Apparent Density g/cm^3
YQS1	6.6309	3.32
YQS2	6.6218	3.31
YQS3	6.6107	3.31
YQS4	6.6413	3.32
YQS5	6.6079	3.30
YQS6	6.6131	3.31

Average Apparent Density = 3.31 g/cm^3

Standard Deviation = 0.01

II. Using Density Cup Z having a Capacity of 3.03^8 cm^3

Run No.	Weight of Copper Powder, g	Apparent Density g/cm^3
ZQS1	10.0531	3.32
ZQS2	10.0179	3.31
ZQS3	10.0341	3.31
ZQS4	10.0083	3.30
ZQS5	10.0478	3.32
ZQS6	10.0216	3.31

Average Apparent Density = 3.31 g/cm^3

Standard Deviation = 0,01

Table C14

Determination of Apparent Density of Copper Powder Produced in Run TK (Table D25)

Using Density Cup Y having a Capacity of 1.997 cm^3

Run No.	Weight of Copper Powder, g	Apparent Density g/cm^3
YTK1	6.6130	3.31
YTK2	6.5578	3.29
YTK3	6.6291	3.31
YTK4	6.6089	3.30
YTK5	6.5773	3.29
YTK6	6.6873	3.34

Average Apparent Density = 3.31 g/cm^3

Standard Deviation = 0.02

Table C15

Determination of Apparent Density of Copper Powder Produced in Run TM (Table D25)

I. Using Density Cup Y having a Capacity of 1.997 cm^3

Run No.	Weight of Copper Powder, g	Apparent Density g/cm^3
YTM1	6.6501	3.33
YTM2	6.6478	3.32
YTM3	6.6701	3.34
YTM4	6.6379	3.32
YTM5	6.6681	3.33
YTM6	6.6839	3.34

Average Apparent Density = 3.33 g/cm^3

Standard Deviation = 0.01

II. Using Density Cup Z having a Capacity of 3.038 cm^3

Run No.	Weight of Copper Powder, g	Apparent Density g/cm^3
ZTM1	10.1210	3.34
ZTM2	10.1379	3.35
ZTM3	10.1189	3.34
ZTM4	10.1309	3.34
ZTM5	10.1091	3.34
ZTM6	10.1451	3.35

Average Apparent Density = 3.34 g/cm^3

Standard Deviation = 0.01

Table C16

Determination of Apparent Density of Copper Powder Produced in Run TN (Table D25)

Using Density Cup Y having a Capacity of 1.99^7 cm^3

Run No.	Weight of Copper Powder, g	Apparent Density g/cm^3
YTN1	6.6989	3.35
YTN2	6.6777	3.34
YTN3	6.6509	3.33
YTN4	6.6679	3.33
YTN5	6.6806	3.34
YTN6	6.6409	3.32

Average Apparent Density = 3.34 g/cm^3

Standard Deviation = 0.01

Table C17

Determination of Apparent Density of Copper Powder Produced in Run TO (Table D25)

Using Density Cup Y Having a Capacity of 1.997 cm^3

Run No.	Weight of Copper Powder, g	Apparent Density g/cm^3
YT01	6.7379	3.37
YT02	6.7201	3.36
YT03	6.7108	3.36
YT04	6.7589	3.38
YT05	6.7678	3.38
YT06	6.7422	3.37

Average Apparent Density = 3.37 g/cm^3

Standard Deviation = 0.01

Table C18

Determination of Apparent Density of Copper Powder Produced in Run TP (Table D25)

I. Using Density Cup Y having a Capacity of 1.99^7 cm^3

Run No.	Weight of Copper Powder, g	Apparent Density g/cm^3
YTP1	6.6340	3.32
YTP2	6.6403	3.32
YTP3	6.6389	3.32
YTP4	6.6291	3.31
YTP5	6.6109	3.31
YTP6	6.6378	3.32

Average Apparent Density = 3.32 g/cm^3

Standard Deviation = 0.01

II. Using Density Cup Z having a Capacity of 3.03^8 cm^3

Run No.	Weight of Copper Powder, g	Apparent Density g/cm^3
ZTP1	9.9680	3.29
ZTP2	10.0371	3.31
ZTP3	10.0701	3.32
ZTP4	10.0232	3.31
ZTP5	10.0111	3.30
ZTP6	10.0424	3.31

Average Apparent Density = 3.31 g/cm^3

Standard Deviation = 0.01

Table C19

Determination of Apparent Density of Copper Powder Produced in Run TR (Tables D25, D28)

I. Using Density Cup Y having a Capacity of 1.99^7 cm^3

Run No.	Weight of Copper Powder, g	Apparent Density g/cm^3
YTR1	6.6149	3.31
YTR2	6.5721	3.29
YTR3	6.5320	3.27
YTR4	6.6138	3.31
YTR5	6.5424	3.27
YTR6	6.5809	3.29

Average Apparent Density = 3.29 g/cm^3

Standard Deviation = 0.02

II. Using Density Cup Z having a Capacity of 3.03^8 cm^3

Run No.	Weight of Copper Powder, g	Apparent Density g/cm^3
ZTR1	10.0634	3.32
ZTR2	9.9079	3.27
ZTR3	9.9552	3.29
ZTR4	9.9269	3.28
ZTR5	9.9344	3.28
ZTR6	9.9891	3.29

Average Apparent Density = 3.29 g/cm^3

Standard Deviation = 0.02

Table C20

Determination of Apparent Density of Copper Powder Produced in Run M (Tables D14, D16)

Using Density Cup X having a Capacity of 25.00 ± 0.05 cm^3

Run No.	Weight of Copper Powder, g	Apparent Density g/cm^3
XM1	86.1646	3.45
XM2	85.9723	3.44
XM3	86.4802	3.46
XM4	86.3028	3.45
XM5	86.1709	3.45
XM6	85.9079	3.44
XM7	86.2874	3.45
XM8	85.9903	3.44
XM9	86.3313	3.45
XM10	86.3979	3.46

Average Apparent Density = 3.45 g/cm^3

Standard Deviation = 0.01

Table C21

Determination of Apparent Density of Copper Powder Produced in Run TR (Tables D25, D28)

Using Density Cup X having a Capacity of 25.00 ± 0.05 cm^3

Run No.	Weight of Copper Powder, g	Apparent Density g/cm^3
XTR1	81.4195	3.26
XTR2	80.9897	3.24
XTR3	81.4809	3.26
XTR4	81.2107	3.25
XTR5	81.0783	3.24
XTR6	81.4880	3.26
XTR7	81.3367	3.25
XTR8	80.9691	3.24
XTR9	81.1274	3.24
XTR10	81.3879	3.26

Average Apparent Density = 3.25 g/cm^3

Standard Deviation = 0.01

Table C22

Determination of Apparent Density of Copper Powder Produced in Run QS (Tables D24, D27)

Using Density Cup X having a Capacity of 25.00 ± 0.05 cm^3

Run No.	Weight of Copper Powder, g	Apparent Density g/cm^3
XQS1	81.7148	3.27
XQS2	82.0308	3.28
XQS3	82.9176	3.32
XQS4	81.9809	3.28
XQS5	82.3761	3.29
XQS6	81.9383	3.28
XQS7	81.9701	3.28
XQS8	82.4173	3.30
XQS9	82.0070	3.28
XQS10	81.8301	3.27

Average Apparent Density = 3.29 g/cm^3

Standard Deviation = 0.02

Table C23

Value of the Apparent Density and Standard Deviation for Standard Copper Powder Sample in the Reproducibility Run

Using Density Cup Y having a Capacity of 1.99^7 cm^3

Run No.	Weight of Copper Powder, g	Apparent Density g/cm^3
Y1	5.4221	2.71
Y2	5.4843	2.74
Y3	5.4230	2.71
Y4	5.4179	2.71
Y5	5.4701	2.74
Y6	5.4409	2.72
Y7	5.4901	2.74
Y8	5.4783	2.74
Y9	5.4469	2.72
Y10	5.4369	2.72

Average Apparent Density = 2.73 g/cm^3

Standard Deviation = 0.01

Table C24

Value of the Apparent Density and Standard Deviation for the Standard Copper Powder Sample in the Reproducibility Run

Using Density Cup Z having a Capacity of 3.03^8 cm^3

Run No.	Weight of Copper Powder, g	Apparent Density g/cm^3
Z1	8.2415	2.72
Z2	8.2686	2.73
Z3	8.3522	2.76
Z4	8.2909	2.74
Z5	8.2860	2.73
Z6	8.2757	2.73
Z7	8.3350	2.75
Z8	8.2799	2.73
Z9	8.2803	2.73
Z10	8.3078	2.74

Average Apparent Density = 2.74 g/cm^3

Standard Deviation = 0.01

Table C25

Effect of Median Diameter of Copper Powder Produced at different Flow Rates on Apparent Density[d]

Run	Flow Rate	Median Diameter	Apparent Density, g/cm^3		
No.	cc/min	microns	a	b	c
D	13.5	23.31	3.34±0.01	3.35±0.01	
G	28.0	22.39	3.37±0.01	3.38±0.01	
I	43.0	20.42	3.38±0.01	3.40±0.01	
K	62.0	18.84	3.45±0.01		
M	92.0	16.41	3.46±0.01	3.46±0.01	3.45±0.01
N	112.0	15.56	3.51±0.02	3.51±0.01	
O	122.0	15.14	3.56±0.01	3.58±0.02	
P	138.0	18.20	3.45±0.02	3.44±0.01	

[a]Apparent Density determined using Density Cup Number Y.

[b]Apparent Density determined using Density Cup Number Z.

[c]Apparent Density determined using Density Cup Number X.

[d]Temperature at the filtration unit 25±3°C.

Table C26

Effect of Median Diameter of Copper Powder Produced at different Flow Rates on Apparent Density[d]

Run No.	Flow Rate cc/min	Median Diameter microns	Apparent Density, g/cm^3 a	b	c
QI	43.0	23.71	3.34±0.01		
QK	62.0	21.88	3.39±0.01		
QM	92.0	19.05	3.45±0.01		
QR	152.0	21.63	3.38±0.01	3.41±0.01	
QS	164.0	24.55	3.31±0.01	3.31±0.01	3.29±0.02

[a]Apparent Density determined using Density Cup Number Y.

[b]Apparent Density determined using Density Cup Number Z.

[c]Apparent Density determined using Density Cup Number X.

[d]Température at the filtration unit 33±3°C.

Table C27

Effect of Median Diameter of Copper Powder Produced at different Flow Rate on Apparent Density[d]

Run No.	Flow Rate cc/min	Median Diameter microns	Apparent Density, g/cm^3 a	b	c
TK	62.0	25.12	3.31±0.01		
TM	92.0	23.66	3.33±0.01	3.34±0.01	
TN	112.0	23.17	3.34±0.01		
TO	122.0	22.65	3.37±0.01		
TP	138.0	24.27	3.32±0.01	3.31±0.01	
TR	154.0	26.61	3.29±0.02	3.29±0.02	3.25±0.01

[a]Apparent Density determined using Density Cup Number Y.

[b]Apparent Density determined using Density Cup Number Z.

[c]Apparent Density determined using Density Cup Number X.

[d]Temperature at the filtration unit 44±3°C.

APPENDIX D

Yields of copper powder, as functions of:

- Duration of experiment
- Temperature of crystallization
- Flow rate of solution
- Weight of copper wire
- Cupric sulphate concentration

Table D1

Cumulative Yield for Run NC-1[a]

Duration hrs	Yield g	Cumulative Duration hrs	Cumulative Yield, g
22	2.1400	22	2.1400
22	2.6088	44	4.7488
22	2.4515	66	7.2003

[a]Series of experiment done on Apparatus 1 designed by de Ga (3).

Table D2

Copper Powder Yield at Flow Rate 15.0 cc/min[a]

Run No.	Duration hrs	Yield g
FC1	22	3.5480
FC2	47	7.3127
FC3	55	8.4564

[a]Series of experiment done on Apparatus 2 designed after de Ga (3).

Table D3

Variation of Copper Yield with Weight of Copper Wire[a] at the Flow Rate of 36.0 cc/min

(Temperature at the filtration unit 25±3°C)

Run No.	Weight[b] of wire, g	Duration hrs	Yield g	Yield/hour g/hr
1B	100	5	3.9836	0.7967
2B	200	5	4.5250	0.9050
3B	400	5	4.5667	0.9133
4B	700	5	4.5600	0.9120
5B	1000	5	4.5524	0.9105
6B	1310	5	4.2595	0.8519

[a]Copper Cable wire used in all runs.

[b]Weight of copper wire before treatment with Nitric Acid.

Table D4

Copper Powder Yield at Flow Rate 10.0 cc/min[a]

(Temperature at the filtration unit 25±3°C)

Run No.	Duration hrs	Yield g	Yield/hour g/hr
1C	6	1.0984	0.1813
2C	5	0.8977	0.1795
3C	6	1.4940	0.2490
4C	6	1.2115	0.2019
5C	10	2.2838	0.2284
6C	3	0.5519	0.1840

Average yield/hour = 0.2043 g/hr

[a]Commercial grade copper wire was used in all runs.

Table D5

Copper Powder Yield at Flow Rate 13.5 cc/min[a]

(Temperature at the filtration unit 25±3°C)

Run No.	Duration hrs	Yield g	Yield/hour g/hr
1D	5	1.4077	0.2815
2D	10	3.3528	0.3353
3D	7	2.0954	0.2993
4D	10	3.2485	0.3248
5D	5	1.3879	0.2776
6D	10	3.4809	0.3481
7D	7	2.2062	0.3152
8D	10	3.0869	0.3087
9D	10	3.1756	0.3176

Average yield/hour = 0.3120 g/hr

[a]Commercial grade copper wire used in all runs.

Table D6

Copper Powder Yield at Flow Rate 18.0 cc/min[a]

(Temperature at the filtration unit 25±3°C)

Run No.	Duration, hrs	Yield g	Yield/hour g/hr
1E	5	1.7306	0.3461
2E	3	1.0653	0.3551
3E	8	3.1696	0.3962
4E	10	4.1073	0.4107

Average yield/hour = 0.3770 g/hr

[a] Commercial grade copper wire was used in all runs.

Table D7

Copper Powder Yield at Flow Rate 24.0 cc/min[a]

(Temperature at the filtration unit 25±3°C)

Run No.	Duration hrs	Yield g	Yield/hour g/hr
1F	4	1.8872	0.4718
2F	6	2.8129	0.4688
3F	2	0.8824	0.4412
4F	8	3.8017	0.4752

Average yield/hour = 0.4643 g/hr

[a]Commercial grade copper wire used in all runs.

Table D8

Copper Powder Yield at Flow Rate 28.0 cc/min[a]

(Temperature at the filtration unit 25±3°C)

Run No.	Duration hrs	Yield g	Yield/hour g/hr
1G	6	3.9286	0.6548
2G	4	2.4249	0.6062
3G	8	5.0816	0.6352
4G	2	1.2509	0.6255

Average yield/hour = 0.6304 g/hr

[a]Commercial grade copper wire was used in all runs.

Table D9

Copper Powder Yield at Flow Rate 36.0 cc/min

(Temperature at the filtration unit 25±3°C)

Run No.	Duration hrs	Yield g	Yield/hour g/hr
1H	6	5.0125	0.8354
2H	4	3.2582	0.8367
3H	2	1.6713	0.8367

Average yield/hour = 0.8289 g/hr

Table D10

Copper Powder Yield at Flow Rate 43.0 cc/min

(Temperature at the filtration unit 25±3°C)

Run No.	Duration hrs	Yield g	Yield/hour g/hr
1I	4	3.7527	0.9382
2I	6	6.1020	1.0170
3I	5	4.8564	0.9713

Average yield/hour = 0.9755 g/hr

Table D11

Copper Powder Yield at Flow Rate 50.0 cc/min.

(Temperature at the filtration unit 25±3°C)

Run No.	Duration hrs	Yield g	Yield/hour g/hr
1J	5	5.8822	1.1764
2J	4	4.7761	1.1940
3J	3	3.6733	1.2244
4J	2	2.3498	1.1749

Average yield/hour = 1.1924 g/hr

Table D12

Copper Powder Yield at Flow Rate 62.0 cc/min

(Temperature at the filtration unit 25±3°C)

Run No.	Duration hrs	Yield g	Yield/hour g/hr
1K	5	7.5165	1.5033
2K	4	5.8523	1.4631
3K	3	4.3562	1.4521
4K	2	2.8960	1.4480

Average yield/hour = 1.4666 g/hr

Table D13

Copper Powder Yield at Flow Rate 76.0 cc/min.

(Temperature at the filtration unit 25±3°C)

Run No.	Duration hrs	Yield g	Yield/hour g/hr
1L	4	7.5632	1.8908
2L	6	11.9385	1.9898
3L	5	9.4932	1.8986

Average yield/hour = 1.9264 g/hr

Table D14.

Copper Powder Yield at Flow Rate 92.0 cc/min

(Temperature at the filtration unit 25±3°C)

Run No.	Duration hrs	Yield g	Yield/hour g/hr
1M	5	9.9375	1.9875
2M	5	10.8118	2.1624
3M	5	10.9819	2.1964

Average yield/hour = 2.1154 g/hr

Table D15

Copper Powder Yield at Flow Rate 112.0 cc/min

(Temperature at the filtrarion unit 25±3°C)

Run No.	Duration hrs	Yield g	Yield/hour g/hr
1N	5	13.1466	2.6293
2N	5	13.0177	2.6035

Average yield/hour = 2.6164 g/hr

Table D16

Copper Powder Yield at Flow Rate 122.0 cc/min

(Temperature at the filtration unit 25±3°C)

Run No.	Duration hrs	Yield g	Yield/hour g/hr
10	5	14.8866	2.9773
20	5	14.7455	2.9491

Average yield/hour = 2.9632 g/hr

Table D17

Copper Powder Yield at Flow Rate 108.0 cc/min

(Temperature at the filtration unit 25±3°C)

Run No.	Duration, hrs	Yield g	Yield/hour g/hr
1P	5	15.4545	3.0909
2P	5	15.6622	3.1324

Average yield/hour = 3.1116 g/hr

Table D18

Summary of Tables D4 to D17, Average Yield/hour of Copper Powder at different Flow Rates.

(Temperature at the filtration unit 25±3°C)

Flow Rate cc/min	Average Yield/hour g/hr
10.0	0.2043
13.5	0.3120
18.0	0.3770
24.0	0.4643
28.0	0.6304
36.0	0.8289
43.0	0.9755
50.0	1.1924
62.0	1.4666
76.0	1.9264
92.0	2.1154
112.0	2.6164
122.0	2.9632
138.0	3.1116

Table D19

Copper Powder Yield at Flow Rate 43.0 cc/min

(Temperature at the filtration unit 33±3°C)

Run No.	Duration hrs	Yield g	Yield/hour g/hr
QI	10	9.8671	0.9867

Table D20

Copper Powder Yield at Flow Rate 62.0 cc/min

(Temperature at the filtration unit 33±3°C)

Run No.	Duration hrs	Yield g	Yield/hour g/hr
QK	7	9.9309	1.4187

Table D21

Copper Powder Yield at Flow Rate 92.0 cc/min

(Temperature at the filtration unit 33±3°C)

Run No.	Duration hrs	Yield g	Yield/hour g/hr
QM	7	15.2799	2.1857

Table D22

Copper Powder Yield at Flow Rate 152.0 cc/min

(Temperature at the filtration unit 33±3°C)

Run No.	Duration hrs	Yield g	Yield/hour g/hr
1QR	5	16.6669	3.3333
2QR	5	17.1075	3.4215

Average yield/hour = 3.3774 g/hr

Table D23

Copper Powder Yield at Flow Rate 164.0 cc/min

(Temperature at the filtration unit 33±3°C)

Run No.	Duration hrs	Yield g	Yield/hour g/hr
1QS	5	17.5485	3.5097

Table D24

Summary of Tables D19 to D23, Yield/hour of Copper Powder at different Flow Rates

(Temperature at the filtration unit 33±3°C)

Flow Rate cc/min	Yield/hour g/hr
43.0	0.9867
62.0	1.4187
92.0	2.1857
152.0	3.3774
164.0	3.5097

Table D25

Copper Powder Yield at different Flow Rate

(Temperature at the filtration unit 44±3°C)

Run No.	Flow Rate cc/min	Duration hrs	Yield g	Yield/hour g/hr
TK	62.0	8	12.3512	1.5439
TM	92.0	7	15.2706	2.1815
TN	112.0	4	10.3968	2.5987
TO	122.0	4	11.8536	2.9634
TP	138.0	8	24.9102	3.1137
1TR	152.0	7	23.5214	3.3602

Table D26

Copper Powder Yield at Flow Rate 92.0 cc/min[a]

(Temperature at the filtration unit 25±3°C)

Run No.	Duration hrs	Yield g	Yield/hour g/hr
4M	7	15.2045	2.1727
5M	7	15.2168	2.1781
6M	7	15.2418	2.1774
7M	7	15.2327	2.1761
8M	8	17.3672	2.1709
9M	7	15.3107	2.1875
10M	7	15.2977	2.1875

Average yield/hour = 2.1783 g/hr

Total weight of Copper Powder Produced = 108.8714 g.

[a]Copper Powder produced for the Sintering Process.

Table D27

Copper Powder Yield at Flow Rate 164.0 cc/min[a]

(Temperature at the filtration unit 33±3°C)

Run No.	Duration hrs	Yield g	Yield/hour g/hr
2QS	3	10.6728	3.5576
3QS	6	21.0872	3.5162
4QS	6	21.3719	3.5619
5QS	6	21.2879	3.5482
6QS	7	24.7306	3.5329
7QS	4	14.3148	3.5787

Average yild/hour = 3.5493 g/hr

Total weight of Copper Powder produced = 113.4670 g.

[a]Copper Powder produced for the Sintering Process

Table D28

Copper powder Yield at Flow Rate 152.0 cc/min[a]

(Temperature at the filtration unit 44±3°C)

Run No.	Duration hrs	Yield g	Yield/hour g/hr
2TR	7	23.5214	3.3602
3TR	8	26.8152	3.3519
4TR	8	26.7823	3.3478
5TR	8½	28.6458	3.3730
6TR	4	13.3516	3.3379

Average yield/hour = 3.3542 g/hr

Total weight of Copper Powder produced = 119.1163 g.

[a]Copper Powder produced for the Sintering Process.

Table D29

Variation of Yield with Cupric Sulphate Solution at 15.0 cc/min[a]

(All Solutions are in 1N Sulphuric Acid)

Run No.	Salt Concentration M	Duration hrs	Yield g
1A	0.50	22	3.5011
2A	1.00	22	5.8644
3A[b]	2.00	—	—

[a]Series of experiment done on Apparatus 2 designed by de Ga (3).

[b]Cupric Sulphate precipitated out in the cooling Condenser.

APPENDIX E

Effect of liquid flow rate on median diameter.

Table E1

Effect of Liquid Flow Rate on Median Diameter

(Temperature at the filtration unit 25±3°C)

Run No.	Flow Rate cc/min	Median Diameter micron	G.S.D.
D	13.5	23.11	1.87
G	28.0	22.39	1.79
I	43.0	20.42	2.17
K	62.0	18.84	2.06
M	92.0	16.41	1.84
N	112.0	15.56	1.92
O	122.0	15.14	1.85
P	138.0	13.20	1.77

Table E2

Effect of Liquid Flow Rate on Median Diameter

(Temperature at the filtration unit 33±3°C)

Run No.	Flow Rate cc/min	Median Diameter microns	G.S.D.
QI	43.0	23.71	1.75
QK	62.0	21.88	1.74
QM	92.0	19.05	1.80
QR	152.0	21.63	1.64
QS	164.0	24.55	1.69

Table E3

Effect of Liquid Flow Rate on Median Diameter

(Temperature at the filtration unit 44±3°C)

Run No.	Flow Rate cc/min	Median Diameter micron	G.S.D.
TK	62.0	25.12	1.94
TM	92.0	23.66	1.86
TN	112.0	23.17	1.84
TO	122.0	22.65	1.79
TP	138.0	24.27	1.91
TR	152.0	26.61	2.07

APPENDIX F

Determination of tensile strength of sintered specimens from copper powders.

Table F1

Determination of Tensile Strength of Sintered Specimen from Copper Powder Produced by Cyclone Technique

Specimen No.	Cross-sectional Area, in^2	Maximum Force Applied, lb.	Tensile Strength psi
TSD1	0.06210	1175	18921
TSD2	0.05700	1051	18439
TSD3	0.05625	1075	19111
TSD4	0.05500	1000	18182
TSD5*	0.05675	1040	18326

Tensile Strength (Average) = 18596 ± 336 psi

*Tensile Strength is higher than it should be as the specimen broke at the grip.

Table F2

Determination of Tensile Strength of Sintered Specimen from Copper Powder Produced in Run M

Specimen No.	Cross-sectional Area, in^2	Maximum Force Applied, lb.	Tensile Strength psi
TSM1	0.05800	1530	26379
TSM2	0.05725	1500	26201

Tensile Strength (Average) = 26290 $\pm$ 89 psi

Table F3

Determination of Tensile Strength of Sintered Specimen from Copper Powder Produced in Run QS

Specimen No.	Cross-sectional Area, in^2	Maximum Force Applied, lb.	Tensile Strength psi
TSQS1	0.04400	1050	23864
TSQS2	0.05625	1350	24000
TSQS3	0.05738	1350	23527

Tensile Strength (Average) = 23797 ± 179 psi

Table F4

Determination of Tensile Strength of Sintered Specimen from Copper Powder Produced in Run TR

Specimen No.	Cross-sectional Area, in^2	Maximum Force Applied, lb.	Tensile Srength psi
TSTR1	0.05625	1360	24178
TSTR2*	0.05738	1410	24573

Tensile Strength (Average) = 24375 ± 197 psi

*Tensile Strength is higher than what it should be as the specimen broke at the grip.